
8-2012

Evaluation Of The Effectiveness Of Anisotropic Analytical Algorithm In Flattened And Flattening-Filter-Free Beams For High Energy Lung Dose Delivery Using The Radiological Physics Center Lung Phantom

Roman Repchak

David Scott Followill

Follow this and additional works at: https://digitalcommons.library.tmc.edu/utgsbs_dissertations



Part of the [Medicine and Health Sciences Commons](#)

Recommended Citation

Repchak, Roman and Followill, David Scott, "Evaluation Of The Effectiveness Of Anisotropic Analytical Algorithm In Flattened And Flattening-Filter-Free Beams For High Energy Lung Dose Delivery Using The Radiological Physics Center Lung Phantom" (2012). *Dissertations and Theses (Open Access)*. 274.
https://digitalcommons.library.tmc.edu/utgsbs_dissertations/274

This Thesis (MS) is brought to you for free and open access by the MD Anderson UTHealth Houston Graduate School at DigitalCommons@TMC. It has been accepted for inclusion in Dissertations and Theses (Open Access) by an authorized administrator of DigitalCommons@TMC. For more information, please contact digcommons@library.tmc.edu.

EVALUATION OF THE EFFECTIVENESS OF ANISOTROPIC ANALYTICAL ALGORITHM
IN FLATTENED AND FLATTENING-FILTER-FREE BEAMS FOR HIGH ENERGY LUNG
DOSE DELIVERY USING THE RADIOLOGICAL PHYSICS CENTER LUNG PHANTOM

by

Roman Repchak, M.S.

APPROVED:

David Followill, Ph.D.
Supervisory Professor

Carol J. Etzel, Ph.D.

Rebecca M. Howell, Ph.D.

Stephen F. Kry, Ph.D.

Andrea Molineu, M.S.

Richard Popple, Ph.D.

APPROVED:

Dean, The University of Texas Health Science Center at Houston
Graduate School of Biomedical Sciences

EVALUATION OF THE EFFECTIVENESS OF ANISOTROPIC ANALYTICAL ALGORITHM
IN FLATTENED AND FLATTENING-FILTER-FREE BEAMS FOR HIGH ENERGY LUNG
DOSE DELIVERY USING THE RADIOLOGICAL PHYSICS CENTER LUNG PHANTOM

A
THESIS

Presented to the Faculty of
The University of Texas
Health Science Center at Houston
and
The University of Texas
M. D. Anderson Cancer Center
Graduate School of Biomedical Sciences

in Partial Fulfillment
of the Requirements
for the Degree of

MASTER OF SCIENCE

by

Roman Repchak, M.S.

Houston, Texas
August, 2012

Acknowledgements

I am grateful to many people without whom this project would not be possible. First and foremost, I would like to thank my advisor Dr. David Followill for his understanding, guidance and continuous support. I want to express my gratitude to all the members of my supervisory committee for all their much appreciated help with this project, their ideas and suggestions. Their constant guidance throughout the whole project was crucial to its success.

I want to thank the entire staff of the Radiological Physics Center for their assistance and support with different aspects of this work. Special thanks go to Paola Alvarez for many very useful tips and help with data analysis, to Nadia Hernandez and Carrie Amador for their very valuable help with the phantom, to Jackie Tonigan for helping me with the irradiations of the phantom, to Lynda McDonald for her support with TLDs, and to Elizabeth Siller for coordinating and making arrangements that made it possible to finish the project on time.

This investigation was supported by PHS grants CA10953 and CA81647 awarded by the NCI, DHHS.

EVALUATION OF THE EFFECTIVENESS OF ANISOTROPIC ANALYTICAL ALGORITHM
IN FLATTENED AND FLATTENING-FILTER-FREE BEAMS FOR HIGH ENERGY LUNG
DOSE DELIVERY USING THE RADIOLOGICAL PHYSICS CENTER LUNG PHANTOM

Publication No.: _____

Roman Repchak, M.S.

Supervisory Professor: David Followill, PhD

The effectiveness of the Anisotropic Analytical Algorithm (AAA) implemented in the Eclipse treatment planning system (TPS) was evaluated using the Radiological Physics Center anthropomorphic lung phantom using both flattened and flattening-filter-free high energy beams. Radiation treatment plans were developed following the Radiation Therapy Oncology Group and the Radiological Physics Center guidelines for lung treatment using Stereotactic Radiation Body Therapy. The tumor was covered such that at least 95% of Planning Target Volume (PTV) received 100% of the prescribed dose while ensuring that normal tissue constraints were followed as well. Calculated doses were exported from the Eclipse TPS and compared with the experimental data as measured using thermoluminescence detectors (TLD) and radiochromic films that were placed inside the phantom. The results demonstrate that the AAA superposition-convolution algorithm is able to calculate SBRT treatment plans with all clinically used photon beams in the range from 6 MV to 18 MV. The measured dose distribution showed a good agreement with the calculated distribution using clinically acceptable criteria of $\pm 5\%$ dose or 3mm distance to agreement.

These results show that in a heterogeneous environment a 3D pencil beam superposition-convolution algorithms with Monte Carlo pre-calculated scatter kernels, such as AAA, are able to reliably calculate dose, accounting for increased lateral scattering due to the loss of electronic equilibrium in low density medium. The data for high energy plans (15 MV and 18 MV) showed very good tumor coverage in contrast to findings by other investigators for less sophisticated dose

calculation algorithms, which demonstrated less than expected tumor doses and generally worse tumor coverage for high energy plans compared to 6MV plans. This demonstrates that the modern superposition-convolution AAA algorithm is a significant improvement over previous algorithms and is able to calculate doses accurately for SBRT treatment plans in the highly heterogeneous environment of the thorax for both lower (≤ 12 MV) and higher (greater than 12 MV) beam energies.

TABLE OF CONTENTS

CHAPTER 1	INTRODUCTION	1
1.1	INTRODUCTION AND BACKGROUND.....	1
1.2	STATEMENT OF PROBLEM	2
1.3	ANISOTROPIC ANALYTICAL ALGORITHM	5
1.4	HYPOTHESIS AND SPECIFIC AIMS.....	7
CHAPTER 2	METHODS AND MATERIALS	8
2.1	THE RPC ANTHROPOMORPHIC THORAX PHANTOM	8
2.1.1	<i>Design and Construction.....</i>	8
2.1.2	<i>CT Simulation of the RPC Phantom.....</i>	12
2.2	TREATMENT PLANNING.....	13
2.2.1	<i>SBRT Plans: Dose Prescription and Limits</i>	13
2.2.2	<i>SBRT Plans: 6 MV and 18 MV MDACC.....</i>	15
2.2.3	<i>SBRT Plans: 6 MV FFF, 6 MV, 10 MV FFF, and 15 MV UAB MC.....</i>	17
2.3	TREATMENT PLAN DELIVERY	18
2.3.1	<i>MD Anderson Cancer Center.....</i>	18
2.3.2	<i>University of Alabama at Birmingham Medical Center.....</i>	18
2.4	DOSIMETRY	19
2.4.1	<i>Gafchromic® EBT2 Film.....</i>	19
2.4.1.1	Film Preparation.....	21
2.4.1.2	Film Scanning	24
2.4.2	<i>Thermoluminescence Dosimeters.....</i>	26
2.4.2.1	TL Design and Placement	26
2.4.2.2	TL Dose Calculation	26

2.5	DATA PROCESSING AND ANALYSIS.....	31
2.5.1	<i>Plan Export</i>	31
2.5.2	<i>TLD Data</i>	32
2.5.3	<i>Film Data Processing</i>	32
2.5.4	<i>Film Data Analysis</i>	37
CHAPTER 3	RESULTS AND DISCUSSION	40
3.1	DOSE RESPONSE CURVE.....	40
3.2	MD ANDERSON CANCER CENTER TREATMENT PLANS	41
3.2.1	<i>MD Anderson: 3D SBRT 6 MV Plan</i>	42
3.2.1.1	Plan Details	42
3.2.1.2	Target TLD Results.....	45
3.2.1.3	2D Gamma Index Analysis Results	47
3.2.1.4	Dose Profiles Results	51
3.2.2	<i>MD Anderson: 3D SBRT 18 MV Plan</i>	53
3.2.2.1	Plan Details	53
3.2.2.2	Target TLD Results.....	56
3.2.2.3	2D Gamma Index Analysis Results	57
3.2.2.4	Dose Profiles Results	61
3.3	UNIVERSITY OF ALABAMA AT BIRMINGHAM MEDICAL CENTER TREATMENT PLANS.....	63
3.3.1	<i>UAB: 3D SBRT 6 MV Plan</i>	63
3.3.1.1	Plan Details	63
3.3.1.2	Target TLD Results.....	65
3.3.1.3	2D Gamma Index Analysis Results	66
3.3.1.4	Dose Profiles Results	70
3.3.2	<i>UAB: 3D SBRT 15 MV Plan</i>	72
3.3.2.1	Plan Details	72

3.3.2.2	Target TLD Results	74
3.3.2.3	2D Gamma Index Analysis Results	75
3.3.2.4	Dose Profiles Results	79
3.3.3	<i>UAB: 3D SBRT 6 MV FFF Plan</i>	81
3.3.3.1	Plan Details	81
3.3.3.2	Target TLD Results	83
3.3.3.3	2D Gamma Index Analysis Results	84
3.3.3.4	Dose Profiles Results	88
3.3.4	<i>UAB: 3D SBRT 10 MV FFF Plan</i>	90
3.3.4.1	Plan Details	90
3.3.4.2	Target TLD Results	92
3.3.4.3	2D Gamma Index Analysis Results	93
3.3.4.4	Dose Profiles Results	97
3.4	RESULTS DISCUSSION	99
CHAPTER 4 CONCLUSION		103
4.1	GENERAL	103
4.2	FUTURE WORK	108
CHAPTER 5 APPENDIX		110
5.1	6 MV SBRT MD ANDERSON CANCER CENTER 2D GAMMA INDEX MAPS AND DOSE PROFILES	110
5.2	18 MV SBRT MD ANDERSON CANCER CENTER 2D GAMMA INDEX MAPS AND DOSE PROFILES	124
5.3	6 MV SBRT UNIVERSITY OF ALABAMA MEDICAL CENTER 2D GAMMA INDEX MAPS AND DOSE PROFILES	138

5.4	15 MV SBRT UNIVERSITY OF ALABAMA MEDICAL CENTER 2D GAMMA INDEX MAPS AND DOSE PROFILES	152
5.5	6 MV FFF SBRT UNIVERSITY OF ALABAMA MEDICAL CENTER 2D GAMMA INDEX MAPS AND DOSE PROFILES	166
5.6	10 MV FFF SBRT UNIVERSITY OF ALABAMA MEDICAL CENTER 2D GAMMA INDEX MAPS AND DOSE PROFILES	180
BIBLIOGRAPHY		194

LIST OF ILLUSTRATIONS

<i>Figure 2.1 Orthogonal Film Arrangement Inside The Phantom Insert</i>	<i>10</i>
<i>Figure 2.2 Heart And Spine TLD Inserts With The Open Target Insert</i>	<i>11</i>
<i>Figure 2.3 A Fully Assembled RPC Lung Phantom.....</i>	<i>12</i>
<i>Figure 2.4 An Axial CT Slice Of The Phantom That Contains The Target. Fiducials, Marked With Arrows, Can Be Seen On The Phantom Surface</i>	<i>13</i>
<i>Figure 2.5 3D View Of The Beam Arrangement Used In All Plans.....</i>	<i>16</i>
<i>Figure 2.6 Beams Configuration Used In a) 6 MV Plan (MDA) and b) 18 MV Plan (MDA)</i>	<i>16</i>
<i>Figure 2.7 Varian Linear Accelerator Head Components.....</i>	<i>17</i>
<i>Figure 2.8 Structure Of Gafchromic ® EBT2 Film (Not To Scale) [23].....</i>	<i>21</i>
<i>Figure 2.9 Irradiated Axial Film With Registration Pricks</i>	<i>22</i>
<i>Figure 2.10 Irradiated Coronal Film With Registration Pricks</i>	<i>22</i>
<i>Figure 2.11 Irradiated Sagittal Film With Registration Pricks</i>	<i>23</i>
<i>Figure 2.12 Phantom Used In Dose Response Film Irradiation</i>	<i>24</i>
<i>Figure 2.13 Polynomial Fit Of K_L Vs Apparent Dose Relationship For TLD Batch B11.....</i>	<i>29</i>
<i>Figure 2.14 Eclipse Export Wizard Settings Window</i>	<i>31</i>
<i>Figure 2.15 RPCFILM With Loaded And Registered Axial Film Image File.....</i>	<i>33</i>
<i>Figure 2.16 CERR Window With Loaded Plan.....</i>	<i>36</i>
<i>Figure 2.17 2D Gamma Index Using Dose And Distance To Agreement Criteria.....</i>	<i>37</i>
<i>Figure 3.1 Plot Of Dose Response Curve And Its Polynomial Fit.....</i>	<i>41</i>
<i>Figure 3.2 3D SBRT 6 MV Plan - Axial Plane Beam Placement.....</i>	<i>43</i>
<i>Figure 3.3 3D SBRT 6 MV Plan - Axial Plane Colorwash Dose Distribution</i>	<i>43</i>
<i>Figure 3.4 3-Plane View Of The Tumor And The Isodose Map.....</i>	<i>44</i>
<i>Figure 3.5 A Magnified Axial Plane View Of The Tumor And The Isodose Map.....</i>	<i>44</i>
<i>Figure 3.6 3D SBRT plan – Dose Volume Histogram</i>	<i>45</i>

<i>Figure 3.7 Measured-To-Predicted Dose Ratios Of Target TLDs For 6 MV Plan (MDA CC).....</i>	<i>46</i>
<i>Figure 3.8 2D Gamma Index Results: $\pm 5\%/3\text{mm}$, Axial Plane For 6 MV Plan</i>	<i>47</i>
<i>Figure 3.9 2D Gamma Index Results: $\pm 5\%/3\text{mm}$, Coronal Plane For 6 MV Plan</i>	<i>48</i>
<i>Figure 3.10 2D Gamma Index Results: $\pm 5\%/3\text{mm}$, Sagittal Plane For 6 MV Plan</i>	<i>48</i>
<i>Figure 3.11 2D Gamma Index Results Using $\pm 5\%/3\text{mm}$ Criteria For 6 MV Plan.....</i>	<i>50</i>
<i>Figure 3.12 2D Gamma Index Results Using $\pm 8\%/3\text{mm}$ Criteria For 6 MV Plan.....</i>	<i>50</i>
<i>Figure 3.13 Right-Left Profiles In Axial And Coronal Planes Compared To The Calculated Dose Profiles For 6 MV Plan.....</i>	<i>51</i>
<i>Figure 3.14 Anterior-Posterior Profiles In Axial And Sagittal Planes Compared To The Calculated Dose Profiles For 6 MV Plan.....</i>	<i>52</i>
<i>Figure 3.15 Superior-Inferior Profiles In Coronal And Sagittal Planes Compared To The Calculated Dose Profiles For 6 MV Plan.....</i>	<i>52</i>
<i>Figure 3.16 3D SBRT 18 MV Plan - Axial Plane Beam Placement.....</i>	<i>53</i>
<i>Figure 3.17 3D SBRT 18 MV Plan - Axial Plane Colorwash Dose Distribution</i>	<i>54</i>
<i>Figure 3.18 3-Plane View Of The Tumor And The Isodose Map.....</i>	<i>54</i>
<i>Figure 3.19 A Magnified Axial Plane View Of The Tumor And The Isodose Map.....</i>	<i>55</i>
<i>Figure 3.20 3D SBRT plan – Dose Volume Histogram</i>	<i>56</i>
<i>Figure 3.21 Measured-To-Predicted Dose Ratios Of Target TLDs For 18 MV Plan (MDA CC).....</i>	<i>57</i>
<i>Figure 3.22 2D Gamma Index Results: $\pm 5\%/3\text{mm}$, Axial Plane For 18 MV Plan</i>	<i>58</i>
<i>Figure 3.23 2D Gamma Index Results: $\pm 5\%/3\text{mm}$, Coronal Plane For 18 MV Plan</i>	<i>58</i>
<i>Figure 3.24 2D Gamma Index Results: $\pm 5\%/3\text{mm}$, Sagittal Plane For 18 MV Plan</i>	<i>59</i>
<i>Figure 3.25 2D Gamma Index Results Using $\pm 5\%/3\text{mm}$ Criteria For 18 MV Plan.....</i>	<i>60</i>
<i>Figure 3.26 2D Gamma Index Results Using $\pm 8\%/3\text{mm}$ Criteria For 18 MV Plan.....</i>	<i>60</i>
<i>Figure 3.27 Right-Left Profiles In Axial And Coronal Planes Compared To The Calculated Dose Profiles For 18 MV Plan.....</i>	<i>61</i>

<i>Figure 3.28 Anterior-Posterior profiles in axial and sagittal planes compared to the calculated dose profiles for 18 MV plan.....</i>	<i>62</i>
<i>Figure 3.29 Superior-Inferior Profiles In Coronal And Sagittal Planes Compared To The Calculated Dose Profiles For 18 MV Plan.....</i>	<i>62</i>
<i>Figure 3.30 3-Plane View Of The Tumor And The Isodose Map.....</i>	<i>64</i>
<i>Figure 3.31 A Magnified Axial Plane View Of The Tumor And The Isodose Map.....</i>	<i>64</i>
<i>Figure 3.32 6MV 3D SBRT Plan – Dose Volume Histogram</i>	<i>65</i>
<i>Figure 3.33 Measured-to-predicted dose ratios of target TLDs for 6 MV plan (UAB MC)</i>	<i>66</i>
<i>Figure 3.34 2D Gamma Index Results: $\pm 5\%/3\text{mm}$, Axial Plane For 6 MV Plan</i>	<i>67</i>
<i>Figure 3.35 2D Gamma Index Results: $\pm 5\%/3\text{mm}$, Coronal Plane For 6 MV Plan</i>	<i>67</i>
<i>Figure 3.36 2D Gamma Index Results: $\pm 5\%/3\text{mm}$, Sagittal Plane For 6 MV Plan</i>	<i>68</i>
<i>Figure 3.37 2D Gamma Index Results Using $\pm 5\%/3\text{mm}$ Criteria For 6 MV Plan.....</i>	<i>69</i>
<i>Figure 3.38 2D Gamma Index Results Using $\pm 8\%/3\text{mm}$ Criteria For 6 MV Plan.....</i>	<i>69</i>
<i>Figure 3.39 Right-Left Profiles In Axial And Coronal Planes Compared To The Calculated Dose Profiles For 6 MV Plan.....</i>	<i>70</i>
<i>Figure 3.40 Anterior-Posterior Profiles In Axial And Sagittal Planes Compared To The Calculated Dose Profiles For 6 MV Plan.....</i>	<i>71</i>
<i>Figure 3.41 Superior-Inferior Profiles In Coronal And Sagittal Planes Compared To The Calculated Dose Profiles For 6 MV Plan.....</i>	<i>71</i>
<i>Figure 3.42 3-Plane View Of The Tumor And The Isodose Map.....</i>	<i>72</i>
<i>Figure 3.43 A Magnified Axial Plane View Of The Tumor And The Isodose Map.....</i>	<i>73</i>
<i>Figure 3.44 15MV 3D SBRT Plan – Dose Volume Histogram</i>	<i>73</i>
<i>Figure 3.45 Measured-To-Predicted Dose Ratios Of Target TLDs For 15 MV Plan (UAB MC)</i>	<i>74</i>
<i>Figure 3.46 2D Gamma Index Results: $\pm 5\%/3\text{mm}$, Axial Plane For 15 MV Plan</i>	<i>75</i>
<i>Figure 3.47 2D Gamma Index Results: $\pm 5\%/3\text{mm}$, Coronal Plane For 15 MV Plan</i>	<i>76</i>
<i>Figure 3.48 2D Gamma Index Results: $\pm 5\%/3\text{mm}$, Sagittal Plane For 15 MV Plan</i>	<i>76</i>

<i>Figure 3.49 2D Gamma Index Results Using $\pm 5\%/3\text{mm}$ Criteria For 15 MV Plan</i>	78
<i>Figure 3.50 2D Gamma Index Results Using $\pm 8\%/3\text{mm}$ Criteria For 15 MV Plan</i>	78
<i>Figure 3.51 Right-Left profiles in axial and coronal planes compared to the calculated dose profiles for 15 MV plan</i>	79
<i>Figure 3.52 Anterior-Posterior profiles in axial and sagittal planes compared to the calculated dose profiles for 15 MV plan</i>	80
<i>Figure 3.53 Superior-Inferior profiles in coronal and sagittal planes compared to the calculated dose profiles for 15 MV plan</i>	80
<i>Figure 3.54 3-Plane View Of The Tumor And The Isodose Map</i>	81
<i>Figure 3.55 A Magnified Axial Plane View Of The Tumor And The Isodose Map</i>	82
<i>Figure 3.56 6MV FFF 3D SBRT Plan – Dose Volume Histogram</i>	82
<i>Figure 3.57 Measured-To-Predicted Dose Ratios Of Target TLDs For 6 MV FFF Plan (UAB MC)</i>	83
<i>Figure 3.58 2D Gamma Index Results: $\pm 5\%/3\text{mm}$, Axial Plane For 6 MV FFF Plan</i>	84
<i>Figure 3.59 2D Gamma Index Results: $\pm 5\%/3\text{mm}$, Coronal Plane For 6 MV FFF Plan</i>	85
<i>Figure 3.60 2D Gamma Index Results: $\pm 5\%/3\text{mm}$, Sagittal Plane For 6 MV FFF Plan</i>	85
<i>Figure 3.61 2D Gamma Index Results Using $\pm 5\%/3\text{mm}$ Criteria For 6 MV FFF Plan</i>	87
<i>Figure 3.62 2D Gamma Index Results Using $\pm 8\%/3\text{mm}$ Criteria For 6 MV FFF Plan</i>	87
<i>Figure 3.63 Right-Left Profiles In Axial And Coronal Planes Compared To The Calculated Dose Profiles For 6 MV FFF Plan</i>	88
<i>Figure 3.64 Anterior-Posterior Profiles In Axial And Sagittal Planes Compared To The Calculated Dose Profiles For 6 MV FFF Plan</i>	89
<i>Figure 3.65 Superior-Inferior Profiles In Coronal And Sagittal Planes Compared To The Calculated Dose Profiles For 6 MV FFF Plan</i>	89
<i>Figure 3.66 3-Plane View Of The Tumor And The Isodose Map</i>	90
<i>Figure 3.67 A Magnified Axial Plane View Of The Tumor And The Isodose Map</i>	91
<i>Figure 3.68 10MV FFF 3D SBRT Plan – Dose Volume Histogram</i>	92

<i>Figure 3.69 Measured-To-Predicted Dose Ratios Of Target TLDs For 10 MV FFF Plan (UAB MC)</i>	93
<i>Figure 3.70 2D Gamma Index Results: $\pm 5\%/3\text{mm}$, Axial Plane For 10 MV FFF Plan</i>	94
<i>Figure 3.71 2D Gamma Index Results: $\pm 5\%/3\text{mm}$, Coronal Plane For 10 MV FFF Plan</i>	94
<i>Figure 3.72 2D Gamma Index Results: $\pm 5\%/3\text{mm}$, Sagittal Plane For 10 MV FFF Plan</i>	95
<i>Figure 3.73 2D Gamma Index Results Using $\pm 5\%/3\text{mm}$ Criteria For 10 MV FFF Plan</i>	96
<i>Figure 3.74 2D Gamma Index Results Using $\pm 8\%/3\text{mm}$ Criteria For 10 MV FFF Plan</i>	96
<i>Figure 3.75 Right-Left Profiles In Axial And Coronal Planes Compared To The Calculated Dose Profiles For 10 MV FFF Plan</i>	97
<i>Figure 3.76 Anterior-Posterior Profiles In Axial And Sagittal Planes Compared To The Calculated Dose Profiles For 10 MV FFF Plan</i>	98
<i>Figure 3.77 Superior-Inferior Profiles In Coronal And Sagittal Planes Compared To The Calculated Dose Profiles For 10 MV FFF Plan</i>	98
<i>Figure 3.78 Measured-to-Predicted Dose Ratio vs Beam Energy</i>	102
<i>Figure 4.1 Measured-To-Predicted TLD Dose Ratios, 3-Irradiation Per Plan Average</i>	104
<i>Figure 4.2 Plot Of Averaged Points Passing $\pm 5\%/3\text{mm}$ Criteria 2D Gamma Analysis For All Plans</i>	106
<i>Figure 4.3 Plot Of Averaged Points Passing $\pm 8\%/3\text{mm}$ Criteria 2D Gamma Analysis For All Plans</i>	107
<i>Figure 5.1 6 MV SBRT MDA 2D Gamma Index Results: $\pm 5\%/3\text{mm}$, Axial Plane, Irradiation #1</i>	110
<i>Figure 5.2 6 MV SBRT MDA 2D Gamma Index Results: $\pm 8\%/3\text{mm}$, Axial Plane, Irradiation #1</i>	111
<i>Figure 5.3 6 MV SBRT MDA 2D Gamma Index Results: $\pm 5\%/3\text{mm}$, Coronal Plane, Irradiation #1</i>	111
<i>Figure 5.4 6 MV SBRT MDA 2D Gamma Index Results: $\pm 8\%/3\text{mm}$, Coronal Plane, Irradiation #1</i>	112

<i>Figure 5.5 6 MV SBRT MDA 2D Gamma Index Results: $\pm 5\%/3\text{mm}$, Sagittal Plane, Irradiation #1</i>	112
<i>Figure 5.6 6 MV SBRT MDA 2D Gamma Index Results: $\pm 8\%/3\text{mm}$, Sagittal Plane, Irradiation #1</i>	113
<i>Figure 5.7 6 MV SBRT MDA 1D Right-Left Dose Profiles: Irradiation #1</i>	113
<i>Figure 5.8 6 MV SBRT MDA 1D Anterior-Posterior Dose Profiles: Irradiation #1</i>	114
<i>Figure 5.9 6 MV SBRT MDA 1D Superior-Inferior Dose Profiles: Irradiation #1</i>	114
<i>Figure 5.10 6 MV SBRT MDA 2D Gamma Index Results: $\pm 5\%/3\text{mm}$, Axial Plane, Irradiation #2</i>	115
<i>Figure 5.11 6 MV SBRT MDA 2D Gamma Index Results: $\pm 8\%/3\text{mm}$, Axial Plane, Irradiation #2</i>	115
<i>Figure 5.12 6 MV SBRT MDA 2D Gamma Index Results: $\pm 5\%/3\text{mm}$, Coronal Plane, Irradiation #2</i>	116
<i>Figure 5.13 6 MV SBRT MDA 2D Gamma Index Results: $\pm 8\%/3\text{mm}$, Coronal Plane, Irradiation #2</i>	116
<i>Figure 5.14 6 MV SBRT MDA 2D Gamma Index Results: $\pm 5\%/3\text{mm}$, Sagittal Plane, Irradiation #2</i>	117
<i>Figure 5.15 6 MV SBRT MDA 2D Gamma Index Results: $\pm 8\%/3\text{mm}$, Sagittal Plane, Irradiation #2</i>	117
<i>Figure 5.16 6 MV SBRT MDA 1D Right-Left Dose Profiles: Irradiation #2</i>	118
<i>Figure 5.17 6 MV SBRT MDA 1D Anterior-Posterior Dose Profiles: Irradiation #2</i>	118
<i>Figure 5.18 6 MV SBRT MDA 1D Superior-Inferior Dose Profiles: Irradiation #2</i>	119
<i>Figure 5.19 6 MV SBRT MDA 2D Gamma Index Results: $\pm 5\%/3\text{mm}$, Axial Plane, Irradiation #3</i>	119
<i>Figure 5.20 6 MV SBRT MDA 2D Gamma Index Results: $\pm 8\%/3\text{mm}$, Axial Plane, Irradiation #3</i>	120
<i>Figure 5.21 6 MV SBRT MDA 2D Gamma Index Results: $\pm 5\%/3\text{mm}$, Coronal Plane, Irradiation #3</i>	120
<i>Figure 5.22 6 MV SBRT MDA 2D Gamma Index Results: $\pm 8\%/3\text{mm}$, Coronal Plane, Irradiation #3</i>	121

<i>Figure 5.23 6 MV SBRT MDA 2D Gamma Index Results: $\pm 5\%/3\text{mm}$, Sagittal Plane, Irradiation #3</i>	121
<i>Figure 5.24 6 MV SBRT MDA 2D Gamma Index Results: $\pm 8\%/3\text{mm}$, Sagittal Plane, Irradiation #3</i>	122
<i>Figure 5.25 6 MV SBRT MDA 1D Right-Left Dose Profiles: Irradiation #3</i>	122
<i>Figure 5.26 6 MV SBRT MDA 1D Anterior-Posterior Dose Profiles: Irradiation #3</i>	123
<i>Figure 5.27 6 MV SBRT MDA 1D Superior-Inferior Dose Profiles: Irradiation #3</i>	123
<i>Figure 5.28 18 MV SBRT MDA 2D Gamma Index Results: $\pm 5\%/3\text{mm}$, Axial Plane, Irradiation #1</i>	124
<i>Figure 5.29 18 MV SBRT MDA 2D Gamma Index Results: $\pm 8\%/3\text{mm}$, Axial Plane, Irradiation #1</i>	124
<i>Figure 5.30 18 MV SBRT MDA 2D Gamma Index Results: $\pm 5\%/3\text{mm}$, Coronal Plane, Irradiation #1</i>	125
<i>Figure 5.31 18 MV SBRT MDA 2D Gamma Index Results: $\pm 8\%/3\text{mm}$, Coronal Plane, Irradiation #1</i>	125
<i>Figure 5.32 18 MV SBRT MDA 2D Gamma Index Results: $\pm 5\%/3\text{mm}$, Sagittal Plane, Irradiation #1</i>	126
<i>Figure 5.33 18 MV SBRT MDA 2D Gamma Index Results: $\pm 8\%/3\text{mm}$, Sagittal Plane, Irradiation #1</i>	126
<i>Figure 5.34 18 MV SBRT MDA 1D Right-Left Dose Profiles: Irradiation #1</i>	127
<i>Figure 5.35 18 MV SBRT MDA 1D Anterior-Posterior Dose Profiles: Irradiation #1</i>	127
<i>Figure 5.36 18 MV SBRT MDA 1D Superior-Inferior Dose Profiles: Irradiation #1</i>	128
<i>Figure 5.37 18 MV SBRT MDA 2D Gamma Index Results: $\pm 5\%/3\text{mm}$, Axial Plane, Irradiation #2</i>	128
<i>Figure 5.38 18 MV SBRT MDA 2D Gamma Index Results: $\pm 8\%/3\text{mm}$, Axial Plane, Irradiation #2</i>	129

<i>Figure 5.39 18 MV SBRT MDA 2D Gamma Index Results: $\pm 5\%/3\text{mm}$, Coronal Plane, Irradiation #2</i>	129
<i>Figure 5.40 18 MV SBRT MDA 2D Gamma Index Results: $\pm 8\%/3\text{mm}$, Coronal Plane, Irradiation #2</i>	130
<i>Figure 5.41 18 MV SBRT MDA 2D Gamma Index Results: $\pm 5\%/3\text{mm}$, Sagittal Plane, Irradiation #2</i>	130
<i>Figure 5.42 18 MV SBRT MDA 2D Gamma Index Results: $\pm 8\%/3\text{mm}$, Sagittal Plane, Irradiation #2</i>	131
<i>Figure 5.43 18 MV SBRT MDA 1D Right-Left Dose Profiles: Irradiation #2</i>	131
<i>Figure 5.44 18 MV SBRT MDA 1D Anterior-Posterior Dose Profiles: Irradiation #2</i>	132
<i>Figure 5.45 18 MV SBRT MDA 1D Superior-Inferior Dose Profiles: Irradiation #2</i>	132
<i>Figure 5.46 18 MV SBRT MDA 2D Gamma Index Results: $\pm 5\%/3\text{mm}$, Axial Plane, Irradiation #3</i>	133
<i>Figure 5.47 18 MV SBRT MDA 2D Gamma Index Results: $\pm 8\%/3\text{mm}$, Axial Plane, Irradiation #3</i>	133
<i>Figure 5.48 18 MV SBRT MDA 2D Gamma Index Results: $\pm 5\%/3\text{mm}$, Coronal Plane, Irradiation #3</i>	134
<i>Figure 5.49 18 MV SBRT MDA 2D Gamma Index Results: $\pm 8\%/3\text{mm}$, Coronal Plane, Irradiation #3</i>	134
<i>Figure 5.50 18 MV SBRT MDA 2D Gamma Index Results: $\pm 5\%/3\text{mm}$, Sagittal Plane, Irradiation #3</i>	135
<i>Figure 5.51 18 MV SBRT MDA 2D Gamma Index Results: $\pm 8\%/3\text{mm}$, Sagittal Plane, Irradiation #3</i>	135
<i>Figure 5.52 18 MV SBRT MDA 1D Right-Left Dose Profiles: Irradiation #3</i>	136
<i>Figure 5.53 18 MV SBRT MDA 1D Anterior-Posterior Dose Profiles: Irradiation #3</i>	136
<i>Figure 5.54 18 MV SBRT MDA 1D Superior-Inferior Dose Profiles: Irradiation #3</i>	137

<i>Figure 5.55 6 MV SBRT UAB 2D Gamma Index Results: $\pm 5\%/3\text{mm}$, Axial Plane, Irradiation #1</i>	138
<i>Figure 5.56 6 MV SBRT UAB 2D Gamma Index Results: $\pm 8\%/3\text{mm}$, Axial Plane, Irradiation #1</i>	138
<i>Figure 5.57 6 MV SBRT UAB 2D Gamma Index Results: $\pm 5\%/3\text{mm}$, Coronal Plane, Irradiation #1</i>	139
<i>Figure 5.58 6 MV SBRT UAB 2D Gamma Index Results: $\pm 8\%/3\text{mm}$, Coronal Plane, Irradiation #1</i>	139
<i>Figure 5.59 6 MV SBRT UAB 2D Gamma Index Results: $\pm 5\%/3\text{mm}$, Sagittal Plane, Irradiation #1</i>	140
<i>Figure 5.60 6 MV SBRT UAB 2D Gamma Index Results: $\pm 8\%/3\text{mm}$, Sagittal Plane, Irradiation #1</i>	140
<i>Figure 5.61 6 MV SBRT UAB 1D Right-Left Dose Profiles: Irradiation #1</i>	141
<i>Figure 5.62 6 MV SBRT UAB 1D Anterior-Posterior Dose Profiles: Irradiation #1</i>	141
<i>Figure 5.63 6 MV SBRT UAB 1D Superior-Inferior Dose Profiles: Irradiation #1</i>	142
<i>Figure 5.64 6 MV SBRT UAB 2D Gamma Index Results: $\pm 5\%/3\text{mm}$, Axial Plane, Irradiation #2</i>	142
<i>Figure 5.65 6 MV SBRT UAB 2D Gamma Index Results: $\pm 8\%/3\text{mm}$, Axial Plane, Irradiation #2</i>	143
<i>Figure 5.66 6 MV SBRT UAB 2D Gamma Index Results: $\pm 5\%/3\text{mm}$, Coronal Plane, Irradiation #2</i>	143
<i>Figure 5.67 6 MV SBRT UAB 2D Gamma Index Results: $\pm 8\%/3\text{mm}$, Coronal Plane, Irradiation #2</i>	144
<i>Figure 5.68 6 MV SBRT UAB 2D Gamma Index Results: $\pm 5\%/3\text{mm}$, Sagittal Plane, Irradiation #2</i>	144
<i>Figure 5.69 6 MV SBRT UAB 2D Gamma Index Results: $\pm 8\%/3\text{mm}$, Sagittal Plane, Irradiation #2</i>	145
<i>Figure 5.70 6 MV SBRT UAB 1D Right-Left Dose Profiles: Irradiation #2</i>	145
<i>Figure 5.71 6 MV SBRT UAB 1D Anterior-Posterior Dose Profiles: Irradiation #2</i>	146
<i>Figure 5.72 6 MV SBRT UAB 1D Superior-Inferior Dose Profiles: Irradiation #2</i>	146

<i>Figure 5.73 6 MV SBRT UAB 2D Gamma Index Results: $\pm 5\%/3\text{mm}$, Axial Plane, Irradiation #3</i>	147
<i>Figure 5.74 6 MV SBRT UAB 2D Gamma Index Results: $\pm 8\%/3\text{mm}$, Axial Plane, Irradiation #3</i>	147
<i>Figure 5.75 6 MV SBRT UAB 2D Gamma Index Results: $\pm 5\%/3\text{mm}$, Coronal Plane, Irradiation #3</i>	148
<i>Figure 5.76 6 MV SBRT UAB 2D Gamma Index Results: $\pm 8\%/3\text{mm}$, Coronal Plane, Irradiation #3</i>	148
<i>Figure 5.77 6 MV SBRT UAB 2D Gamma Index Results: $\pm 5\%/3\text{mm}$, Sagittal Plane, Irradiation #3</i>	149
<i>Figure 5.78 6 MV SBRT UAB 2D Gamma Index Results: $\pm 8\%/3\text{mm}$, Sagittal Plane, Irradiation #3</i>	149
<i>Figure 5.79 6 MV SBRT UAB 1D Right-Left Dose Profiles: Irradiation #3</i>	150
<i>Figure 5.80 6 MV SBRT UAB 1D Anterior-Posterior Dose Profiles: Irradiation #1</i>	150
<i>Figure 5.81 6 MV SBRT UAB 1D Superior-Inferior Dose Profiles: Irradiation #1</i>	151
<i>Figure 5.82 15 MV SBRT UAB 2D Gamma Index Results: $\pm 5\%/3\text{mm}$, Axial Plane, Irradiation #1</i>	152
<i>Figure 5.83 15 MV SBRT UAB 2D Gamma Index Results: $\pm 8\%/3\text{mm}$, Axial Plane, Irradiation #1</i>	152
<i>Figure 5.84 15 MV SBRT UAB 2D Gamma Index Results: $\pm 5\%/3\text{mm}$, Coronal Plane, Irradiation #1</i>	153
<i>Figure 5.85 15 MV SBRT UAB 2D Gamma Index Results: $\pm 8\%/3\text{mm}$, Coronal Plane, Irradiation #1</i>	153
<i>Figure 5.86 15 MV SBRT UAB 2D Gamma Index Results: $\pm 5\%/3\text{mm}$, Sagittal Plane, Irradiation #1</i>	154
<i>Figure 5.87 15 MV SBRT UAB 2D Gamma Index Results: $\pm 8\%/3\text{mm}$, Sagittal Plane, Irradiation #1</i>	154
<i>Figure 5.88 15 MV SBRT UAB 1D Right-Left Dose Profiles: Irradiation #1</i>	155
<i>Figure 5.89 15 MV SBRT UAB 1D Anterior-Posterior Dose Profiles: Irradiation #1</i>	155
<i>Figure 5.90 15 MV SBRT UAB 1D Superior-Inferior Dose Profiles: Irradiation #1</i>	156

<i>Figure 5.91 15 MV SBRT UAB 2D Gamma Index Results: $\pm 5\%/3\text{mm}$, Axial Plane, Irradiation #2</i>	156
<i>Figure 5.92 15 MV SBRT UAB 2D Gamma Index Results: $\pm 8\%/3\text{mm}$, Axial Plane, Irradiation #2</i>	157
<i>Figure 5.93 15 MV SBRT UAB 2D Gamma Index Results: $\pm 5\%/3\text{mm}$, Coronal Plane, Irradiation #2</i>	157
<i>Figure 5.94 15 MV SBRT UAB 2D Gamma Index Results: $\pm 8\%/3\text{mm}$, Coronal Plane, Irradiation #2</i>	158
<i>Figure 5.95 15 MV SBRT UAB 2D Gamma Index Results: $\pm 5\%/3\text{mm}$, Sagittal Plane, Irradiation #2</i>	158
<i>Figure 5.96 15 MV SBRT UAB 2D Gamma Index Results: $\pm 8\%/3\text{mm}$, Sagittal Plane, Irradiation #2</i>	159
<i>Figure 5.97 15 MV SBRT UAB 1D Right-Left Dose Profiles: Irradiation #2</i>	159
<i>Figure 5.98 15 MV SBRT UAB 1D Anterior-Posterior Dose Profiles: Irradiation #2</i>	160
<i>Figure 5.99 15 MV SBRT UAB 1D Superior-Inferior Dose Profiles: Irradiation #2</i>	160
<i>Figure 5.100 15 MV SBRT UAB 2D Gamma Index Results: $\pm 5\%/3\text{mm}$, Axial Plane, Irradiation #3</i>	161
<i>Figure 5.101 15 MV SBRT UAB 2D Gamma Index Results: $\pm 8\%/3\text{mm}$, Axial Plane, Irradiation #3</i>	161
<i>Figure 5.102 15 MV SBRT UAB 2D Gamma Index Results: $\pm 5\%/3\text{mm}$, Coronal Plane, Irradiation #3</i>	162
<i>Figure 5.103 15 MV SBRT UAB 2D Gamma Index Results: $\pm 8\%/3\text{mm}$, Coronal Plane, Irradiation #3</i>	162
<i>Figure 5.104 15 MV SBRT UAB 2D Gamma Index Results: $\pm 5\%/3\text{mm}$, Sagittal Plane, Irradiation #3</i>	163
<i>Figure 5.105 15 MV SBRT UAB 2D Gamma Index Results: $\pm 8\%/3\text{mm}$, Sagittal Plane, Irradiation #3</i>	163
<i>Figure 5.106 15 MV SBRT UAB 1D Right-Left Dose Profiles: Irradiation #3</i>	164

<i>Figure 5.107 15 MV SBRT UAB 1D Anterior-Posterior Dose Profiles: Irradiation #3.....</i>	<i>164</i>
<i>Figure 5.108 15 MV SBRT UAB 1D Superior-Inferior Dose Profiles: Irradiation #3.....</i>	<i>165</i>
<i>Figure 5.109 6 MV FFF SBRT UAB 2D Gamma Index Results: $\pm 5\%/3\text{mm}$, Axial Plane, Irradiation #1.....</i>	<i>166</i>
<i>Figure 5.110 6 MV FFF SBRT UAB 2D Gamma Index Results: $\pm 8\%/3\text{mm}$, Axial Plane, Irradiation #1.....</i>	<i>166</i>
<i>Figure 5.111 6 MV FFF SBRT UAB 2D Gamma Index Results: $\pm 5\%/3\text{mm}$, Coronal Plane, Irradiation #1.....</i>	<i>167</i>
<i>Figure 5.112 6 MV FFF SBRT UAB 2D Gamma Index Results: $\pm 8\%/3\text{mm}$, Coronal Plane, Irradiation #1.....</i>	<i>167</i>
<i>Figure 5.113 6 MV FFF SBRT UAB 2D Gamma Index Results: $\pm 5\%/3\text{mm}$, Sagittal Plane, Irradiation #1.....</i>	<i>168</i>
<i>Figure 5.114 6 MV FFF SBRT UAB 2D Gamma Index Results: $\pm 8\%/3\text{mm}$, Sagittal Plane, Irradiation #1.....</i>	<i>168</i>
<i>Figure 5.115 6 MV FFF SBRT UAB 1D Right-Left Dose Profiles: Irradiation #1</i>	<i>169</i>
<i>Figure 5.116 6 MV FFF SBRT UAB 1D Anterior-Posterior Dose Profiles: Irradiation #1</i>	<i>169</i>
<i>Figure 5.117 6 MV FFF SBRT UAB 1D Superior-Inferior Dose Profiles: Irradiation #1.....</i>	<i>170</i>
<i>Figure 5.118 6 MV FFF SBRT UAB 2D Gamma Index Results: $\pm 5\%/3\text{mm}$, Axial Plane, Irradiation #2.....</i>	<i>170</i>
<i>Figure 5.119 6 MV FFF SBRT UAB 2D Gamma Index Results: $\pm 8\%/3\text{mm}$, Axial Plane, Irradiation #2.....</i>	<i>171</i>
<i>Figure 5.120 6 MV FFF SBRT UAB 2D Gamma Index Results: $\pm 5\%/3\text{mm}$, Coronal Plane, Irradiation #2.....</i>	<i>171</i>
<i>Figure 5.121 6 MV FFF SBRT UAB 2D Gamma Index Results: $\pm 8\%/3\text{mm}$, Coronal Plane, Irradiation #2.....</i>	<i>172</i>

<i>Figure 5.122 6 MV FFF SBRT UAB 2D Gamma Index Results: $\pm 5\%/3\text{mm}$, Sagittal Plane, Irradiation #2.....</i>	<i>172</i>
<i>Figure 5.123 6 MV FFF SBRT UAB 2D Gamma Index Results: $\pm 8\%/3\text{mm}$, Sagittal Plane, Irradiation #2.....</i>	<i>173</i>
<i>Figure 5.124 6 MV FFF SBRT UAB 1D Right-Left Dose Profiles: Irradiation #2</i>	<i>173</i>
<i>Figure 5.125 6 MV FFF SBRT UAB 1D Anterior-Posterior Dose Profiles: Irradiation #2</i>	<i>174</i>
<i>Figure 5.126 6 MV FFF SBRT UAB 1D Superior-Inferior Dose Profiles: Irradiation #2.....</i>	<i>174</i>
<i>Figure 5.127 6 MV FFF SBRT UAB 2D Gamma Index Results: $\pm 5\%/3\text{mm}$, Axial Plane, Irradiation #3.....</i>	<i>175</i>
<i>Figure 5.128 6 MV FFF SBRT UAB 2D Gamma Index Results: $\pm 8\%/3\text{mm}$, Axial Plane, Irradiation #3.....</i>	<i>175</i>
<i>Figure 5.129 6 MV FFF SBRT UAB 2D Gamma Index Results: $\pm 5\%/3\text{mm}$, Coronal Plane, Irradiation #3.....</i>	<i>176</i>
<i>Figure 5.130 6 MV FFF SBRT UAB 2D Gamma Index Results: $\pm 8\%/3\text{mm}$, Coronal Plane, Irradiation #3.....</i>	<i>176</i>
<i>Figure 5.131 6 MV FFF SBRT UAB 2D Gamma Index Results: $\pm 5\%/3\text{mm}$, Sagittal Plane, Irradiation #3.....</i>	<i>177</i>
<i>Figure 5.132 6 MV FFF SBRT UAB 2D Gamma Index Results: $\pm 8\%/3\text{mm}$, Sagittal Plane, Irradiation #3.....</i>	<i>177</i>
<i>Figure 5.133 6 MV FFF SBRT UAB 1D Right-Left Dose Profiles: Irradiation #3</i>	<i>178</i>
<i>Figure 5.134 6 MV FFF SBRT UAB 1D Anterior-Posterior Dose Profiles: Irradiation #3</i>	<i>178</i>
<i>Figure 5.135 6 MV FFF SBRT UAB 1D Superior-Inferior Dose Profiles: Irradiation #3.....</i>	<i>179</i>
<i>Figure 5.136 10 MV FFF SBRT UAB 2D Gamma Index Results: $\pm 5\%/3\text{mm}$, Axial Plane, Irradiation #1.....</i>	<i>180</i>
<i>Figure 5.137 10 MV FFF SBRT UAB 2D Gamma Index Results: $\pm 8\%/3\text{mm}$, Axial Plane, Irradiation #1.....</i>	<i>180</i>

<i>Figure 5.138 10 MV FFF SBRT UAB 2D Gamma Index Results: $\pm 5\%/3\text{mm}$, Coronal Plane, Irradiation #1</i>	181
<i>Figure 5.139 10 MV FFF SBRT UAB 2D Gamma Index Results: $\pm 8\%/3\text{mm}$, Coronal Plane, Irradiation #1</i>	181
<i>Figure 5.140 10 MV FFF SBRT UAB 2D Gamma Index Results: $\pm 5\%/3\text{mm}$, Sagittal Plane, Irradiation #1</i>	182
<i>Figure 5.141 10 MV FFF SBRT UAB 2D Gamma Index Results: $\pm 8\%/3\text{mm}$, Sagittal Plane, Irradiation #1</i>	182
<i>Figure 5.142 10 MV FFF SBRT UAB 1D Right-Left Dose Profiles: Irradiation #1</i>	183
<i>Figure 5.143 10 MV FFF SBRT UAB 1D Anterior-Posterior Dose Profiles: Irradiation #1</i>	183
<i>Figure 5.144 10 MV FFF SBRT UAB 1D Superior-Inferior Dose Profiles: Irradiation #1</i>	184
<i>Figure 5.145 10 MV FFF SBRT UAB 2D Gamma Index Results: $\pm 5\%/3\text{mm}$, Axial Plane, Irradiation #2</i>	184
<i>Figure 5.146 10 MV FFF SBRT UAB 2D Gamma Index Results: $\pm 8\%/3\text{mm}$, Axial Plane, Irradiation #2</i>	185
<i>Figure 5.147 10 MV FFF SBRT UAB 2D Gamma Index Results: $\pm 5\%/3\text{mm}$, Coronal Plane, Irradiation #2</i>	185
<i>Figure 5.148 10 MV FFF SBRT UAB 2D Gamma Index Results: $\pm 8\%/3\text{mm}$, Coronal Plane, Irradiation #2</i>	186
<i>Figure 5.149 10 MV FFF SBRT UAB 2D Gamma Index Results: $\pm 5\%/3\text{mm}$, Sagittal Plane, Irradiation #2</i>	186
<i>Figure 5.150 10 MV FFF SBRT UAB 2D Gamma Index Results: $\pm 8\%/3\text{mm}$, Sagittal Plane, Irradiation #2</i>	187
<i>Figure 5.151 10 MV FFF SBRT UAB 1D Right-Left Dose Profiles: Irradiation #2</i>	187
<i>Figure 5.152 10 MV FFF SBRT UAB 1D Anterior-Posterior Dose Profiles: Irradiation #2</i>	188
<i>Figure 5.153 10 MV FFF SBRT UAB 1D Superior-Inferior Dose Profiles: Irradiation #2</i>	188

<i>Figure 5.154 10 MV FFF SBRT UAB 2D Gamma Index Results: $\pm 5\%/3\text{mm}$, Axial Plane, Irradiation #3.....</i>	<i>189</i>
<i>Figure 5.155 10 MV FFF SBRT UAB 2D Gamma Index Results: $\pm 8\%/3\text{mm}$, Axial Plane, Irradiation #3.....</i>	<i>189</i>
<i>Figure 5.156 10 MV FFF SBRT UAB 2D Gamma Index Results: $\pm 5\%/3\text{mm}$, Coronal Plane, Irradiation #3.....</i>	<i>190</i>
<i>Figure 5.157 10 MV FFF SBRT UAB 2D Gamma Index Results: $\pm 8\%/3\text{mm}$, Coronal Plane, Irradiation #3.....</i>	<i>190</i>
<i>Figure 5.158 10 MV FFF SBRT UAB 2D Gamma Index Results: $\pm 5\%/3\text{mm}$, Sagittal Plane, Irradiation #3.....</i>	<i>191</i>
<i>Figure 5.159 10 MV FFF SBRT UAB 2D Gamma Index Results: $\pm 8\%/3\text{mm}$, Sagittal Plane, Irradiation #3.....</i>	<i>191</i>
<i>Figure 5.160 10 MV FFF SBRT UAB 1D Right-Left Dose Profiles: Irradiation #3.....</i>	<i>192</i>
<i>Figure 5.161 10 MV FFF SBRT UAB 1D Anterior-Posterior Dose Profiles: Irradiation #3</i>	<i>192</i>
<i>Figure 5.162 10 MV FFF SBRT UAB 1D Superior-Inferior Dose Profiles: Irradiation #3.....</i>	<i>193</i>

LIST OF TABLES

<i>Table 2.1 RPC Phantom Material Densities and CT Numbers.....</i>	<i>9</i>
<i>Table 2.2 RPC/RTOG List Of SBRT Lung Treatment Protocols</i>	<i>14</i>
<i>Table 2.3 Normal Tissues Constraints (RPC Protocol).....</i>	<i>15</i>
<i>Table 2.4 L23 RPC Lung Phantom Profile Data</i>	<i>34</i>
<i>Table 3.1 Dose Response Film Data Points.....</i>	<i>40</i>
<i>Table 3.2 Target TLD Results. 6 MV, MD Anderson.....</i>	<i>46</i>
<i>Table 3.3 6 MV Plan 2D Gamma Index Results, MD Anderson.....</i>	<i>49</i>
<i>Table 3.4 Target TLD Results. 18 MV, MD Anderson.....</i>	<i>56</i>
<i>Table 3.5 18 MV Plan 2D Gamma Index Results, MD Anderson.....</i>	<i>59</i>
<i>Table 3.6 Target TLD Results. 6 MV, UAB.....</i>	<i>65</i>
<i>Table 3.7 6 MV Plan 2D Gamma Index Results, UAB.....</i>	<i>68</i>
<i>Table 3.8 Target TLD Results. 15 MV, UAB.....</i>	<i>74</i>
<i>Table 3.9 15 MV Plan 2D Gamma Index Results, UAB.....</i>	<i>77</i>
<i>Table 3.10 Target TLD Results. 6 MV FFF, UAB</i>	<i>83</i>
<i>Table 3.11 6 MV FFF Plan 2D Gamma Index Results, UAB</i>	<i>86</i>
<i>Table 3.12 Target TLD Results. 10 MV FFF, UAB</i>	<i>92</i>
<i>Table 3.13 10 MV FFF Plan 2D Gamma Index Results, UAB</i>	<i>95</i>

Chapter 1 Introduction

1.1 Introduction and Background

The Radiological Physics Center (RPC) is a quality assurance office (QAO) funded by the National Cancer Institute (NCI) that is tasked to provide quality assurance services to institutions participating in clinical trials funded by NCI and its cooperative study groups. The RPC evaluates radiotherapy programs, develops protocols and QA procedures, and helps correct institutional deficiencies. The goal of the RPC is to make sure that prescribed radiation doses that are being delivered are clinically comparable, accurate and consistent.

The RPC provides services to over 1,800 institutions (over 14,000 beams) in the United States and abroad. Over the past 44 years the RPC has developed an extensive Quality Assurance (QA) program that includes on-site audit and remote audit tools. The on-site audits include dose measurements on therapy machines, review of patient dose calculations and quality control (QC) procedures, as well as interviewing the oncology staff. The remote audit tools consist of development and implementation of credentialing processes for participation in specific protocols, analysis of patient dose calculations, and verification of beam calibration. Anthropomorphic QA phantoms employing optically-stimulated luminescence or thermoluminescence dosimeters (OSLD/TLD) and radiochromic film are used to verify the actually delivered doses and compare them to doses calculated by the Treatment Planning Systems (TPS). Additionally, the RPC helps institutions in identifying the sources of inconsistencies and works with them on corrective actions.

The RPC's remote audit QA program employs a multitude of different anthropomorphic phantoms, among which the pelvic-prostate, head-and-neck, and thorax phantoms are the most common. Each phantom is constructed in such a way that it would allow the RPC to test and evaluate if the institutions providing radiation therapy services are able to develop and deliver treatment plans that satisfy specific clinical trial protocol requirements.

The thorax (Lung) RPC phantom is used to verify dose delivery from two commonly used radiation therapy techniques: 3D conformal (3D CRT) and intensity-modulated (IMRT). It represents a hollow plastic case shaped as a human thorax that fills with water. The phantom contains specific structures simulating human organs, such as heart, spine, lungs, and tumor [1].

Two types of dosimeters are used within the lung phantom: TLD for point dose and radiochromic film for two-dimensional dose distribution measurements. After an institution, that requests credentialing, irradiates the phantom, it is shipped back to the RPC for analysis. The data, measured by the dosimeters inside the phantom, is compared to the calculated values that are provided by the institution as well as to RPC established dosimetric parameters. This remote audit phantom QA program provides a reliable and cost effective tool in evaluating the institution's abilities to develop and deliver a specific radiation treatment in order to participate in cooperative group trials. Furthermore, the program helps institutions to identify potential problems in their treatment process.

The reproducibility of results with the thorax phantom, as described by Followill *et al*, proved its effectiveness in the credentialing process, making it very useful as an all encompassing test of the entire heterogeneity calculation algorithm of different TPSs [1, 2].

1.2 Statement of Problem

As reported by Mah & Van Dyk [3], calculated doses that were not corrected for heterogeneities resulted in the radiation pneumonitis risk underestimates of up to 19%. They concluded that heterogeneity corrections should be used in all multi-center clinical trials to determine correct dose in each case.

When high energy photon beams enter the air in the lungs the electron range in the lateral direction is increased which results in a loss of electronic equilibrium along the central axis [4]. Earlier studies that measured doses calculated with the algorithms that do not take into account the increased lateral scatter [5] advise against the use of small field sizes and high energy beams (18

MV) in heterogeneous environments such as the thorax and recommend selecting a lower beam energy (6 MV) when developing plans and calculating doses to a tumor surrounded by lung tissue.

Due to dose escalation and high dose gradients in modern delivery techniques such as IMRT or Stereotactic Radiation Body Therapy (SBRT) for lung tumors, it is becoming increasingly important to correct for such heterogeneities. Heterogeneity dose calculation corrections in many contemporary planning systems use different dose calculation algorithms that are based on superposition-convolution models with pre-calculated Monte Carlo (MC) kernels. Techniques that take into account electron disequilibrium due to increased lateral electron scattering in low density medium result in dose calculations that are in better agreement with measured dose distributions and, therefore, should be used in place of those that ignore lateral scattering component (such as pencil beam superposition) [6].

The superposition-convolution calculation typically has two components: first is the energy distribution that is released in the medium at the interaction site and the second component (kernel) represents the scatter distribution from this interaction. The latter component is typically obtained either analytically or by using Monte Carlo simulations. The superposition-convolution algorithm by itself integrates the first element (energy distribution at the primary interaction site) and second element (3D scatter distribution) over the entire body volume. The dose calculation in this case becomes a function of the algorithm itself, the geometry and the number of beams, as well as the resolution of the dose calculation grid [7].

According to the RPC data based on their remote audit QA program's TLD and radiochromic film measurements in anthropomorphic thorax phantoms, the heterogeneity corrected tumor doses calculated by different TPS in the lungs result in a wide range of delivered doses with Monte Carlo based methods having the best agreement with actual measurements [8, 9]. Even though heterogeneity correction of MC-based dose calculations are superior to the currently implemented superposition-convolution algorithms, Monte Carlo based techniques are largely impractical for clinical use due to substantial computational resources and time requirements.

While most dose calculation algorithms work well in a homogeneous medium they have been shown to not work well under certain specific, more challenging situations, such as higher photon beam energies and small field sizes. A Monte Carlo simulation study that looked into the differences between doses delivered using 6 MV and 15 MV energies [10] found that lower energy (6 MV) was preferable for lung cancer treatment to the MC simulated 15 MV beam since the latter resulted in a considerable loss of lateral equilibrium and significantly worse target coverage of planning treatment volume (PTV). One of the more recent studies that looked into the effectiveness of one of the modern superposition-convolution algorithms, Analytical Anisotropic Algorithm (AAA), implemented in the Varian Eclipse treatment planning system found that compared to Monte Carlo a 10 MV beam dose distribution in lung calculated by the AAA was inferior, while 6 MV beam resulted in an accurate dose calculation with much better agreement [11] highlighting potential difficulties that even the most up-to-date dose calculation algorithms face when used to plan treatments with tumors inside of the lungs utilizing high energy beams (>12 MV) and small fields. Due to complexities with accurate dose calculation in such conditions, at present, the SBRT lung treatments are performed using multiple fields (not less than 7) and beam energies of less than 10 MV. It has been shown [11] that in most clinical situations the superposition-convolution algorithms that account for 3D scatter have proven to be adequate for use in radiation treatment planning.

As was mentioned earlier, the Varian Eclipse TPS employs the Analytical Anisotropic Algorithm for volumetric heterogeneity corrected dose calculations. New data from the Radiological Physics Center (February, 2011) obtained using AAA in RPC's Lung phantom showed excellent agreement (0.98 measured-to-predicted ratio for point dose using TLDs and 100% pixel pass rate using $\pm 5\%/5\text{mm}$ gamma index for planar dose distribution using films) for a lung treatment using 15 MV x-ray beams. These data suggest that recent development in the AAA algorithm may have improved the volumetric heterogeneity corrected dose calculation so that it is now possible to use this algorithm for dose calculations in highly heterogeneous medium (such a lung) with beam

energies greater than 10 MV with dosimetric results that, prior to that, were only possible with 6 MV beams.

1.3 Anisotropic Analytical Algorithm

The Eclipse treatment planning system designed by Varian Medical Systems (Palo Alto, CA) was first introduced in 2001 and since then has been constantly evolving and adding many new features including intensity-modulated, image-guided, and arc radiation therapy, radiosurgery capabilities, conformal optimization, biological optimization and evaluation and many more. The planning system is capable of generating treatment plans using photon, electron, and proton beams making it one of the most popular commercially available TPS around the world with estimated over 10,000 systems being deployed.

The AAA essentially is a 3D pencil beam superposition-convolution algorithm. It employs separate Monte Carlo calculated models for primary and scattered extra-focal photons, as well as for the electrons scattered from the collimators. A total of six exponential functions are used in its model to calculate the dose distribution in the lateral direction. This allows the use of analytical convolution in the algorithm greatly reducing calculation time. The AAA has been originally implemented in stereotactic radiation therapy planning and later was included in Eclipse TPS [12].

Clinically the AAA is separated into two individual components: configuration and dose calculation. The first part is designed to acquire the necessary fundamental parameters of the clinical beam, i.e. energy spectra, photon and electron fluence, which are later used for the actual dose calculation. To account for complex composition of clinical beam, the AAA uses multiple sources to model the beam with only primary photons being considered primary source. Scattered and extra-focal photons along with electrons are treated as separate secondary sources.

To model the primary source, the AAA employs a phase space model that uses physical parameters obtained during the commissioning process. To determine the energy spectrum, the

algorithm takes into account the flattening filter characteristics and the beam mean energy dependence on the radial distance from the central axis. The secondary source model employs a virtual source that is located at the exit point of the flattening filter and includes an energy spectrum which is scaled to achieve a specified mean energy without any off-axis variations.

The original scatter kernels are obtained from the Monte Carlo pre-calculated data, but they also can be acquired from the energy spectrum during the configuration step of the algorithm. The scatter kernels provide the information on scatter characteristics for different beams. Since the actual beam is polyenergetic, multiple monoenergetic kernels were calculated in water using the Monte Carlo method from which the polyenergetic kernel is created as a weighted sum of the specific set of these kernels. In actual dose calculation, scaling accounts for differences between water density and the densities obtained from computed tomography (CT) simulated images. The clinical beam is divided into many finite-size beamlets with multiple convolutions performed for primary and secondary sources and the final 3D dose calculation is completed by superposing the beamlets [12].

The heterogeneity correction in the AAA has two components: the lateral scatter and the depth-directed component. Modeling of the lateral component using exponential functions provides an accurate representation of lateral scatter in a heterogeneous environment. The depth-directed component represents the total deposited energy, calculated using the lateral scatter functions on each plane. The convolution of this component accounts for tissue interface effects. With enough distance from the low-high density interface the AAA calculated results are comparable to Monte Carlo simulations. As was mentioned earlier, this technique has some limitation in treatment planning in lungs involving small field sizes and higher energies due to loss of electronic equilibrium along the central axis [13]. Improvements have been made to the AAA dose calculation algorithm in the area of tissue heterogeneity modeling and the accuracy of the scattered dose calculation making the AAA one of the most accurate commercially available non-MC-based algorithms at this time.

1.4 Hypothesis and Specific Aims

The hypothesis of this research is:

There will NOT be a difference of greater than $\pm 5\%$ or 3 mm distance to agreement (DTA) on average between radiotherapy treatments using 6 MV beam and energies greater than 10 MV using flattened and flattening filter free (FFF) photons beams as measured with the RPC's Lung phantoms.

The specific aims of this work are:

1. Create clinically relevant 6x/18x, and 6x/15x, 6x/10x FFF (TrueBeam) SBRT treatment plans for the RPC Lung phantom from a typical prescription and dose constraints for flattened and FFF beams.
2. Compare the flattened and FFF treatment plans to the respective higher energies plans to determine if they are clinically comparable.
3. Deliver 3 planned treatments to the RPC Lung phantom for each developed plan and measure the dose distribution from each.
4. Compare the measured and calculated doses delivered by flattened and FFF beams using clinically acceptable criteria 90% of points passing $\pm 5\%/3\text{mm}$ gamma index for 2D dose distribution and $\pm 5\%$ for point dose.

Chapter 2 Methods and Materials

2.1 The RPC Anthropomorphic Thorax Phantom

2.1.1 *Design and Construction*

The phantom used in this study was the RPC Lung Phantom #23. It is commonly used by the RPC as a remote QA tool. The primary use of this phantom is for credentialing institutions who intend to take part in clinical trials for the treatment of lung tumors supported by the NCI. In order to create a realistic clinical scenario the phantom was created to simulate the major anatomical structures of the thoracic cavity, such as chest wall, heart, spine, and lungs with a tumor inside of the left lung. All the structures are made of material with similar radiological properties to that of the human body, such as material density, CT number, and effective atomic number. Table 2.1 contains the characteristics of the materials used in the phantom. The body of the phantom is made of half a centimeter polyvinyl chloride (PVC) that creates a hollow case that is filled with water during CT simulation and dose delivery. This construction allows the phantom to be relatively light when not in use and drained of water. At the same time, water that fills the phantom has comparable radiological characteristics to that of the surrounding soft tissues. The structures that represent major organs have simplified shapes such as the spherically shaped heart located in the center of the phantom. The spine is represented by a cylinder located posterior-medially, and the tumor is in the shape of rounded cylinder. The external dimensions of phantom (including edges) are 39 cm in length, 41 cm in width, and 27 cm / 32 cm in height (front/back). The target (tumor), located in the center of the left lung, is divided into two equal superior and inferior parts with the overall dimensions 3 cm in diameter and 5 cm in length.

Table 2.1 RPC Phantom Material Densities and CT Numbers

Phantom Structure	Substitute Material	Density [g / cm ³]	Material CT Number [HU]
Phantom Shell	PVC	1.37	630
Tumor	HIPS	1.04	-50
Lung Insert	Compressed Cork	0.33	-640
Lungs	CIRS Lung (Inhale)	0.21	-660
Heart	Nylon	1.08	97
Spine	Acrylic	1.17	230

Four TLDs and three orthogonal radiochromic films are used to verify the accuracy of the dose delivered during each phantom irradiation. Two TLDs, labeled HEART_TLD and CORD_TLD, one for heart and one for spine, respectively, are placed inside two acrylic rods and inserted in their respective anatomical location holes in the phantom to position the heart TLD superior to the target and the spine TLD inferior to tumor.

The target, made of high impact polystyrene, is embedded inside of a separate insert made of compressed cork that is enclosed in the plastic cylindrical housing. The housing has a hole at the bottom that serves as a key when it is fully inserted into the phantom and prevents it from moving. The housing can be disassembled by unscrewing two top plastic screws and removing handle and lid. This insert represents the posterior part of the left lung and consists of two parts. The tumor inside of this imaging/dosimetry insert is also divided into superior and inferior parts. Each part of the target has an opening ~3mm off of the center of the target for its own TLD, labeled PTV_TLD_sup and PTV_TLD_inf. TLDs were used for absolute dose measurement and are described further in chapter 2.6.3. Two-dimensional dose distributions were measured using radiochromic films (chapter 2.5.1). Three orthogonal slots for radiochromic films are made in the axial, coronal, and sagittal directions inside of the imaging/dosimetry insert and tumor. The coronal and sagittal films have ~ 2 cm long central cuts that allow them to be inserted perpendicular to each other inside the target. Both films

are also cut in half into superior and inferior pieces. This allows the axial film to be placed between the superior and inferior films and target TLDs and in the middle of the two halves of the insert (Figure 2.1).

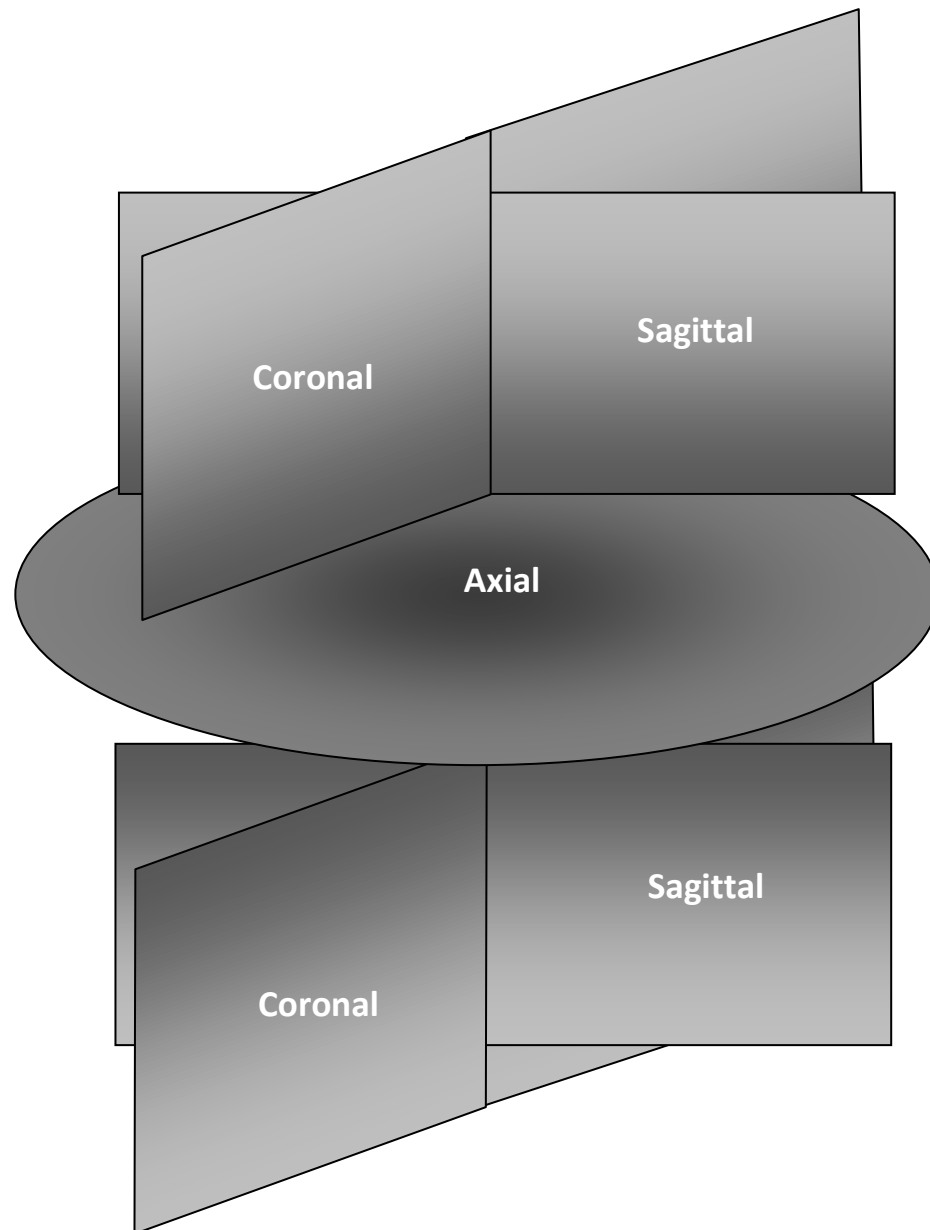


Figure 2.1 Orthogonal Film Arrangement Inside The Phantom Insert

After all TLDs and films were placed in their proper positions the two parts of the imaging/dosimetry insert are put into the plastic housing, the lid is closed, and the handle is screwed back in. The plastic housing has eight side holes and three holes on top of the lid that are used for film registration. In order to know the exact position of the films a sharp metal pin was used to make a four registration pricks in each coronal and sagittal film through the housing side holes and three pricks through the lid in the axial film before the superior part of the insert was lowered in the plastic housing. After the imaging/dosimetry insert was assembled it was placed inside the phantom and keyed into place to prevent any movement. Figure 2.2 shows two heart and spine TLD inserts, as well as the open target insert removed from the housing. Figure 2.3 shows a fully assembled phantom.



Figure 2.2 Heart And Spine TLD Inserts With The Open Target Insert



Figure 2.3 A Fully Assembled RPC Lung Phantom

2.1.2 CT Simulation of the RPC Phantom

CT simulation is a process of imaging the patient or phantom with the goal of using the obtained series of axial images in the treatment planning process. For the purpose of this study, the RPC phantom was scanned on an *AcQSim 2 CT* scanner (Philips Medical System, Bothell, WA). Simulation localization is the process of aligning the center of the phantom with the two lateral and sagittal CT localization lasers. In order to remain consistent, the location of the lasers on the phantom (LAP of America LC, Boynton Beach, FL) employed during CT simulation were the same as those used during the dose delivery in the linear accelerator vault. During the localization step the phantom was marked at the cross-section of the three pairs of lasers with small fiducial markers (metal spheres ~3mm in diameter). These markers are routinely employed in most clinical cases to

help establish the center of coordinate in the patient or phantom during the planning process (chapter 2.3). After the phantom was set up and aligned on the table, it was scanned using a typical clinical protocol for thoracic cancer patients: 120 kVp, 383 mAs, pitch of 1, 1.5 mm slice thickness, and 500 mm Field of View (FoV). A total of 410 axial CT images were acquired and transferred to Eclipse TPS for planning (Figure 2.4).

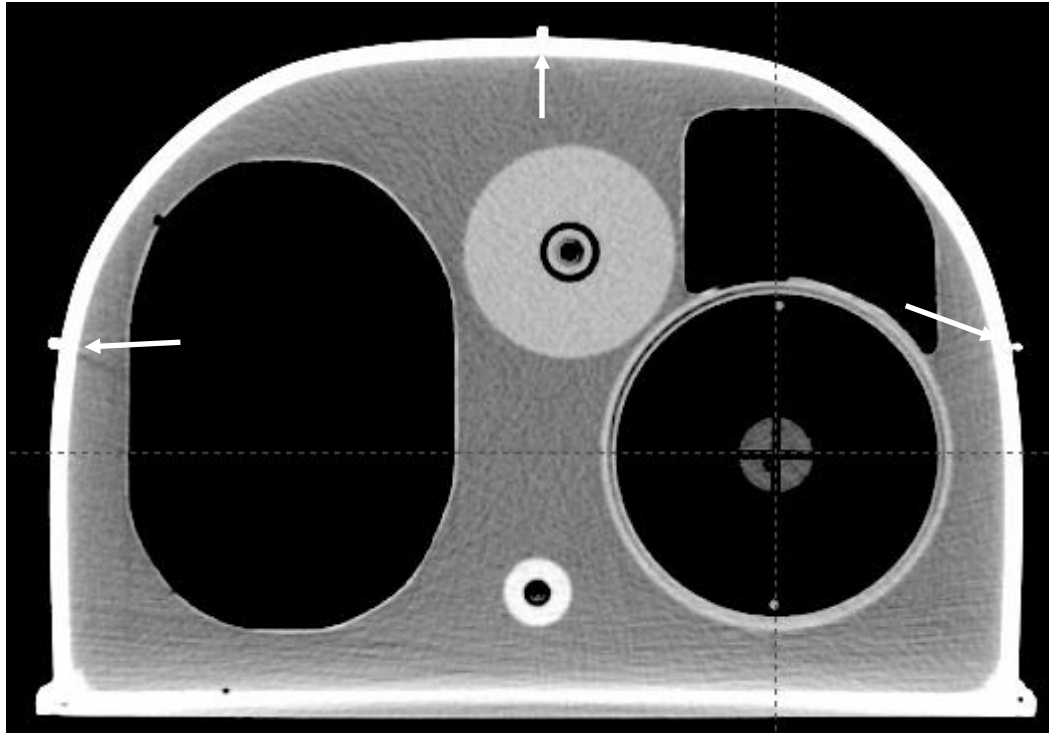


Figure 2.4 An Axial CT Slice Of The Phantom That Contains The Target. Fiducials, Marked With Arrows, Can Be Seen On The Phantom Surface

2.2 Treatment Planning

2.2.1 SBRT Plans: Dose Prescription and Limits

The SBRT plans were designed according to the “Guidelines for Planning and Irradiating the RPC Lung Phantom” (March 2010 Revision) [14]. Three critical organs at risk were contoured in the Eclipse TPS – lung (left and right), heart, and spine. The spine was contoured 10 cm above and below the PTV and the body contour was expanded by 0.5 cm according to various RTOG protocols (Table 2.2). Per the RPC instructions [14] and RTOG protocols [15, 16, 17, 18] the Clinical Target

Volume (CTV) was equal to Gross Tumor Volume (GTV). The Planning Target Volume (PTV) was created by expanding the GTV by 0.5 cm axially and by 1 cm in superior-inferior direction.

Table 2.2 RPC/RTOG List Of SBRT Lung Treatment Protocols

	RPC – 03/10	RTOG 1021 – 05/11	RTOG 0915 – 08/10	RTOG 0813 – 02/10	RTOG 0618 – 02/09
Dose (Gy) x frac	6 x 1	18 x 3	34 x 1, 12 x 4	10 x 5	20 x 3
CT Scan Slice, mm	Lung ≤3mm	Lung ≤3mm	Lung ≤3mm	Lung ≤3mm	Lung ≤3mm
Static beams (min. recom'd)	7 ≥10	7 ≥10	7 ≥10	7 ≥10	7 ≥10
Arc, angle	>340°	>340°	>340°	>340°	>340°
Energy, MV	4-10	4-10, 10-15 <50% beams	4-10, 10-15 ≤2 beams	4-10, 10-15 ≤2 beams	4-10, 10-15 ≤2 beams
PTV V _{95% Dx}	100%	100%	100%	100%	100%
PTV V _{90% Dx}	>99%	>99%	>99%	>99%	>99%
Spillage (NT)		>105% Dx <15% PTV	>105% Dx <15% PTV	>105% Dx <15% PTV	>105% Dx <15% PTV
Conformality Index		<1.2 Protocol spec.	<1.2 Protocol spec.	<1.2 Protocol spec.	<1.2 Protocol spec.
Field size/shape	PTV	PTV	PTV	PTV	PTV
Spinal cord	Any point ≤5Gy	Protocol spec.	Protocol spec.	Protocol spec.	Protocol spec.
Heart (% volume receiving X Gy)	<33% - ≤6 Gy <66% - ≤4.5 Gy <100% - ≤4 Gy	Protocol spec.	Protocol spec.	Protocol spec.	Protocol spec.
Lungs (% volume receiving X Gy)	<37% - ≤2 Gy	Protocol spec.	Protocol spec.	Protocol spec.	Protocol spec.
Contouring					
CTV	GTV	GTV	GTV	GTV	GTV
PTV _{axial}	GTV+0.5 cm	GTV+0.5 cm	GTV+0.5 cm	GTV+0.5 cm	GTV+0.5 cm
PTV _{long}	GTV+1 cm	GTV+1 cm	GTV+1 cm	GTV+1 cm	GTV+1 cm
D _{2cm}		PTV + 2 cm	PTV + 2 cm	PTV + 2 cm	PTV + 2 cm
Spinal cord		10 cm above and below PTV	10 cm above and below PTV	10 cm above and below PTV	10 cm above and below PTV
Skin		Body + 0.5 cm	Body + 0.5 cm	Body + 0.5 cm	Body + 0.5 cm

For the phantom irradiation, a single fraction of 6 Gy was prescribed and normalized to be delivered to at least 95% of the PTV. The secondary dosimetric objective of 90% of the prescribed dose to at least 99% of the PTV was also met. Plans were verified to make sure that conformity indices (CI) were <1.2 according to the RTOG recommendation. A Dose Volume Histogram (DVH) was used to verify that the calculated doses to critical structures (spinal cord, heart, and lung) were below their corresponding limits specified for the RPC Lung phantom Table 2.3.

Table 2.3 Normal Tissues Constraints (RPC Protocol)

Normal structure	Volume	Dose
Spinal Cord	Any point	≤5.0 Gy
Heart	<33% total vol	≤6.0 Gy
	<66% total vol	≤4.5 Gy
	<100% total vol	≤4.0 Gy
Whole Lung (Right & Left)	<37% total vol	<2.0 Gy

The four TLDs were contoured: CORD_TLD (spine), HEART_TLD (heart), PTV_TLD_sup (superior half of the target), and PTV_TLD_inf (inferior half of the target). These volumes were used to calculate the measured-to-predicted dose ratio and for dose correction in 2D film dose analysis (chapter2.6.3).

A total of six phantom irradiation plans were developed. Two SBRT plans - 6 MV and 18 MV - were designed to be delivered on the MD Anderson Varian Clinac 2100CD and 21EX linear accelerators (Varian Associates, Palo Alto, CA). The other four plans - 6 MV FFF, 6 MV, 10 MV FFF, and 15 MV – were created to be delivered on a Varian TrueBeam STx linear accelerator at The University of Alabama (UAB) at Birmingham Medical Center.

2.2.2 SBRT Plans: 6 MV and 18 MV MDACC

RPC instructions called for a minimum of 7 non-opposing static beams [14]. A total of nine beams were utilized in each of the six treatment plans at 25°, 60°, 115°, 150°, 180°, 220°, 260°, 285°, and 300°.

and 345° (Figure 2.5). To minimize the setup uncertainty, beams angles, couch, and gantry orientations were kept identical for all plans (Figure 2.6).

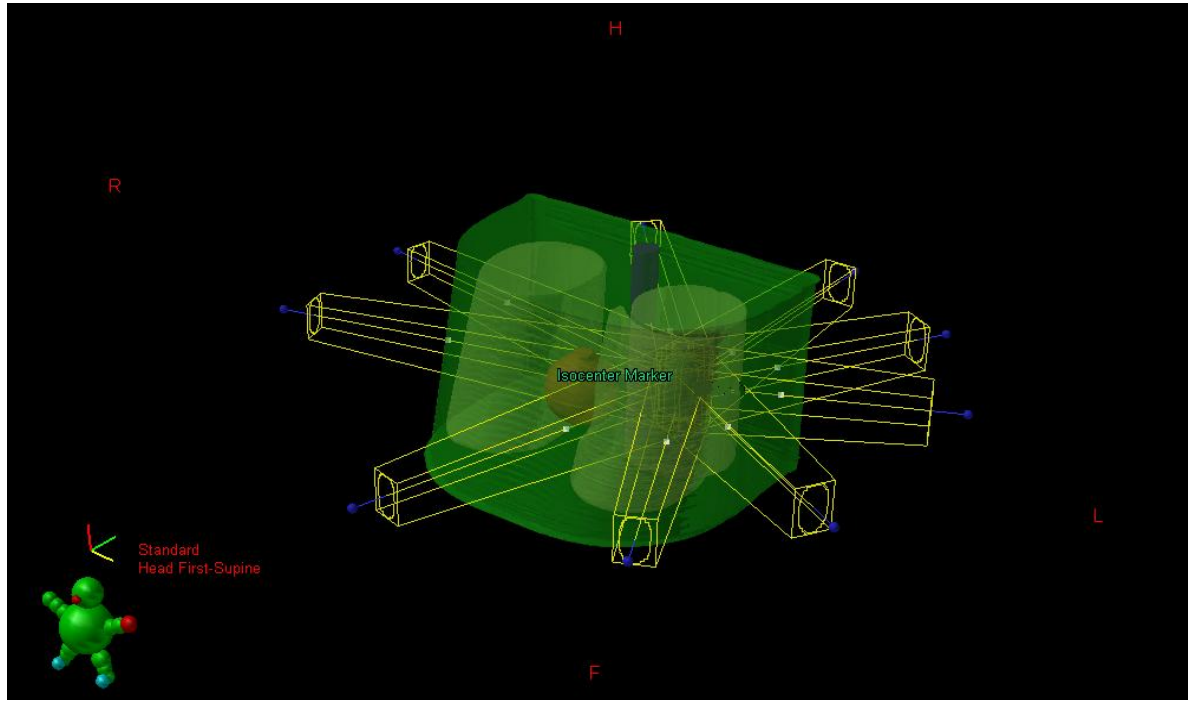


Figure 2.5 3D View Of The Beam Arrangement Used In All Plans

a)

Fields		Dose Prescription		<input type="checkbox"/> Field Alignments	<input type="checkbox"/> Plan Objectives	<input type="checkbox"/> Optimization Objectives	Dose Statistics		Calculation Models		Plan Sum											
Group	Field ID	Technique	Machine/Energy	MLC	Field Weight	Scale	Gantry Rtn [deg]	Coll Rtn [deg]	Couch Rtn [deg]	Wedge	Field X [cm]	X1 [cm]	X2 [cm]	Field Y [cm]	Y1 [cm]	Y2 [cm]	X [cm]	Y [cm]	Z [cm]	SSD [cm]	MU	Ref. D [cGy]
<input checked="" type="checkbox"/>	Field 1	STATIC-I	Research_2300IX - 6X	Static	1.000	Varian IEC	345.0	0.0	0.0	None	6.0	+3.0	+3.0	7.9	+4.2	+3.7	8.8	4.2	-0.5	83.9	112	152.9
<input checked="" type="checkbox"/>	Field 2	STATIC-I	Research_2300IX - 6X	Static	1.000	Varian IEC	25.0	0.0	0.0	None	6.0	+3.0	+3.0	7.9	+4.2	+3.7	8.8	4.2	-0.5	87.4	99	121.3
<input checked="" type="checkbox"/>	Field 3	STATIC-I	Research_2300IX - 6X	Static	1.000	Varian IEC	60.0	0.0	0.0	None	6.0	+3.0	+3.0	7.9	+4.2	+3.7	8.8	4.2	-0.5	89.9	100	119.0
<input checked="" type="checkbox"/>	Field 4	STATIC-I	Research_2300IX - 6X	Static	1.000	Varian IEC	115.0	0.0	0.0	None	6.0	+3.0	+3.0	7.9	+4.2	+3.7	8.8	4.2	-0.5	89.7	102	121.6
<input checked="" type="checkbox"/>	Field 5	STATIC-I	Research_2300IX - 6X	Static	1.000	Varian IEC	150.0	0.0	0.0	None	6.0	+3.0	+3.0	7.9	+4.2	+3.7	8.8	4.2	-0.5	88.7	107	131.0
<input checked="" type="checkbox"/>	Field 6	STATIC-I	Research_2300IX - 6X	Static	1.000	Varian IEC	180.0	0.0	0.0	None	6.0	+3.0	+3.0	7.9	+4.2	+3.7	8.8	4.2	-0.5	90.2	100	118.7
<input checked="" type="checkbox"/>	Field 7	STATIC-I	Research_2300IX - 6X	Static	1.000	Varian IEC	220.0	0.0	0.0	None	6.0	+3.0	+3.0	7.9	+4.2	+3.7	8.8	4.2	-0.5	86.9	117	147.3
<input checked="" type="checkbox"/>	Field 8	STATIC-I	Research_2300IX - 6X	Static	1.000	Varian IEC	260.0	0.0	0.0	None	6.0	+3.0	+3.0	7.9	+4.2	+3.7	8.8	4.2	-0.5	72.2	165	302.5
<input checked="" type="checkbox"/>	Field 9	STATIC-I	Research_2300IX - 6X	Static	1.000	Varian IEC	285.0	0.0	0.0	None	6.0	+3.0	+3.0	7.9	+4.2	+3.7	8.8	4.2	-0.5	72.7	154	278.6

b)

Fields	Dose Prescription		<input type="checkbox"/> Field Alignments	<input type="checkbox"/> Plan Objectives	<input type="checkbox"/> Optimization Objectives	Dose Statistics		Calculation Models		Plan Sum												
Group	Field ID	Technique	Machine/Energy	MLC	Field Weight	Scale	Gantry Rtn [deg]	Coll Rtn [deg]	Couch Rtn [deg]	Wedge	Field X [cm]	X1 [cm]	X2 [cm]	Field Y [cm]	Y1 [cm]	Y2 [cm]	X [cm]	Y [cm]	Z [cm]	SSD [cm]	MU	Ref. D [cGy]
<input checked="" type="checkbox"/>	Field 1	STATIC-I	Research_2300IX - 18X	Static	1.000	Varian IEC	345.0	0.0	0.0	None	6.0	+3.0	+3.0	7.9	+4.2	+3.7	8.8	4.2	-0.5	83.9	102	136.0
<input checked="" type="checkbox"/>	Field 2	STATIC-I	Research_2300IX - 18X	Static	1.000	Varian IEC	25.0	0.0	0.0	None	6.0	+3.0	+3.0	7.9	+4.2	+3.7	8.8	4.2	-0.5	87.4	94	102.8
<input checked="" type="checkbox"/>	Field 3	STATIC-I	Research_2300IX - 18X	Static	1.000	Varian IEC	60.0	0.0	0.0	None	6.0	+3.0	+3.0	7.9	+4.2	+3.7	8.8	4.2	-0.5	89.9	94	109.3
<input checked="" type="checkbox"/>	Field 4	STATIC-I	Research_2300IX - 18X	Static	1.000	Varian IEC	115.0	0.0	0.0	None	6.0	+3.0	+3.0	7.9	+4.2	+3.7	8.8	4.2	-0.5	89.7	95	111.7
<input checked="" type="checkbox"/>	Field 5	STATIC-I	Research_2300IX - 18X	Static	1.000	Varian IEC	150.0	0.0	0.0	None	6.0	+3.0	+3.0	7.9	+4.2	+3.7	8.8	4.2	-0.5	88.7	98	118.0
<input checked="" type="checkbox"/>	Field 6	STATIC-I	Research_2300IX - 18X	Static	1.000	Varian IEC	180.0	0.0	0.0	None	6.0	+3.0	+3.0	7.9	+4.2	+3.7	8.8	4.2	-0.5	90.2	94	110.1
<input checked="" type="checkbox"/>	Field 7	STATIC-I	Research_2300IX - 18X	Static	1.000	Varian IEC	220.0	0.0	0.0	None	6.0	+3.0	+3.0	7.9	+4.2	+3.7	8.8	4.2	-0.5	86.9	104	128.1
<input checked="" type="checkbox"/>	Field 8	STATIC-I	Research_2300IX - 18X	Static	1.000	Varian IEC	260.0	0.0	0.0	None	6.0	+3.0	+3.0	7.9	+4.2	+3.7	8.8	4.2	-0.5	72.2	129	231.1
<input checked="" type="checkbox"/>	Field 9	STATIC-I	Research_2300IX - 18X	Static	1.000	Varian IEC	285.0	0.0	0.0	None	6.0	+3.0	+3.0	7.9	+4.2	+3.7	8.8	4.2	-0.5	72.7	123	215.2

Figure 2.6 Beams Configuration Used In a) 6 MV Plan (MDA) and b) 18 MV Plan (MDA)

X and Y collimator jaws were fixed at 6.0 cm and 7.9 cm, respectively, and the multi-leaf collimator was aligned with the PTV borders.

Heterogeneity corrected dose calculations for the six treatment plans were performed using the AAA version **8.9.08** with a dose calculation grid size of $2.5 \times 2.5 \text{ mm}^2$.

2.2.3 SBRT Plans: 6 MV FFF, 6 MV, 10 MV FFF, and 15 MV UAB MC

After the 6 MV treatment plan was completed and verified it was exported from the research Eclipse TPS at MD Anderson Cancer Center to the clinical Eclipse TPS at the UAB Medical Center and recalculated using UAB MC TrueBeam 6 MV beam model. A 15 MV plan was created and recalculated using the same 6 MV primary and secondary dose objectives. The flattening filter (Figure 2.7) was in place for the 6 MV and 15 MV beams plans, but it was removed for the 6 MV FFF and 10 MV FFF configurations. The UAB plans were recalculated with a small isocenter shift, as compared to the MD Anderson plans, to simplify the setup in new geometry of the TrueBeam STx linear accelerator.

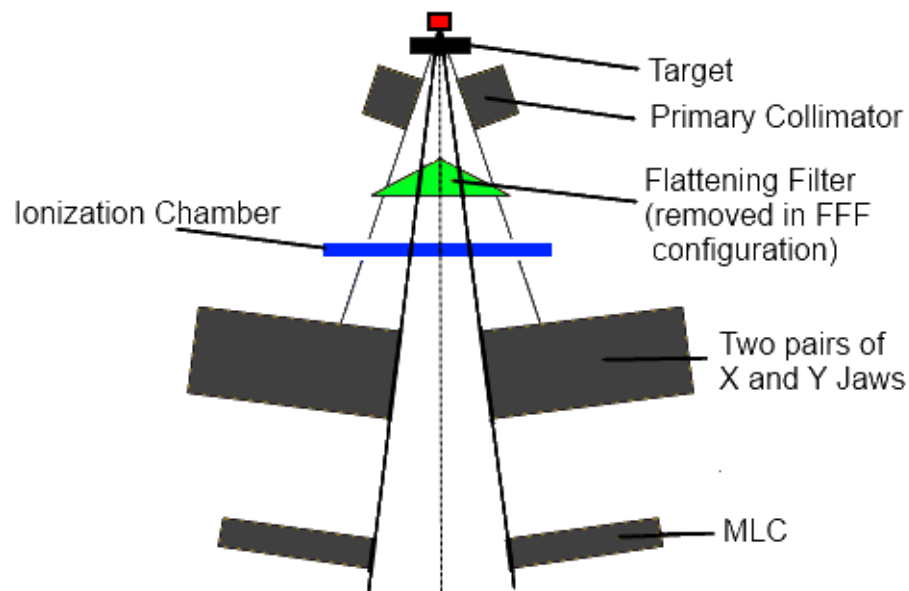


Figure 2.7 Varian Linear Accelerator Head Components

Flattening-filter-free beams have a lower effective energy as well as a beam profile that, unlike a flattened beam, peaks in the middle. This profile shape along with the increased beam output (by 2-4 times) makes FFF very efficient in treatment of small targets using stereotactic radiosurgery (SRS) and SBRT [19]. Additionally, removal of the flattening filter leads to a reduction in linear accelerator head radiation leakage by more than half and results in overall lower peripheral doses to the patient, which is even more substantial for higher energies [20].

2.3 Treatment Plan Delivery

2.3.1 MD Anderson Cancer Center

As was mentioned in chapter 2.2.1, 6 MV and 18 MV plans were delivered to the phantom at the MD Anderson Cancer Center using Clinac 2100CD (Rm 2104) and Clinac 21EX (Rm ACB3). These dosimetrically matched linear accelerators used Millennium 120 multi-leaf collimators (MLC). MLC files for both plans (6 and 18 MV) were loaded on the accelerator treatment computer. The alignment of the phantom was performed using the installed treatment room laser system identical to the one installed in the CT simulation room. After the alignment was complete the couch was shifted 8.8 cm to the right, 4.2 cm in anterior, and 0.5 cm in superior direction. This effectively moved the center of the target to the machine isocenter according to Eclipse calculated distances. Every beam was delivered in service mode using beam parameters calculated in Eclipse for a total of nine beams per plan. Each phantom plan irradiation was repeated three times. Films and TLDs were replaced with new ones after each irradiation for a total of 6 irradiation sets. The beam data for 6 MV and 18 MV are shown in chapter 2.2.2 (Figure 2.6).

2.3.2 University of Alabama at Birmingham Medical Center

A total of four plans, 6 MV FFF, 6 MV, 10 MV FFF, and 15 MV, were each delivered three times at UAB MC. The TrueBeam STx (S/N #1005) linear accelerator was capable of performing clinical flattening-filter-free irradiations and was commissioned for use with 6 and 10 MV FFF beam

energies. The TrueBeam STx linear accelerator also uses a new collimator system - high definition 120 multi-leaf collimator (HDMLC). As was mentioned in chapter 2.2.3, the plans were recalculated using UAB commissioned beam models for each respective energy. The plans were delivered in DICOM filemode. To ensure proper alignment of the phantom on the treatment table, an on-board imaging (OBI) system was employed in addition to using the lasers. During this imaging the unloaded phantom was used, so no extra dose from the OBI had to be accounted for. Once the phantom position had been confirmed, the insert was loaded with films, TLDs were inserted, and each plan was delivered. After each plan irradiation, a visual inspection of the films to confirm the correct phantom positioning was performed prior to another set of four plans being delivered, followed by the final, third set of irradiations of all four plans. Films and TLDs were replaced with the new ones after each irradiation for a total of 12 irradiation sets.

2.4 Dosimetry

2.4.1 Gafchromic® EBT2 Film

Radiochromic films are two-dimensional dosimeters with high spatial resolution and low spectral sensitivity variation. Their daylight sensitivity is minimal which allows them to be handled in well-lit rooms. These films change color directly in response to radiation and do not require any chemical processing. Image forms during a polymerization process, in which energy is transferred from the high energy photons or particles to the photomonomer molecule resulting in a chemical reaction that leads to color change [21]. Because of their excellent dosimetric characteristics and ease of use radiochromic films have been widely adopted and, along with TLDs, have been used by RPC for many years as an important remote audit tool in multiple generations of RPC phantoms and research.

Radiochromic film used in this study was Gafchromic® EBT2 (Lot # A06271103, Exp. date: June, 2013) manufactured by Ashland (Covington, KY). EBT2 film is well suited for use in

dosimetry of radiotherapy beams because of its low energy dependence, high spatial resolution, negligible sensitivity to light, and no need for wet chemical processing. This film has a spatial resolution <0.1 mm and near-tissue equivalent density ($Z_{\text{eff}}^{\text{EBT2}}=6.84$). [22].

EBT2 film is a newer version of EBT film that has been improved in a couple of key areas. Yellow dye was added to minimize differences resulted from nonuniform film coating. It is less sensitive to day light and more resistant to damage when cut into pieces. It has very little energy dependence and can be used in an energy range from 50 keV to 20 MeV. EBT2 is made by combining clear layers of polyester with the active film coating that contains a chemical polymer [23]. A 175 micron-thick clear layer of polyester substrate is covered by a 30 micron-thick film of active layer and a 5 micron-thick topcoat. Finally, a 50 micron-thick protective layer of over-laminate is glued to the layer of topcoat by a 25 micron thick adhesive layer (Figure 2.8).

After exposure to radiation the active monomers in EBT2 film form a polymer that is visible to the naked eye with two absorption peaks at 585 and 636 nm. Due to film self-development the increase in optical density (OD) reaches 99% of its maximum after 2-3 days for films exposed to 1-15 Gy [22]. Therefore all films were scanned 3 days post-irradiation to reduce the self-development effect.

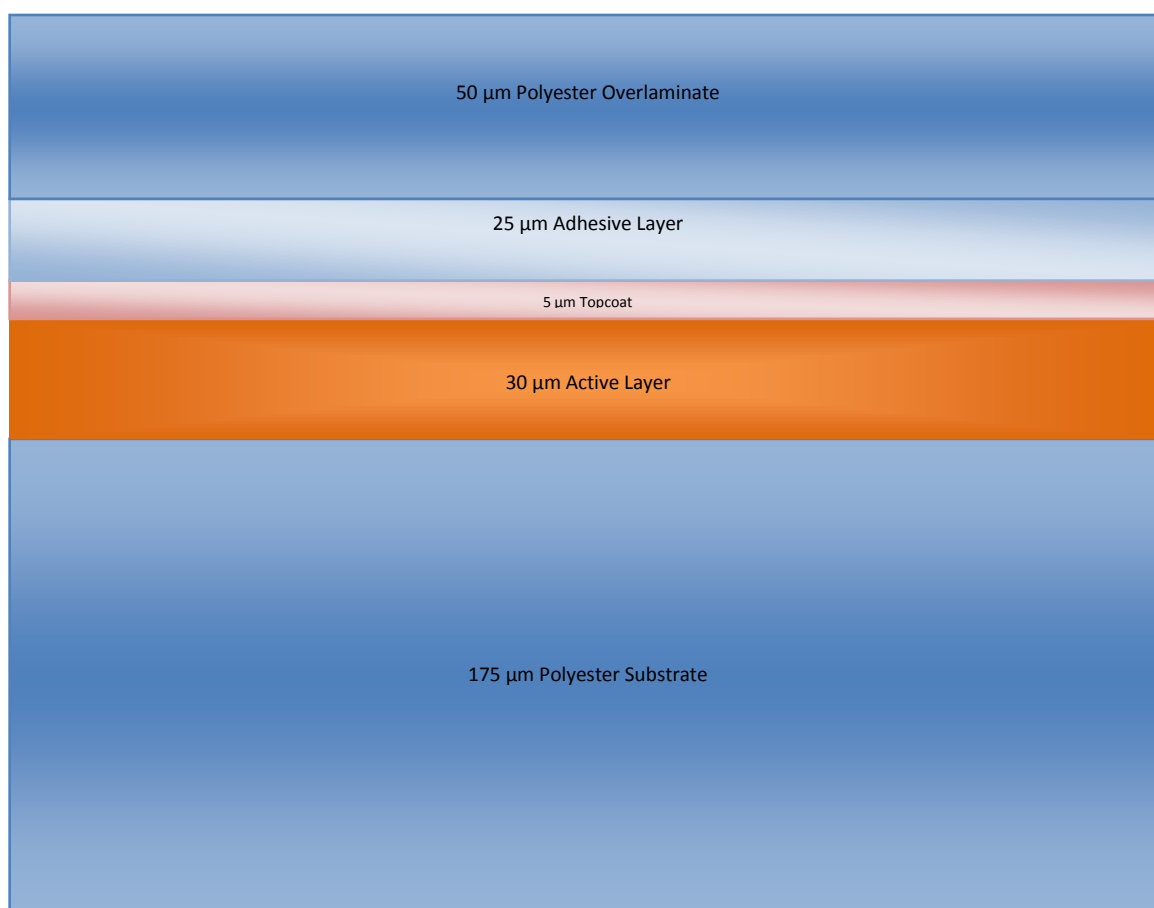


Figure 2.8 Structure Of Gafchromic ® EBT2 Film (Not To Scale) [23]

2.4.1.1 Film Preparation

EBT2 film used in this study came in an 8”x10” format with 25 sheets per box. Film was cut into multiple pieces according to the RPC templates. The axial film was cut to fit in the middle of the two halves of the target insert and marked with permanent marker at the opposite edges to indicate film orientation (Figure 2.9). Coronal and sagittal films were cut in half as was described in chapter 2.2.1 (Figures 2.10 and 2.11)

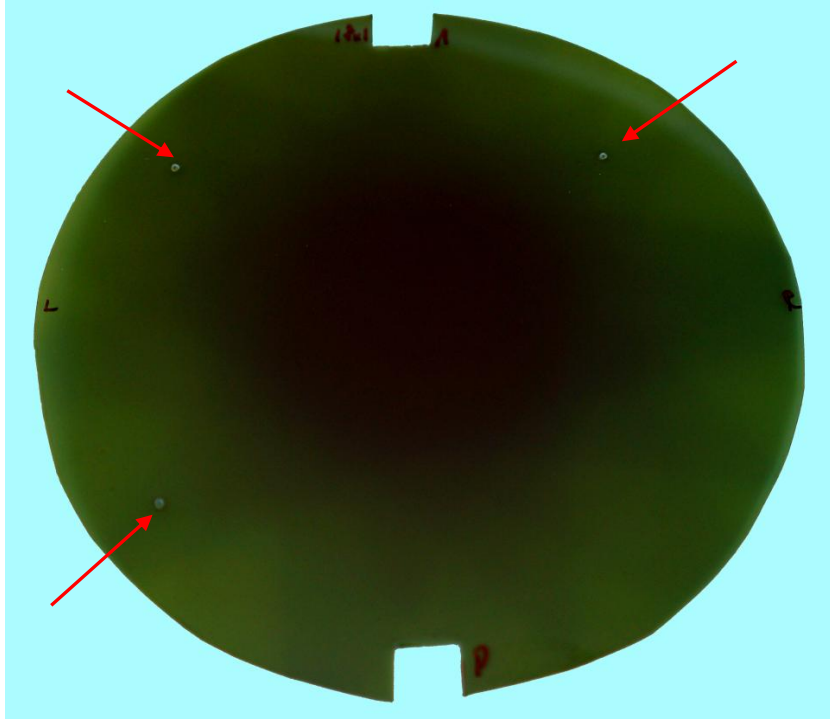


Figure 2.9 Irradiated Axial Film With Registration Pricks

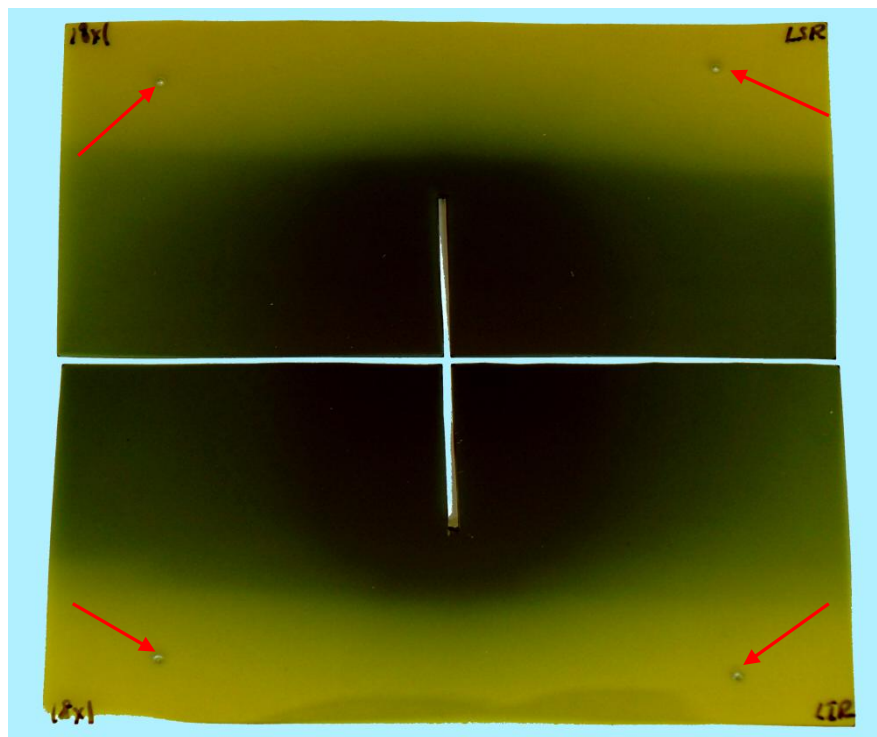


Figure 2.10 Irradiated Coronal Film With Registration Pricks

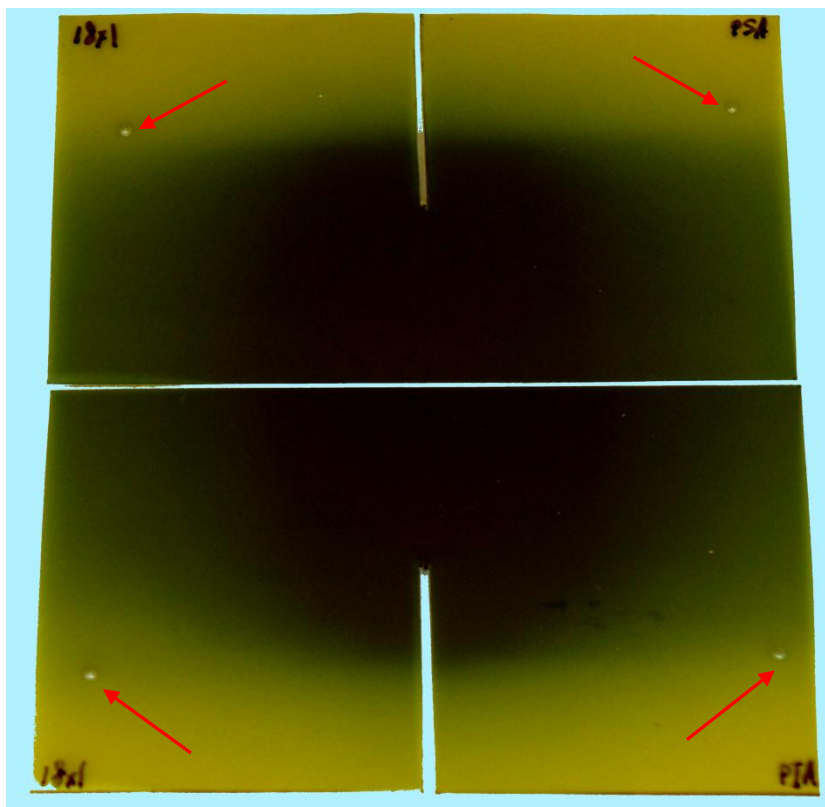


Figure 2.11 Irradiated Sagittal Film With Registration Pricks

In order to reliably relate ODs of the films to the dose, a dose response relationship between a known dose and fixed ODs was determined using the following method. A set of dose values were selected from the low and the high range of exposures. For this work a total of 8 dose values were selected to be delivered using 0.55, 1.64, 2.74, 3.83, 6.02, 8.21, 10.40, and 12.59 Gy. Two sheets of EBT2 film were cut into 8 equal (10 x 12.5 cm) pieces, each one marked with the corresponding dose it would receive. Figure 2.12 shows a standard setup for obtaining the dose response curve. Each piece of film was placed on top of 9 cm thick solid water phantom and covered with another 1.5 cm thick block of solid water. The source-to-surface distance (SSD) was set at 100 cm and the field size was 35 x 35cm². Placement and orientation of every film piece was consistent to avoid any directional uncertainties. A field size dependent output factor correction was applied to convert the

MU into dose. The dose response film irradiation and scanning were performed at the same time along with the RPC Lung phantom films (chapter 2.5.1.2).

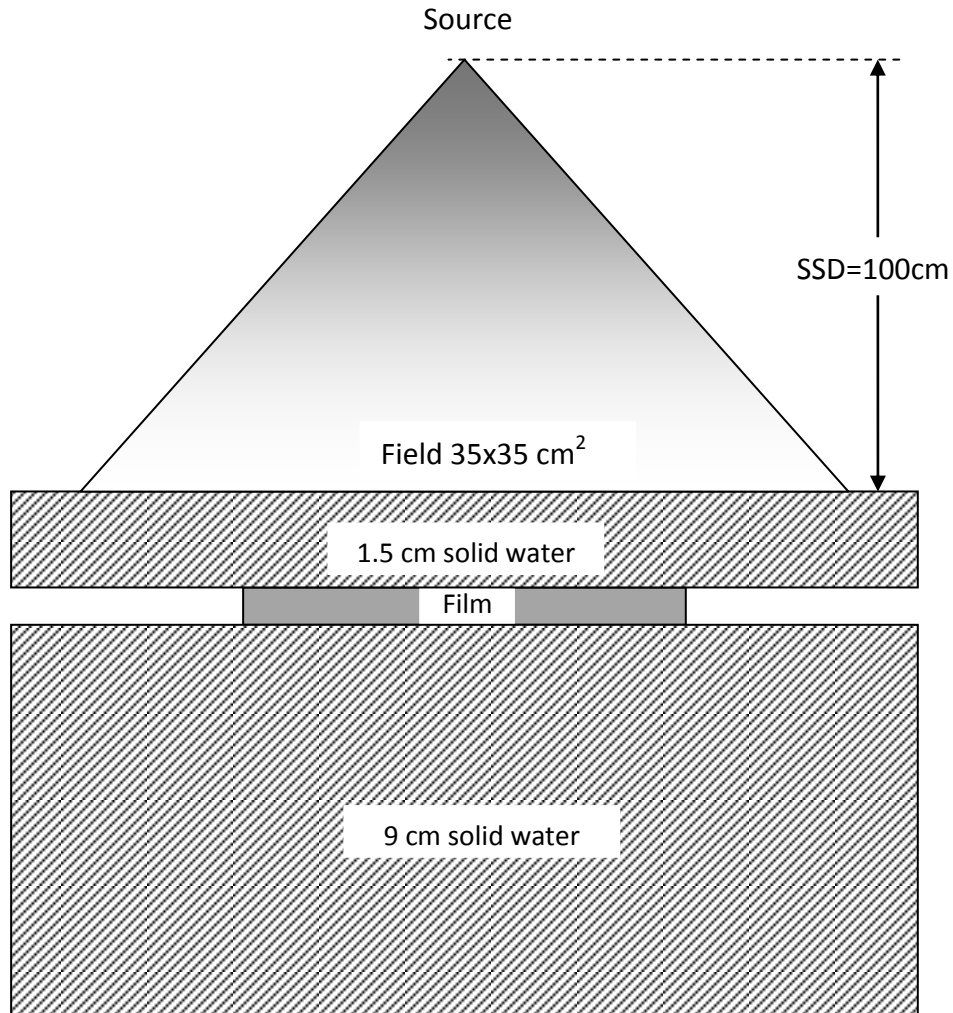


Figure 2.12 Phantom Used In Dose Response Film Irradiation

2.4.1.2 Film Scanning

Three days after irradiating the films, they were scanned on a transmission type microdensitometer PeC CCD100, S/N: 9101077328E (Photoelectron Corporation, North Billerica, MA). The scanner was located inside of a dark cabinet and consisted of 16 bit 512 x 512 pixel charged-coupled device (CCD) camera that could be moved vertically to accommodate different fields of view and a flatbed light source with compression transparent lid on which films were placed. According to the manufacturer, the light-emitting device inside of the scanner bed was

specified at 665 nm which was a close match to one of the absorption peaks of the EBT2 film. This matching is important in order to maximize the signal-to-noise ratio due to CCD camera sensitivity to noise.

After the CCD camera was set to the properly set, a focus scan was performed to verify the resolution of the camera. A black paper mask was used for the rest of the scans to limit the backlit area of the scanner bed to the effective area of films. Before films could be scanned a flatfield file was created using a blank sheet of non-irradiated film. This flatfield was used as a background and was subsequently subtracted from each film scan. A spatial calibration was performed using transparent sheet with a grid of known dimensions and a field of view of 200 x 200mm which resulted in 0.4 mm pixel size. Every film was read in the same orientation to avoid any possible inconsistency within the batch.

During the scan the optical density (OD) of the film was converted into an electrical signal in the CCD camera. This signal was further digitized and digitally processed (including flatfield digital subtraction) and the final image was written into Flexible Image Transport System (FITS) file. This format was specifically designed for storage and transmission of scientific data and includes information about spatial calibration as well as other metadata that were used in the image analysis.

An additional scanning of the dose response films was performed before the phantom films were scanned and average values for the large region of interest (ROI) for each piece of dose response film was recorded and verified. Obtained values were used to correlate the dose to OD (chapter 2.5.1.1). This was done by plotting Dose vs. OD and fitting third order polynomial dose response curve intersecting 0 on the Y axis. The fit coefficients of the dose response equation were imported into a configuration file of the MATLAB package used for the film analysis (chapter 2.6.3).

2.4.2 Thermoluminescence Dosimeters

Thermoluminescence dosimeters (TLD) are a vital tool for measuring the absolute absorbed dose in radiation therapy. As was mentioned in chapter 2.1.1, both films and TLDs have been extensively used in the RPC remote audits. Their cost, flexibility and ease of use have made them ideal dosimeters to be used. The total uncertainty due to random fluctuations was calculated to be $\pm 2.3\%$ dose uncertainty with a 93% confidence interval equal to $\pm 5\%$ [24].

2.4.2.1 TLD Design and Placement

To measure point doses inside the phantom a TLD-100 powder (batch B11) was used. The active component of TLD-100 is LiF powder doped with Mg and Ti that emits light while being heated in a TLD reader. Each “Double-load” TLD plastic capsule was 15mm in length and 4mm in diameter with 1mm thick walls. Each capsule was a two-compartment container with each compartment having about 15 mm^3 of active volume that was filled with 20-22mg of TLD powder. TLD powder in each compartment was weighed and read individually and the final dose was calculated taking the average of the two readings. A total of 4 capsules were used in each irradiation (chapter 2.2.1) – two in superior and inferior tumor inserts and one in each heart and spine inserts. Since the TLD capsules were asymmetric due to one end being sealed, the placement of the TLDs was such that the plugged end of the capsule was facing away from the axial film in the tumor. For axial film TLD correction the calculated doses from both superior and inferior capsules were averaged. For coronal and sagittal films, only doses from their corresponding capsules were used such that superior capsule was used only for superior coronal and superior sagittal films and the inferior capsule – for inferior films only.

2.4.2.2 TLD Dose Calculation

TLD readout and dose calculation was performed according to the RPC “Procedure for Calculating TLD Doses” for batch B11 [25].

In TLD dose calculations it is important to know the dose-to-reading relationship. This was accomplished by using two sets of Standard TLDs irradiated to known doses. Each Standard TLD set consisted of 3 high (8 Gy) and 3 low dose (2 Gy) TLDs. The Standards were put inside a small Lucite phantom and placed in the center of a 10 x 10 cm² irradiation field from a Theratron 780C Co⁶⁰ machine. These Standards were read before the start of each session as well as at the end.

In order to minimize random and systematic uncertainties during the readout process a total of four Control TLDs were read during each TLD reading session. Two Controls were read at the beginning (after the first set of Standards) and at the end of the session (before the second set of Standards). After each set of 6 phantom TLDs were read another set of Controls followed. This was done to make sure that session was consistent from the start to the end and that there weren't any changes in the read sensitivity during the session.

Thermoluminescence is a process that directly depends on the amount of the material being read. Since the mass of the TLD powder is variable in every capsule it had to be accurately determined prior to readout process. The mass was measured using analytical balance AT261 DeltaRange (Mettler Toledo, LLC, Columbus, OH). Charge collected during the heating of the powder was recorded alongside with the powder mass from each capsule compartment to yield a normalized TLD reading in $\mu\text{C}/\text{mg}$ units. Standard deviation of these readings from both compartments of the TLD capsule served as an indicator of how reliable was each normalized TLD dose.

The dose calculated from the TLD readings is determined according to the following equation

$$D = M_{TLD} \times S \times K_F \times K_L \times K_E$$

Where

D – represents dose to a muscle;

M_{TLD} – An average TLD reading per unit mass (mg);

S – System sensitivity;

K_F – Fading correction factor

K_L – Linearity correction factor

K_E – Energy correction factor

The System Sensitivity was determined for each session by dividing the expected Standard dose by M_{TLD} , K_F and K_L . The energy correction for Co⁶⁰ beam is 1.

$$S = D_{expected} / (M_{TLD} \times K_F \times K_L)$$

Readout-to-dose response for TLD changes with time. To correct for differences in fading between phantom TLDs and Standards the following equation was used:

$$K_F = N / (a \cdot e^{-bt} + c \cdot e^{-dt})$$

Where

t – Number of days passed from irradiation date.

a, b, c, d, and N are empiric constants that depend on the TLD. For TLD batch B11 the RPC used the following values:

$$a = 1.2815$$

$$b = 0.00010885$$

$$c = 0.067810$$

$$d = 0.071908$$

$$N = 1.3493$$

Thermoluminescence dosimeters tend to overrespond at higher doses resulting in a supra-linear function. In order for the TLD readings to reliably represent the actual dose it has to be adjusted by a linearity correction factor K_L . K_L was calculated by irradiating multiple sets of three TLD capsules from 1 to 40 Gy using a ^{60}Co machine. Readings from each set were averaged and adjusted for system sensitivity and fading correction factor as was described previously. The linearity correction factor K_L was calculated as ratio of actual dose to the apparent dose and it was plotted against the apparent dose (Figure 2.13).

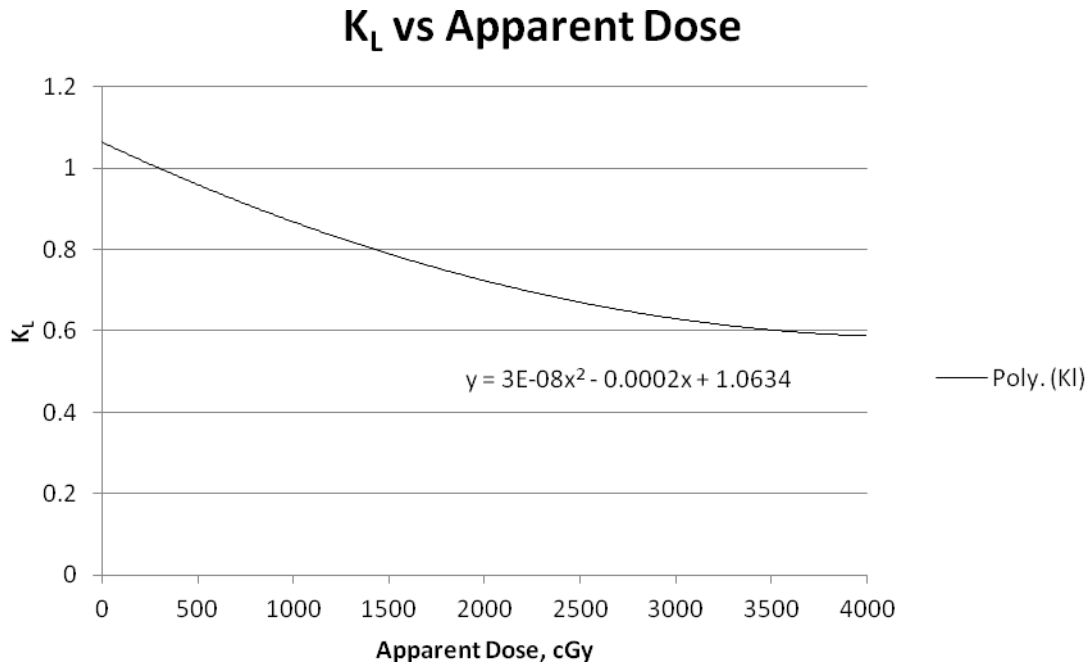


Figure 2.13 Polynomial Fit Of K_L Vs Apparent Dose Relationship For TLD Batch B11

A second order polynomial fit based on the RPC's batch B11 data resulted in the following fit coefficients:

$$K_L = a \times D_i^2 + b \times D_i + c,$$

Where

$$a = 2.552065 \times 10^{-8};$$

$$b = -2.221104 \times 10^{-4};$$

$$c = 1.064337$$

And

D_i – is estimated dose from the previous iteration, while D_0 – being first approximation dose without linearity correction

$$D_0 = (M_{TLD} \times S \times K_F \times K_E)$$

Linearity corrected dose was calculated for a total of six iterations multiplying D_0 by the current iteration linearity correction factor K_L .

The energy correction factor, K_E , is needed to correlate the Standard TLD response in Co^{60} beam to the energies used in this work. K_E takes into account specifics of the scatter medium of the phantom as well as spectral differences between Co^{60} beam and linear accelerator beams of different energies. The following values for energy correction were used for the RPC Lung phantom [26].

<u>Energy, MV</u>	<u>K_E</u>
6	1.011
10-12	1.023
15-20	1.036

2.5 Data Processing and Analysis

2.5.1 Plan Export

For data analysis to take place the plans designed in Eclipse TPS were exported using the Export Wizard (Figure 2.14) tool.

Every plan was exported using Digital Imaging and Communications in Medicine (DICOM) format and included a full set of CT images, defined structures, and total absolute doses. Having all these data allows extracting doses calculated by the Eclipse TPS at any point or in any plane in the phantom and comparison to the doses measured by radiochromic films and TLDs.

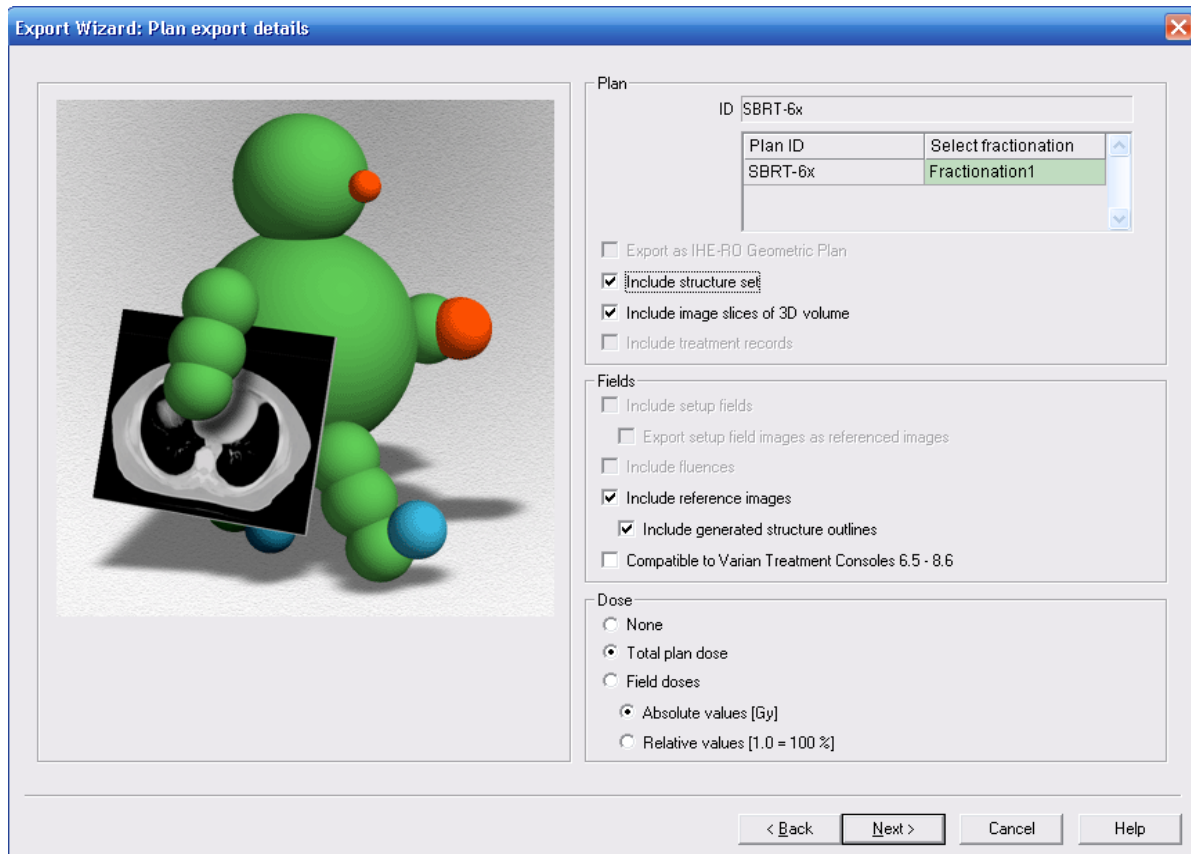


Figure 2.14 Eclipse Export Wizard Settings Window

The analysis of the data was performed in a Computational Environment for Radiotherapy Research (CERR) v.3.3 implemented within the numerical computing environment of MATLAB (R2008b) (MathWorks®, Natick, MA). CERR allows conversion of the information from different TPSs into a common file format and provides powerful tools for development and assessment of multiple treatment planning concepts [27].

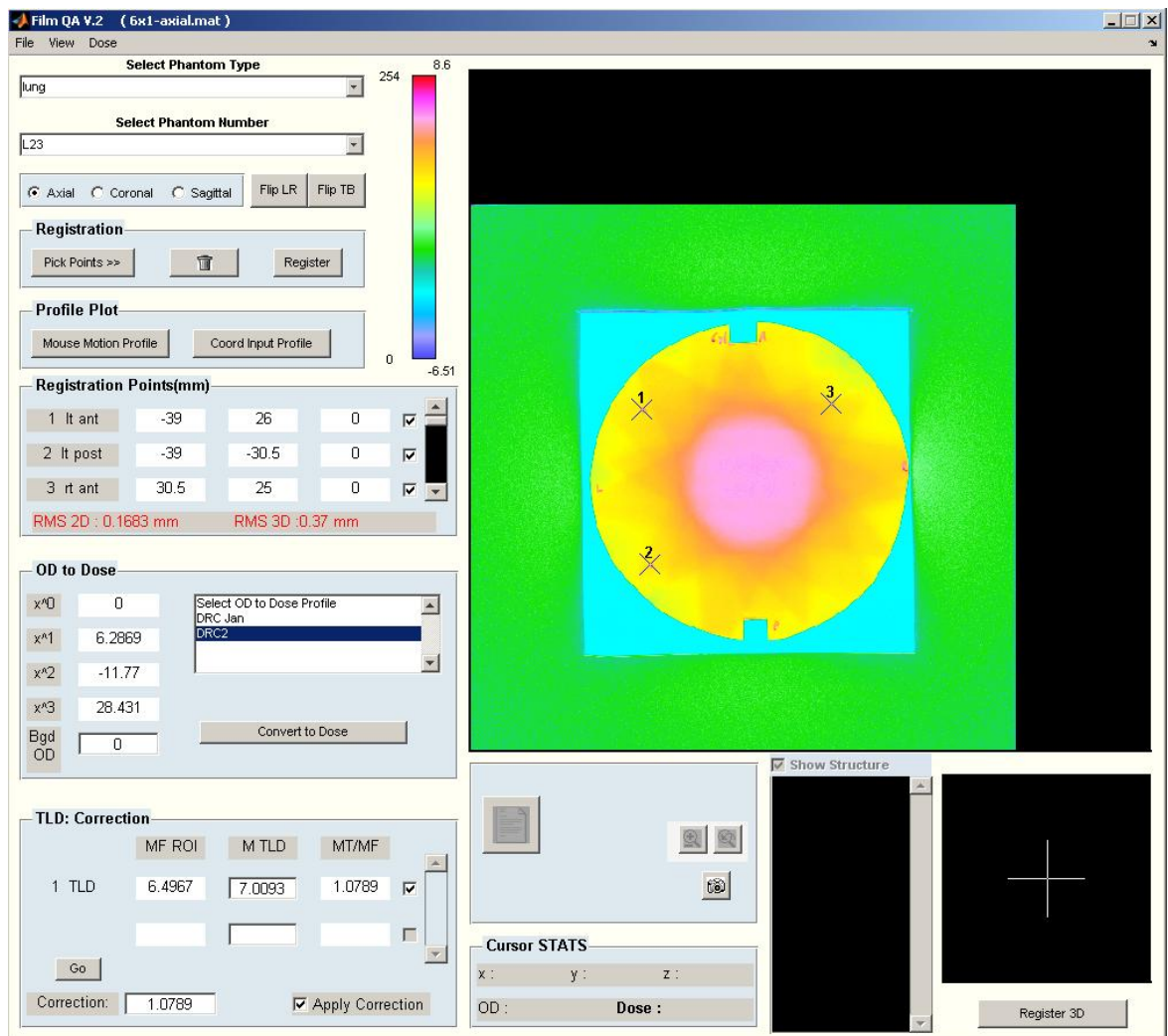
Every exported plan was converted and saved into a single MATLAB file format containing information about CT scans, outlined structures, and calculated 3D dose distributions. Single point, volume doses, as well as 2D doses distributions in any plane could be easily extracted from this file and analyzed.

2.5.2 *TLD Data*

As was mentioned in (chapter 2.3.1) four TLD regions of interest were created for every plan. The location of these ROIs was selected to be the same as geometrical locations of physical TLD capsules placed in heart, spine, and tumor inserts. The Eclipse TPS calculated the mean volume dose to each outlined ROI. These values were used to determine one of this work's objectives: measured-to-predicted TLD ratios.

2.5.3 *Film Data Processing*

The 2D film data analysis was performed using an in-house developed code RPCFILM (Figure 2.15). To streamline the workflow and to be able to access the treatment planning system data this code functioned within the same computational environment of MATLAB as CERR. This integration allows RPCFILM code to register film data to the data calculated by Eclipse TPS.



Before this code could be used for film analysis it required some additional data. To correct the information obtained from the films, RPCFILM uses doses measured by the TLDs, and therefore it is important to have the TLD dose calculations done prior to analysis. Since every phantom used by the RPC is unique, a full phantom profile had to be created. This profile contains the coordinates of all film perforations and was done using following method. A clear template that copies the shape of films was placed inside the phantom in the same way the actual film would go and insert was fully assembled. A pinprick was used to puncture the template the same way as if a film was used. The insert was opened and the template was removed. Distances from the center of coordinates (center of

the tumor) to the holes in the template were measured. Positions of the TLD capsules were also marked on each film. 3D coordinates were associated with each film in such way that the axial film only uses (X,Y) pair, coronal (X,Z) pair, and sagittal (Y,Z) pair. The profile for the L23 RPC Lung phantom had the following coordinates (Table 2.4).

Table 2.4 L23 RPC Lung Phantom Profile Data

		X, mm	Y, mm	Z, mm
		Film		
Axial	Left anterior	-39	26	0
	Left posterior	-39	-30.5	0
	Right anterior	30.5	25	0
Coronal	Superior left	-42.5	0	50
	Superior right	41	0	53
	Inferior left	-39.5	0	-52
	Inferior right	42.5	0	-49.5
Sagittal	Superior posterior	0	-45	40.5
	Superior anterior	0	41.5	37.5
	Inferior posterior	0	-45	-38.5
	Inferior anterior	0	44.5	-40.5
		TLD		
Axial	Superior/Inferior	3.5	-3.5	0
Coronal	Superior	4	0	6
	Inferior	4	0	-6
Sagittal	Superior	0	-3.5	6
	Inferior	0	-3.5	-6

Another file was created that contained information on regions of interest for the 2D gamma analysis. In this work a single gamma index region of interest of PTV + 2cm was chosen. The last

piece of data required for the film analysis was the dose response curve (chapter 2.5.1.1). The polynomial fit coefficients for the dose response curve were loaded into the third configuration file.

After the launch of the RPCFILM in MATLAB the following step-by-step procedure was used to prepare film data for analysis.

1. A file containing the film image in .fit format (chapter 2.4.1.2) was loaded into memory.
2. From the drop-down menu the correct phantom profile containing registration information was selected
3. Since every axial, coronal, and sagittal film was analyzed separately, an orthogonal plane that corresponded to the loaded image file was selected.
4. Depending on the film plane selected, a set of registration points in a specific order was loaded from the phantom profile file. Each point was assigned a numeric coordinate value by marking corresponding pricks (chapter 2.2.1) on the film image. To verify the accuracy of the 2D registration a root mean square (RMS) error value was calculated after “Register” button was pressed.
5. After the successful 2D registration of the film the proper Dose Response Curve profile was selected. After the DRC was loaded, the program calculated the dose at the TLD position by converting optical densities of the film using the coordinates from the phantom profile. The axial films had one value assigned to TLD dose corresponding to the average of both superior and inferior TLDs, while coronal and sagittal films had separate values for each TLD. Once the TLD position dose was obtained from the film OD, a correction coefficient was calculated by dividing the film dose by that obtained for the corresponding TLD capsule (chapter 2.5.2.2).

6. After all corrections were applied, the final step was registering the film to a 3D volume dose dataset. In this step, after pressing “Register 3D” RPCFILM launched the CERR environment and asks the user to load the corresponding plan (Figure 2.16). A total of five points were used in the 3D registration: superior and inferior edges of the tumor, anterior edge of the lung insert, center of the tumor along the central axis, and the final point was registering the medial edge of the tumor in the central axial plane. After the successful registration, CERR will produce a 2D dose distribution that corresponds to the same plane as the film being analyzed. Similar to 2D registration, after the 3D registration has been completed the RPCFILM calculates 3D RMS Error.

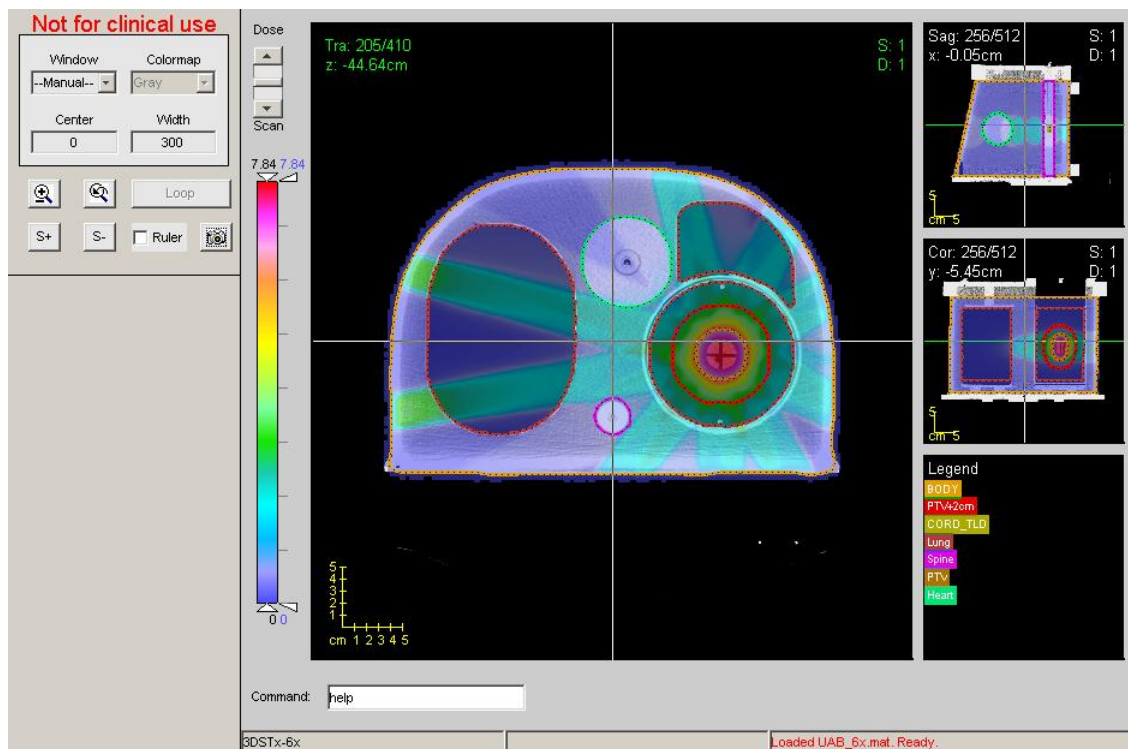


Figure 2.16 CERR Window With Loaded Plan

7. Following the last step, the film image with matching registration data, OD-to-Dose conversion, TLD corrections, and 2D dose distribution extracted from CERR were

saved into a single MATLAB file. This file provides a convenient way of presenting all the necessary information for further analysis.

2.5.4 Film Data Analysis

After the film data processing was completed and saved into file a 2D gamma analysis was performed. This was done using RPCFILM code - the same software code that was used in film data processing. Gamma analysis requires input of two values for dose-to-agreement (in %) and distance-to-agreement (in mm) (Figure 2.17).

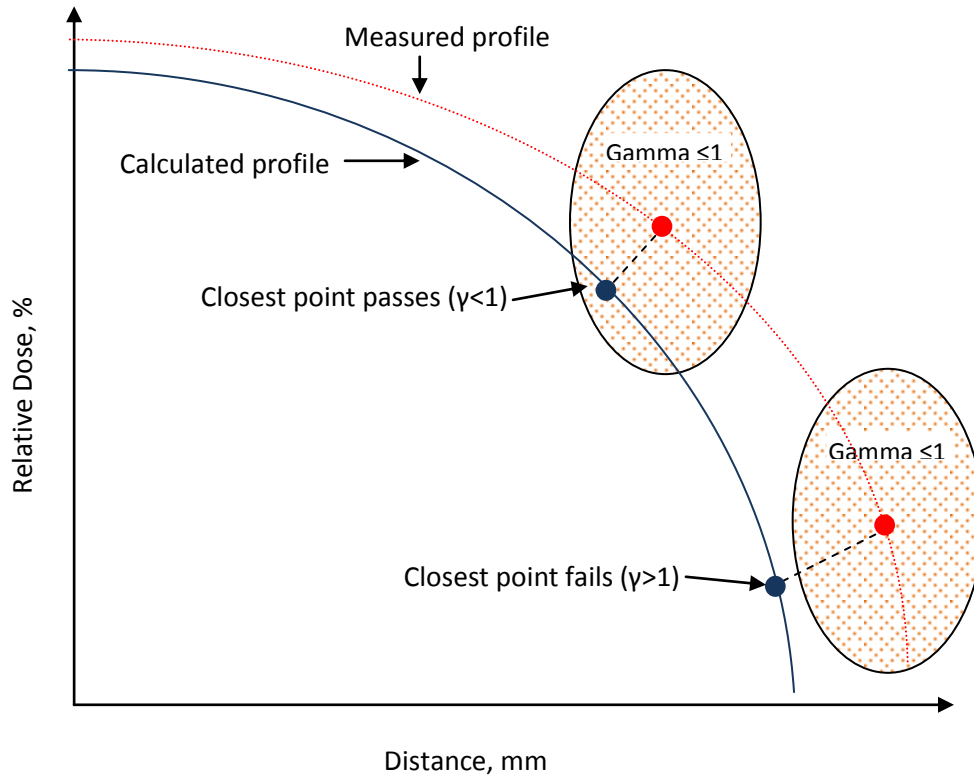


Figure 2.17 2D Gamma Index Using Dose And Distance To Agreement Criteria

The actual gamma index $\gamma(\vec{r}_r)$ is calculated as a minimum value of $\Gamma(\vec{r}_r, \vec{r}_e)$ according to the following formulas:

$$\gamma(\vec{r}_r) = \min_{\vec{r}_e} \Gamma(\vec{r}_r, \vec{r}_e)$$

And

$$\Gamma(\vec{r}_r, \vec{r}_e) = \sqrt{\frac{|\vec{r}_e - \vec{r}_r|^2}{\Delta d^2} + \frac{|D_e(\vec{r}_e) - D_r(\vec{r}_r)|^2}{\Delta D^2}},$$

Where

\vec{r}_r and \vec{r}_e are the evaluated and reference vector point positions, $D_e(\vec{r}_e)$ and $D_r(\vec{r}_r)$ are the evaluated and reference doses, respectively and Δd and ΔD are the distance-to-agreement and dose difference criteria, respectively [28].

Two sets of criteria, $\pm 5\%/3\text{mm}$ and $\pm 8\%/3\text{mm}$, were used in this work. RPCFILM code calculates a passing rate of pixels (gamma index < 1) around unity using these criteria. A first set of criteria of $\pm 5\%/3\text{mm}$ was stated in the hypothesis (chapter 1.4). The reason for the second set was that for the heterogeneity-corrected dose in anthropomorphic thorax phantoms the RPC uses gamma index around ratio of 0.97 instead of 1. This was done based on the RPC data [29, 30] that demonstrated that the average measured-to-calculated dose ratio in the target was 0.97 (0.92-0.99 range). In order to be able to perform a comparison of the plans created in this study to the standards used by the RPC, gamma index analysis using $\pm 8\%/3\text{mm}$ criteria was also performed on all plans.

After the appropriate criteria were entered, the correct region of interest was selected. As was pointed out in chapter 2.6.3, all films were analyzed using single ROI equal to PTV+2cm. Axial PTV+2 was equal to 8 cm (-4...+4 cm) in the axial plane, while coronal and sagittal films had PTV+2cm ROIs equal to 11 cm (-5.5...+5.5 cm) in the superior-inferior and 8 cm in the lateral and anterior-posterior directions. Selecting ROI for gamma analysis opens a new window showing dose distributions limited to this region. The option to mask some areas of this image was used to exclude from gamma index analysis any pixels that were part of pinprick marks that were used in film registration, coronal and sagittal film slits that were cut in order to load the axial film (chapter 2.2.1), as well as any dust particles, scratches, or other damage that could have happened prior to scanning

in the process of film handling. After the masking was complete, RPCFILM code calculated and displayed the gamma index map and a number of pixels (in %) that passed the specified criteria. This map has two options of displaying the results. The color-coded (standard) option displays pixel map using color spectrum from dark blue (value of 0 having the best agreement) to dark red (gamma index greater than 2 having the worst agreement) with color green being 1. Values greater than 2 are truncated to 2. The second option, binary, presents passing pixels (gamma index <1) as white while failing pixels (gamma index >1) as dark grey. Binary mode doesn't show how close each pixel is to passing or failing while first option could provide some additional information about spatial dose distribution or profile shapes. The color-coded gamma index maps of every film were saved into a file and the passing rates were analyzed and plotted using Microsoft® Excel (Redmond, WA) software.

The second part of film analysis consisted of extracting dose profiles. In this step, a total of two sets of two dose profiles each were pulled from every film data file. A single set represented a measured and calculated dose profiles in one of the directions depending on the film being analyzed. Axial film produced two sets in X (right-left) and Y (anterior-posterior) directions, coronal resulted in X and Z (superior-inferior) profiles, and sagittal in Y and Z directions. These profiles were imported into an Excel spreadsheet. A 10-point Simple Moving Average smoothing was applied to every measured profile that was plotted along with calculated dose profile and the PTV boundaries.

Chapter 3 Results and Discussion

3.1 Dose Response Curve

The Dose Response Curve was calculated following the procedure described in chapter 2.5.1.1. As was mentioned earlier, in order to relate an unknown dose to a known film optical density the relationship between a known dose and known OD had to be established. In order to have a reliable dose-OD relationship a range of doses for the dose response films had to be irradiated that covered both lower and higher limits of expected doses. Eight different doses in fixed geometry were delivered to films resulting in 8 distinct levels of optical density. Table 3.1 shows the delivered doses and their corresponding ODs for the EBT2 (Lot # A06271103) radiochromic film. The same lot was used throughout the whole study for all phantom irradiations.

Table 3.1 Dose Response Film Data Points

MU	Dose, Gy	OD
50	0.548	0.137
150	1.643	0.306
250	2.738	0.416
350	3.833	0.497
550	6.023	0.618
750	8.213	0.702
950	10.403	0.756
1150	12.593	0.811

The function, relating Dose to OD, was plotted (Figure 3.1) and a third order polynomial fit based on these data points resulted in the following equation:

$$D = 28.431 \cdot OD^3 - 11.77 \cdot OD^2 + 6.2869 \cdot OD$$

Where

D – Dose received by film;

OD – Film optical density.

Since during the film scanning step (chapter 2.5.1.2) optical densities of background (flatfield) was subtracted from the optical densities of dose response and phantom films this polynomial regression was calculated with the X and Y intercept at 0. This means that 0 OD will equate to 0 Gy. To verify “goodness of fit”, R^2 , coefficient was determined. It shows how well a function fits the set of observations with 1 being an ideal fit and 0 being the worst match. R^2 was calculated to be 0.999 demonstrating that obtained equation describes experimental data very well.

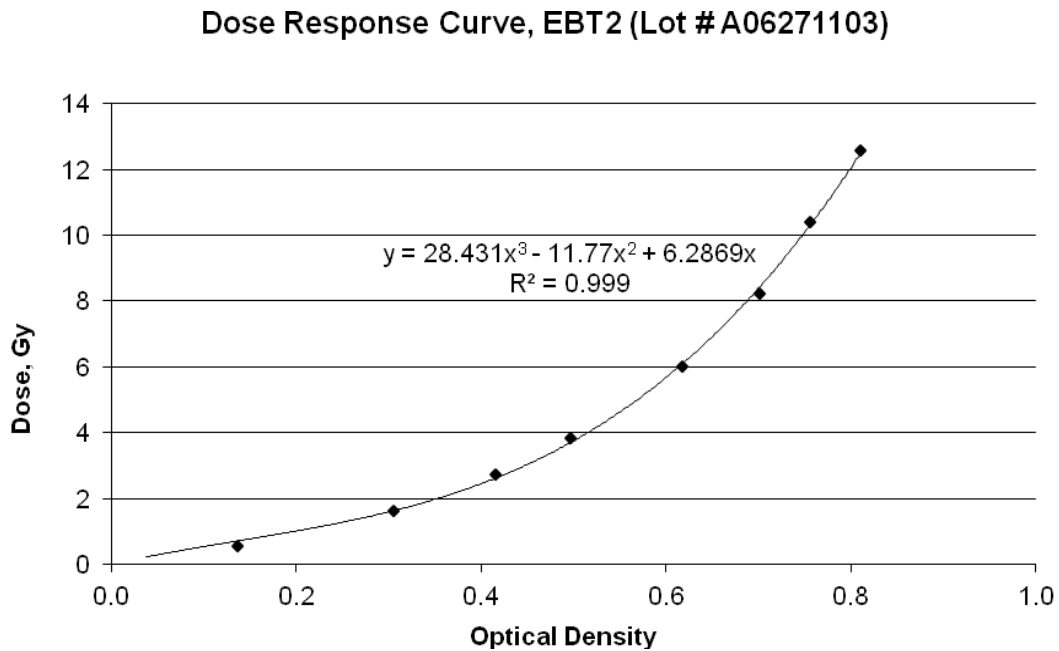


Figure 3.1 Plot Of Dose Response Curve And Its Polynomial Fit

3.2 MD Anderson Cancer Center Treatment Plans

Both 6 MV and 18 MV plans were developed in Research Eclipse treatment planning system. AAA v.8.9.08 heterogeneity correction was applied for volume dose calculations in both plans. Plan dose prescription and limits were discussed in chapter 2.3.1. Each plan was normalized so that 6 Gy in single fraction was to be delivered to at least 95% of the PTV volume using a total of nine fields at

25°, 60°, 115°, 150°, 180°, 220°, 260°, 285°, and 345° (Figure 2.5). In each case the tumor coverage was achieved by using only beams of specified energy, such as the only photon energy allowed in 3D SBRT 6 MV plan was 6 MV x-rays etc. Keeping all other variables(isocenter, fields setup, dose rate, and collimator jaws and MLC positions) constant and only changing the energy of the treatment beam, allows relating any changes in the final dose distribution to the effectiveness of the dose calculation and heterogeneity correction of the anisotropic analytical algorithm itself.

To minimize the effect of fading, all TLD capsules were read 14 days post-irradiation. TLD readings (in charge per unit mass [$\mu\text{C}/\text{mg}$]) were converted into dose (in cGy) as described in chapter 2.5.2.2. Each plan was delivered three times to the phantom, resulting in two target TLDs per irradiation for a total of 36 target doses. Corresponding doses were extracted from the treatment planning system and a measured-to-predicted ratio was calculated. Each TLD dose was corrected for the variations in linear accelerator daily output. The RPC currently uses passing criteria of 0.97 ± 0.05 . In this work, if this ratio was within $\pm 5\%$ of the absolute dose the TLD was passing otherwise it was considered to be failing the point dose test.

3.2.1 MD Anderson: 3D SBRT 6 MV Plan

3.2.1.1 Plan Details

After all required structures were contoured a number of beam placements were tested to find an optimal configuration that met the plan objectives. Figure 3.2 shows phantom axial plane with final beam placement, while Figure 3.3 shows the colorwash dose distribution on the same axial slice. Colorwash display maps out dose intensity from the lowest (blue) to the highest (red). The dose range (window) was selected to display the doses between 15% of the prescribed dose to maximum (in this case 120.8%). The plan's calculated dose was in a good agreement with RTOG requirements for Conformality Index, normal tissue dose spillage and dose restrictions (chapter 2.3.1).

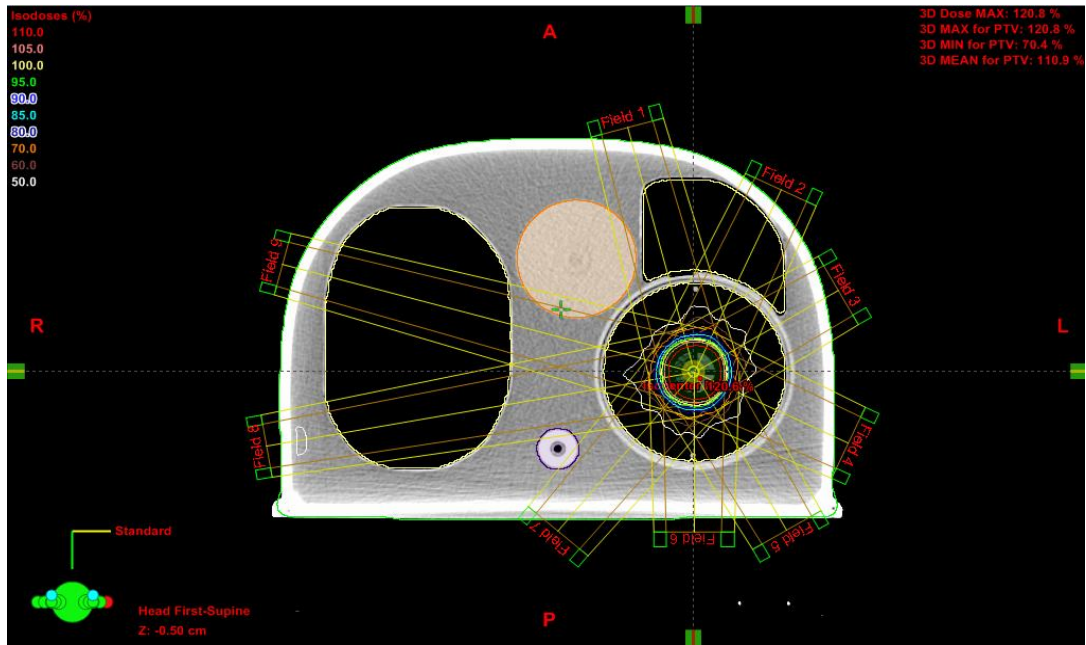


Figure 3.2 3D SBRT 6 MV Plan - Axial Plane Beam Placement

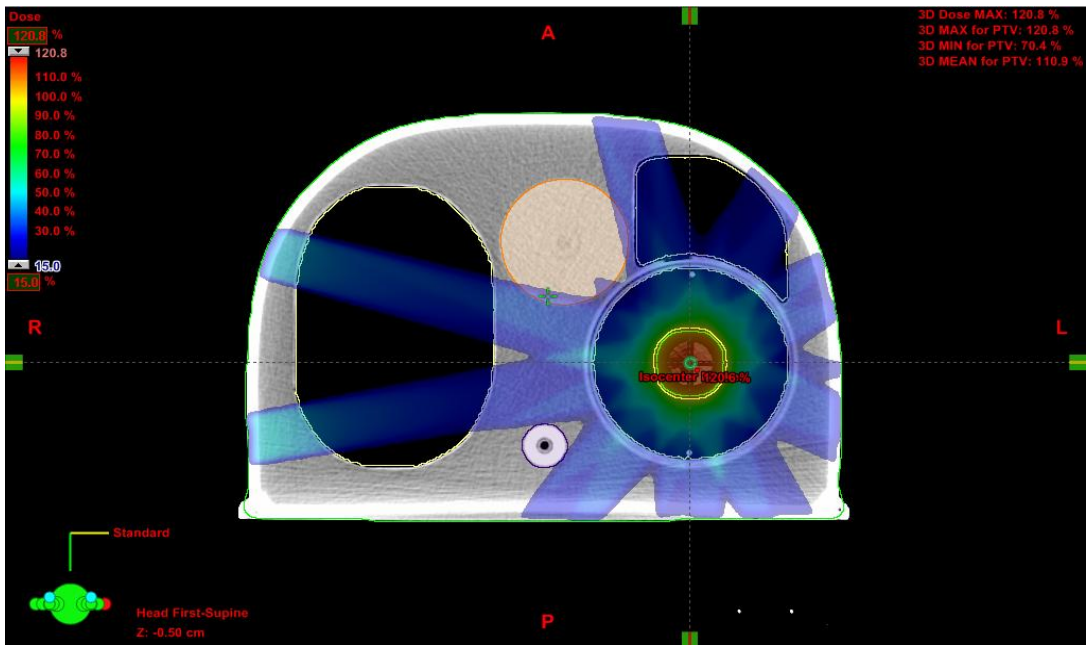


Figure 3.3 3D SBRT 6 MV Plan - Axial Plane Colorwash Dose Distribution

Figure 3.4 represents a 3-plane view of the tumor and the calculated isodose map. Calculated dose takes advantage of AAA heterogeneity correction and demonstrates an excellent conformity in all three planes. A magnified view of the same axial plane is shown in Figure 3.5.

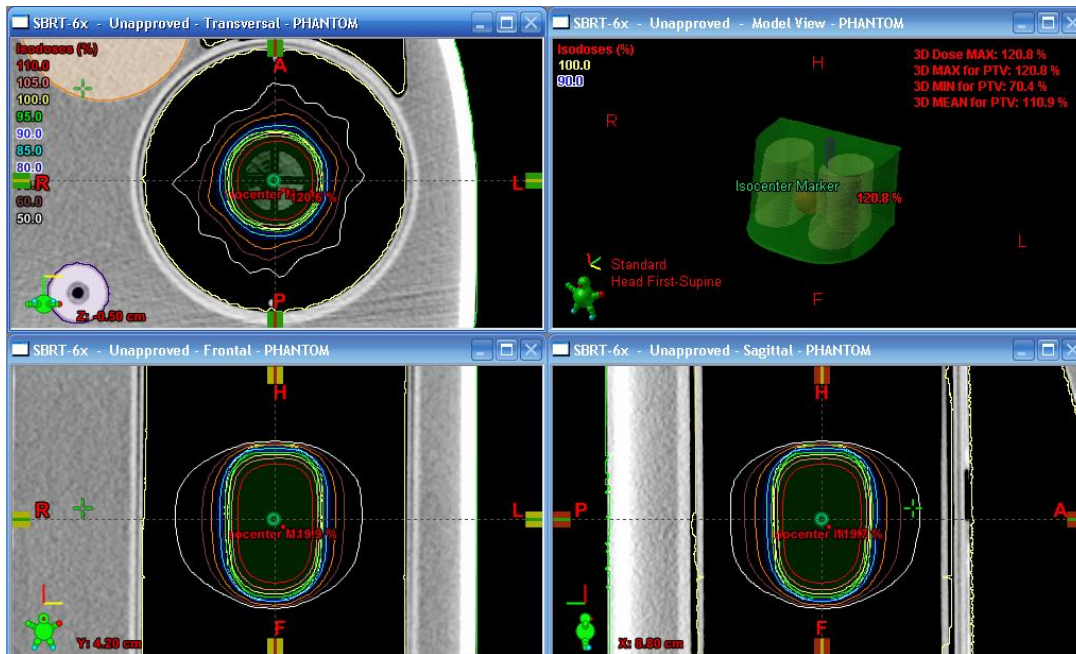


Figure 3.4 3-Plane View Of The Tumor And The Isodose Map

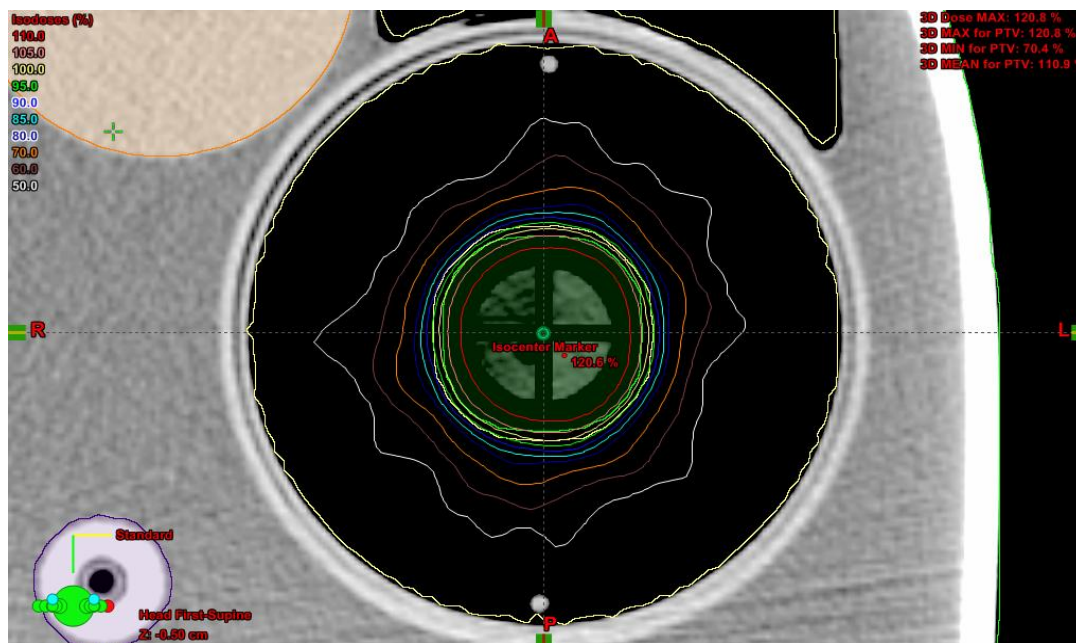


Figure 3.5 A Magnified Axial Plane View Of The Tumor And The Isodose Map

A Dose Volume Histogram (DVH) represents a cumulative relationship between the absolute (or relative) dose and the volume of the region of interest that receives that dose. It can be seen from Figure 3.6 that non-tumor tissues (lung, heart, and spine) received radiation dose well below the established RTOG and RPC limits for normal tissues. At the same time, the tumor coverage complied with the specified prescription described in Treatment Planning section.

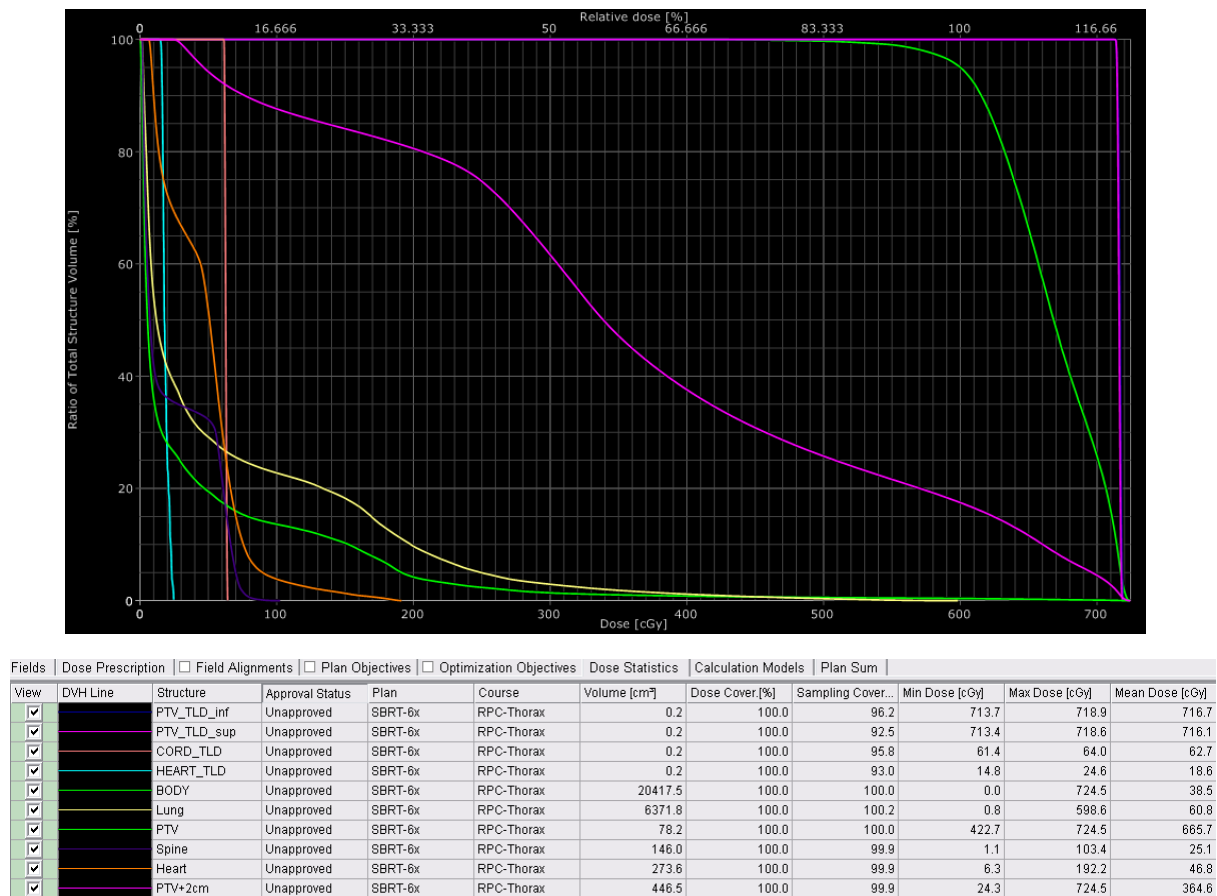


Figure 3.6 3D SBRT plan – Dose Volume Histogram

3.2.1.2 Target TLD Results

Table 3.2 shows superior and inferior target TLD data corrected for daily output and Figure 3.7 displays a histogram of the measured-to-predicted dose ratios for target TLDs. The averages have error bars representing the 95% confidence interval (CI) plotted as well.

Table 3.2 Target TLD Results. 6 MV, MD Anderson

Plan: 6 MV, MD Anderson, Clinac 2100CD							
Phantom Irradiation №	TLD Dose, Gy		Daily Output Correction	Corrected TLD Dose, Gy		Eclipse Calculated Dose, Gy	
	PTV TLD_sup	PTV TLD_inf		PTV TLD_sup	PTV TLD_inf	PTV TLD_sup	PTV TLD_inf
1	6.9899	7.0287	1.015	6.8866	6.9249	7.161	7.167
2	7.1064	7.0618		7.0014	6.9575		
3	7.0897	7.0762		6.9849	6.9716		
Average				6.9576	6.9513	7.164	
Measured/Predicted Ratio				0.972	0.970	0.971	

TLD Results - 6MV Plan, MDA

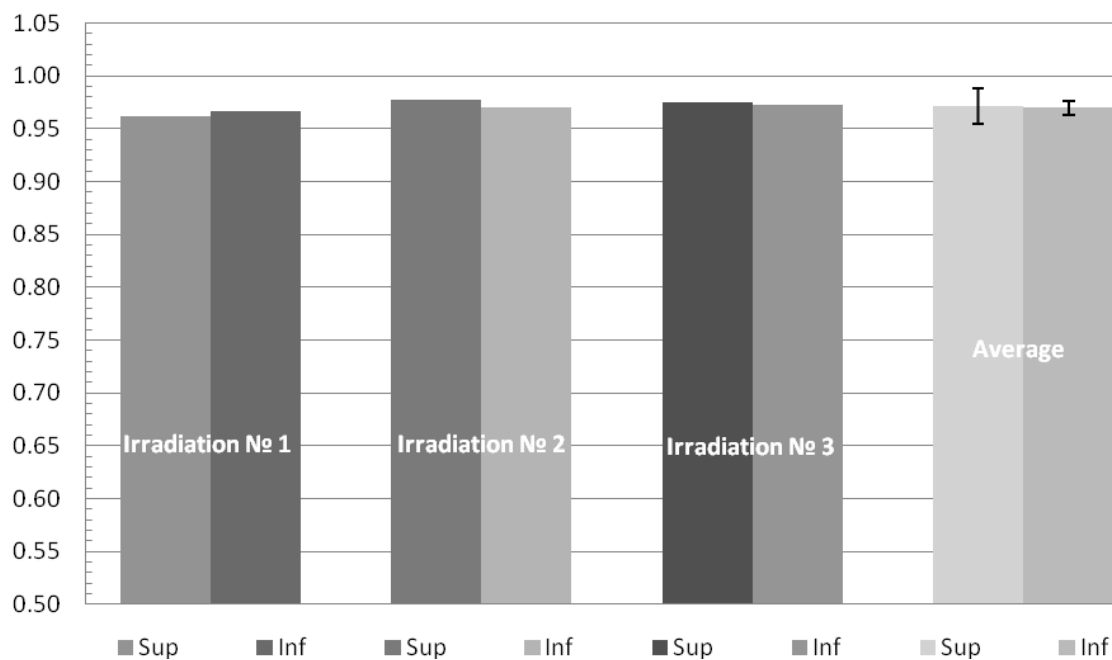


Figure 3.7 Measured-To-Predicted Dose Ratios Of Target TLDs For 6 MV Plan (MDA CC)

3.2.1.3 2D Gamma Index Analysis Results

As was mention in Film Data Analysis (chapter 2.6.4) section, two sets of criteria, $\pm 5\%/3\text{mm}$ and $\pm 8\%/3\text{mm}$, were used in this work. This resulted in two sets of gamma index maps per plane for a total of 18 maps per plan. Figures 3.8-3.10 show examples of the 2D gamma index results for the first irradiation of the phantom at MD Anderson Cancer Center using a 6 MV 3D SBRT plan and $\pm 5\%/3\text{mm}$ gamma criteria. Gamma analysis results using $\pm 8\%/3\text{mm}$ criteria, as well as results for other irradiations are shown in the Appendix.

Table 3.3 summarizes the 2D gamma index results for all three irradiations (using 6 MV plan) of the RPC phantom at MD Anderson.

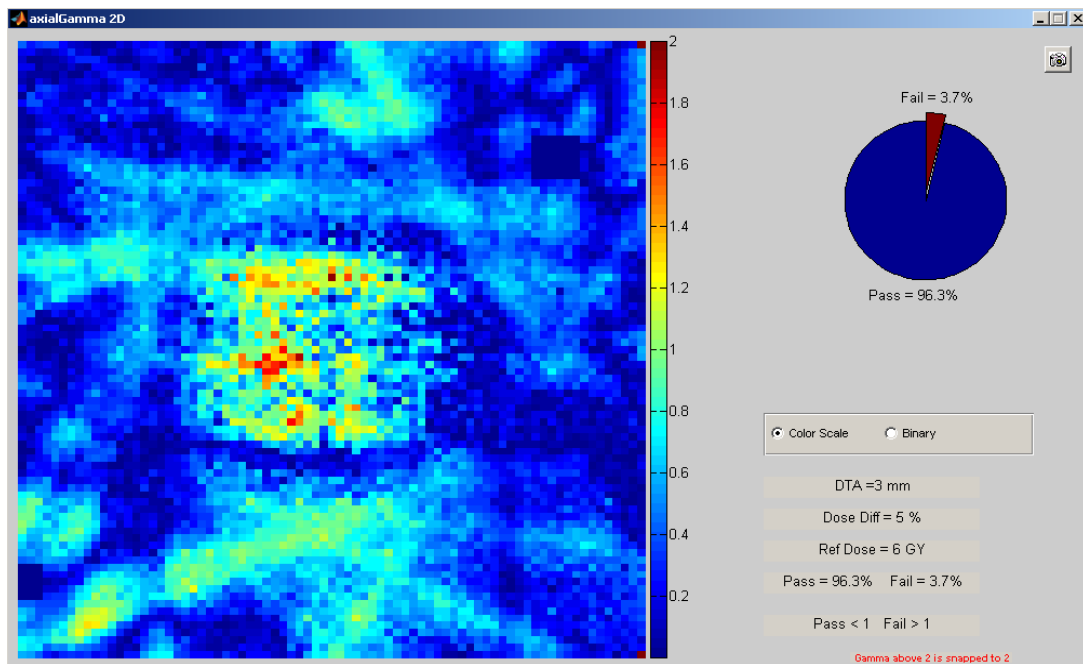


Figure 3.8 2D Gamma Index Results: $\pm 5\%/3\text{mm}$, Axial Plane For 6 MV Plan

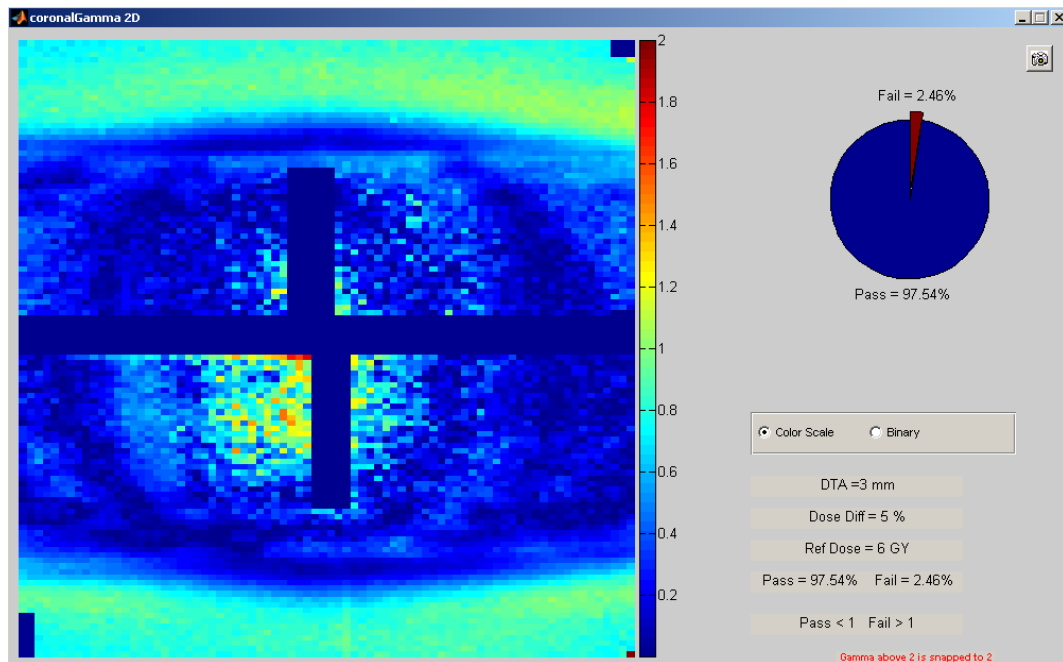


Figure 3.9 2D Gamma Index Results: $\pm 5\%/3\text{mm}$, Coronal Plane For 6 MV Plan

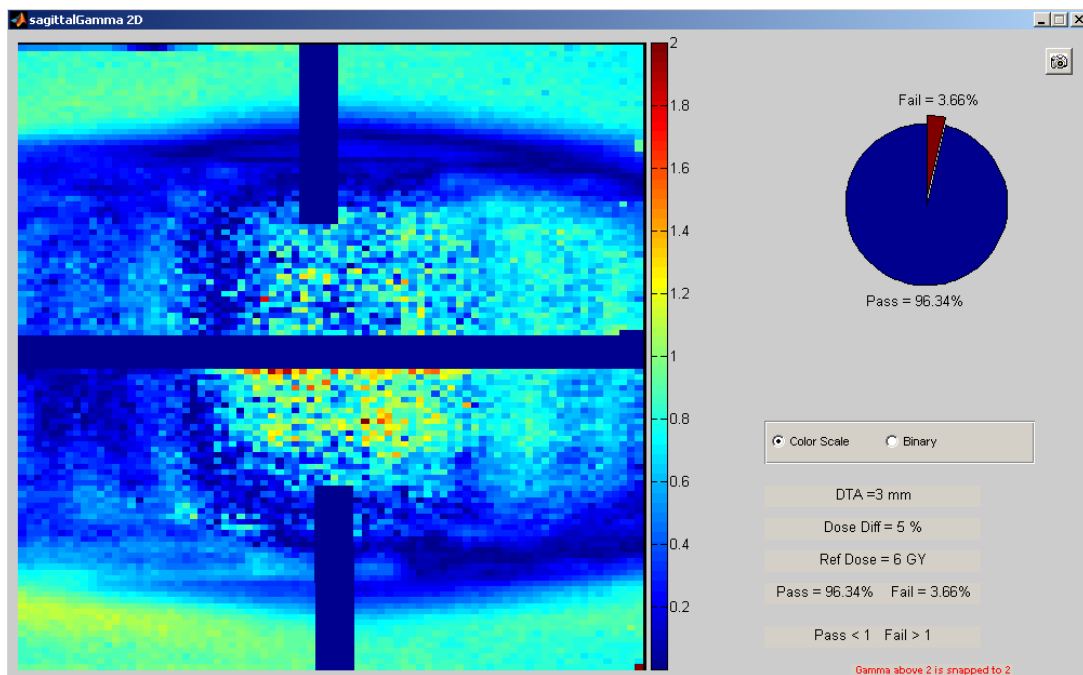


Figure 3.10 2D Gamma Index Results: $\pm 5\%/3\text{mm}$, Sagittal Plane For 6 MV Plan

Table 3.3 6 MV Plan 2D Gamma Index Results, MD Anderson

Plan: 6 MV, MD Anderson, Clinac 2100CD

Phantom Irrad.No	Gamma Index Analysis Criteria	Orthogonal Plane Passing Rate, %			Average 3-planes, %	Standard Deviation 3-planes
		Axial	Coronal	Sagittal		
1	±5%/3mm	96.3%	97.5%	96.3%	96.7%	0.70%
	±8%/3mm	99.7%	99.9%	99.9%	99.8%	0.15%
2	±5%/3mm	96.6%	96.0%	94.4%	95.7%	1.13%
	±8%/3mm	99.6%	99.4%	99.9%	99.7%	0.26%
3	±5%/3mm	95.6%	98.7%	95.1%	96.5%	1.98%
	±8%/3mm	99.7%	99.9%	99.9%	99.8%	0.13%
Ave. Passing Rate – All Irradiations, %	±5%/3mm	96.2%	97.4%	95.3%	96.3%	
	±8%/3mm	99.7%	99.8%	99.9%	99.8%	
Std Deviation – All Irradiations, %	±5%/3mm	0.53%	1.36%	0.98%	0.55%	
	±8%/3mm	0.03%	0.27%	0.03%	0.09%	

A plot of the data in Table 3.3 is presented in Figures 3.11-3.12. Error bars represent the 95% CI.

Gamma Index Results - 6MV MDA, 5%/3mm

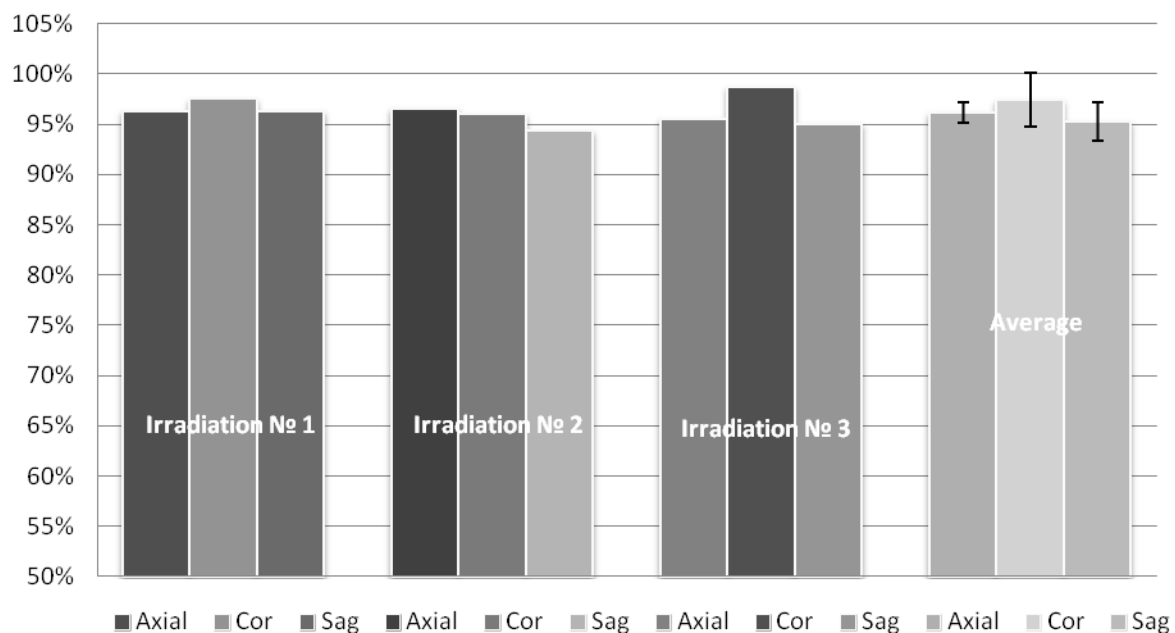


Figure 3.11 2D Gamma Index Results Using $\pm 5\%/3\text{mm}$ Criteria For 6 MV Plan

Gamma Index Results - 6MV MDA, 8%/3mm

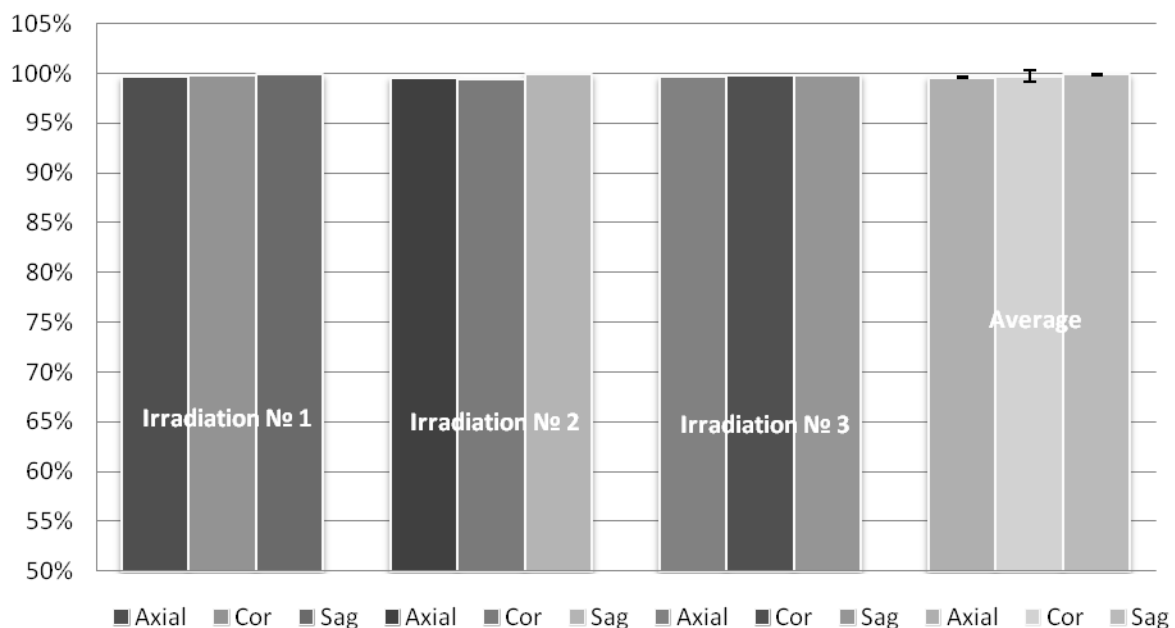


Figure 3.12 2D Gamma Index Results Using $\pm 8\%/3\text{mm}$ Criteria For 6 MV Plan

3.2.1.4 Dose Profiles Results

Two dose profiles per plane were acquired (chapter 2.6.4) and plotted using Excel. The example of Right-Left, Anterior-Posterior, and Superior-Inferior measured (film) and calculated (TPS) profiles for the first irradiation of the phantom in MD Anderson Cancer Center using 6 MV 3D SBRT plan are shown in Figures 3.13-3.15. Plane specific profiles for other irradiations and their corresponding TLD doses are presented in the Appendix.

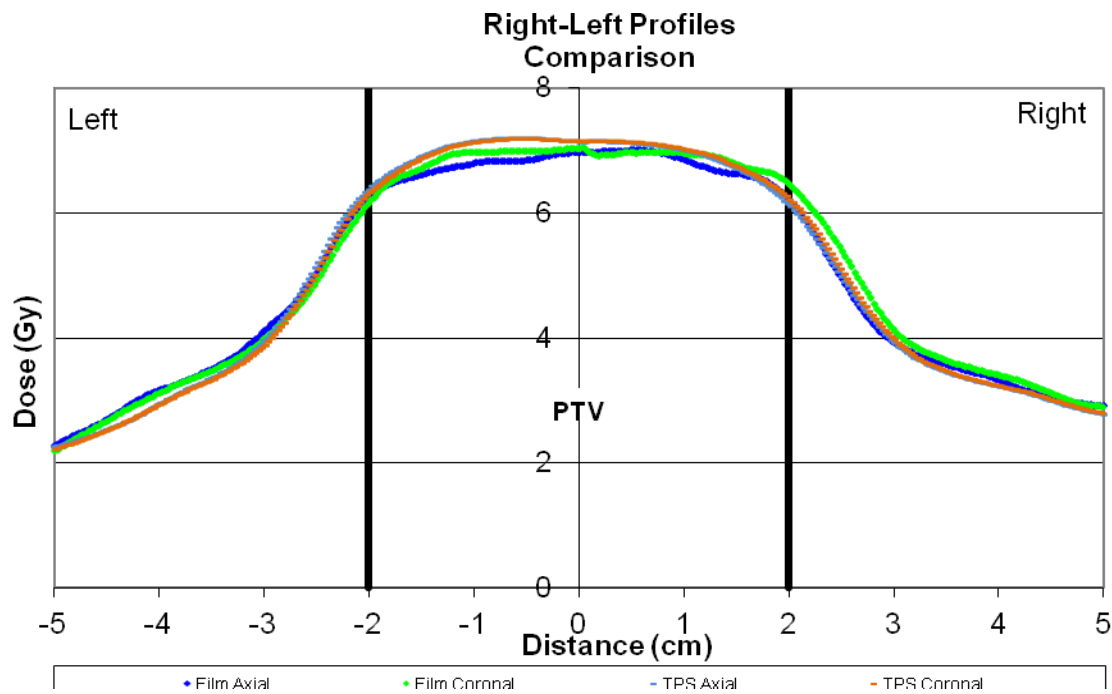


Figure 3.13 Right-Left Profiles In Axial And Coronal Planes Compared To The Calculated Dose Profiles For 6 MV Plan

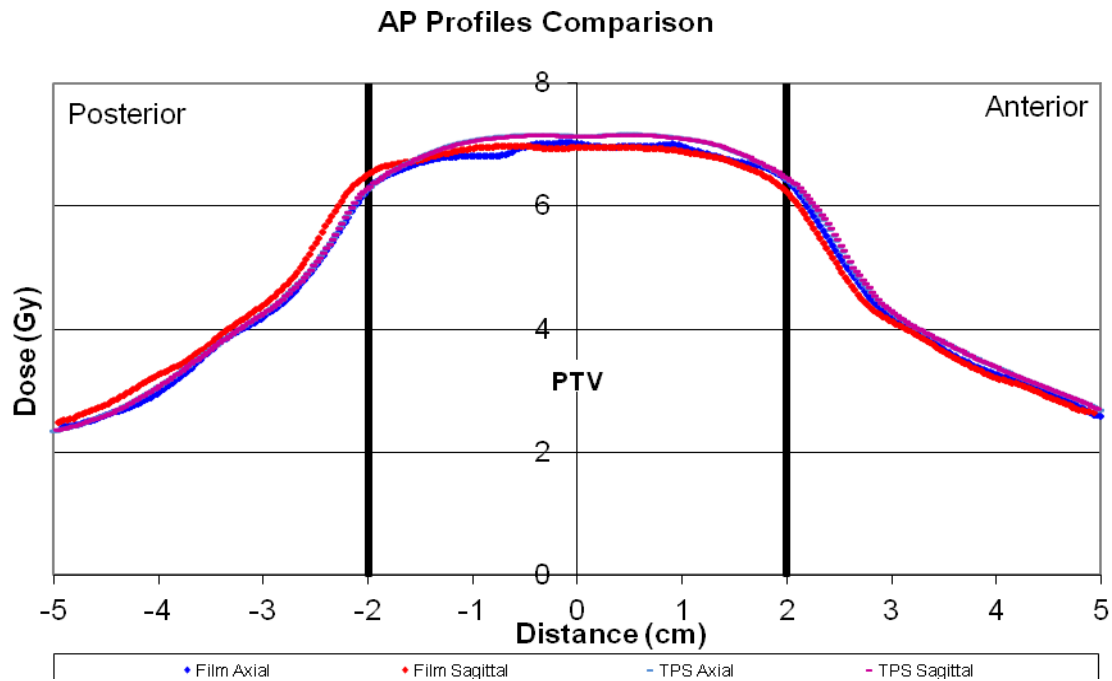


Figure 3.14 Anterior-Posterior Profiles In Axial And Sagittal Planes Compared To The Calculated Dose Profiles For 6 MV Plan

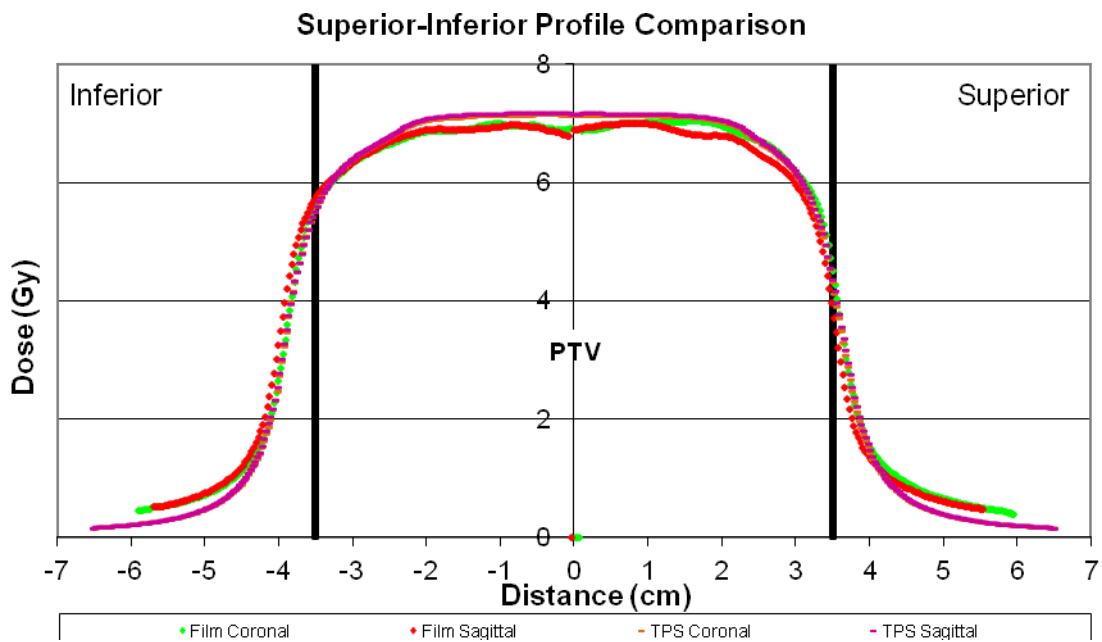


Figure 3.15 Superior-Inferior Profiles In Coronal And Sagittal Planes Compared To The Calculated Dose Profiles For 6 MV Plan

3.2.2 MD Anderson: 3D SBRT 18 MV Plan

3.2.2.1 Plan Details

Figure 3.16 shows phantom axial plane with final beam placement, while Figure 3.17 shows the colorwash dose distribution on the same axial slice. The dose range (window) was selected to display the doses between 15% of the prescribed dose to maximum (in this case 128.5%). Calculated dose was in a good agreement with RTOG requirements for Conformality Index, normal tissue dose spillage and dose restrictions (chapter 2.3.1).

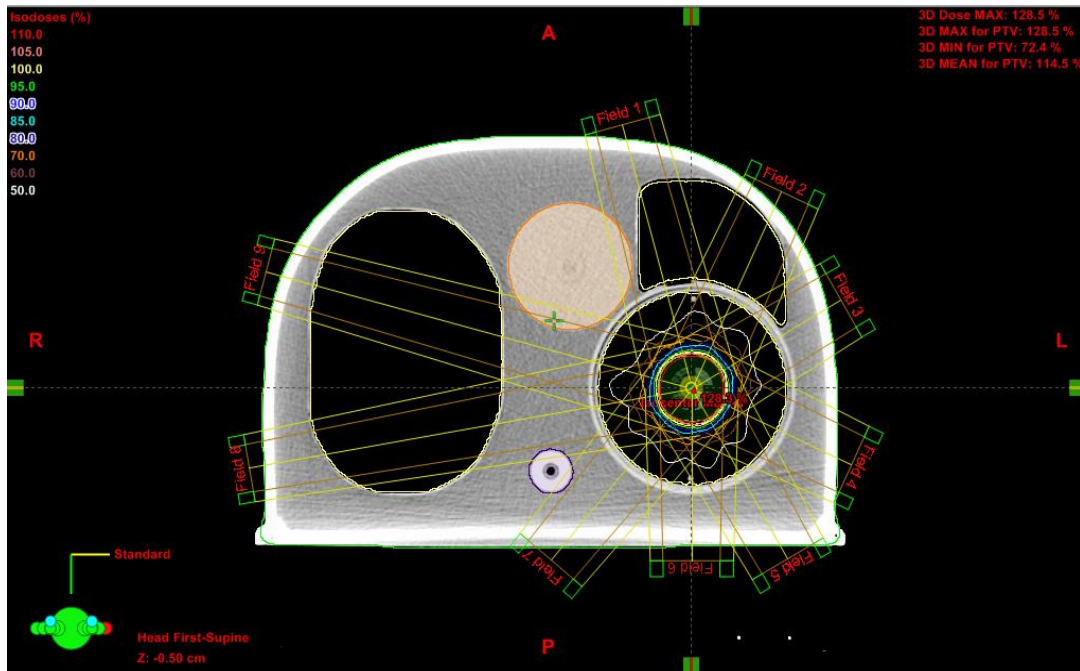


Figure 3.16 3D SBRT 18 MV Plan - Axial Plane Beam Placement

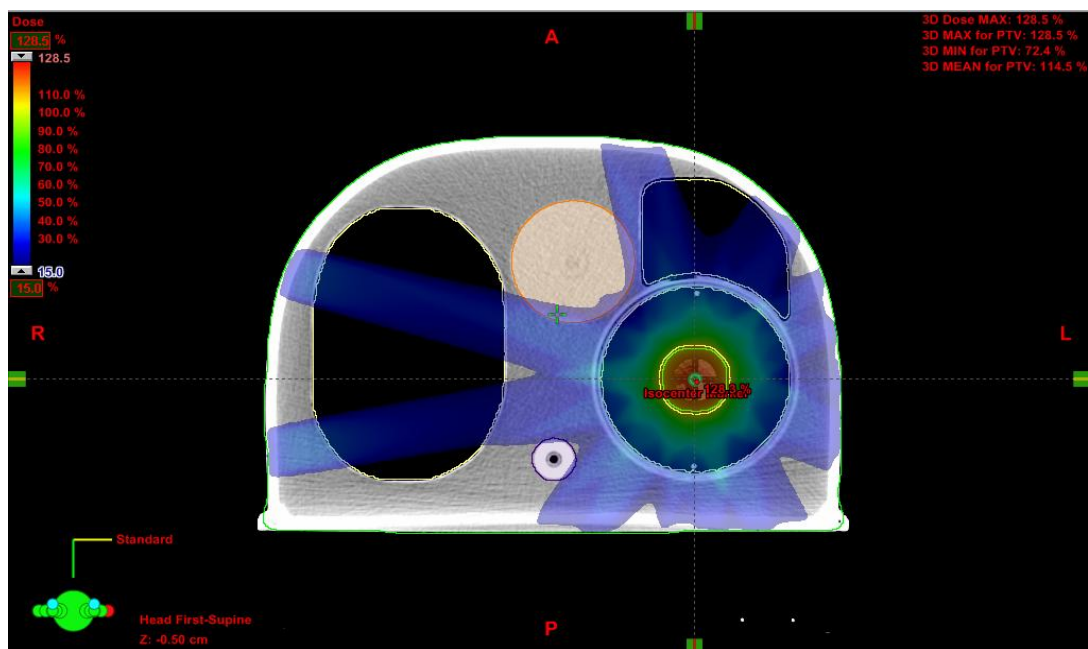


Figure 3.17 3D SBRT 18 MV Plan - Axial Plane Colorwash Dose Distribution

Figure 3.18 shows a 3-plane view of the tumor and the calculated isodose map. Calculated dose takes advantage of AAA heterogeneity correction and demonstrates good conformity in all three planes. A magnified view of the same axial plane is shown in Figure 3.19.

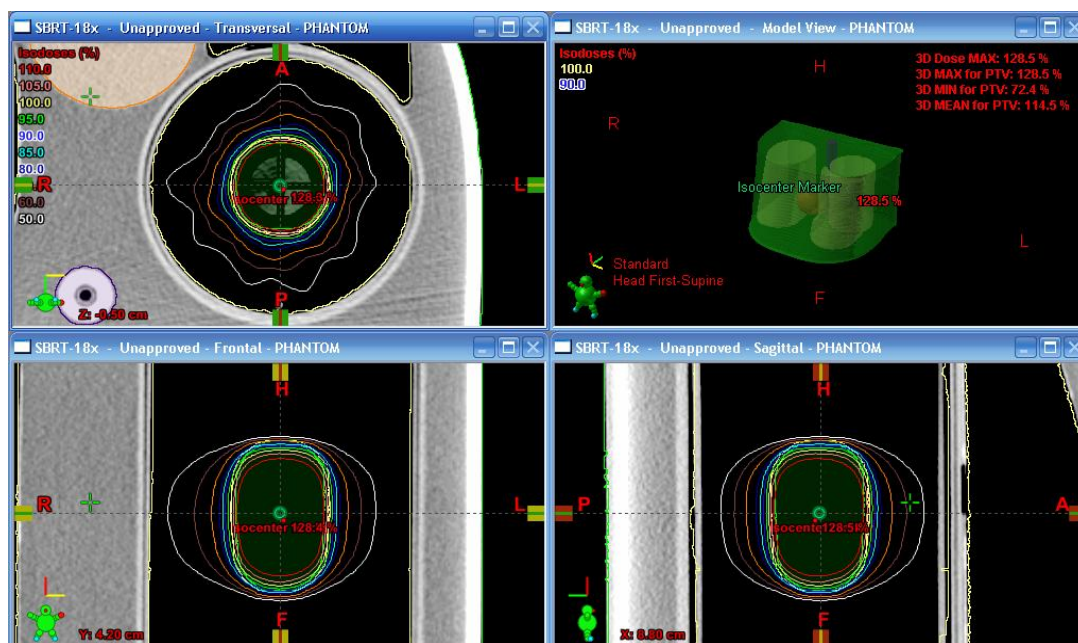


Figure 3.18 3-Plane View Of The Tumor And The Isodose Map

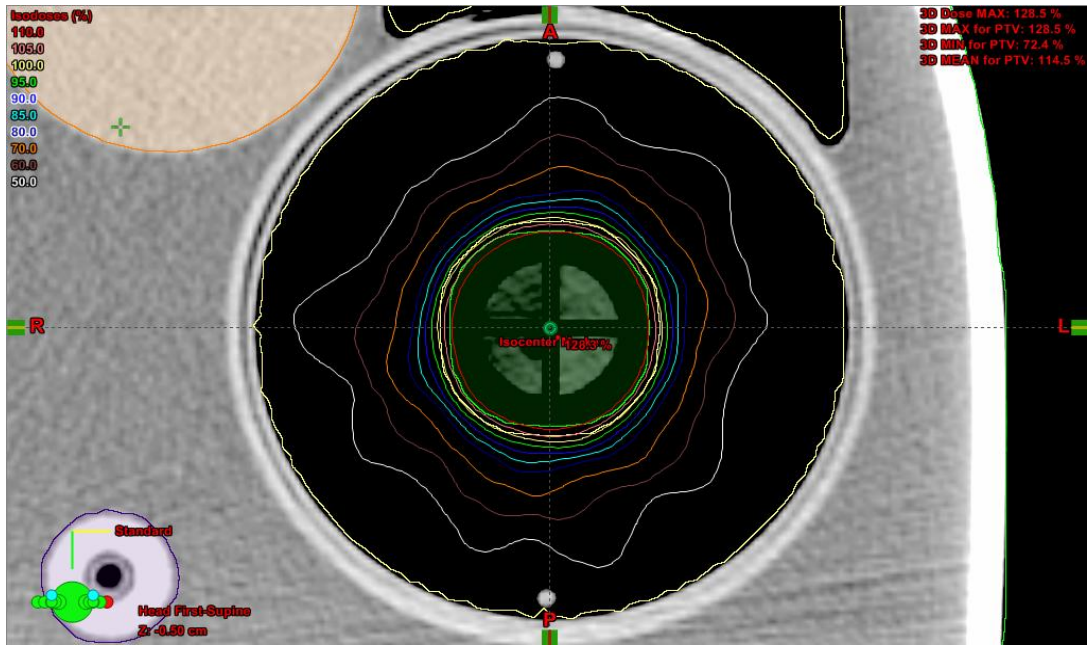
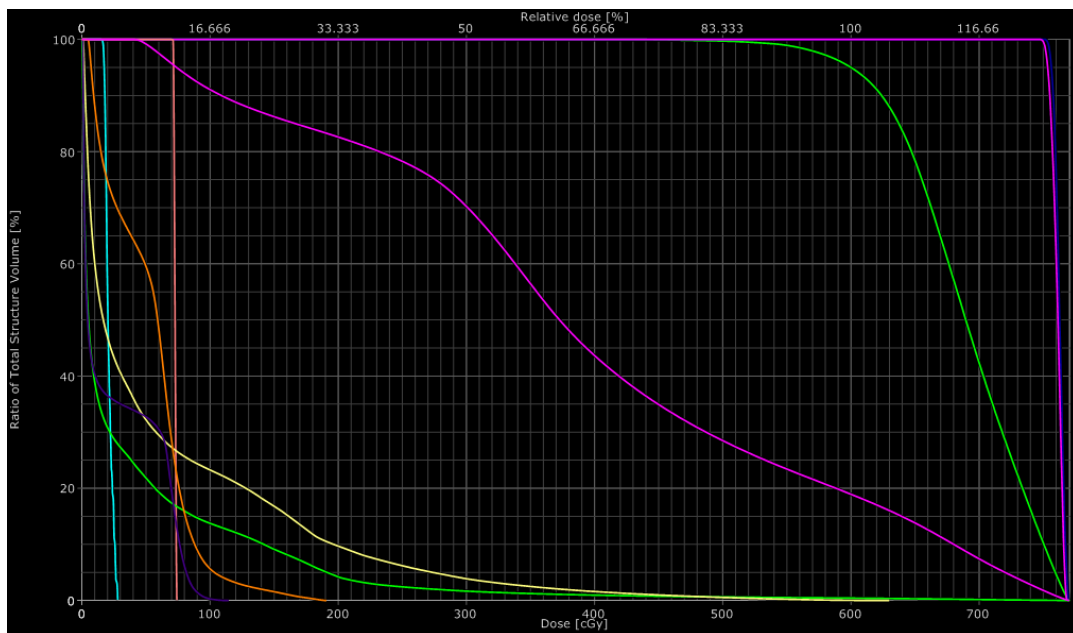


Figure 3.19 A Magnified Axial Plane View Of The Tumor And The Isodose Map

Figure 3.20 shows a Dose Volume Histogram for the calculated dose distribution. As with 6MV plan the radiation doses to non-tumor tissues such as lung, heart, and spine are substantially lower than the established RTOG and RPC limits while the tumor was covered according to the prescribed dose.



Fields	Dose Prescription	<input type="checkbox"/> Field Alignments	<input type="checkbox"/> Plan Objectives	<input type="checkbox"/> Optimization Objectives	Dose Statistics		Calculation Models		Plan Sum		
View	DVH Line	Structure	Approval Status	Plan	Course	Volume [cm³]	Dose Cover [%]	Sampling Cover...	Min Dose [cGy]	Max Dose [cGy]	Mean Dose [cGy]
<input checked="" type="checkbox"/>		PTV_TLD_inf	Unapproved	SBRT-18x	RPC-Thorax	0.2	100.0	96.2	751.9	769.7	762.7
<input checked="" type="checkbox"/>		PTV_TLD_sup	Unapproved	SBRT-18x	RPC-Thorax	0.2	100.0	92.5	748.5	768.6	760.9
<input checked="" type="checkbox"/>		CORD_TLD	Unapproved	SBRT-18x	RPC-Thorax	0.2	100.0	95.8	71.1	74.1	72.7
<input checked="" type="checkbox"/>		HEART_TLD	Unapproved	SBRT-18x	RPC-Thorax	0.2	100.0	93.0	15.9	28.0	21.1
<input checked="" type="checkbox"/>		BODY	Unapproved	SBRT-18x	RPC-Thorax	20417.5	100.0	100.0	0.0	770.9	40.0
<input checked="" type="checkbox"/>		Lung	Unapproved	SBRT-18x	RPC-Thorax	6371.8	100.0	100.2	0.6	630.4	64.9
<input checked="" type="checkbox"/>		PTV	Unapproved	SBRT-18x	RPC-Thorax	78.2	100.0	100.0	434.6	770.9	686.9
<input checked="" type="checkbox"/>		Spine	Unapproved	SBRT-18x	RPC-Thorax	146.0	100.0	99.9	0.5	115.0	27.2
<input checked="" type="checkbox"/>		Heart	Unapproved	SBRT-18x	RPC-Thorax	273.6	100.0	99.9	4.3	191.3	52.9
<input checked="" type="checkbox"/>		PTV+2cm	Unapproved	SBRT-18x	RPC-Thorax	446.5	100.0	99.9	40.8	770.9	393.0

Figure 3.20 3D SBRT plan – Dose Volume Histogram

3.2.2.2 Target TLD Results

Table 3.4 shows superior and inferior target TLD data corrected for daily output and Figure 3.21 displays measured-to-predicted dose ratios for target TLDs. The averages have error bars representing the 95% confidence interval (CI) plotted as well.

Table 3.4 Target TLD Results. 18 MV, MD Anderson

Plan: 18 MV, MD Anderson, Clinac 21EX							
Phantom Irradiation №	TLD Dose, Gy		Daily Output Correction	Corrected TLD Dose, Gy		Eclipse Calculated Dose, Gy	
	PTV TLD_sup	PTV TLD_inf		PTV TLD_sup	PTV TLD_inf	PTV TLD_sup	PTV TLD_inf
1	7.8470	7.7038	0.997	7.8706	7.7270	7.609	7.627
2	7.8012	7.7931		7.8246	7.8166		
3	7.7922	7.7750		7.8156	7.7984		
Average				7.8370	7.7807	7.618	
Measured/Predicted Ratio				1.03	1.02	1.025	

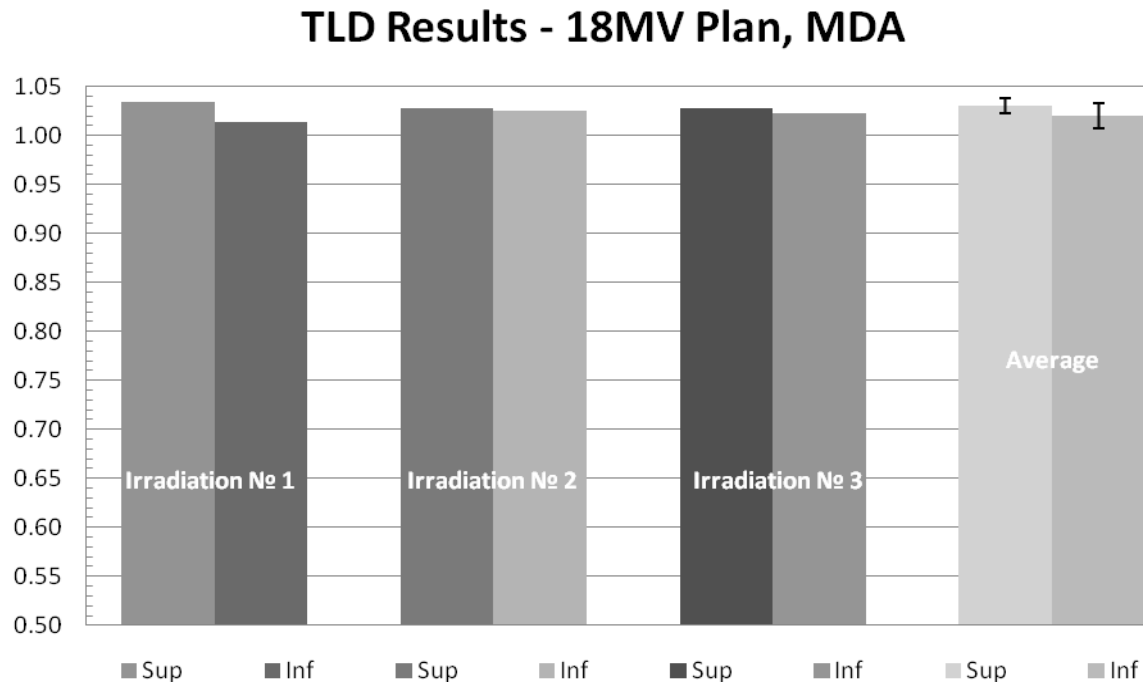


Figure 3.21 Measured-To-Predicted Dose Ratios Of Target TLDs For 18 MV Plan (MDA CC)

3.2.2.3 2D Gamma Index Analysis Results

Figures 3.22-3.24 show examples of 2D gamma index results for one of the irradiations of the phantom in MD Anderson Cancer Center using 18 MV 3D SBRT plan and $\pm 5\%/3\text{mm}$ criteria. Gamma analysis results using $\pm 8\%/3\text{mm}$ criteria, as well as results for other irradiations are presented in the Appendix.

Table 3.5 summarizes 2D gamma index results for all three irradiations (using the 18 MV plan) of the RPC phantom at MD Anderson.

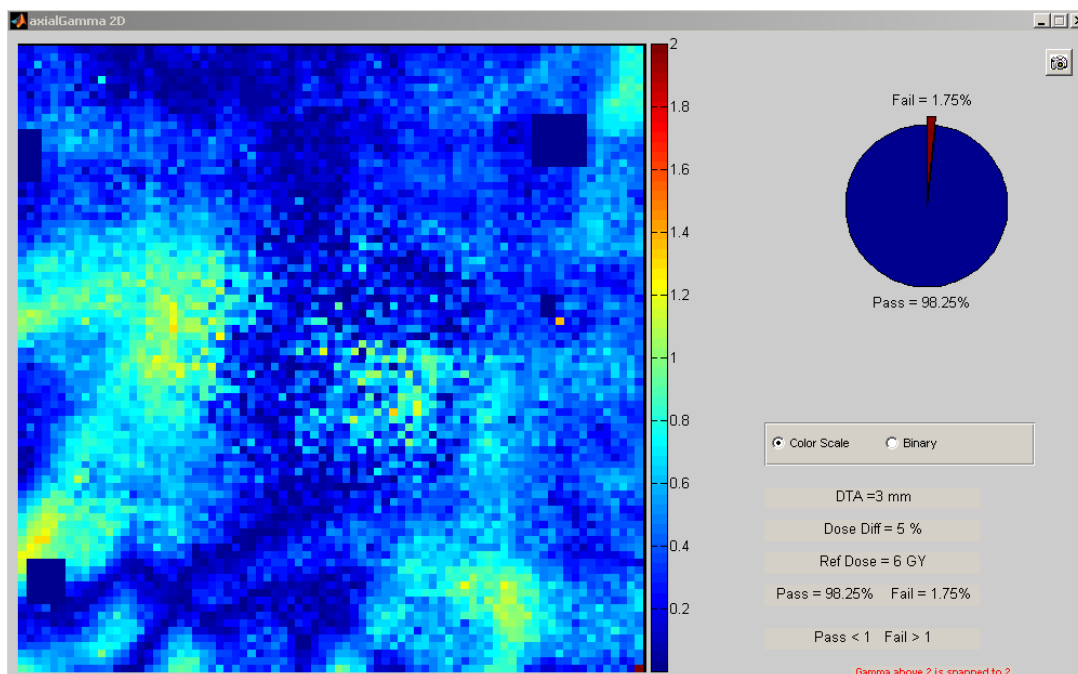


Figure 3.22 2D Gamma Index Results: $\pm 5\%/3\text{mm}$, Axial Plane For 18 MV Plan

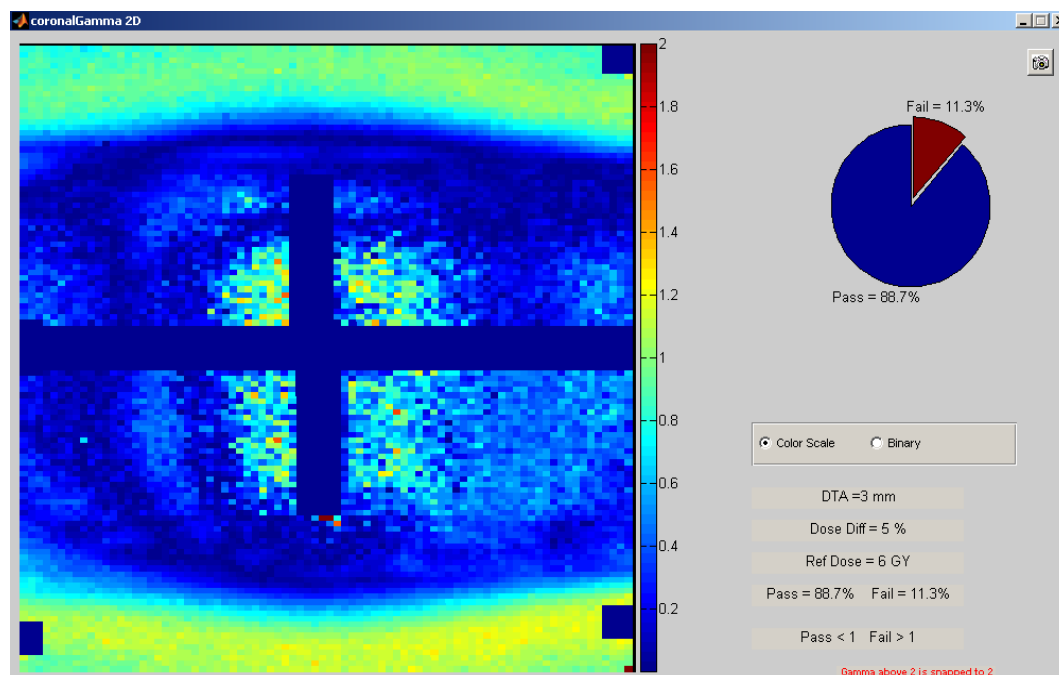


Figure 3.23 2D Gamma Index Results: $\pm 5\%/3\text{mm}$, Coronal Plane For 18 MV Plan

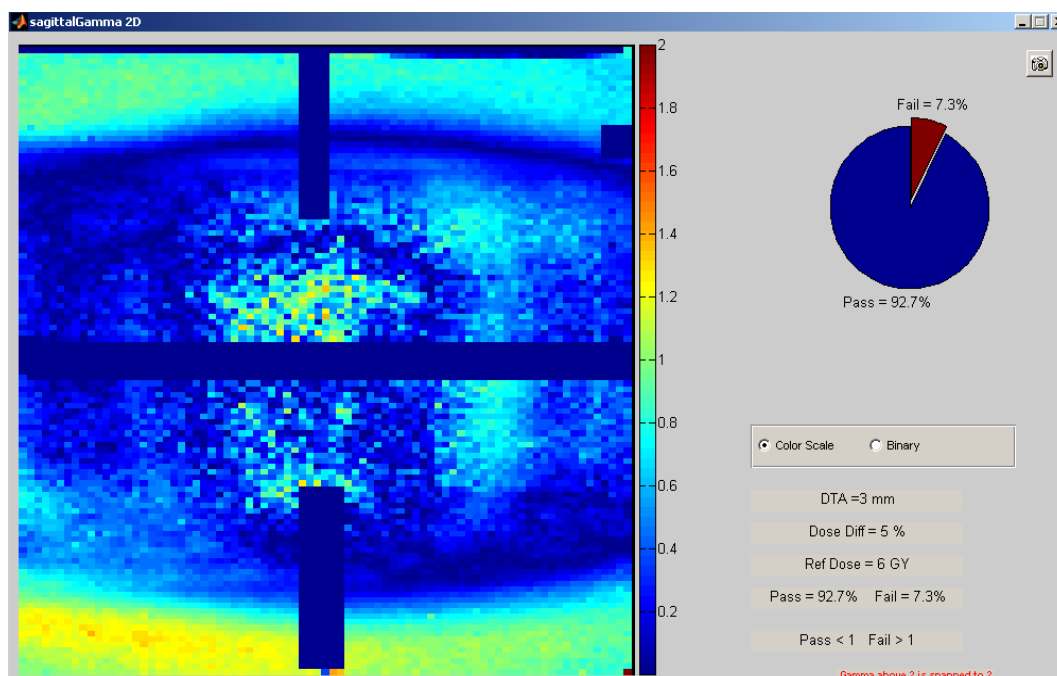


Figure 3.24 2D Gamma Index Results: $\pm 5\%/3\text{mm}$, Sagittal Plane For 18 MV Plan

Table 3.5 18 MV Plan 2D Gamma Index Results, MD Anderson

Plan: 18 MV, MD Anderson, Clinac 21EX						
Phantom Irrad.No	Gamma Index Analysis Criteria	Orthogonal Plane Passing Rate, %			Average 3-planes, %	Standard Deviation 3-planes
		Axial	Coronal	Sagittal		
1	$\pm 5\%/3\text{mm}$	99.1%	86.9%	90.6%	92.2%	6.24%
	$\pm 8\%/3\text{mm}$	100.0%	99.9%	100.0%	100.0%	0.02%
2	$\pm 5\%/3\text{mm}$	94.8%	88.1%	90.9%	91.3%	3.39%
	$\pm 8\%/3\text{mm}$	99.7%	99.6%	100.0%	99.8%	0.20%
3	$\pm 5\%/3\text{mm}$	98.3%	88.7%	92.7%	93.2%	4.80%
	$\pm 8\%/3\text{mm}$	99.8%	99.9%	100.0%	99.9%	0.08%
Ave. Passing Rate – All Irradiations, %	$\pm 5\%/3\text{mm}$	97.4%	87.9%	91.4%	92.2%	
	$\pm 8\%/3\text{mm}$	99.8%	99.8%	100.0%	99.9%	
Std Deviation – All Irradiations, %	$\pm 5\%/3\text{mm}$	2.24%	0.93%	1.15%	0.98%	
	$\pm 8\%/3\text{mm}$	0.14%	0.19%	0.02%	0.10%	

A plot of the data in the Table 3.5 is presented in Figures 3.25-3.26. Error bars represent the 95% CI.

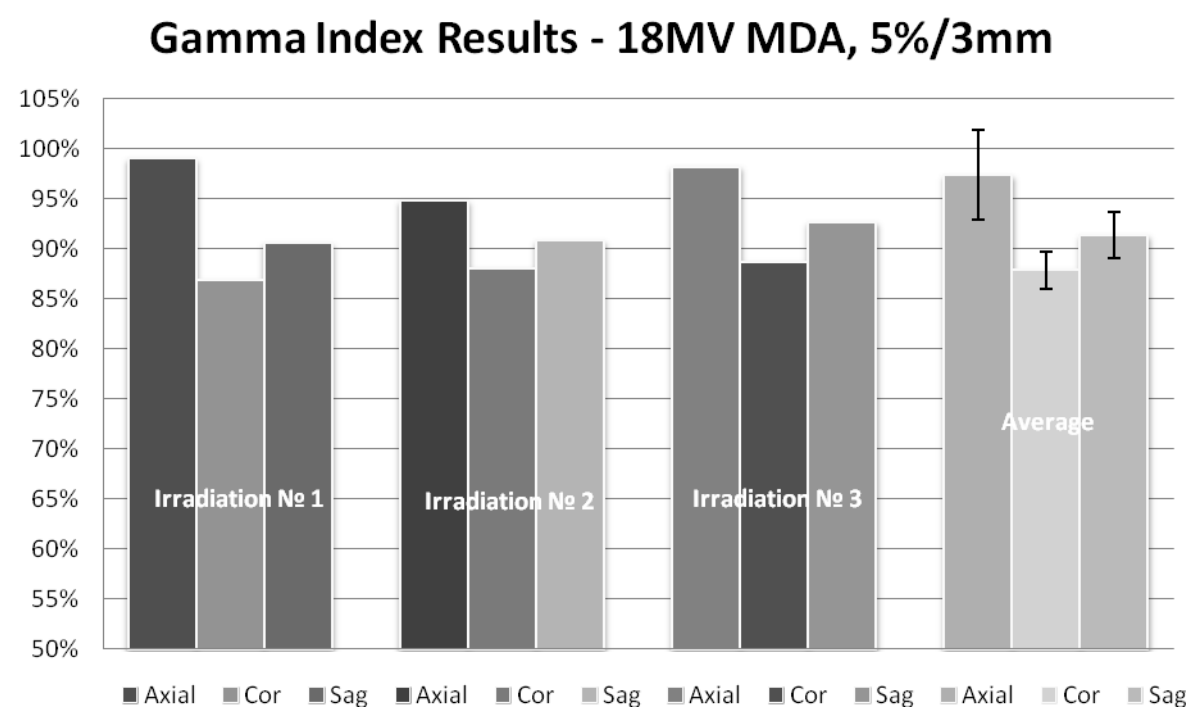


Figure 3.25 2D Gamma Index Results Using $\pm 5\%/3\text{mm}$ Criteria For 18 MV Plan

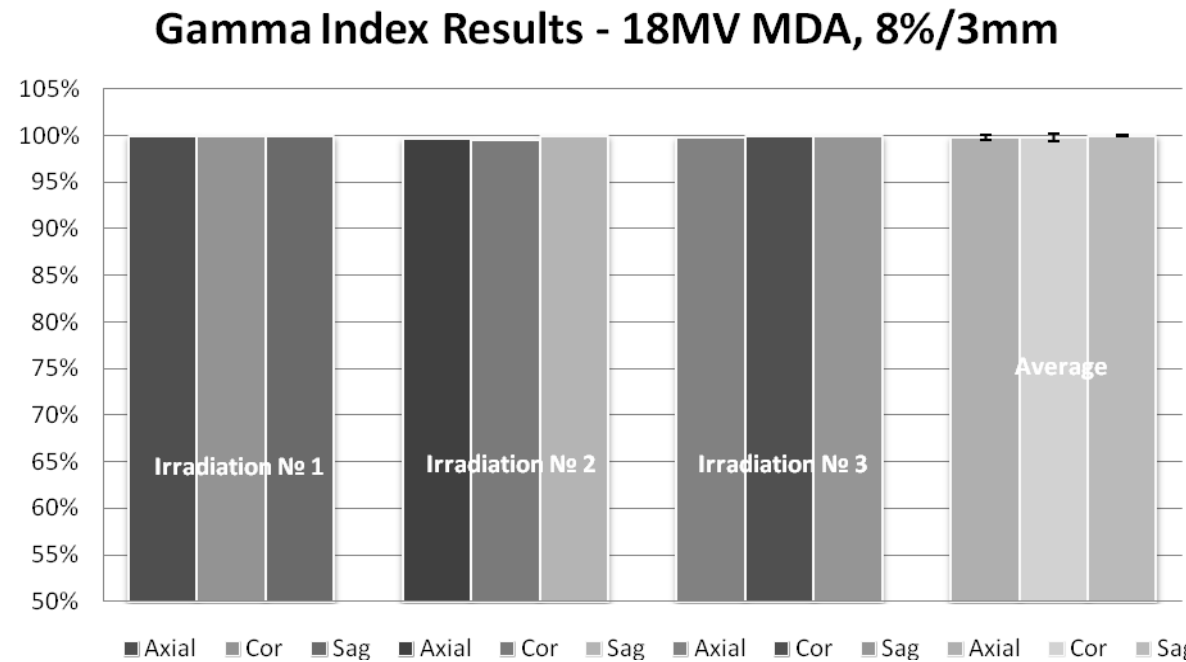


Figure 3.26 2D Gamma Index Results Using $\pm 8\%/3\text{mm}$ Criteria For 18 MV Plan

3.2.2.4 Dose Profiles Results

The example of Right-Left, Anterior-Posterior, and Superior-Inferior measured (film) and calculated (TPS) profiles for the first irradiation of the phantom in MD Anderson using the 18 MV 3D SBRT plan are shown in Figures 3.27-3.29. Plane specific profiles for other irradiations and their corresponding TLD doses are presented in the Appendix.

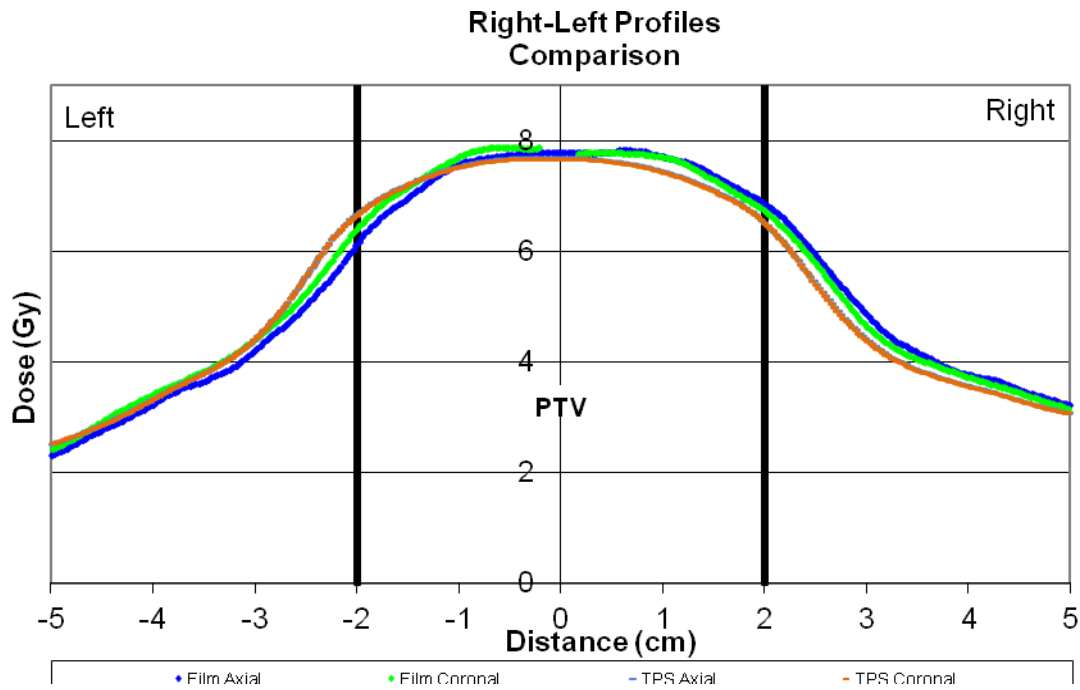


Figure 3.27 Right-Left Profiles In Axial And Coronal Planes Compared To The Calculated Dose Profiles For 18 MV Plan

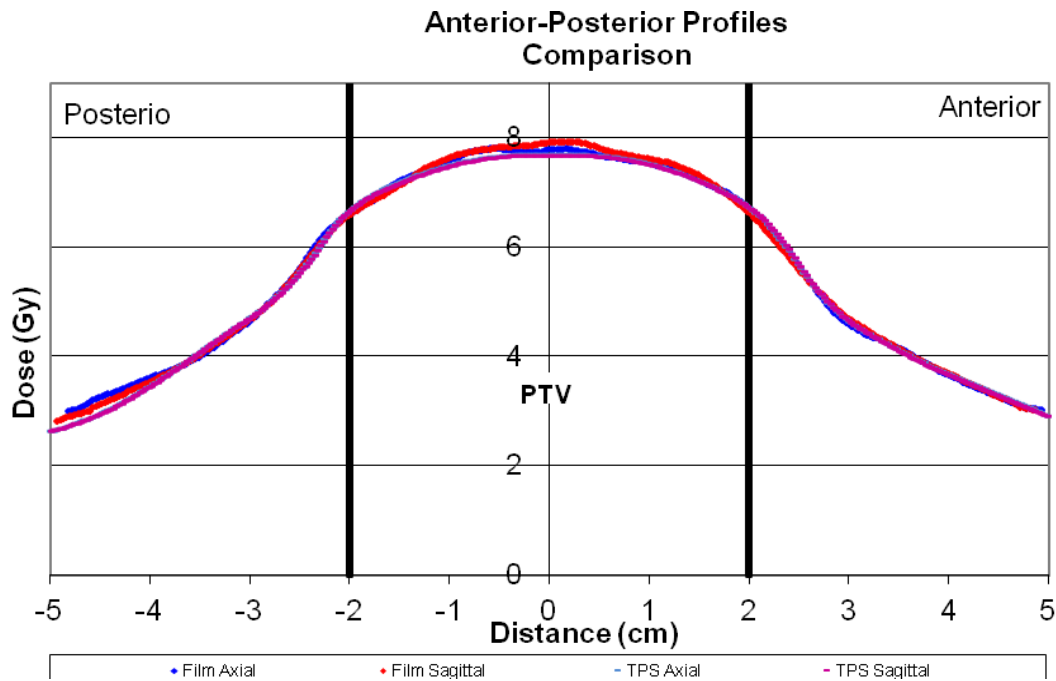


Figure 3.28 Anterior-Posterior profiles in axial and sagittal planes compared to the calculated dose profiles for 18 MV plan

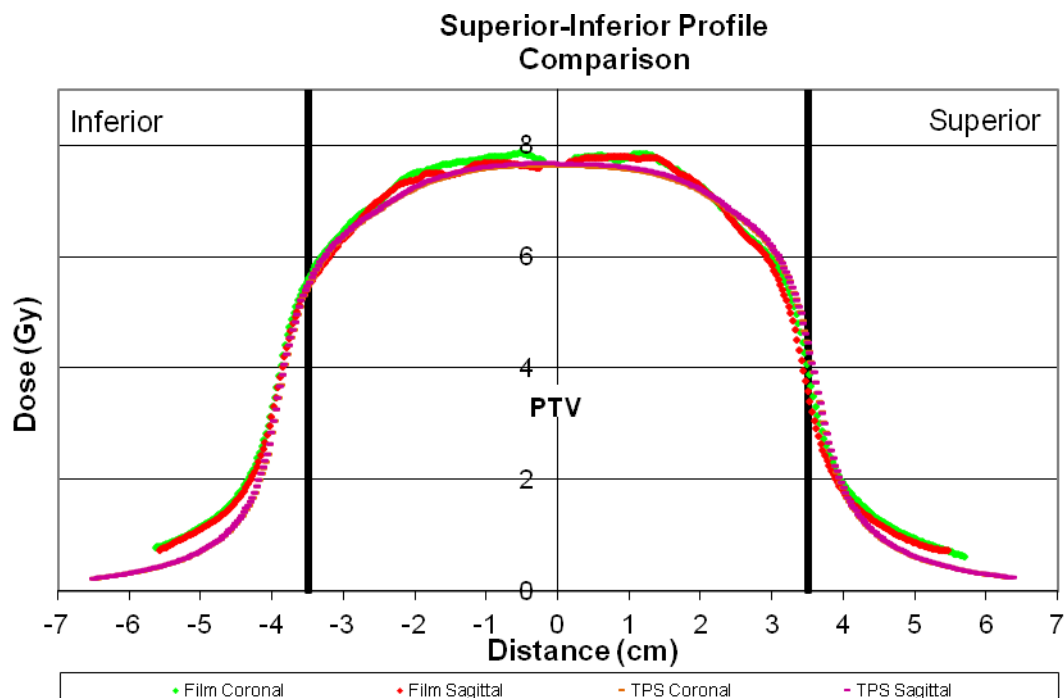


Figure 3.29 Superior-Inferior Profiles In Coronal And Sagittal Planes Compared To The Calculated Dose Profiles For 18 MV Plan

3.3 University of Alabama at Birmingham Medical Center Treatment Plans

The 6 MV treatment plan designed with the research Eclipse treatment planning system at MD Anderson Cancer Center was imported into the University of Alabama Medical Center clinical Eclipse TPS (chapter 2.3.1). The same version of AAA (v.8.9.08) heterogeneity correction was used to recalculate the dose using UAB beam models. Field placements, target coverage, and critical organ dose limits were identical for all plans (chapter 2.3.1). From this plan 15 MV, 6 MV FFF, and 10MV FFF plans were created by modifying each field's beam energy to each plan's respective values while keeping other parameters unchanged.

3.3.1 UAB: 3D SBRT 6 MV Plan

3.3.1.1 Plan Details

Figure 3.30 represents a 3-plane view of the tumor and the calculated isodose map. Calculated dose takes advantage of AAA heterogeneity correction and demonstrates an excellent conformity in all three planes. Figure 3.31 shows a magnified view of the same axial plane.

Figure 3.32 shows a Dose Volume Histogram for the calculated dose distribution. As with previously discussed treatment plans the radiation doses to non-tumor tissues such as lung, heart, and spine were substantially lower than the established RTOG and RPC limits while the tumor was covered according to the prescribed dose.



Figure 3.30 3-Plane View Of The Tumor And The Isodose Map

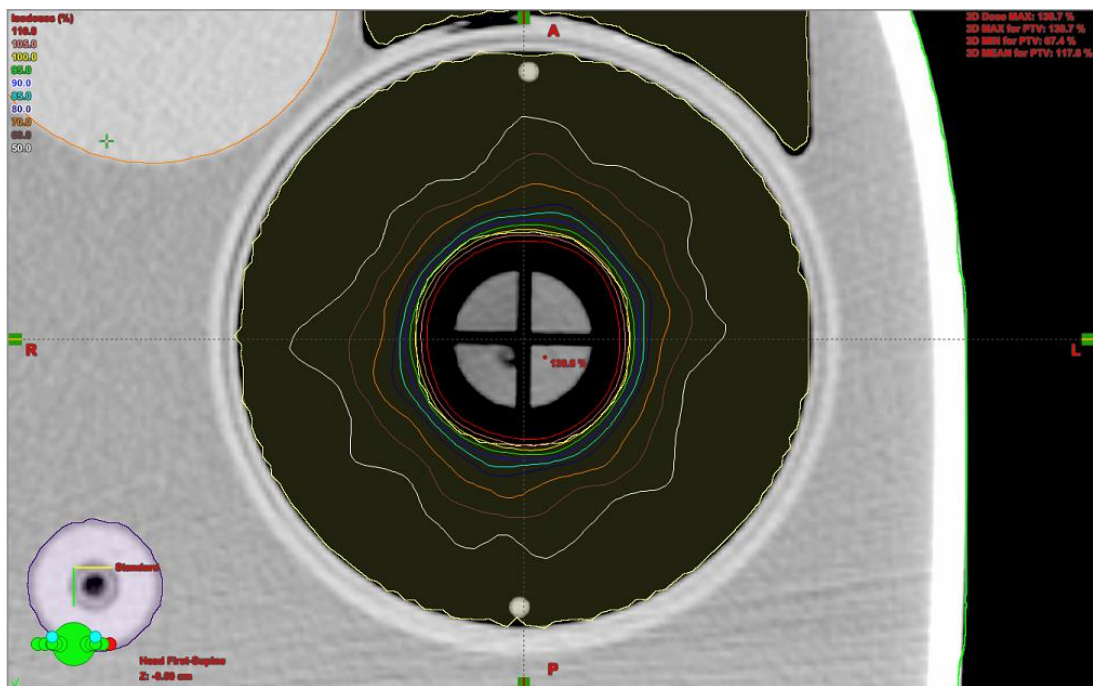


Figure 3.31 A Magnified Axial Plane View Of The Tumor And The Isodose Map

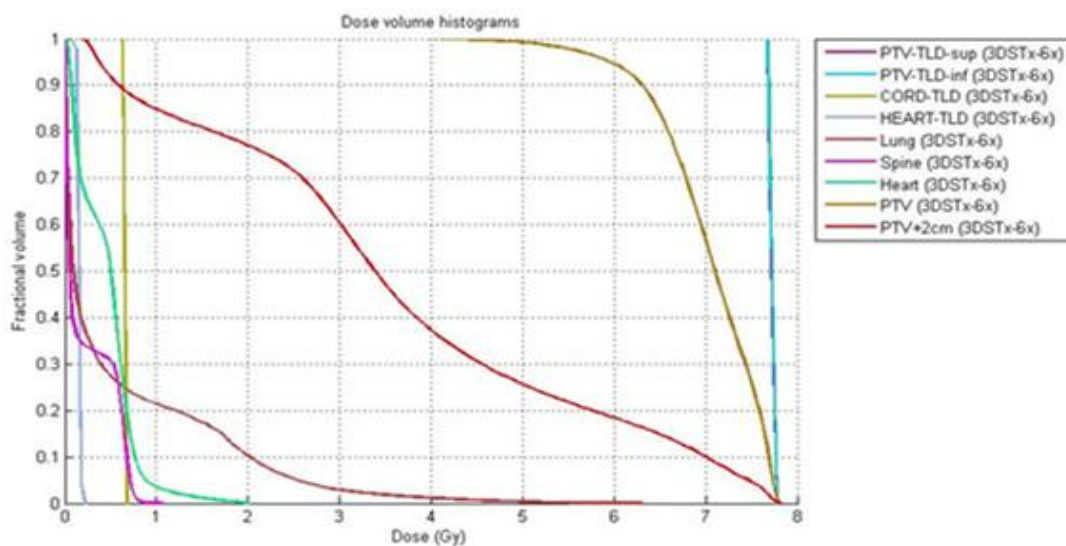


Figure 3.32 6MV 3D SBRT Plan – Dose Volume Histogram

3.3.1.2 Target TLD Results

Table 3.6 shows superior and inferior target TLD data corrected for daily output and Figure 3.33 displays measured-to-predicted dose ratios for target TLDs. The averages have corresponding error bars representing 95% confidence intervals (CI) plotted as well.

Table 3.6 Target TLD Results. 6 MV, UAB

Plan: 6 MV, UAB, TrueBeam STx							
Phantom Irradiation №	TLD Dose, Gy		Daily Output Correction	Corrected TLD Dose, Gy		Eclipse Calculated Dose, Gy	
	PTV TLD_sup	PTV TLD_inf		PTV TLD_sup	PTV TLD_inf	PTV TLD_sup	PTV TLD_inf
1	7.3475	7.2994	0.988	7.4366	7.3879	7.744	7.749
2	7.2584	7.3451		7.3465	7.4342		
3	7.3296	7.3494		7.4185	7.4385		
Average				7.4005	7.4202	7.747	
Measured/Predicted Ratio				0.956	0.958	0.957	

TLD Results - 6MV Plan, UAB

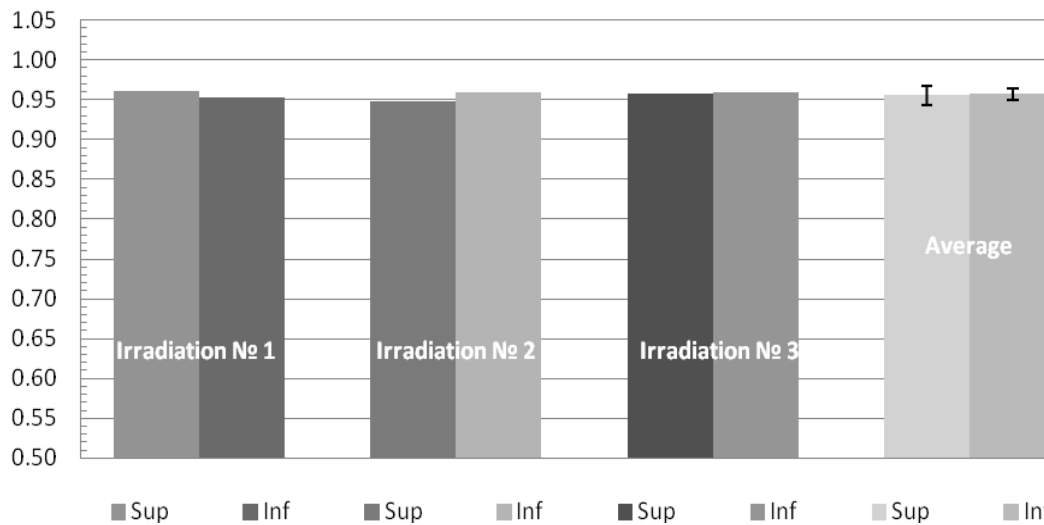


Figure 3.33 Measured-to-predicted dose ratios of target TLDs for 6 MV plan (UAB MC)

3.3.1.3 2D Gamma Index Analysis Results

Figures 3.34-3.36 show examples of 2D gamma index results for the first irradiation of the phantom in UAB Medical Center using 6 MV 3D SBRT plan and a $\pm 5\%/3\text{mm}$ criteria. Gamma analysis results using a $\pm 8\%/3\text{mm}$ criteria, as well as results for other irradiations are presented in the Appendix.

Table 3.7 summarizes the 2D gamma index results for all three irradiations (using the 6 MV plan) of the RPC phantom at University of Alabama at Birmingham.

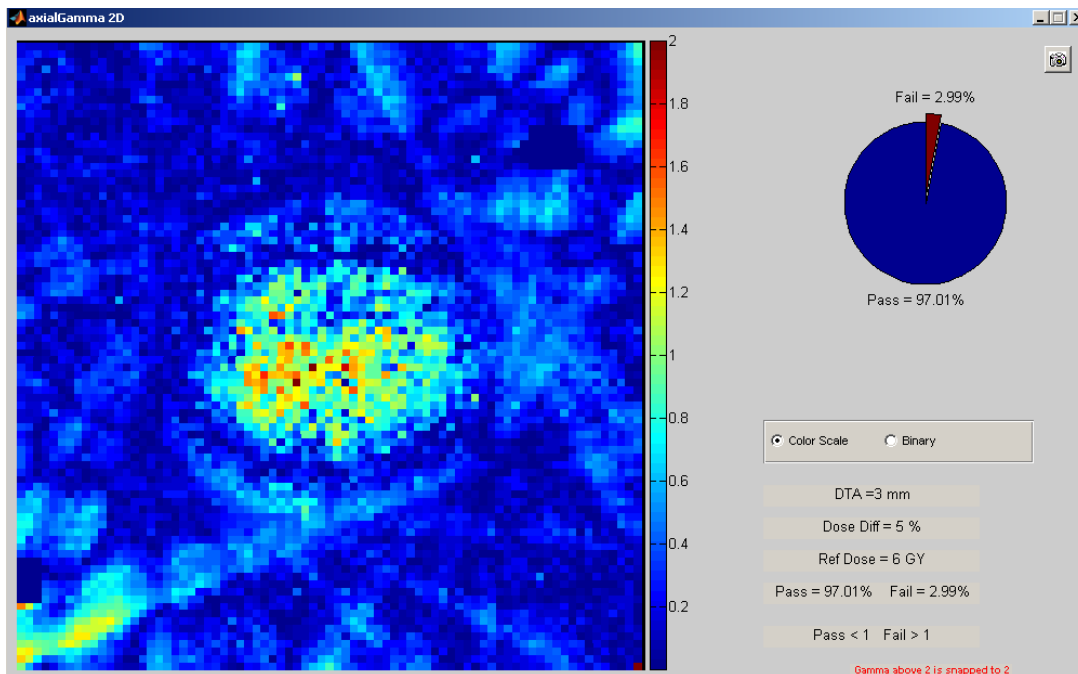


Figure 3.34 2D Gamma Index Results: $\pm 5\%/3\text{mm}$, Axial Plane For 6 MV Plan

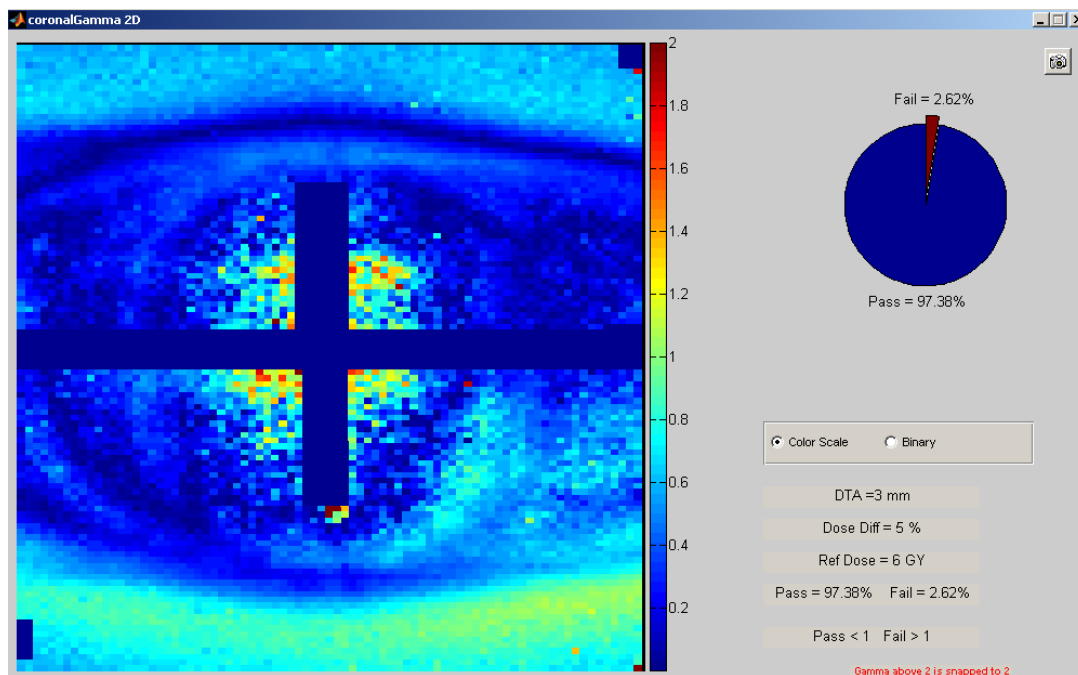


Figure 3.35 2D Gamma Index Results: $\pm 5\%/3\text{mm}$, Coronal Plane For 6 MV Plan

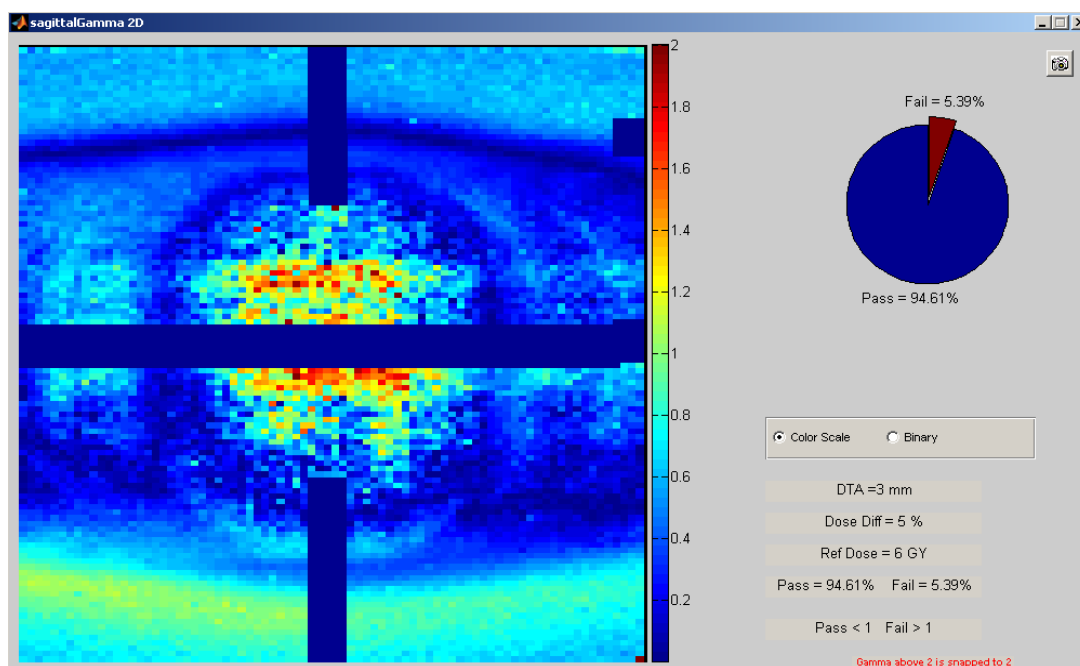


Figure 3.36 2D Gamma Index Results: $\pm 5\%/3\text{mm}$, Sagittal Plane For 6 MV Plan

Table 3.7 6 MV Plan 2D Gamma Index Results, UAB
Plan: 6 MV, UAB, TrueBeam STx

Phantom Irrad.No	Gamma Index Analysis Criteria	Orthogonal Plane Passing Rate, %			Average 3-planes, %	Standard Deviation 3-planes
		Axial	Coronal	Sagittal		
1	$\pm 5\%/3\text{mm}$	97.0%	97.4%	94.6%	96.3%	1.50%
	$\pm 8\%/3\text{mm}$	99.9%	99.7%	99.1%	99.6%	0.40%
2	$\pm 5\%/3\text{mm}$	95.1%	97.0%	93.2%	95.1%	1.90%
	$\pm 8\%/3\text{mm}$	99.1%	99.8%	98.7%	99.2%	0.59%
3	$\pm 5\%/3\text{mm}$	97.7%	97.3%	90.5%	95.2%	4.03%
	$\pm 8\%/3\text{mm}$	99.7%	99.6%	98.6%	99.3%	0.65%
Ave. Passing Rate – All Irradiations, %	$\pm 5\%/3\text{mm}$	96.6%	97.2%	92.8%	95.6%	
	$\pm 8\%/3\text{mm}$	99.6%	99.7%	98.8%	99.4%	
Std Deviation – All Irradiations, %	$\pm 5\%/3\text{mm}$	1.35%	0.20%	2.07%	0.68%	
	$\pm 8\%/3\text{mm}$	0.41%	0.11%	0.30%	0.19%	

A plot of the data in the Table 3.7 is presented in Figures 3.37-3.38. Error bars represent the 95% CI.

Gamma Index Results - 6MV UAB, 5%/3mm

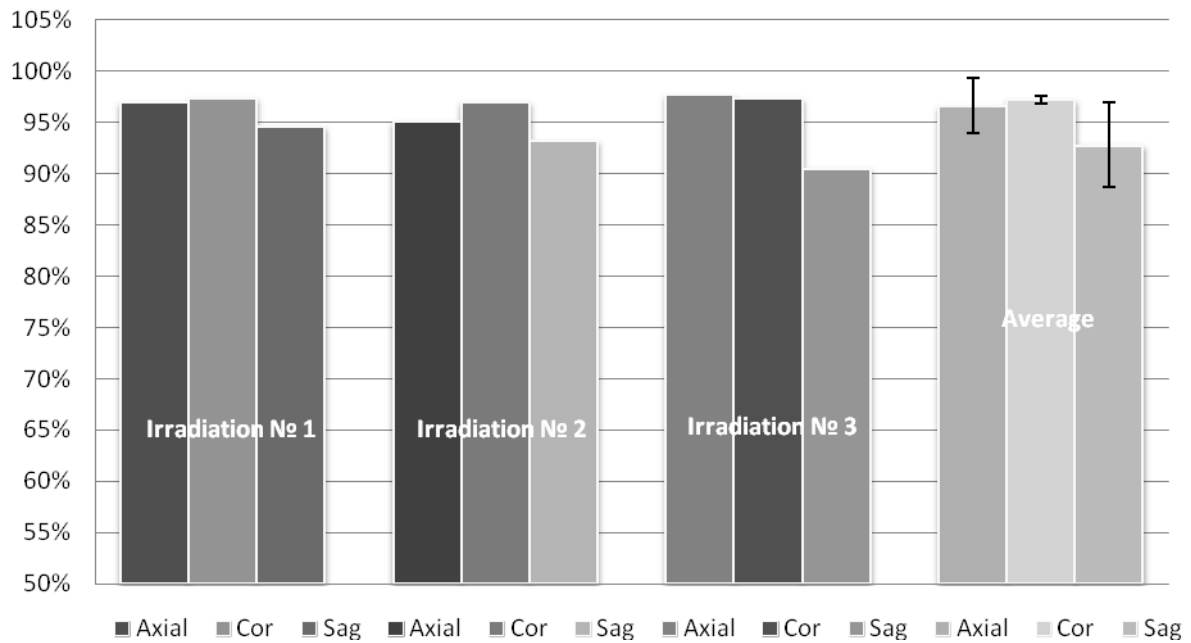


Figure 3.37 2D Gamma Index Results Using $\pm 5\%/3\text{mm}$ Criteria For 6 MV Plan

Gamma Index Results - 6MV UAB, 8%/3mm

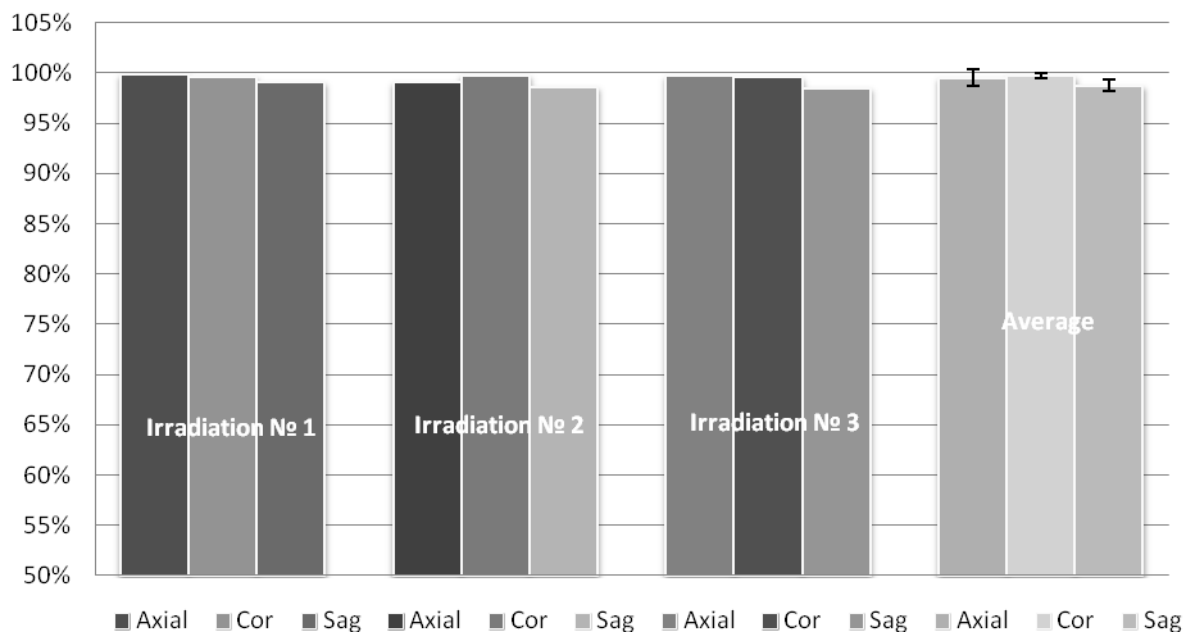


Figure 3.38 2D Gamma Index Results Using $\pm 8\%/3\text{mm}$ Criteria For 6 MV Plan

3.3.1.4 Dose Profiles Results

The example of Right-Left, Anterior-Posterior, and Superior-Inferior measured (film) and calculated (TPS) profiles for the first irradiation of the phantom in UAB Medical Center using the 6 MV 3D SBRT plan are shown in Figures 3.39-3.41. Plane specific profiles for other irradiations and their corresponding TLD doses are presented in the Appendix.

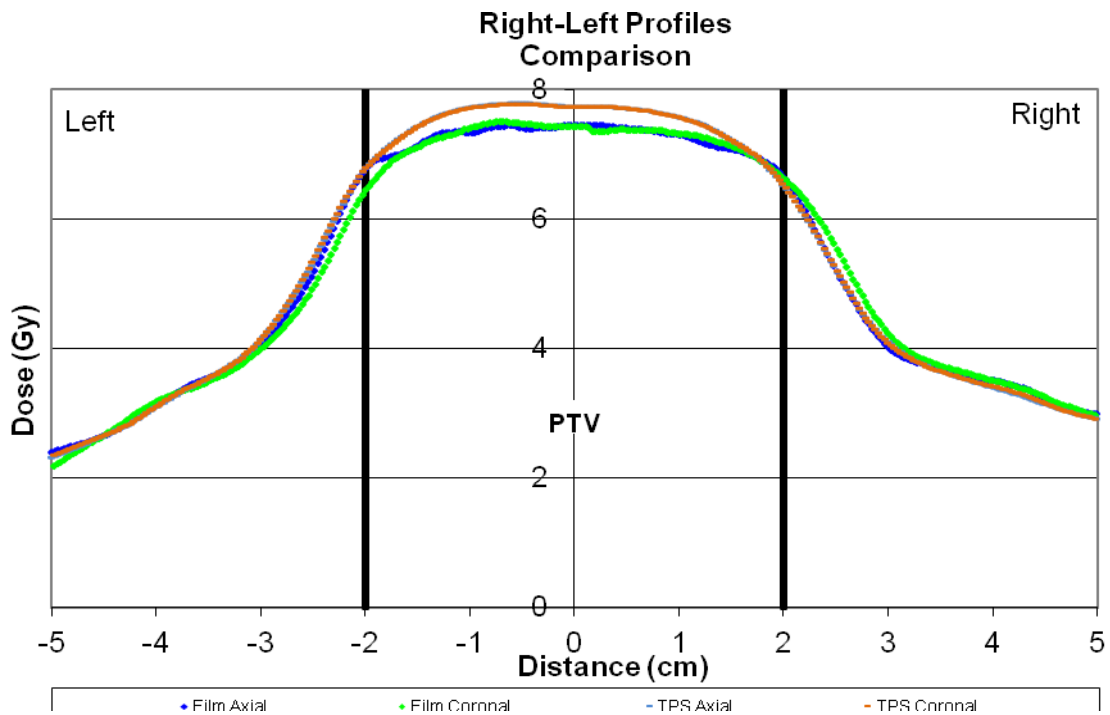


Figure 3.39 Right-Left Profiles In Axial And Coronal Planes Compared To The Calculated Dose Profiles For 6 MV Plan

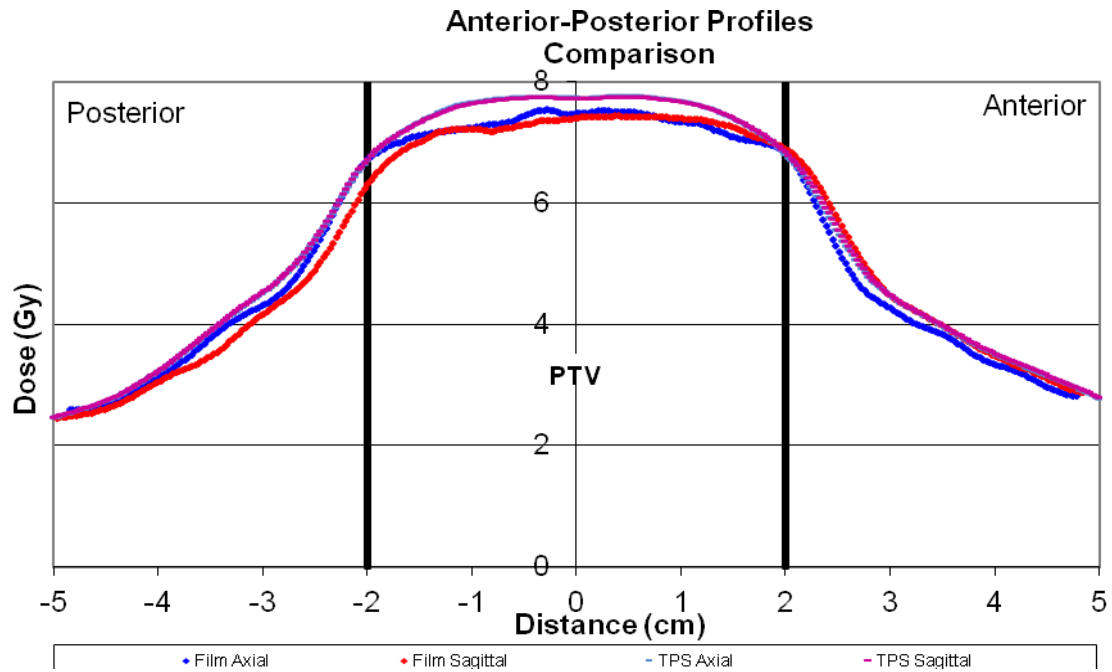


Figure 3.40 Anterior-Posterior Profiles In Axial And Sagittal Planes Compared To The Calculated Dose Profiles For 6 MV Plan

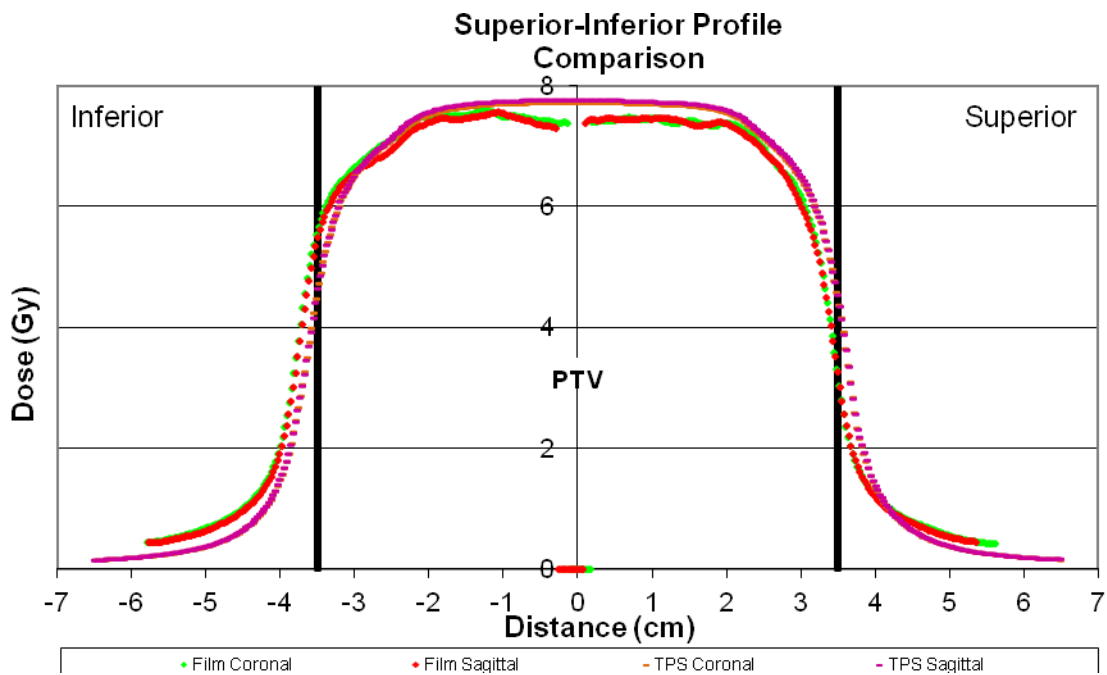


Figure 3.41 Superior-Inferior Profiles In Coronal And Sagittal Planes Compared To The Calculated Dose Profiles For 6 MV Plan

3.3.2 UAB: 3D SBRT 15 MV Plan

3.3.2.1 Plan Details

Figure 3.42 represents a 3-plane view of the tumor and the calculated isodose map. Calculated dose demonstrates a good conformity in all three planes. A magnified view of the same axial plane is shown in Figure 3.43.



Figure 3.42 3-Plane View Of The Tumor And The Isodose Map



Figure 3.43 A Magnified Axial Plane View Of The Tumor And The Isodose Map

Figure 3.44 shows a Dose Volume Histogram for the calculated dose distribution. As with previously discussed treatment plans the radiation doses to non-tumor tissues such as lung, heart, and spine were substantially lower than the established RTOG and RPC limits while the tumor was covered according to the prescribed dose.

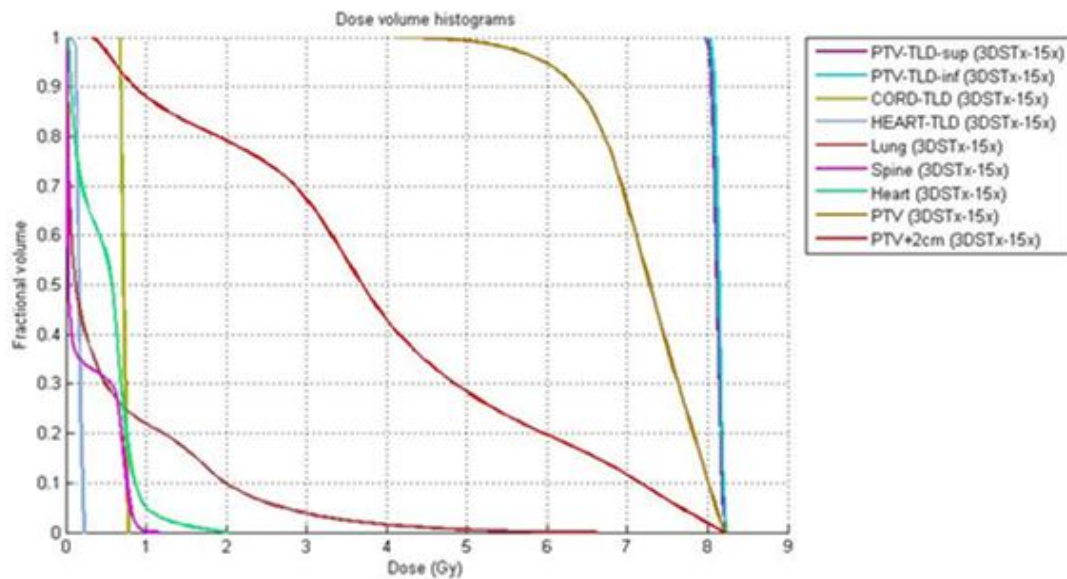


Figure 3.44 15MV 3D SBRT Plan – Dose Volume Histogram

3.3.2.2 Target TLD Results

Table 3.8 shows superior and inferior target TLD data corrected for daily output and Figure 3.45 displays measured-to-predicted dose ratios for target TLDs. The averages have error bars representing the 95% confidence interval (CI) plotted as well.

Table 3.8 Target TLD Results. 15 MV, UAB

Plan: 15 MV, UAB, TrueBeam STx							
Phantom Irradiation №	TLD Dose, Gy		Daily Output Correction	Corrected TLD Dose, Gy		Eclipse Calculated Dose, Gy	
	PTV TLD_sup	PTV TLD_inf		PTV TLD_sup	PTV TLD_inf	PTV TLD_sup	PTV TLD_inf
1	7.9980	8.0035	0.987	8.1031	8.1087	8.143	8.155
2	8.0069	8.0645		8.1122	8.1704		
3	7.9545	7.9686		8.0590	8.0733		
Average				8.0914	8.1175	8.149	
Measured/Predicted Ratio				0.994	0.995	0.995	

TLD Results - 15MV Plan, UAB

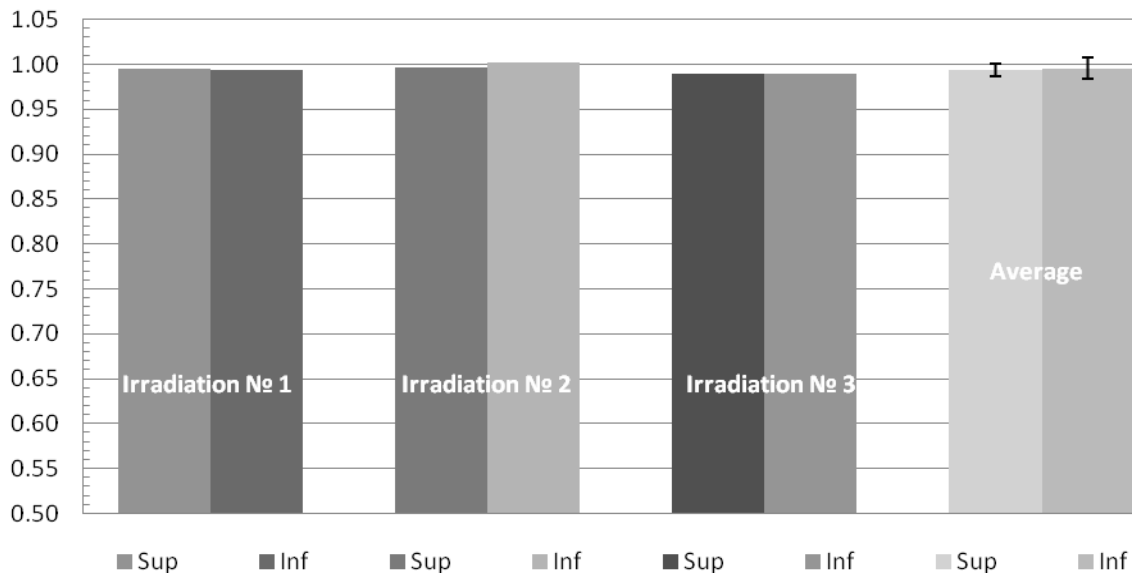


Figure 3.45 Measured-To-Predicted Dose Ratios Of Target TLDs For 15 MV Plan (UAB MC)

3.3.2.3 2D Gamma Index Analysis Results

Figures 3.46-3.48 show examples of 2D gamma index results for one of the irradiations of the phantom in UAB Medical Center using 15 MV 3D SBRT plan and $\pm 5\%/3\text{mm}$ criteria. Gamma analysis results using $\pm 8\%/3\text{mm}$ criteria, and results for other irradiations are presented in the Appendix.

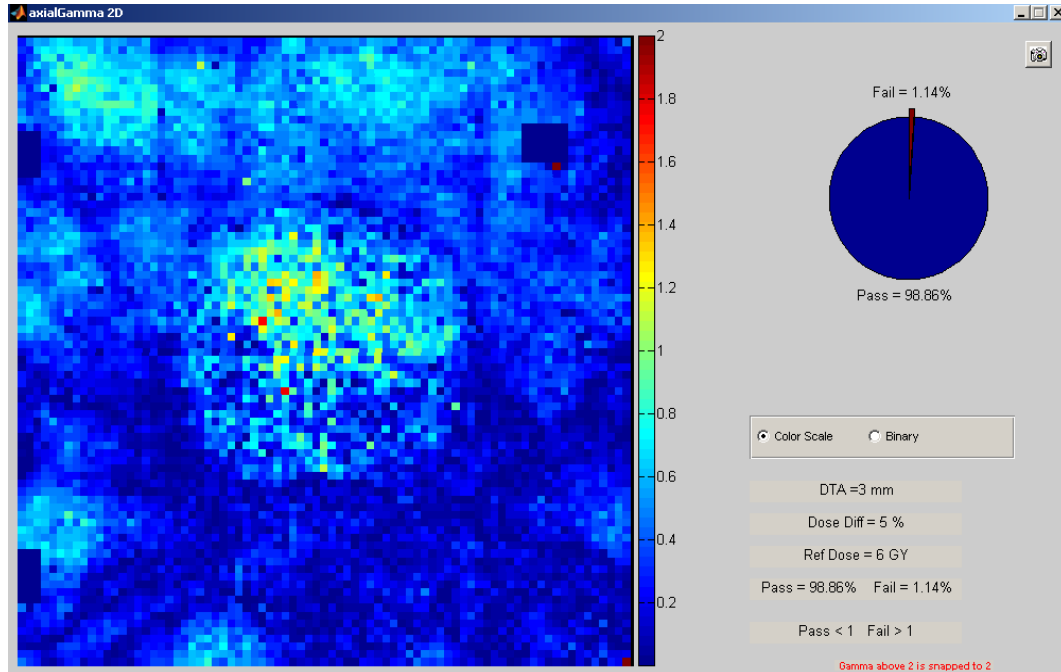


Figure 3.46 2D Gamma Index Results: $\pm 5\%/3\text{mm}$, Axial Plane For 15 MV Plan

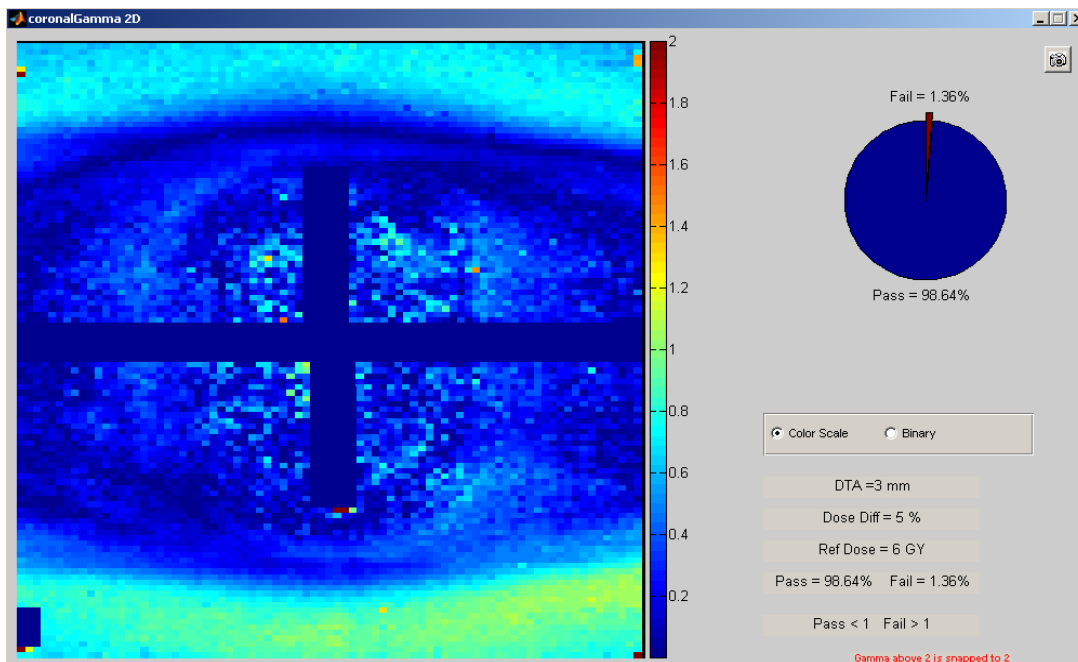


Figure 3.47 2D Gamma Index Results: $\pm 5\%/3\text{mm}$, Coronal Plane For 15 MV Plan

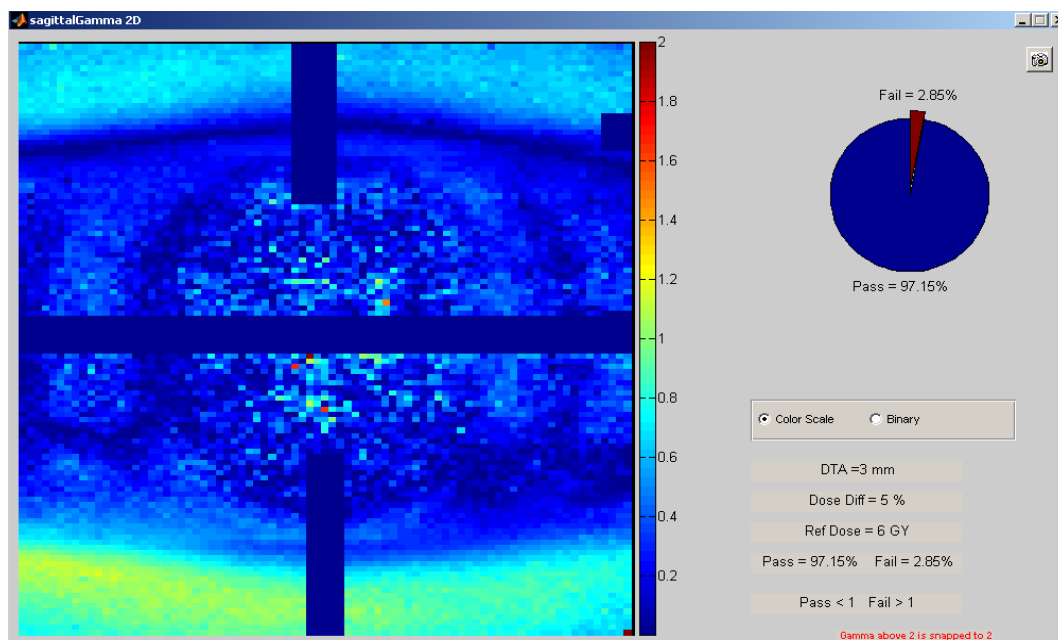


Figure 3.48 2D Gamma Index Results: $\pm 5\%/3\text{mm}$, Sagittal Plane For 15 MV Plan

Table 3.9 summarizes 2D gamma index results for all three irradiations (using the 15 MV plan) of the RPC phantom at University of Alabama at Birmingham.

Table 3.9 15 MV Plan 2D Gamma Index Results, UAB

Plan: 15 MV, UAB, TrueBeam STx						
Phantom Irrad.No	Gamma Index Analysis Criteria	Orthogonal Plane Passing Rate, %			Average 3-planes, %	Standard Deviation 3-planes
		Axial	Coronal	Sagittal		
1	±5%/3mm	100.0%	96.9%	93.0%	96.0%	2.60%
	±8%/3mm	99.9%	99.9%	99.8%	99.9%	0.04%
2	±5%/3mm	99.7%	97.4%	96.8%	98.0%	1.56%
	±8%/3mm	100.0%	99.9%	99.8%	99.9%	0.09%
3	±5%/3mm	98.9%	98.6%	97.2%	98.2%	0.93%
	±8%/3mm	100.0%	100.0%	100.0%	100.0%	0.01%
Ave. Passing Rate – All Irradiations, %	±5%/3mm	98.9%	97.6%	95.7%	97.4%	
	±8%/3mm	99.9%	99.9%	99.9%	99.9%	
Std Deviation – All Irradiations, %	±5%/3mm	0.88%	0.91%	2.27%	1.23%	
	±8%/3mm	0.03%	0.03%	0.08%	0.04%	

A plot of the data in the Table 3.9 is presented in Figures 3.49-3.50. Error bars represent the 95% CI.

Gamma Index Results - 15MV UAB, 5%/3mm

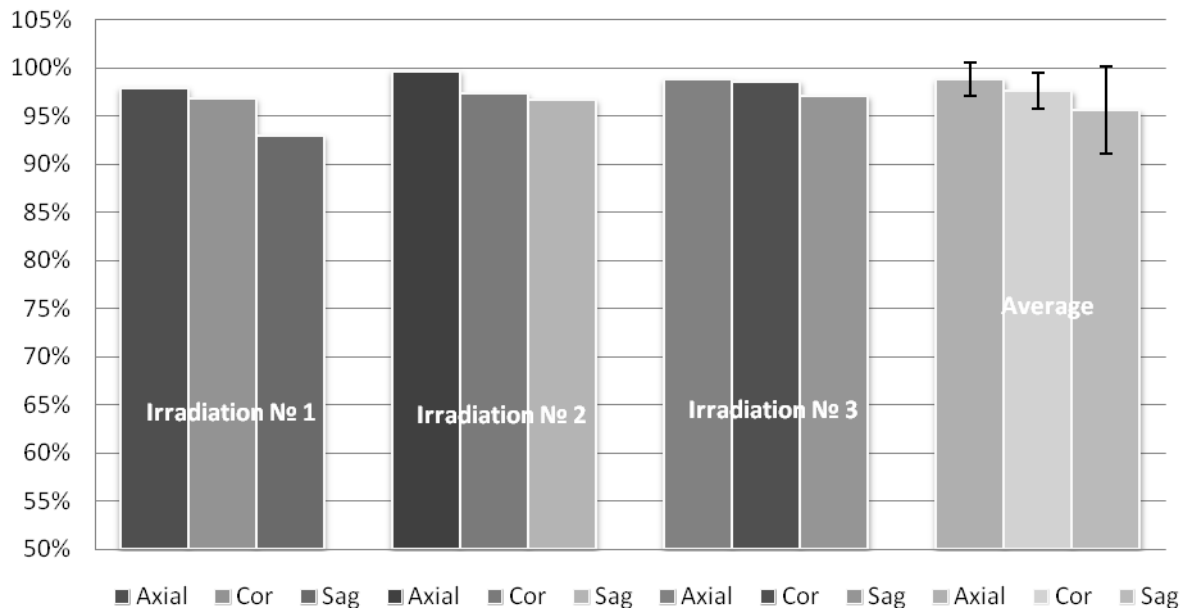


Figure 3.49 2D Gamma Index Results Using $\pm 5\%/3\text{mm}$ Criteria For 15 MV Plan

Gamma Index Results - 15MV UAB, 8%/3mm

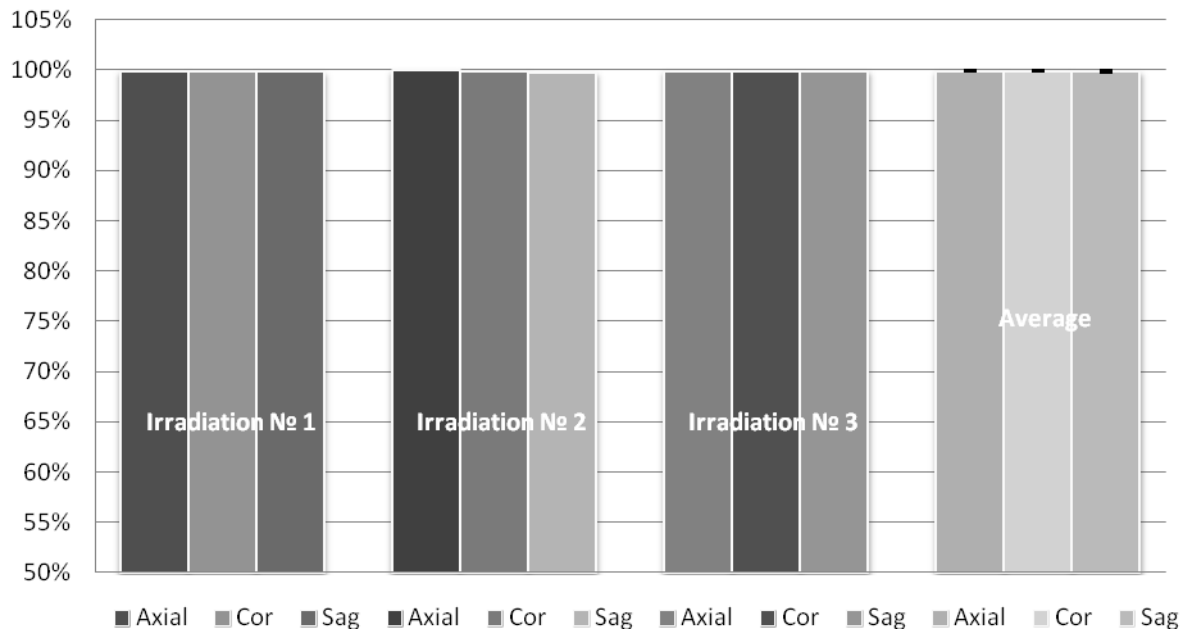


Figure 3.50 2D Gamma Index Results Using $\pm 8\%/3\text{mm}$ Criteria For 15 MV Plan

3.3.2.4 Dose Profiles Results

The example of Right-Left, Anterior-Posterior, and Superior-Inferior measured (film) and calculated (TPS) profiles for the first irradiation of the phantom in UAB Medical Center using the 15 MV 3D SBRT plan are shown in Figures 3.51-3.53. Plane specific profiles for other irradiations and their corresponding TLD doses are presented in the Appendix.

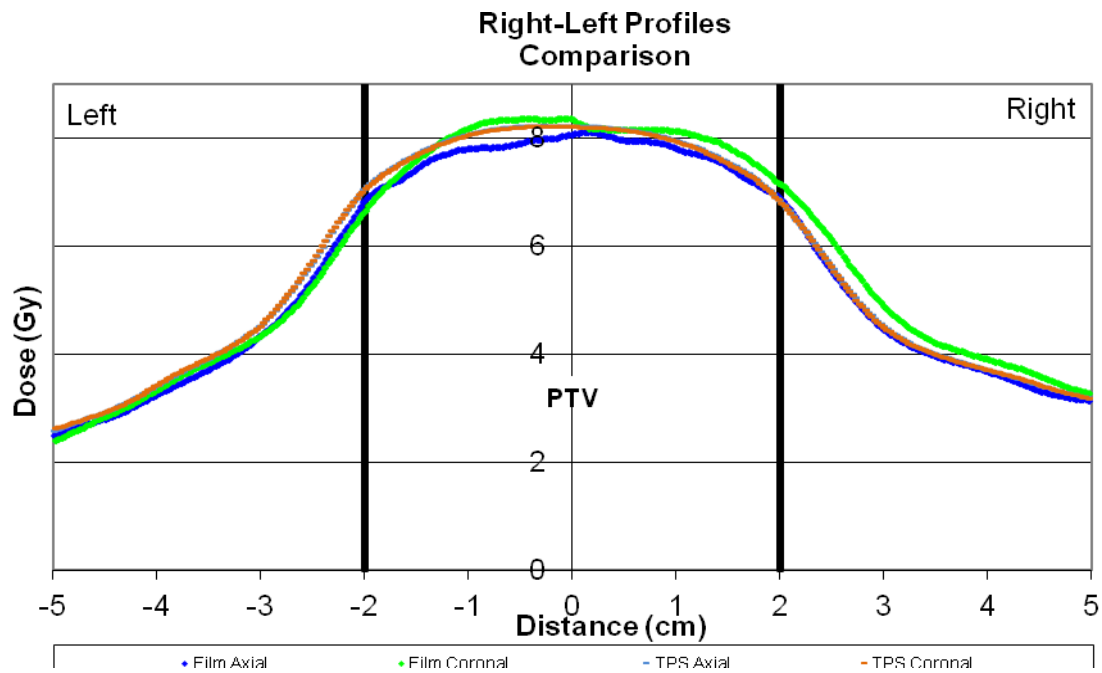


Figure 3.51 Right-Left profiles in axial and coronal planes compared to the calculated dose profiles for 15 MV plan

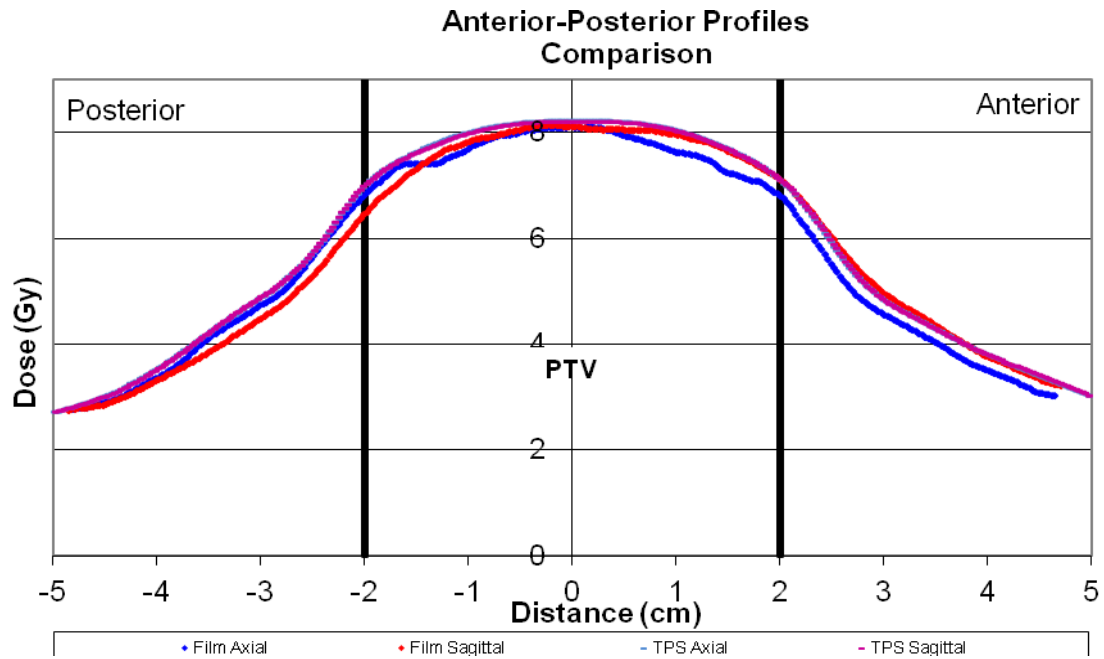


Figure 3.52 Anterior-Posterior profiles in axial and sagittal planes compared to the calculated dose profiles for 15 MV plan

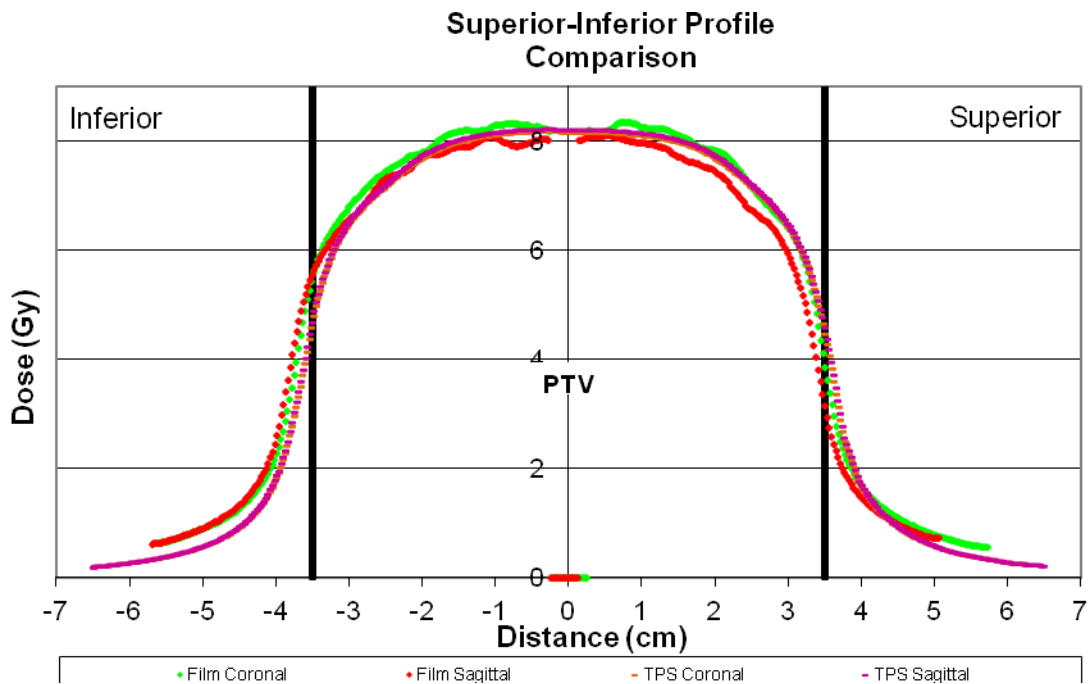


Figure 3.53 Superior-Inferior profiles in coronal and sagittal planes compared to the calculated dose profiles for 15 MV plan

3.3.3 UAB: 3D SBRT 6 MV FFF Plan

3.3.3.1 Plan Details

Figure 3.54 represents a 3-plane view of the tumor and the calculated isodose map. Calculated dose demonstrates a good conformity in all three planes. A magnified view of the same axial plane is shown in Figure 3.55.



Figure 3.54 3-Plane View Of The Tumor And The Isodose Map



Figure 3.55 A Magnified Axial Plane View Of The Tumor And The Isodose Map

Figure 3.56 shows a Dose Volume Histogram for the calculated dose distribution. As with previously discussed treatment plans the radiation doses to non-tumor tissues such as lung, heart, and spine were substantially lower than the established RTOG and RPC limits while the tumor was covered according to the prescribed dose.

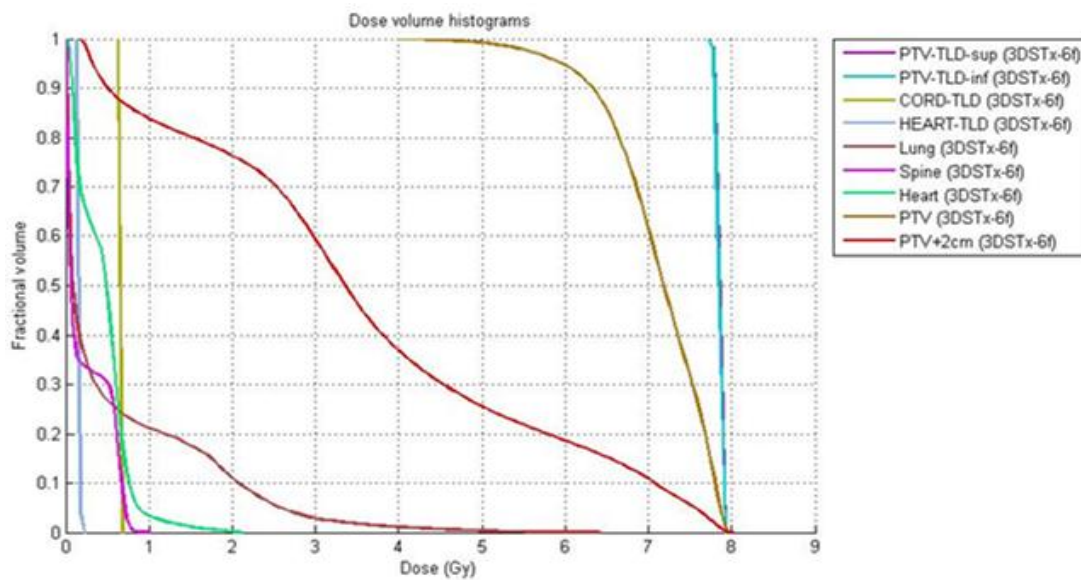


Figure 3.56 6MV FFF 3D SBRT Plan – Dose Volume Histogram

3.3.3.2 Target TLD Results

Table 3.10 shows superior and inferior target TLD data corrected for daily output and Figure 3.57 displays measured-to-predicted dose ratios for target TLDs. The averages have error bars representing the 95% confidence interval (CI) plotted as well.

Table 3.10 Target TLD Results. 6 MV FFF, UAB

Plan: 6 MV FFF, UAB, TrueBeam STx							
Phantom Irradiation №	TLD Dose, Gy		Daily Output Correction	Corrected TLD Dose, Gy		Eclipse Calculated Dose, Gy	
	PTV TLD_sup	PTV TLD_inf		PTV TLD_sup	PTV TLD_inf	PTV TLD_sup	PTV TLD_inf
1	7.4641	7.5838	0.998	7.4796	7.5996	7.874	7.866
2	7.5038	7.5646		7.5194	7.5803		
3	7.4653	7.5203		7.4809	7.5360		
Average				7.4933	7.5720	7.870	
Measured/Predicted Ratio				0.952	0.963	0.957	

TLD Results - 6MV FFF Plan, UAB

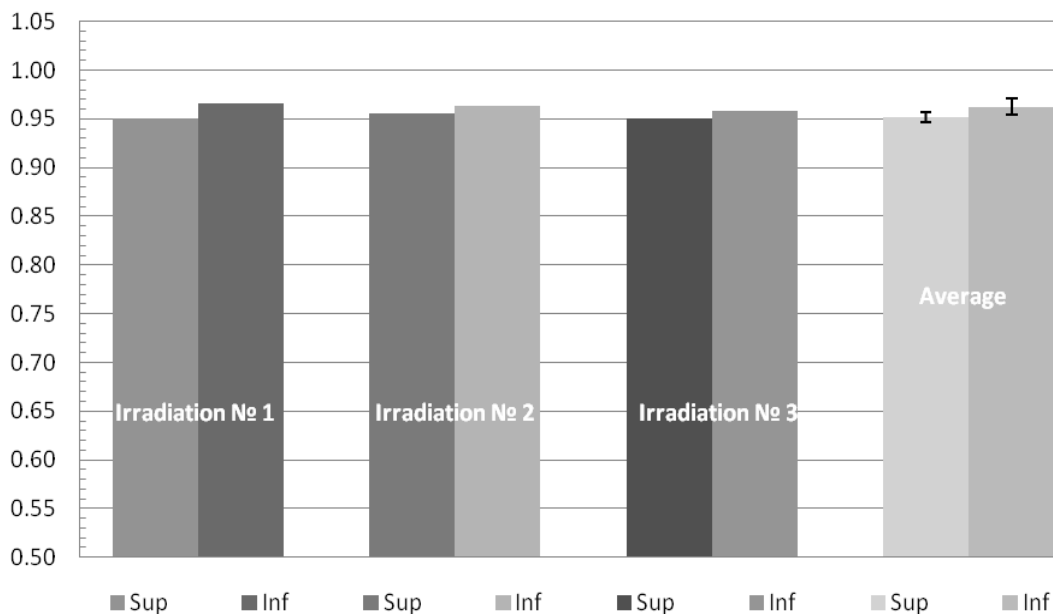


Figure 3.57 Measured-To-Predicted Dose Ratios Of Target TLDs For 6 MV FFF Plan (UAB MC)

3.3.3.3 2D Gamma Index Analysis Results

Figures 3.58-3.60 show examples of 2D gamma index results for one of the irradiations of the phantom in UAB Medical Center using the 6 MV FFF 3D SBRT plan and $\pm 5\%/3\text{mm}$ criteria. Gamma analysis results using $\pm 8\%/3\text{mm}$ criteria, as well as results for other irradiations are presented in the Appendix.

Table 3.11 summarizes 2D gamma index results for all three irradiations (using 6 MV FFF plan) of the RPC phantom at University of Alabama at Birmingham.

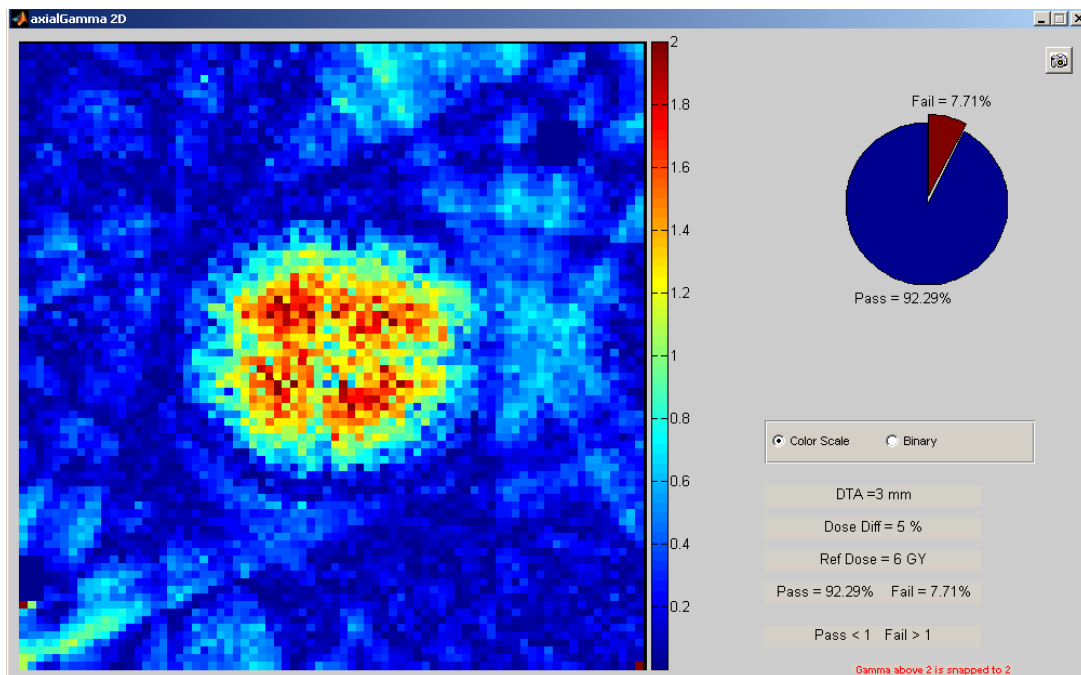


Figure 3.58 2D Gamma Index Results: $\pm 5\%/3\text{mm}$, Axial Plane For 6 MV FFF Plan

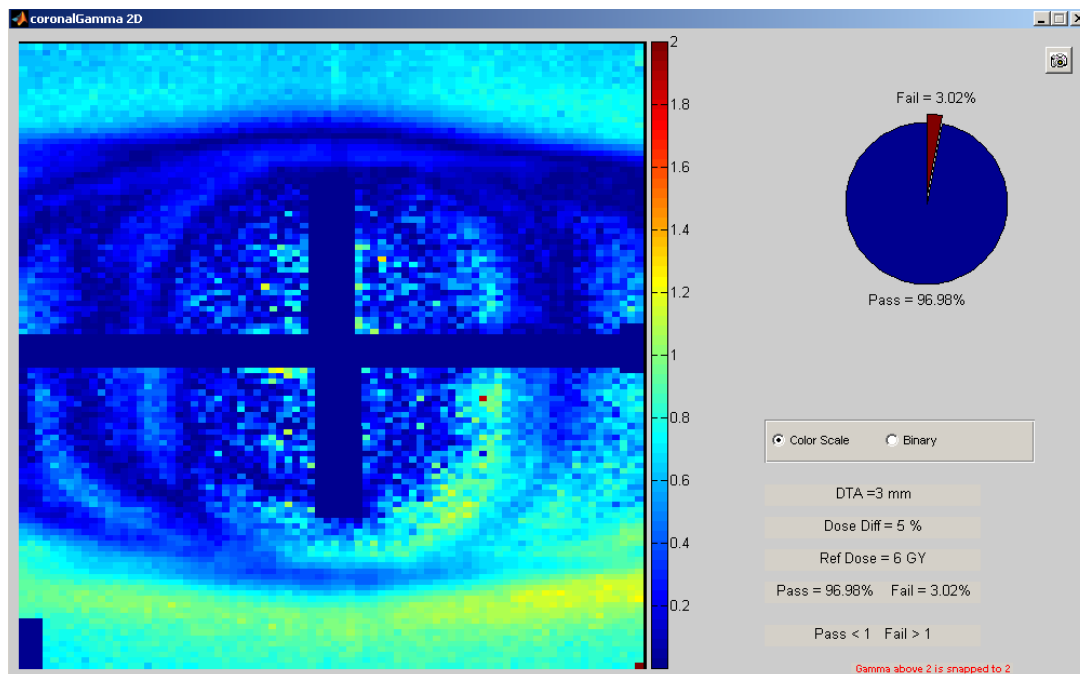


Figure 3.59 2D Gamma Index Results: $\pm 5\%/3\text{mm}$, Coronal Plane For 6 MV FFF Plan

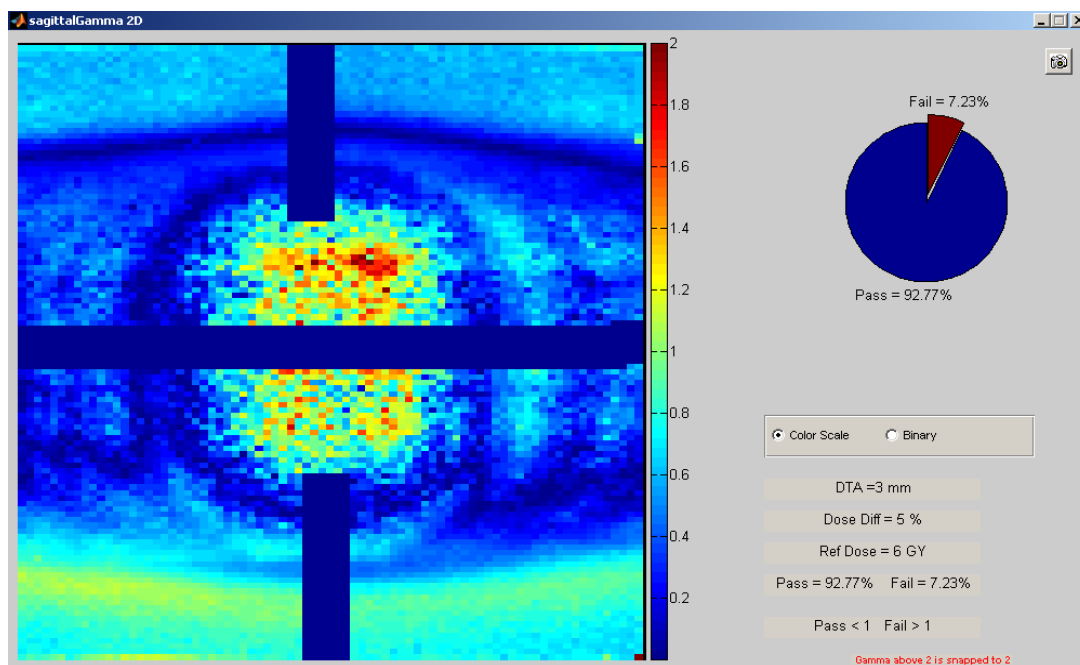


Figure 3.60 2D Gamma Index Results: $\pm 5\%/3\text{mm}$, Sagittal Plane For 6 MV FFF Plan

Table 3.11 6 MV FFF Plan 2D Gamma Index Results, UAB

Plan: 6 MV FFF, UAB, TrueBeam STx

Phantom Irrad.№	Gamma Index Analysis Criteria	Orthogonal Plane Passing Rate, %			Average 3-planes, %	Standard Deviation 3-planes
		Axial	Coronal	Sagittal		
1	±5%/3mm	92.3%	97.0%	92.8%	94.0%	2.58%
	±8%/3mm	99.9%	99.9%	99.2%	99.7%	0.39%
2	±5%/3mm	96.5%	97.2%	88.9%	94.2%	4.62%
	±8%/3mm	99.7%	99.8%	96.4%	98.6%	1.92%
3	±5%/3mm	92.2%	96.3%	90.0%	92.8%	3.22%
	±8%/3mm	97.4%	99.6%	96.7%	97.9%	1.50%
Ave. Passing Rate – All Irradiations, %	±5%/3mm	93.7%	96.8%	90.5%	93.7%	
	±8%/3mm	99.0%	99.8%	97.44%	98.7%	
Std Deviation – All Irradiations, %	±5%/3mm	2.47%	0.47%	2.01%	0.75%	
	±8%/3mm	1.36%	0.18%	1.55%	0.89%	

A plot of the data in the Table 3.11 is presented in Figures 3.61-3.62. Error bars represent the 95% CI.

Gamma Index Results - 6MV FFF UAB, 5%/3mm

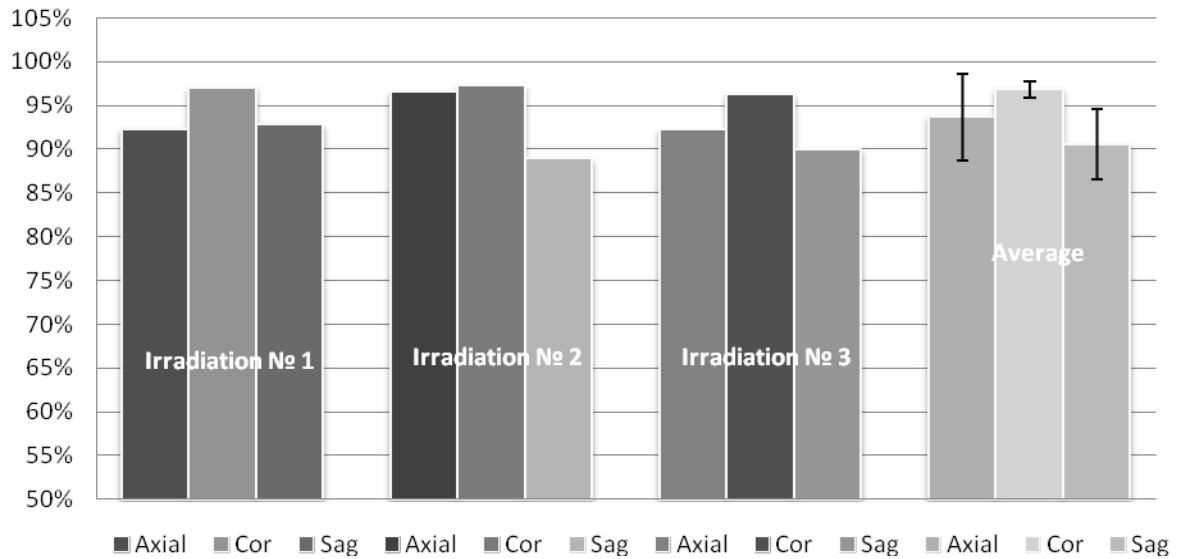


Figure 3.61 2D Gamma Index Results Using $\pm 5\%/3\text{mm}$ Criteria For 6 MV FFF Plan

Gamma Index Results - 6MV FFF UAB, 8%/3mm

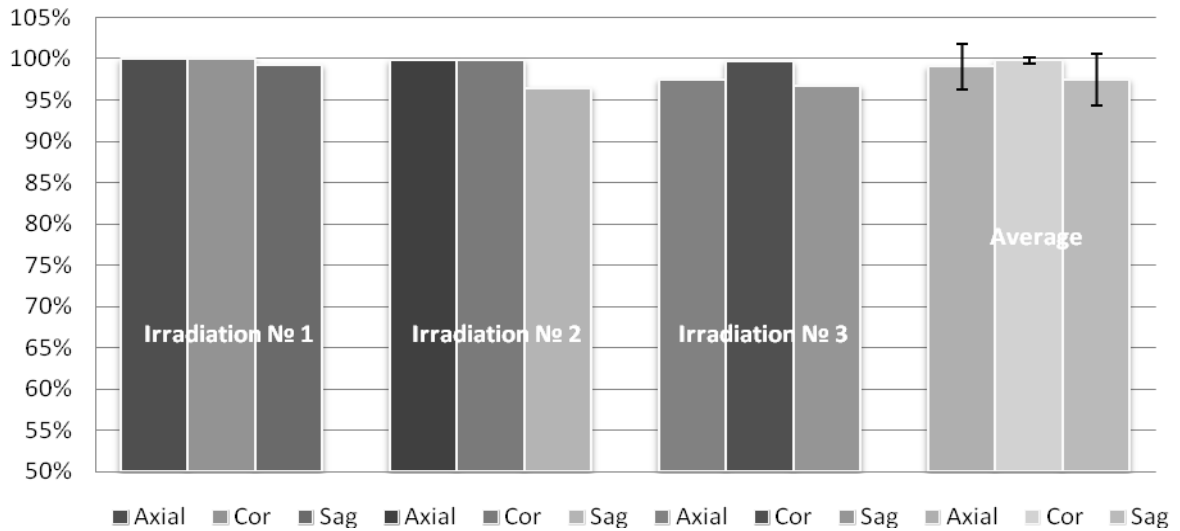


Figure 3.62 2D Gamma Index Results Using $\pm 8\%/3\text{mm}$ Criteria For 6 MV FFF Plan

3.3.3.4 Dose Profiles Results

The example of Right-Left, Anterior-Posterior, and Superior-Inferior measured (film) and calculated (TPS) profiles for the first irradiation of the phantom in UAB Medical Center using the 6 MV FFF 3D SBRT plan are shown in Figures 3.63-3.65. Plane specific profiles for other irradiations and their corresponding TLD doses are presented in the Appendix.

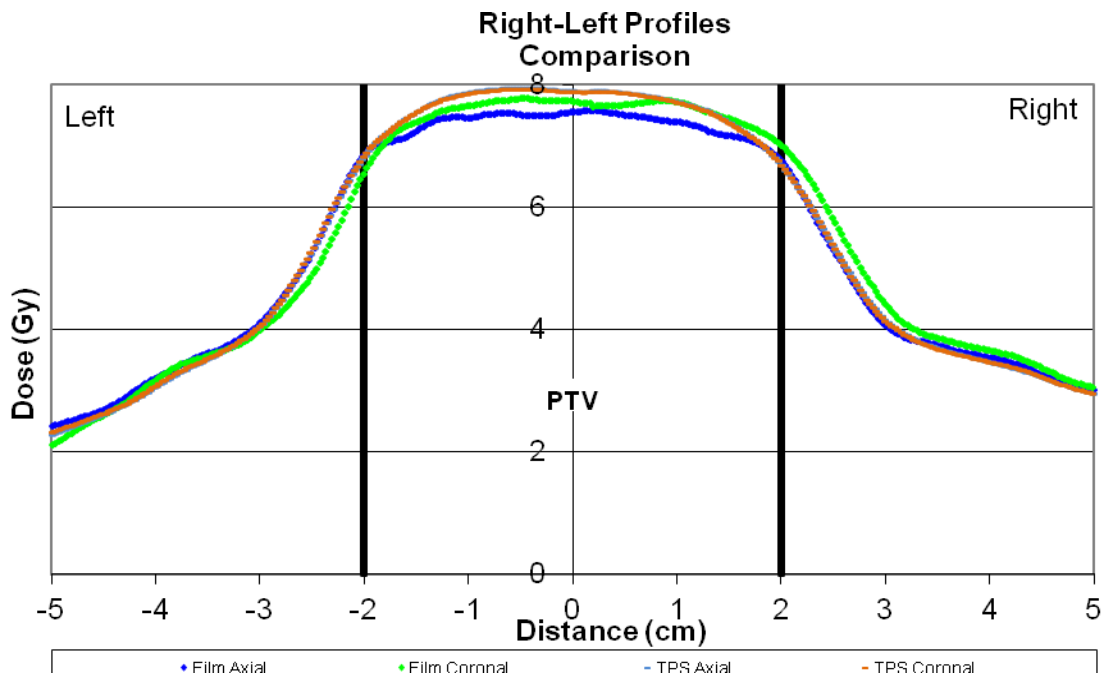


Figure 3.63 Right-Left Profiles In Axial And Coronal Planes Compared To The Calculated Dose Profiles For 6 MV FFF Plan

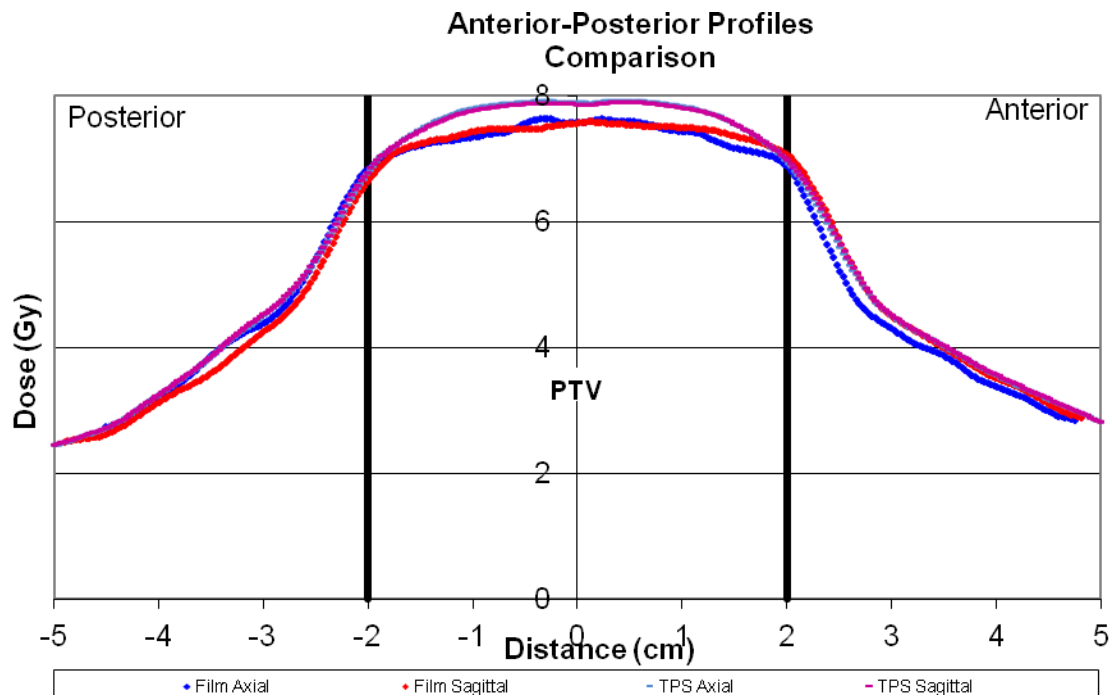


Figure 3.64 Anterior-Posterior Profiles In Axial And Sagittal Planes Compared To The Calculated Dose Profiles For 6 MV FFF Plan

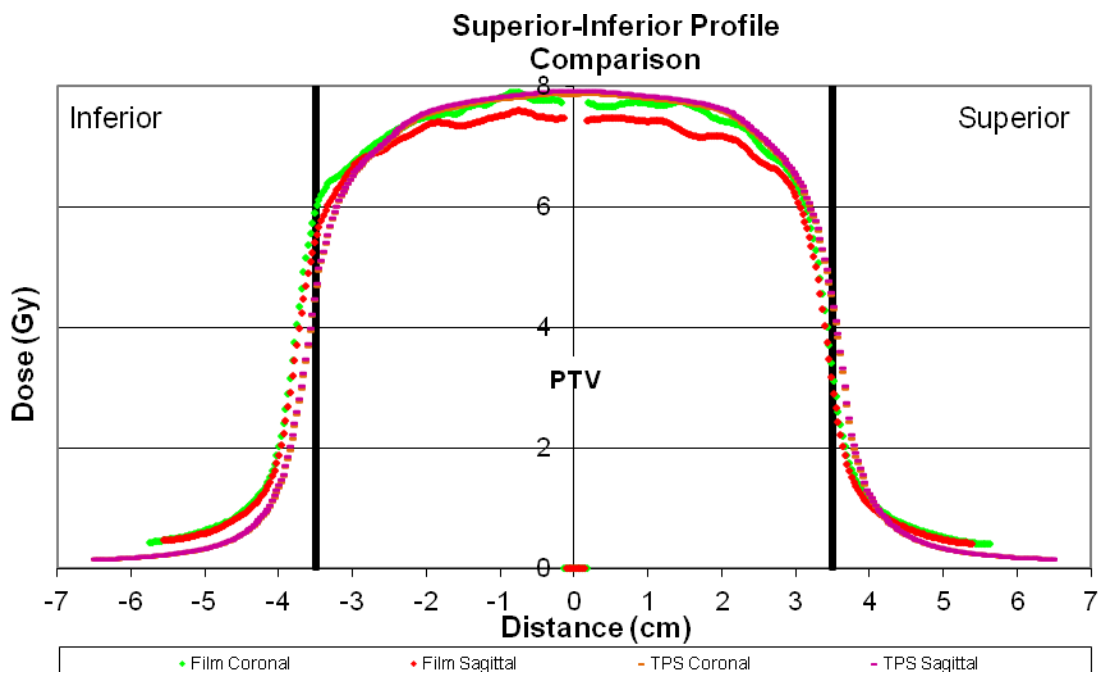


Figure 3.65 Superior-Inferior Profiles In Coronal And Sagittal Planes Compared To The Calculated Dose Profiles For 6 MV FFF Plan

3.3.4 UAB: 3D SBRT 10 MV FFF Plan

3.3.4.1 Plan Details

Figure 3.66 represents a 3-plane view of the tumor and the calculated isodose map. Calculated dose demonstrates a good conformity in all three planes. A magnified view of the same axial plane is shown in Figure 3.67.

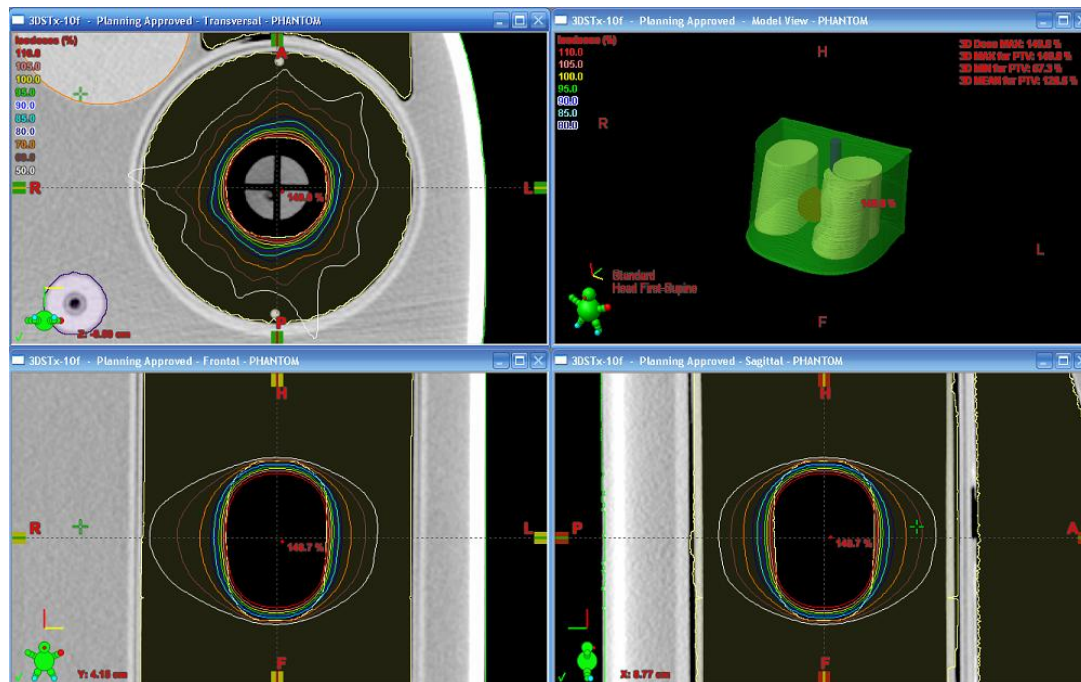


Figure 3.66 3-Plane View Of The Tumor And The Isodose Map



Figure 3.67 A Magnified Axial Plane View Of The Tumor And The Isodose Map

Figure 3.68 shows a Dose Volume Histogram for the calculated dose distribution. As with previously discussed treatment plans the radiation doses to non-tumor tissues such as lung, heart, and spine were substantially lower than the established RTOG and RPC limits while the tumor was covered according to the prescribed dose.

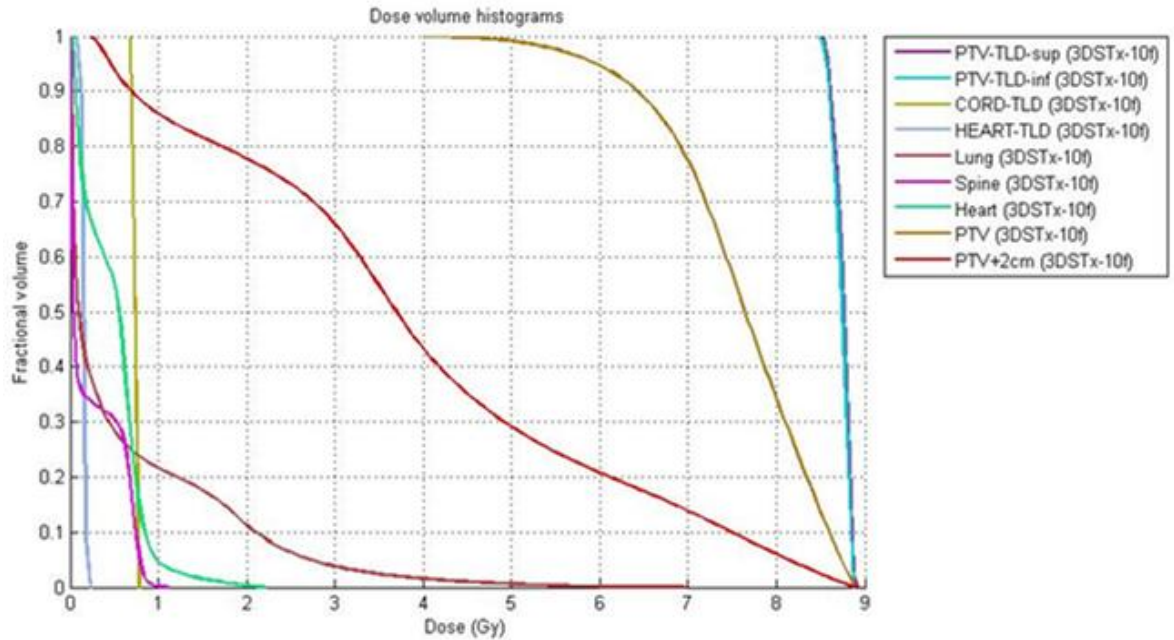


Figure 3.68 10MV FFF 3D SBRT Plan – Dose Volume Histogram

3.3.4.2 Target TLD Results

Table 3.12 shows superior and inferior target TLD data corrected for daily output and Figure 3.69 displays measured-to-predicted dose ratios for target TLDs. The averages have error bars representing the 95% confidence interval (CI) plotted as well.

Table 3.12 Target TLD Results. 10 MV FFF, UAB

Plan: 10 MV FFF, UAB, TrueBeam STx							
Phantom Irradiation №	TLD Dose, Gy		Daily Output Correction	Corrected TLD Dose, Gy		Eclipse Calculated Dose, Gy	
	PTV TLD_sup	PTV TLD_inf		PTV TLD_sup	PTV TLD_inf	PTV TLD_sup	PTV TLD_inf
1	8.5267	8.3748	0.991	8.6043	8.5551	8.776	8.750
2	8.6347	8.4756		8.7132	8.5526		
3	8.4064	8.3074		8.4828	8.3829		
Average				8.6001	8.4969	8763	
Measured/Predicted Ratio				0.980	0.971	0.976	

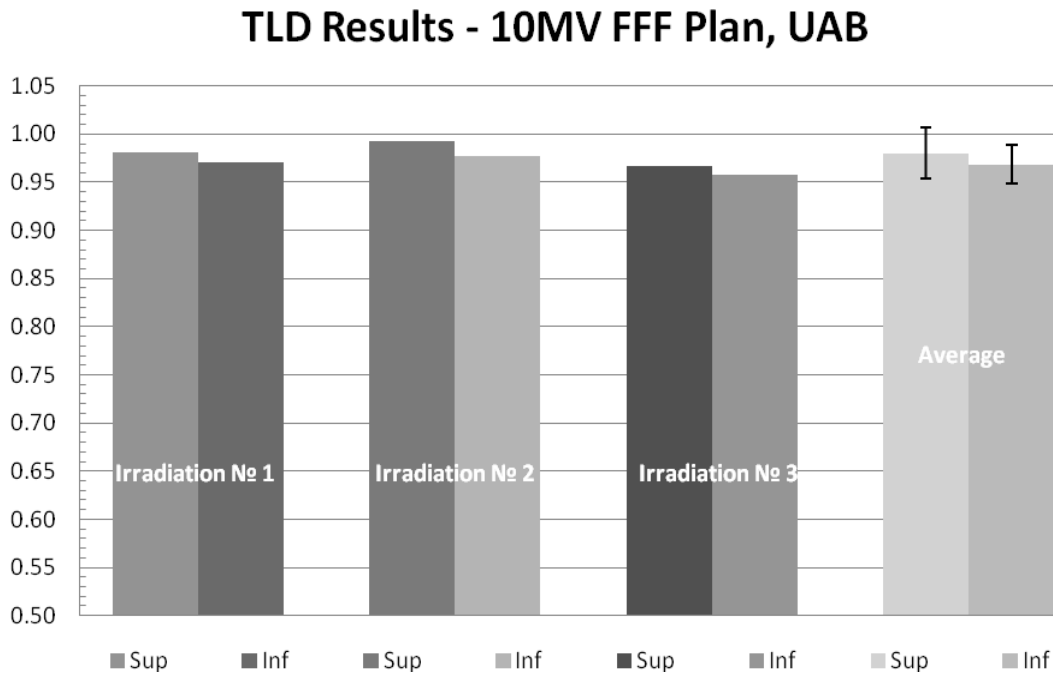


Figure 3.69 Measured-To-Predicted Dose Ratios Of Target TLDs For 10 MV FFF Plan (UAB MC)

3.3.4.3 2D Gamma Index Analysis Results

Figures 3.70-3.72 show examples of 2D gamma index results for one of the irradiations of the phantom in UAB Medical Center using the 10 MV FFF 3D SBRT plan and $\pm 5\%/3\text{mm}$ criteria. Gamma analysis results using a $\pm 8\%/3\text{mm}$ criteria, as well as results for other irradiations are presented in the Appendix.

Table 3.13 summarizes 2D gamma index results for all three irradiations (using the 10 MV FFF plan) of the RPC phantom at University of Alabama at Birmingham.

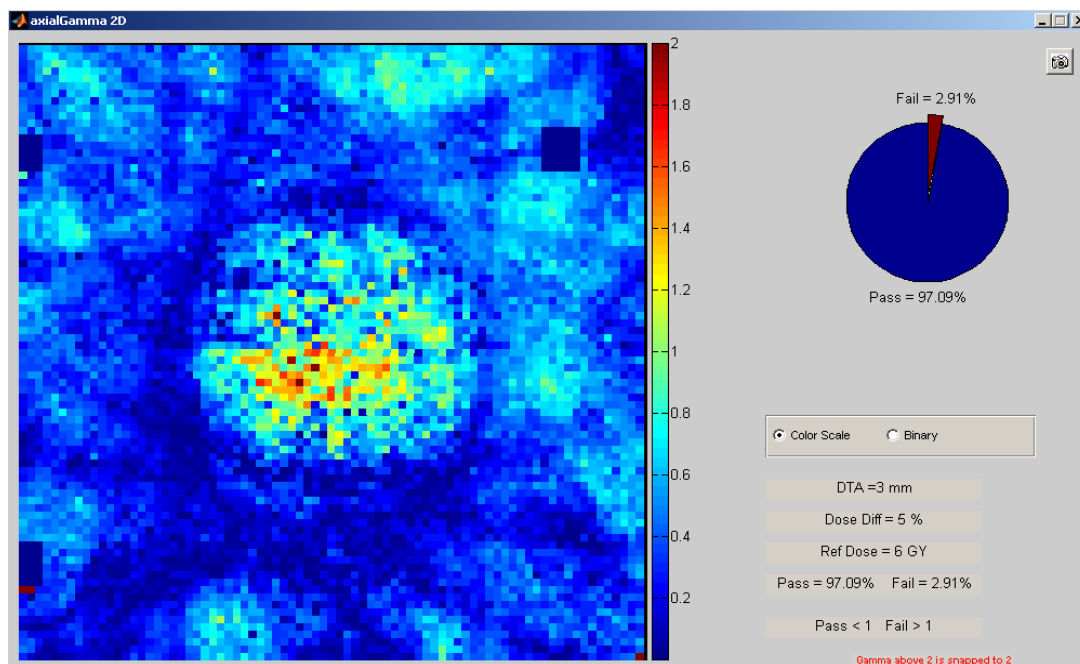


Figure 3.70 2D Gamma Index Results: $\pm 5\%/3\text{mm}$, Axial Plane For 10 MV FFF Plan

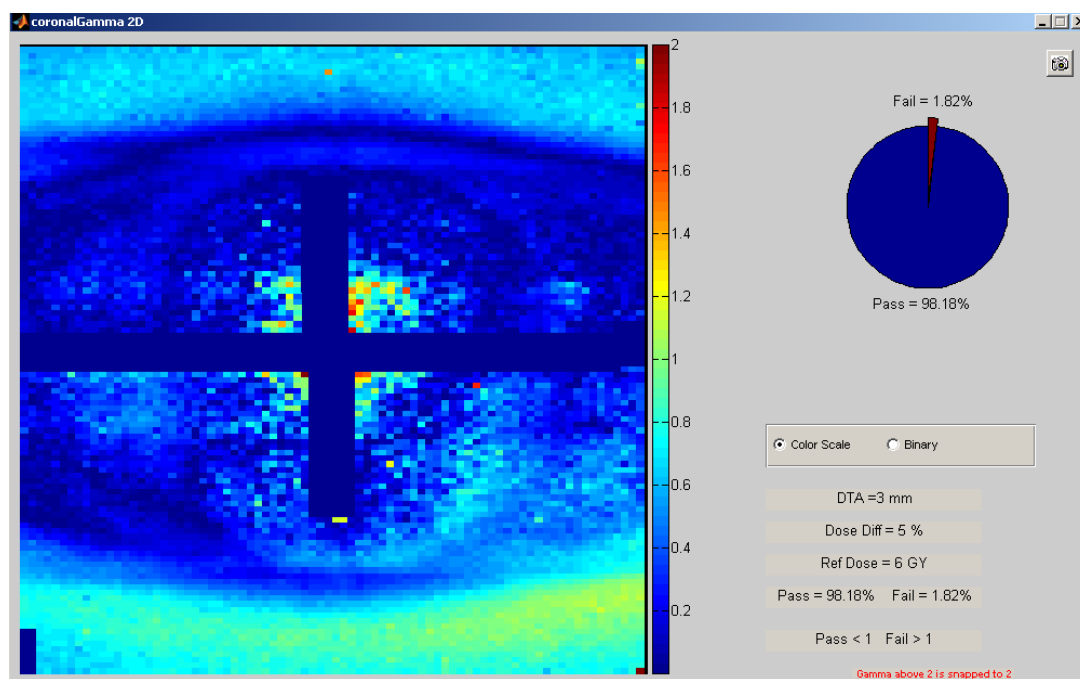


Figure 3.71 2D Gamma Index Results: $\pm 5\%/3\text{mm}$, Coronal Plane For 10 MV FFF Plan

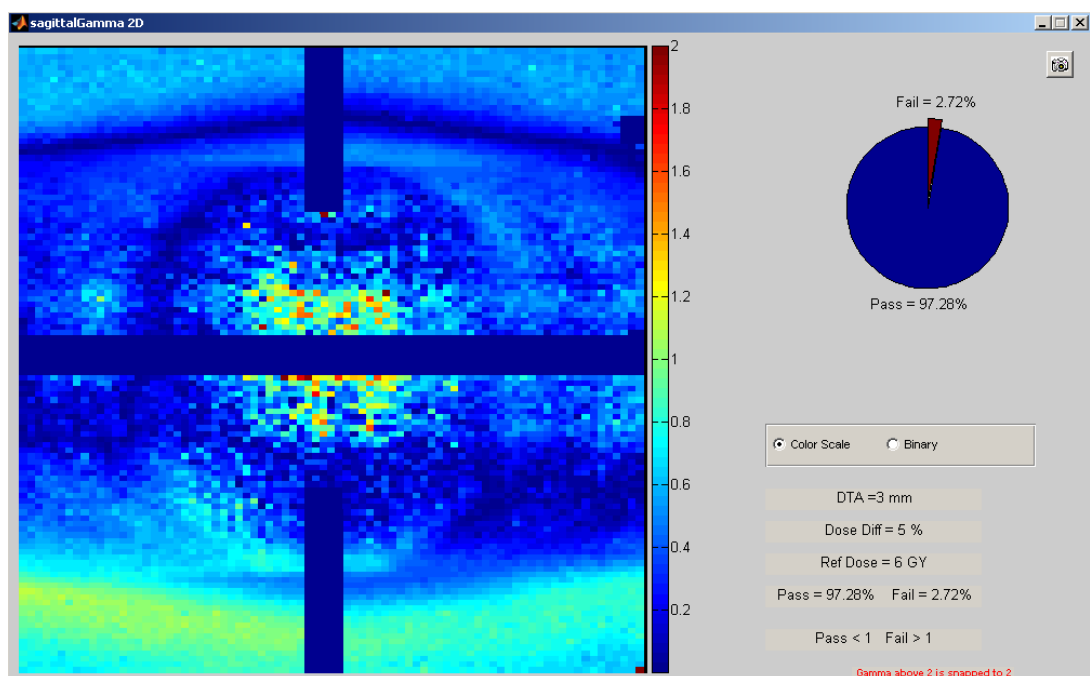


Figure 3.72 2D Gamma Index Results: $\pm 5\%/3\text{mm}$, Sagittal Plane For 10 MV FFF Plan

Table 3.13 10 MV FFF Plan 2D Gamma Index Results, UAB

Plan: 10 MV FFF, UAB, TrueBeam STx

Phantom Irrad.No	Gamma Index Analysis Criteria	Orthogonal Plane Passing Rate, %			Average 3-planes, %	Standard Deviation 3-planes
		Axial	Coronal	Sagittal		
1	$\pm 5\%/3\text{mm}$	97.1%	98.2%	97.3%	97.5%	0.59%
	$\pm 8\%/3\text{mm}$	99.2%	99.9%	99.6%	99.5%	0.36%
2	$\pm 5\%/3\text{mm}$	99.3%	95.2%	96.5%	97.0%	2.06%
	$\pm 8\%/3\text{mm}$	99.9%	99.9%	99.9%	99.9%	0.01%
3	$\pm 5\%/3\text{mm}$	91.2%	98.8%	93.5%	94.5%	3.90%
	$\pm 8\%/3\text{mm}$	96.2%	99.9%	98.4%	98.2%	1.85%
Ave. Passing Rate – All Irradiations, %	$\pm 5\%/3\text{mm}$	95.8%	97.4%	95.8%	96.3%	
	$\pm 8\%/3\text{mm}$	98.4%	99.9%	99.3%	99.2%	
Std Deviation – All Irradiations, %	$\pm 5\%/3\text{mm}$	4.20%	1.89%	2.01%	1.63%	
	$\pm 8\%/3\text{mm}$	1.95%	0.00%	0.80%	0.92%	

A plot of the data in the Table 3.13 is presented in Figures 3.73-3.74. Error bars represent the 95% CI.

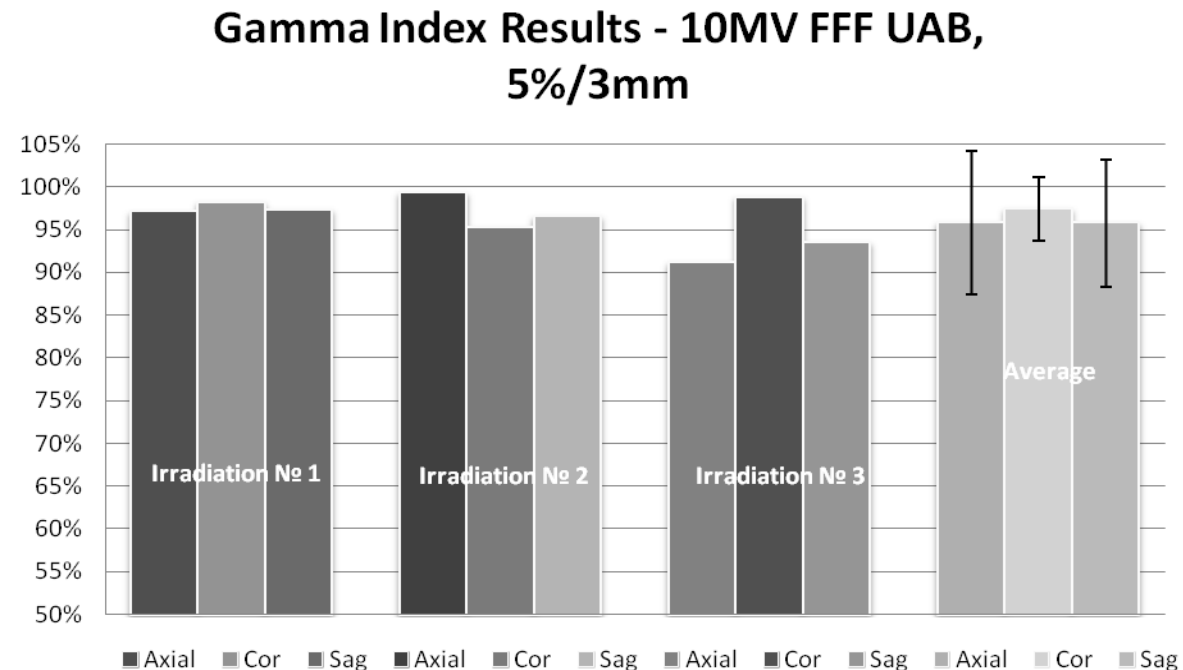


Figure 3.73 2D Gamma Index Results Using $\pm 5\%/3\text{mm}$ Criteria For 10 MV FFF Plan

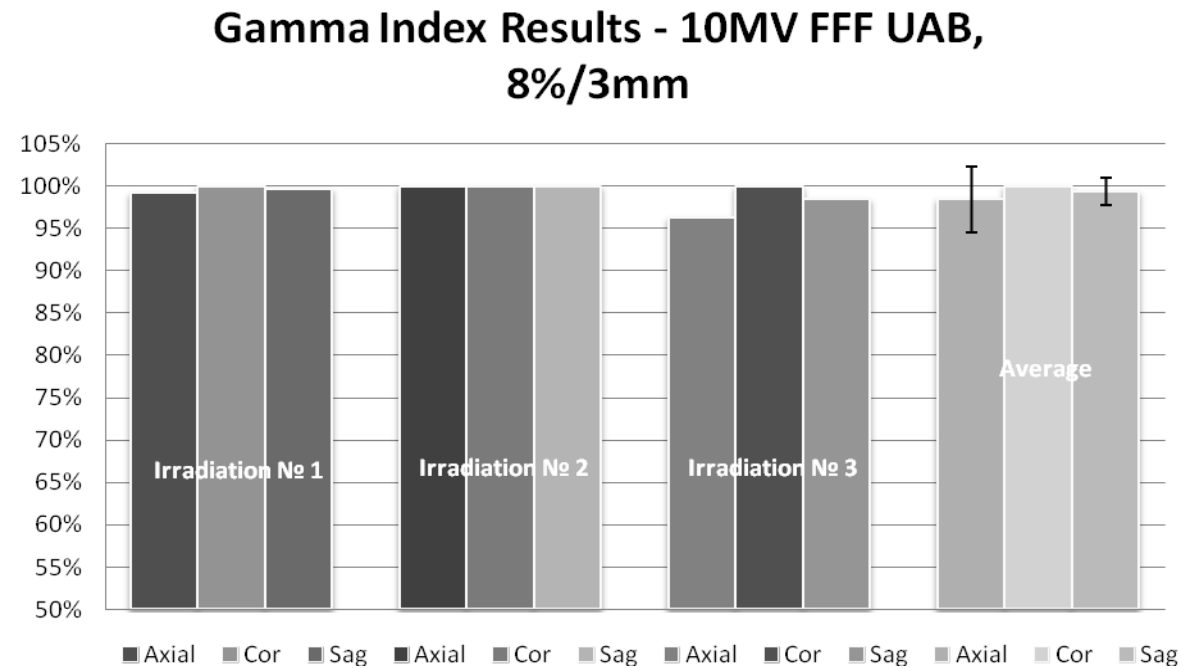


Figure 3.74 2D Gamma Index Results Using $\pm 8\%/3\text{mm}$ Criteria For 10 MV FFF Plan

3.3.4.4 Dose Profiles Results

The example of Right-Left, Anterior-Posterior, and Superior-Inferior measured (film) and calculated (TPS) profiles for the first irradiation of the phantom in the UAB Medical Center using the 10 MV FFF 3D SBRT plan are shown in Figures 3.75-3.77. Plane specific profiles for other irradiations and their corresponding TLD doses are presented in the Appendix.

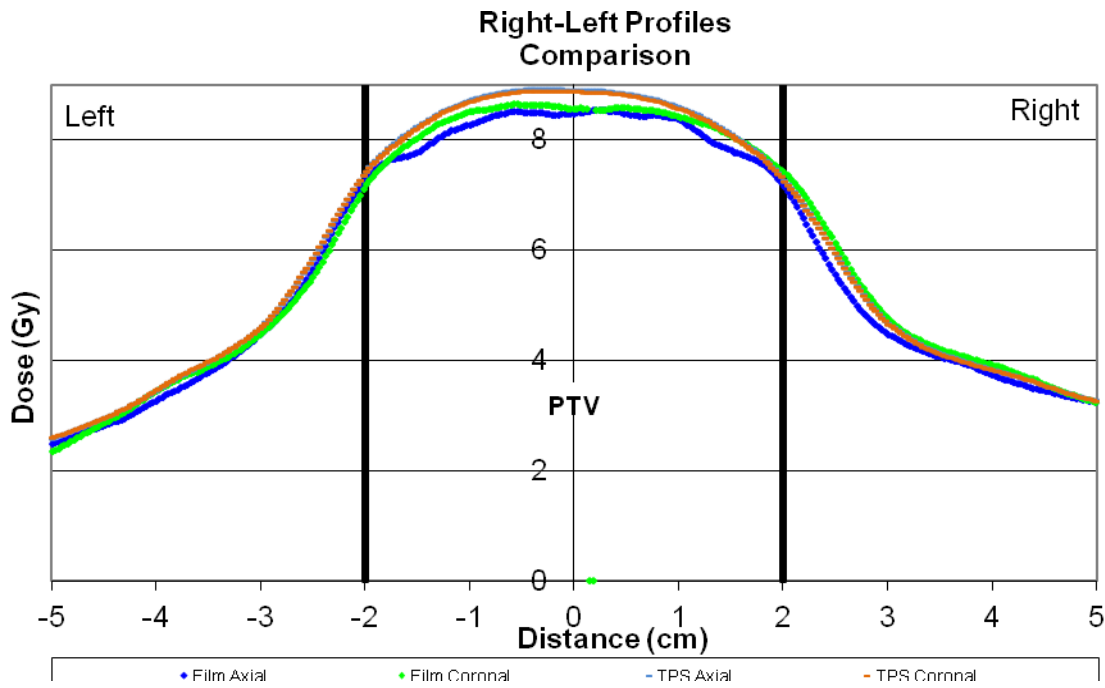


Figure 3.75 Right-Left Profiles In Axial And Coronal Planes Compared To The Calculated Dose Profiles For 10 MV FFF Plan

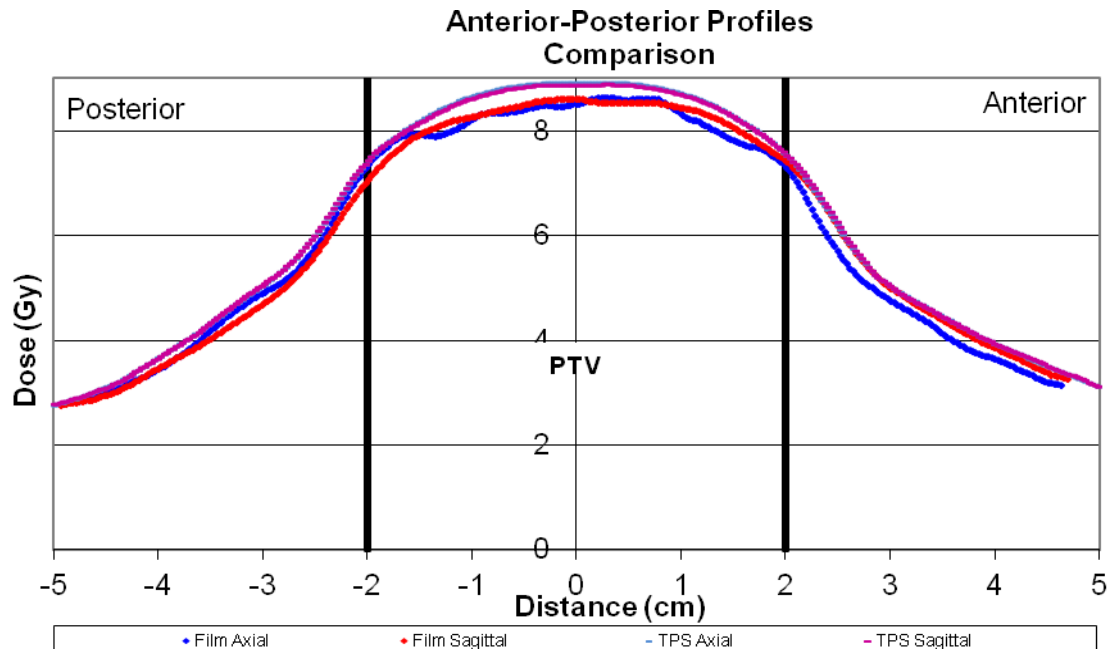


Figure 3.76 Anterior-Posterior Profiles In Axial And Sagittal Planes Compared To The Calculated Dose Profiles For 10 MV FFF Plan

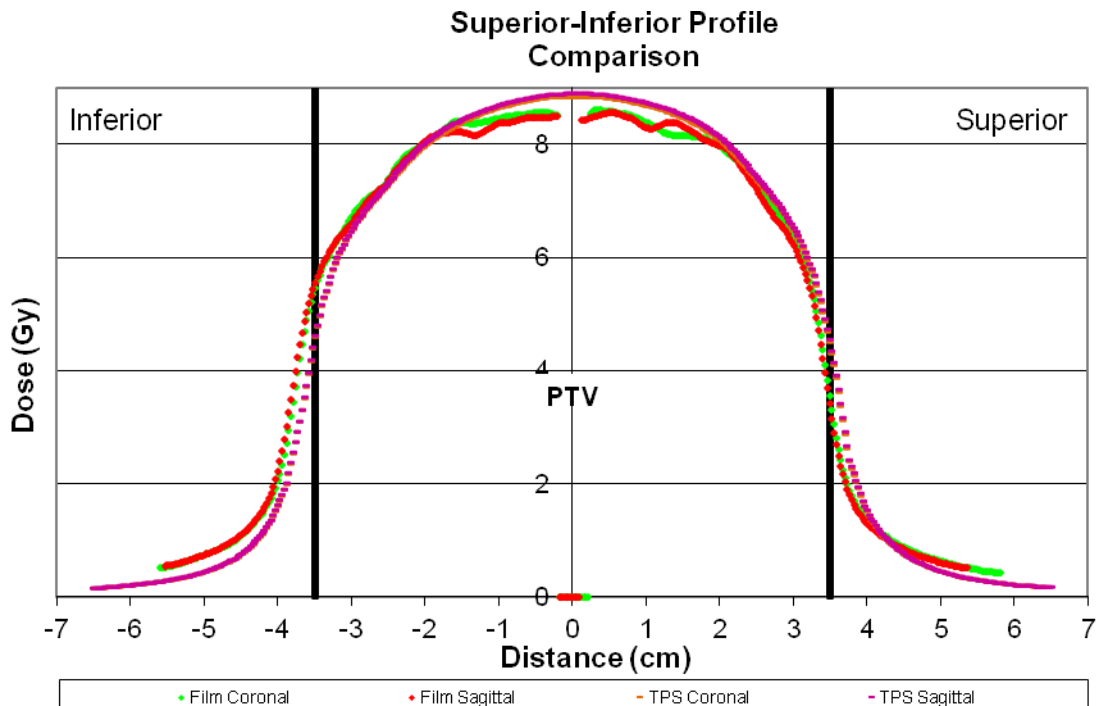


Figure 3.77 Superior-Inferior Profiles In Coronal And Sagittal Planes Compared To The Calculated Dose Profiles For 10 MV FFF Plan

3.4 Results Discussion

All three 6 MV/6 MV FFF 3D SBRT plans that were, delivered at MD Anderson Cancer Center and at the University of Alabama Medical Center resulted in a good agreement of point dose, between that measured by the TLDs, and that calculated in the Eclipse TPS. The average measured/predicted ratio for both target TLDs was 0.971 for 6MV MDA and 0.957/0.957 for 6 MV/6 MV FFF UAB, respectively. This represents measured dose of 2.9% and 4.3% lower than was expected based on the calculations. At the same time both results are in excellent agreement with the RPC expected dose ratio of 0.96-0.97 [8, 9] and are within the $\pm 5\%$ of the calculated dose limit established in this work.

2D gamma index analysis for these three plans resulted in 96.3%/95.6%/93.7% average pixels passing rate over all planes using $\pm 5\%/3\text{mm}$, and 99.8%/99.4%/98.7% using $\pm 8\%/3\text{mm}$ criteria for MDA 6 MV 3D SBRT, UAB 6 MV 3D SBRT and UAB 6 MV FFF 3D SBRT plans, respectively. In this work the lower limit for passing rate using $\pm 5\%/3\text{mm}$ criteria was established at 90% average for all planes while the lower limit for gamma index established by RPC in their credentialing procedures is set to 85% using $\pm 5\%/5\text{mm}$ around 0.97.

Dose profile analysis revealed a good agreement between calculated and measured data. Due to phantom alignment uncertainties there was a $\sim 2\text{mm}$ profile shift to the right on coronal films, and $\sim 2\text{mm}$ posterior and $\sim 1\text{mm}$ inferior shift on sagittal films in an MDA plan. UAB plans had a similar $\sim 1\text{-}2\text{mm}$ profile shift to the right on coronal films and $\sim 2\text{mm}$ anterior and inferior profile shifts on sagittal films. This misalignment resulted in a minor profile mismatch and in slightly higher standard deviation for these planes.

These results show that 6 MV 3D SBRT plans delivered at both institutions were comparable in respect to absolute point dose, as well as 2D planar dose distribution, and are well within the official RPC limits and the limits established in this work.

The 10 MV FFF 3D SBRT plan point dose measured by the TLDs was also in a good agreement with predicted dose that was calculated in Eclipse TPS with an average measured/predicted ratio for both target TLDs of 0.976 which is slightly higher than the ratio obtained in the 6MV plans. This represents measured dose of 2.4% less than was expected and is in excellent agreement with the RPC expected dose ratio of 0.97, as well as is well within $\pm 5\%$ of the calculated dose.

2D gamma index analysis resulted in 96.3% and 99.2% average passing rates using over all planes using $\pm 5\%/3\text{mm}$ and $\pm 8\%/3\text{mm}$ criteria respectively. This agreement was comparable to the 6 MV plans, as well as passing both 90% and 85% limits established in his work and by the RPC, respectively. As with 6 MV, 10 MV FFF measured dose profiles were in a good agreement with the calculated data.

Analysis of the higher energy, 15 MV and 18 MV, 3D SBRT plans revealed that point doses measured by the TLDs resulted in the average measured/predicted dose ratios for both target TLDs of 0.995 for 15 MV and 1.025 for 18 MV. Both ratios are in a good agreement with predicted dose calculated in Eclipse TPS. This represents measured dose of 0.5% lower and 2.5% greater than was expected. 15 MV ratio of 0.995 is slightly higher than the RPC expected dose ratio of 0.97, but it is still within 0.92-1.02 passing range, while the 18 MV dose ratio of 1.025 falls slightly outside the maximum limit of 1.02 allowed by the RPC. At the same time both the 15 MV and 18 MV, measured/predicted point dose ratios are within the criteria of this work of $\pm 5\%$ of the calculated dose. Care should be taken when considering the RPC limits for energies higher than 12 MV. Since the original RPC criteria was established based on the statistical analysis of the large number irradiations in 6-12 MV range [8, 9], its validity has not been verified for energies greater than 12 MV.

2D gamma index analysis for both plans resulted in 97.4%/ 92.2% average passing rate over all planes using $\pm 5\%/3\text{mm}$ and 99.9%/99.9% using $\pm 8\%/3\text{mm}$ for 15 and 18 MV, respectively. This agreement passes both the 90% and 85% limits established in his work and by the RPC for their credentialing process, respectively.

Dose profile analysis revealed a good agreement between calculated and measured data. Small phantom misalignments were observed: a $\sim 1\text{-}2\text{mm}$ profile shift to the right on coronal films and $\sim 2\text{mm}$ anterior and inferior on sagittal films in 15 MV plan, and a similar $\sim 2\text{mm}$ profile shift to the right on coronal and axial films in the 18 MV plan. This resulted in lower gamma index results for coronal planes and subsequently higher standard deviations for these three planes' averages in the 18 MV plan and in slightly higher standard deviation for the sagittal plane in the 15 MV plan.

Further examination of 1D dose profiles reveals a noticeable divergence of the measured profiles from the calculated outside the planning treatment volume in superior-inferior direction for all plans and beam energies. This deviation represents an increased dose to the tissues outside the planned treatment volume and a higher dose to a normal lung by 4-5% of the prescribed dose than what was predicted by the AAA calculation in the Eclipse TPS. Since the gamma index analysis was performed on PTV+2 cm this disagreement could be identified as failing points (yellow and red) on some of the coronal and sagittal gamma index maps outside the superior and inferior edges of the PTV. This region is characterized by the multi-leaf collimators covering larger field and is a subject of the increased beam penumbra.

Plotting the TLD data for all plans and calculating linear regression fit shows that the increase in beam energy results in a corresponding increase in the measured-to-predicted dose ratio of 0.005 MV^{-1} or 0.5% change in ratio for every 1 MV change in beam energy (Figure 3.78).

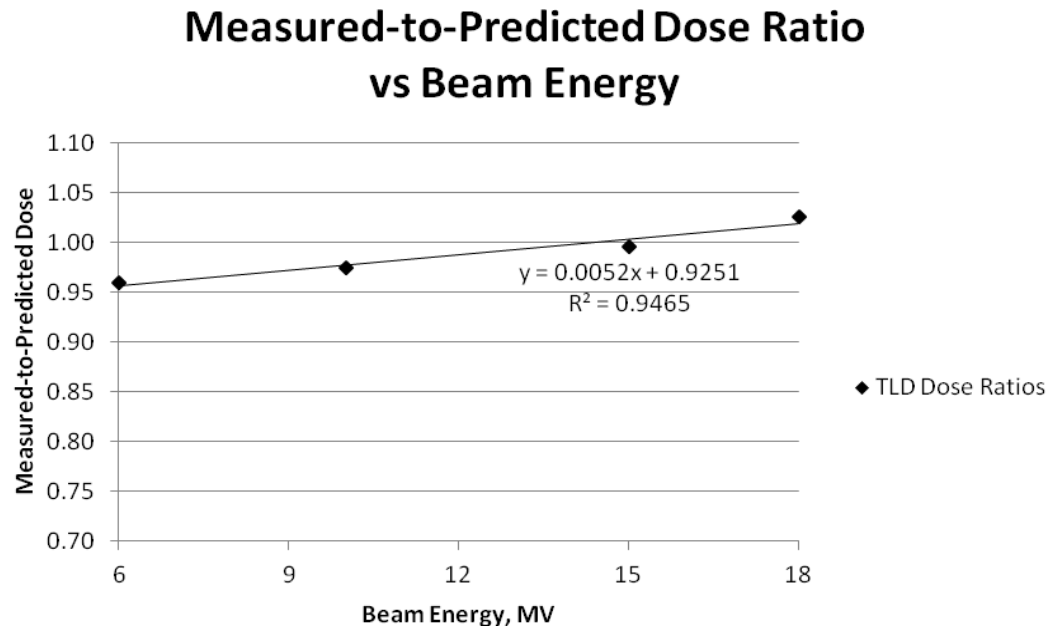


Figure 3.78 Measured-to-Predicted Dose Ratio vs Beam Energy

This dependency agrees with the RPC statistical data for lower beam energies, and also predicts that 15 MV energy plans calculated using AAA heterogeneity correction would result in the most accurate delivered dose with measured-to-calculated dose ratio of 1.00.

Chapter 4 Conclusion

4.1 General

Papanikolau *et al* do not recommend the use of beam energies higher than 12 MV for treatment of tumors surrounded by lung tissue inside the thorax due to the insufficient heterogeneity correction of existing dose calculation algorithms for high energies and small field sizes [7]. In this work the effectiveness of Anisotropic Analytical Algorithm for high energy flattened and flattening-filter-free beams has been evaluated using the Radiological Physics Center Lung phantom.

The verification of the dose calculation by the Varian, Inc. superposition-convolution AAA algorithm for tumor located in the middle of the lung was performed for the range of x-ray energies and beam types that are currently used in radiation therapy. Six stereotactic radiation body therapy treatment plans were designed in the Varian Eclipse treatment planning system using dose prescriptions and constraints that are identical to the RPC's credentialing requirements using thorax anthropomorphic phantom. Each plan was normalized that so at least 95% of PTV volume would receive 100% of prescribed dose. Prior to delivery, all plans were reviewed for the compliance with the current RPC accreditation guidelines as well as with the existing clinical trials recommendations by the Radiation Therapy Oncology Group [15-18]. Since the current guidelines limit the maximum photon energy to not greater than 12 MV [7], some of the existing metrics may not be applicable to higher energy beams, i.e. 15 MV and 18 MV.

In this work the point doses measurements were performed using TLD and the two-dimensional dose distributions were obtained from analyzing EBT2 radiochromic films. The primary acceptance criteria were specified in the research design of this work for the 2D dose distribution as 90% of points on average passing $\pm 5\%$ or 3mm distance to agreement and the measured point doses being within $\pm 5\%$ of the calculated dose.

For the credentialing process of the institutions the RPC has implemented the following acceptance criteria: 0.92-1.02 for measured-to-predicted point dose ratio, $\geq 80\%$ of single plane $\geq 85\%$ three-plane average points passing $\pm 5\%/5\text{mm}$ gamma criteria. The latter criteria are calculated by the RPC around 0.97 which would effectively correspond to $\pm 8\%/5\text{mm}$ around 1.0 using this work's methodology. To make a comparison of the experimental data with the RPC action limits the secondary set of criteria was adopted. In addition to the primary criteria of 0.95-1.05 and $\pm 5\%/3\text{mm}$, the analyzed data was also compared with the existing 0.92-1.02 point dose RPC limits and a more stringent gamma index of $\geq 90\%$ three-plane average points passing $\pm 8\%/3\text{mm}$.

The three irradiation averaged TLD point dose measurements for all six plans are plotted in Figure 4.1.

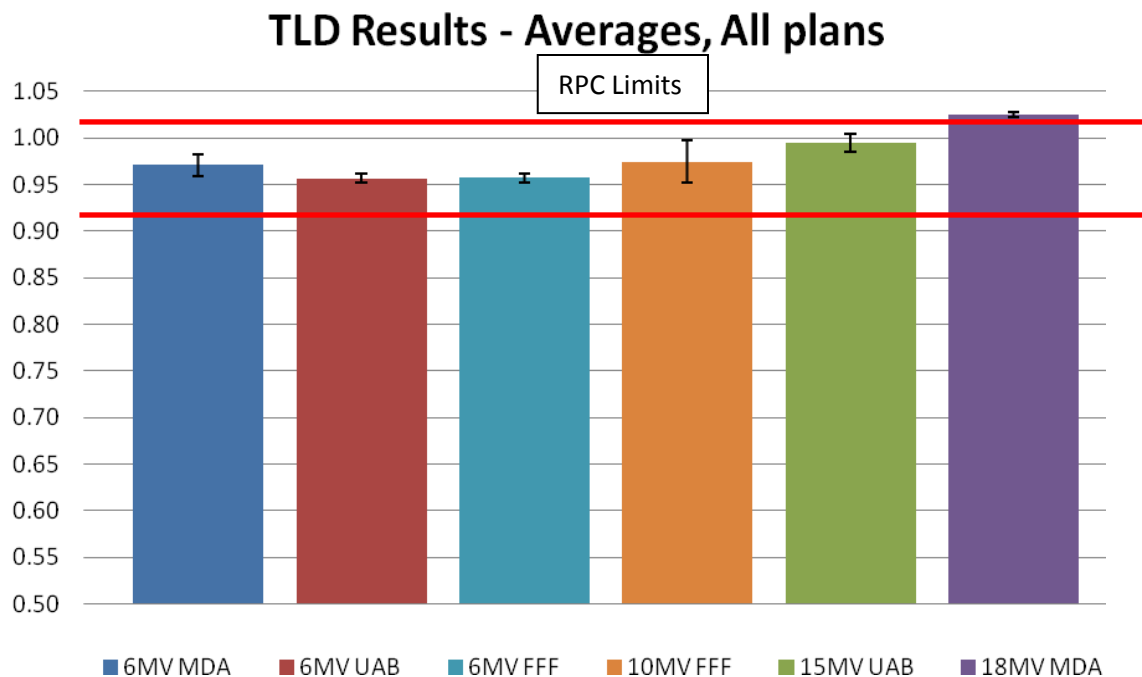


Figure 4.1 Measured-To-Predicted TLD Dose Ratios, 3-Irradiation Per Plan Average

The results demonstrate that all plans meet the passing criteria of $\pm 5\%$ of the calculated absolute dose, as well as the RPC criteria of 0.97 ± 0.05 with one exception. The average measured-

to-predicted ratio of the TLD doses delivered using 18 MV beam energy was calculated to be 1.025, which is below the maximum limit of 1.05 established in this work. This number falls slightly outside the 1.02 which is the maximum ratio allowed by the RPC. As was mentioned earlier in chapter 3.4, the 0.92-1.02 range (or 0.97 ± 0.05) point dose criterion was established by the RPC based on the multi institutional data to maintain consistency among different clinical trials. However, as most clinical trial protocols recommend the use of photon beam energies of less than 12 MV, this RPC limit should only be applied to plans designed and delivered according with these protocols recommendations, i.e. using beam energies in the 6-12 MV range. No criteria currently exist in the RPC regarding point dose limits for energies greater than 12 MV; therefore, the existing limits may not be applicable in this case.

Followill *et al*, in their recent study [9] report that for Monte Carlo based methods new acceptance criterion of 1 ± 0.05 for measured-to-predicted dose ratio will be used. This is the same passing criterion that was used in this work and that were successfully passed by all delivered plans (range 0.957-1.025). Acceptance of this new criterion not only for treatment plans calculated using Monte Carlo based methods, but for all other currently available clinical systems would make it easier to compare the dose calculation accuracy and effectiveness of different methods and algorithms. On the other hand, changing the acceptance criteria would create a substantial problem regarding consistency of clinical trials. Since all historical data was collected and processed using the 0.97 ± 0.05 criterion it would require recalculation of all previously acquired data and possibly even changing the new acceptance criterion of 1.0 ± 0.05 itself.

The gamma index analysis of the 2D dose distribution shows that 90% or more points on average have passed the $\pm 5\%/3\text{mm}$ criteria for all delivered plans with the lowest being 92.2% for the 18MV plan and the highest being 97.4% for the 15MV plan. The 18 MV number was the result of lower gamma indices for coronal planes in all three irradiations. Figure 4.2 shows a three irradiation averaged summary of gamma index analysis using $\pm 5\%/3\text{mm}$ criteria for all six plans.

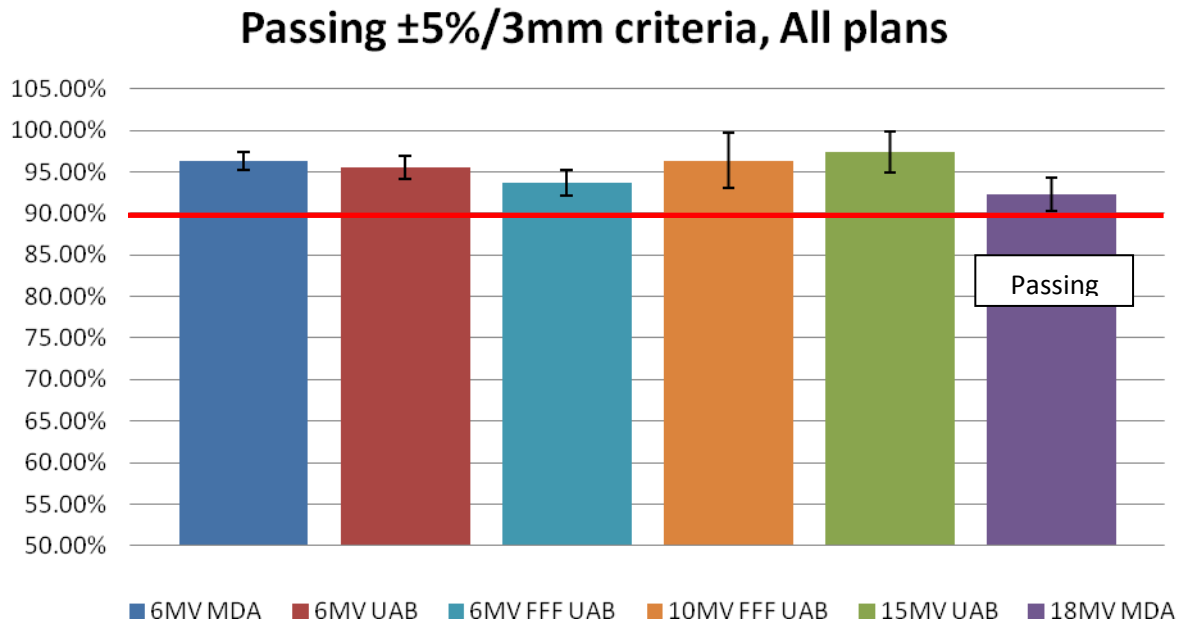


Figure 4.2 Plot Of Averaged Points Passing $\pm 5\%/3\text{mm}$ Criteria 2D Gamma Analysis For All Plans

The gamma index analysis data using secondary criteria of $\pm 8\%/3\text{mm}$ is presented in Figure 4.3. All plans showed an excellent agreement with calculated dose distributions with the lowest being 98.7% of points passing $\pm 8\%/3\text{mm}$ for the 6MV FFF plan and the highest being 99.9% for the 15 MV plan. As was mentioned earlier the $\pm 8\%/3\text{mm}$ criteria were included to compare the plans developed in this work with the RPC standards. Although, this criteria is more stringent than the existing limits it still provides the means to evaluate and compare these plans to the currently existing credentialing standards. Since the RPC criteria were developed based on the existing recommendations for maximum beam energy of 12 MV, the comparison of the gamma indices calculated using $\pm 8\%/3\text{mm}$ criteria with the RPC data should be done only for plans using 6 and 10 MV beams. The results of 2D dose distribution analysis for 15 and 18MV plans using such criteria may not be valid, despite showing an excellent agreement.

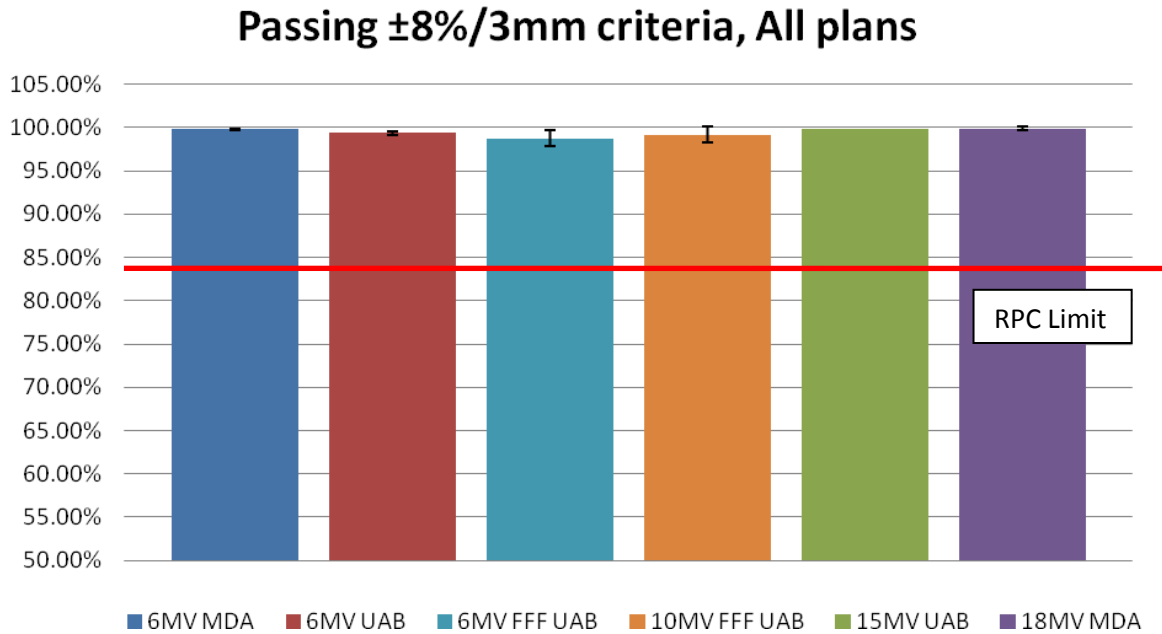


Figure 4.3 Plot Of Averaged Points Passing $\pm 8\%/3\text{mm}$ Criteria 2D Gamma Analysis For All Plans

The one dimensional dose profile analysis revealed a good agreement for all three orthogonal planes. There were occasional 2-3 mm shifts in some planes that resulted in displacement of the measured dose profiles relatively to the calculated profiles and hence in the lower corresponding gamma indices. Proper phantom alignment could further improve these results.

The results from both flattened and flattening-filter-free plans in 6-10 MV range are in a good agreement with the RPC data [8, 9, 29] and show that AAA algorithm is capable of calculating treatment plans in a complex heterogeneous environment consistently and accurately using $\pm 5\%/3\text{mm}$ gamma index and $\pm 5\%$ point dose criteria. This concurs with the existing recommendations of using beams energies of not greater than 12 MV for lung treatments [7].

Regarding the higher energies, neither 15 MV nor 18 MV are typically used in radiation therapy treatments of lung tumors due to the substantial loss of electronic equilibrium and a larger penumbra as reported by Wang *et al* [10]. Klein *et al* reported that plans using 18 MV can underdose the tumor by up to 11% [5] which can significantly compromise the effectiveness of the radiation

treatment and local tumor control. Studies that specifically looked into the AAA dose calculation effectiveness in heterogeneous environment also reported larger standard deviation with plans using 18 MV (up to 8%) as compared to 6 MV [13].

Analyzed data from 15 MV and 18 MV plans calculated in Eclipse TPS using AAA v. 8.9.08 delivered to the RPC anthropomorphic lung phantom shows a very good agreement between the calculated and delivered doses. While there is an increased electronic lateral disequilibrium and a larger penumbra for higher energies, both 15 MV and 18 MV 3D SBRT plans calculated with AAA do not show a decreased dose to the tumor or notably higher standard deviations for these energies. In fact, plans calculated using AAA with higher energies resulted in a higher overall dose to the tumor as compared to the lower energies in 6-10 MV range, as was mentioned in Results Discussion (chapter 3.4). This increase in dose to the tumor with increased energy does not concur with these published studies.

This disagreement could stem from the fact that recent changes in AAA, such as better Monte Carlo pre-calculated kernels as well in algorithm itself, made it able to account for these effects. The results obtained from analyzing this work's data show that delivered 3D SBRT plans calculated using Analytical Anisotropic Algorithm with different beams (flattened and flattening-filter-free) and different energies (6 MV – 18 MV) result in measured doses that are within $\pm 5\%$ of the calculated dose, as well as 90% or more pixels are passing the $\pm 5\%$ dose or 3 mm distance to agreement using 2D gamma index analysis. This demonstrates that AAA implemented in Eclipse TPS is fully capable of calculating treatment doses in heterogeneous medium, such as lung, using both lower and higher photon beam energies.

4.2 Future Work

In this work the effectiveness of the 3D superposition-convolution AAA algorithm with high energies was evaluated using stereotactic radiation body therapy plans. To simplify the data analysis

and identify the potential deficiencies of the AAA algorithm all developed and delivered plans used only static beams. Advanced radiation therapy treatment techniques, such as Intensity Modulated and Arc Radiation Therapy extensively use the MLC to modulate the dose. The continuous changes in MLC leaf position while delivering the high energy dose may pose a challenge to the AAA algorithm due to penumbra broadening of the beam.

The RPC anthropomorphic phantom used in this study was stationary to eliminate any alignment uncertainties due to target movement. During the breathing cycle, respiratory motion of the thorax may result in a sizable displacement of a tumor which could negatively affect the tumor coverage. In order to evaluate the dose delivery with tumor motion the RPC phantom can be placed on the moving platform that was specifically designed to simulate such motion. A 4D computed tomography simulation along with the treatment plan that takes into account this motion would help to evaluate the effectiveness of the AAA algorithm in a more realistic condition.

Finally, Acuros XB dose calculation algorithm was recently introduced by Varian, Inc to be implemented in Eclipse TPS. This new algorithm could lead to an increased accuracy of the dose calculation as compared to the currently used 3D pencil beam superposition-convolution algorithms such as AAA.

Chapter 5 Appendix

5.1 6 MV SBRT MD Anderson CANCER CENTER 2D Gamma Index Maps and Dose Profiles

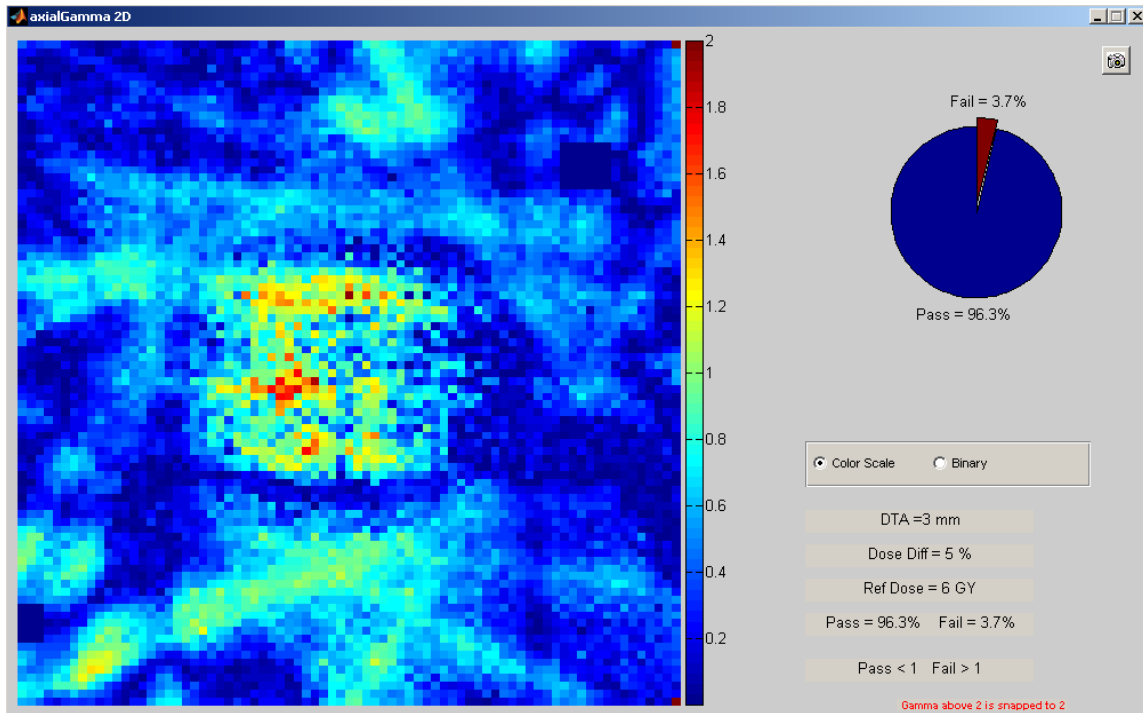


Figure 5.1 6 MV SBRT MDA 2D Gamma Index Results: $\pm 5\%/3\text{mm}$, Axial Plane, Irradiation #1

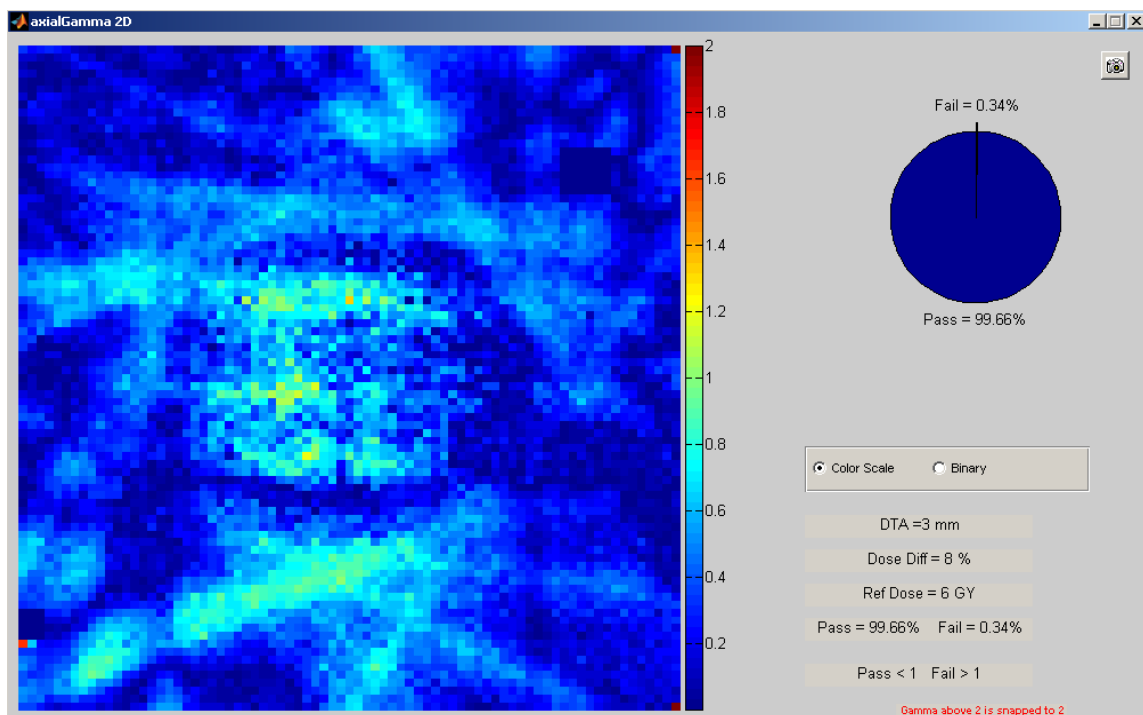


Figure 5.2 6 MV SBRT MDA 2D Gamma Index Results: $\pm 8\%/3\text{mm}$, Axial Plane, Irradiation #1

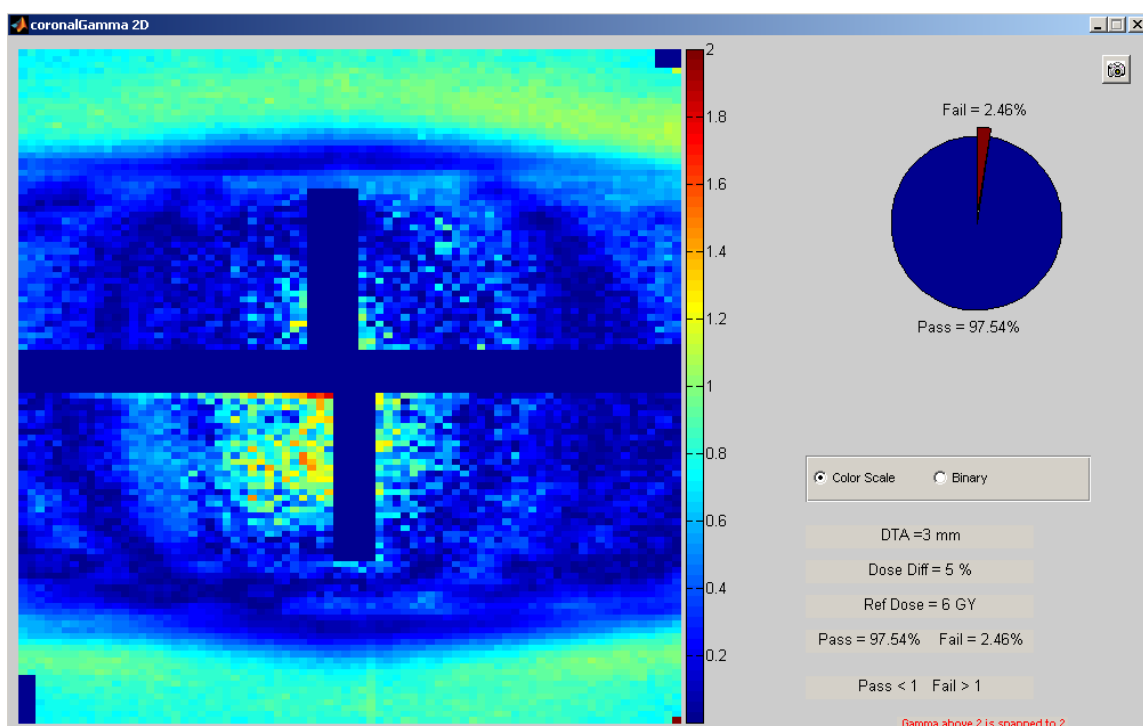


Figure 5.3 6 MV SBRT MDA 2D Gamma Index Results: $\pm 5\%/3\text{mm}$, Coronal Plane, Irradiation #1

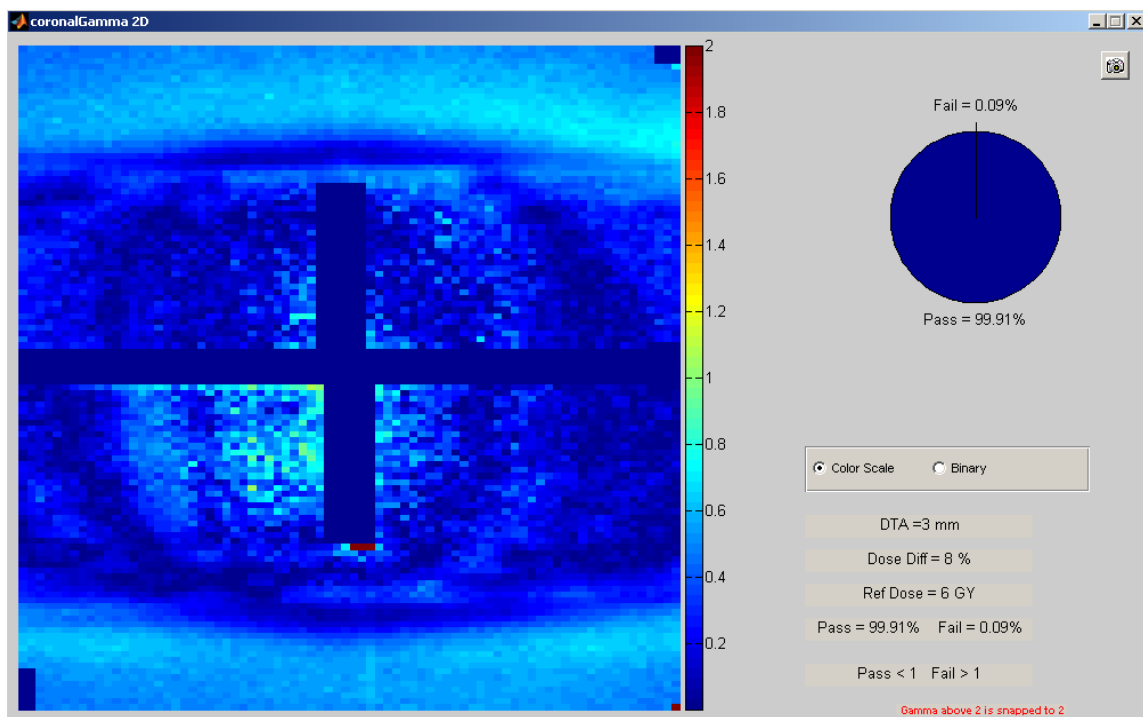


Figure 5.4 6 MV SBRT MDA 2D Gamma Index Results: $\pm 8\%/3\text{mm}$, Coronal Plane, Irradiation #1

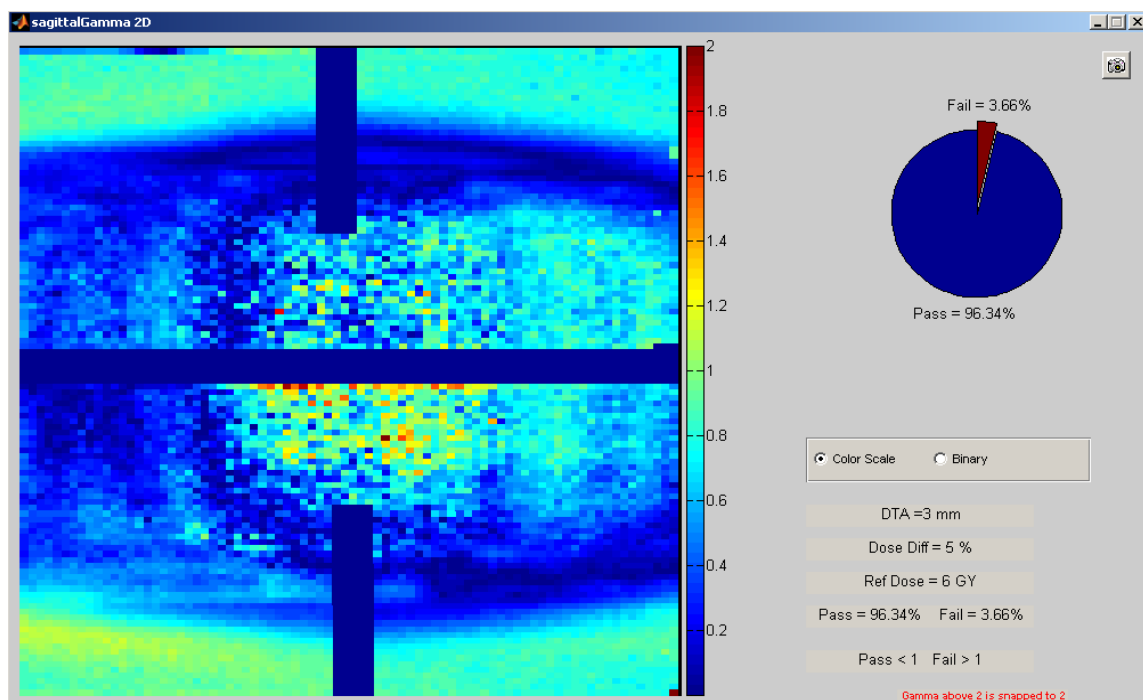


Figure 5.5 6 MV SBRT MDA 2D Gamma Index Results: $\pm 5\%/3\text{mm}$, Sagittal Plane, Irradiation #1

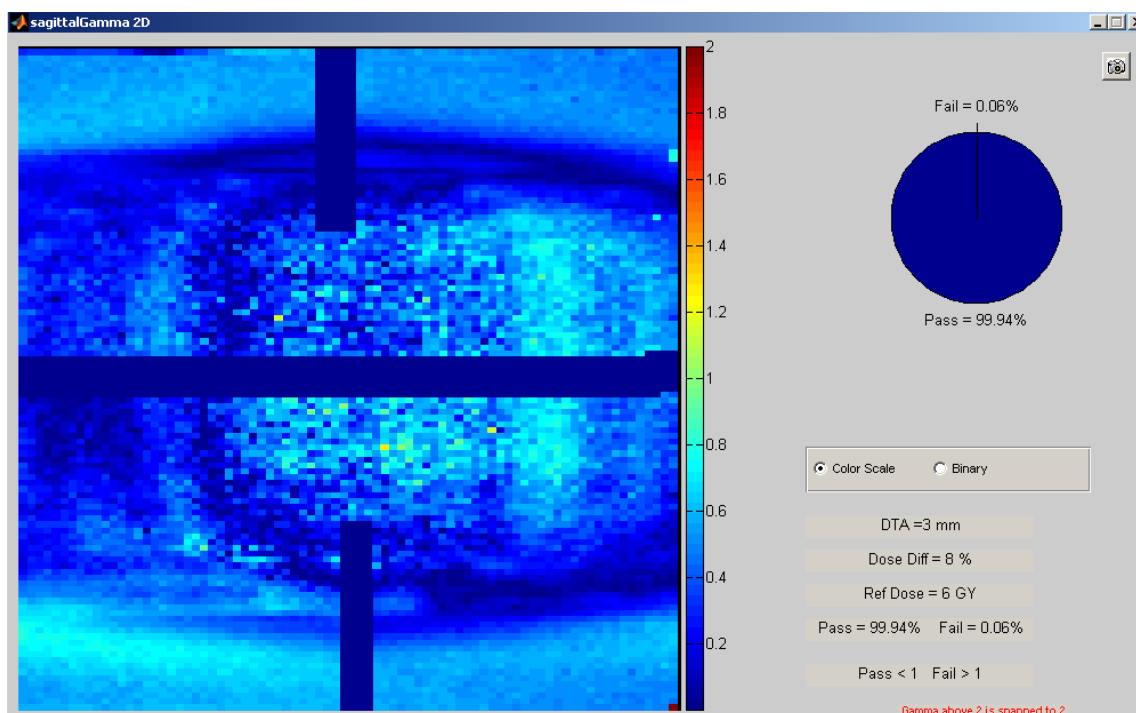


Figure 5.6 6 MV SBRT MDA 2D Gamma Index Results: $\pm 8\%/3\text{mm}$, Sagittal Plane, Irradiation #1

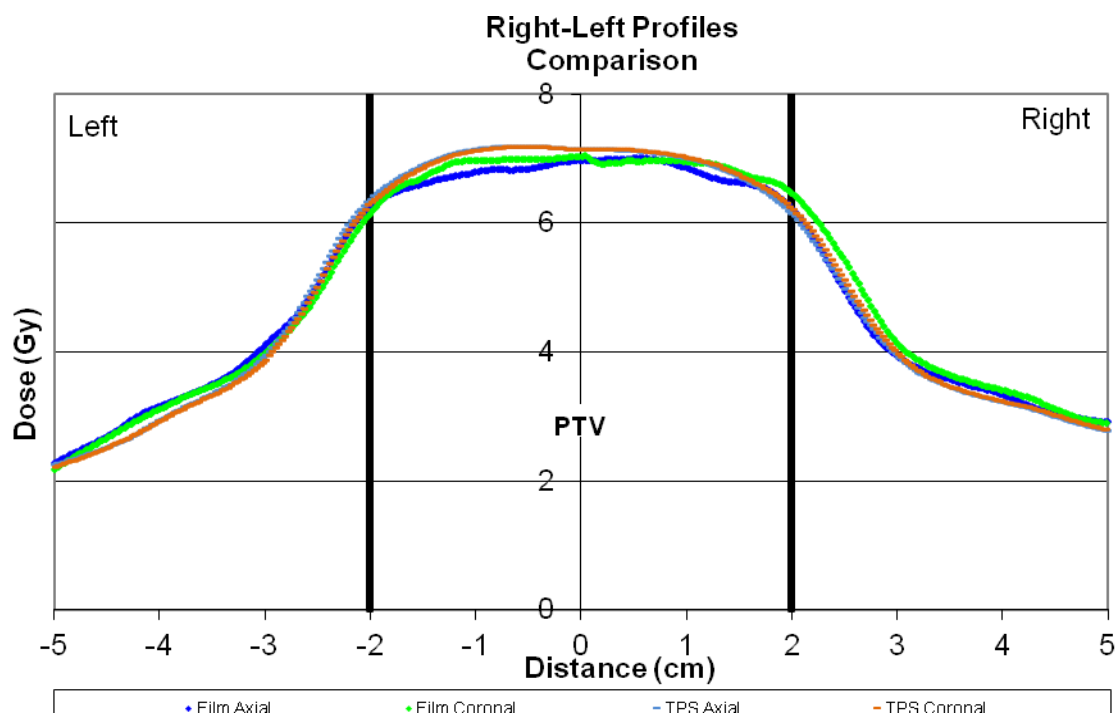


Figure 5.7 6 MV SBRT MDA 1D Right-Left Dose Profiles: Irradiation #1

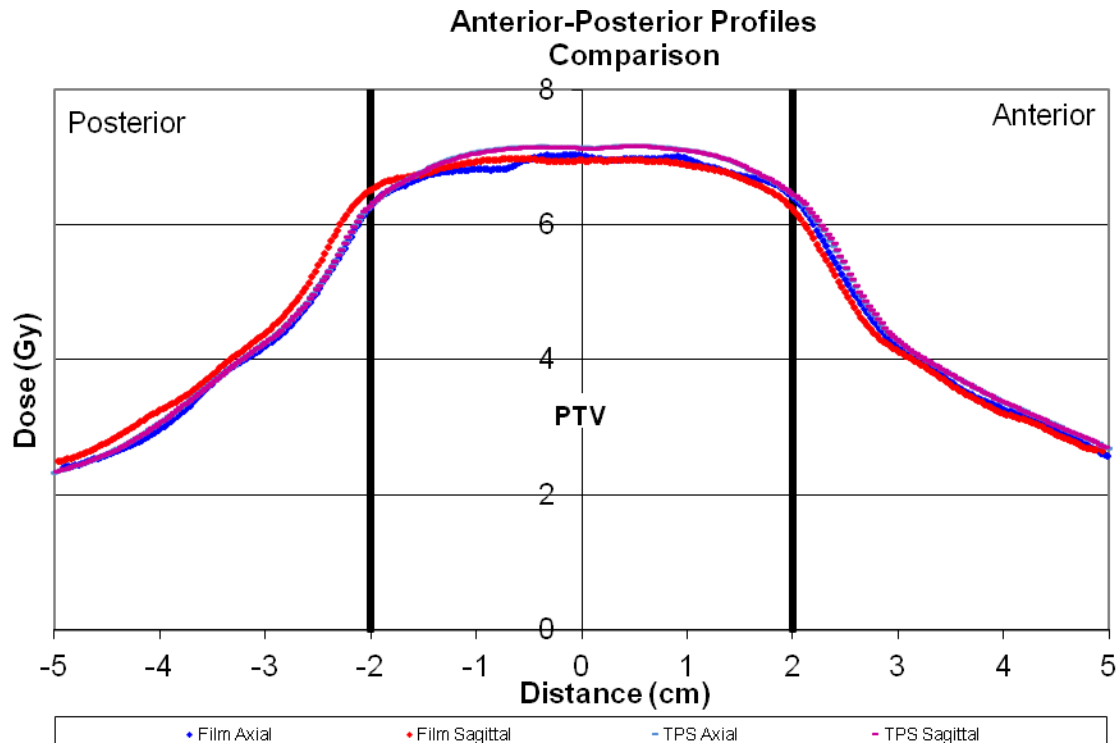


Figure 5.8 6 MV SBRT MDA 1D Anterior-Posterior Dose Profiles: Irradiation #1

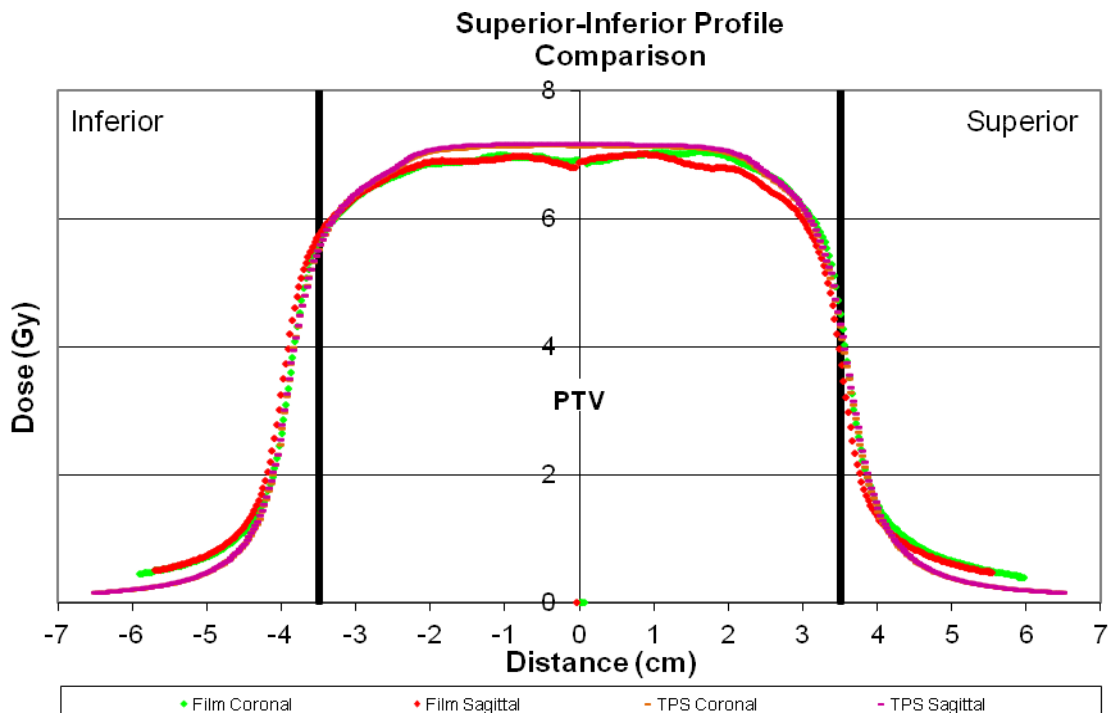


Figure 5.9 6 MV SBRT MDA 1D Superior-Inferior Dose Profiles: Irradiation #1

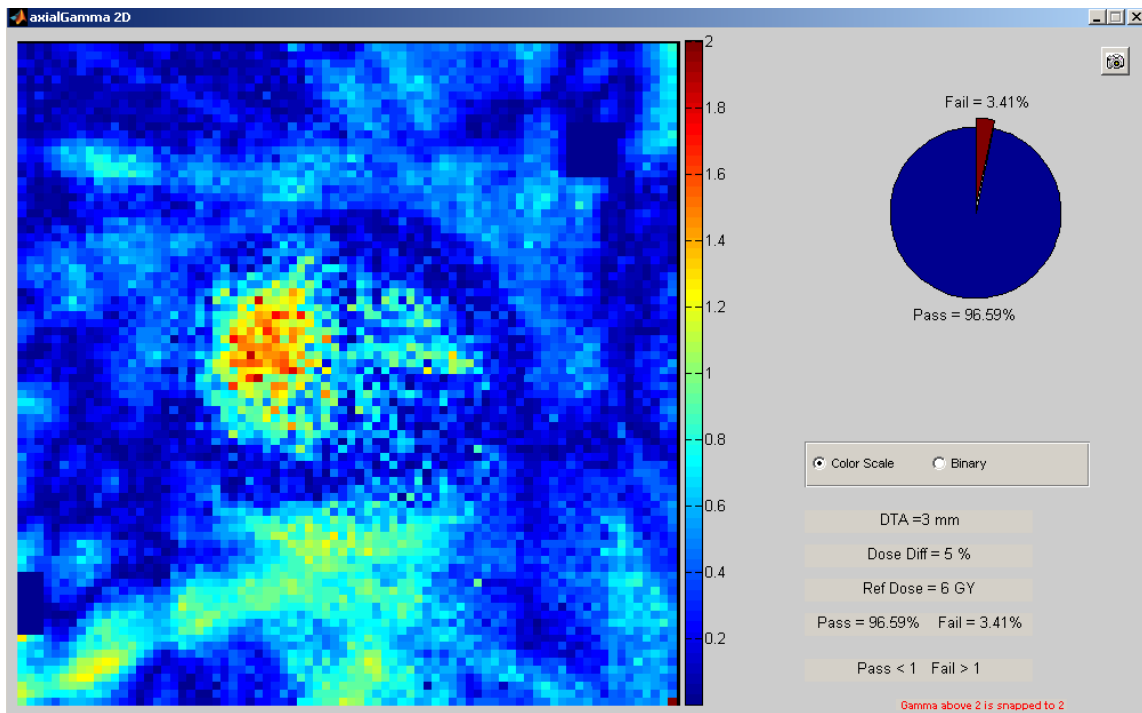


Figure 5.10 6 MV SBRT MDA 2D Gamma Index Results: $\pm 5\%/3\text{mm}$, Axial Plane, Irradiation #2

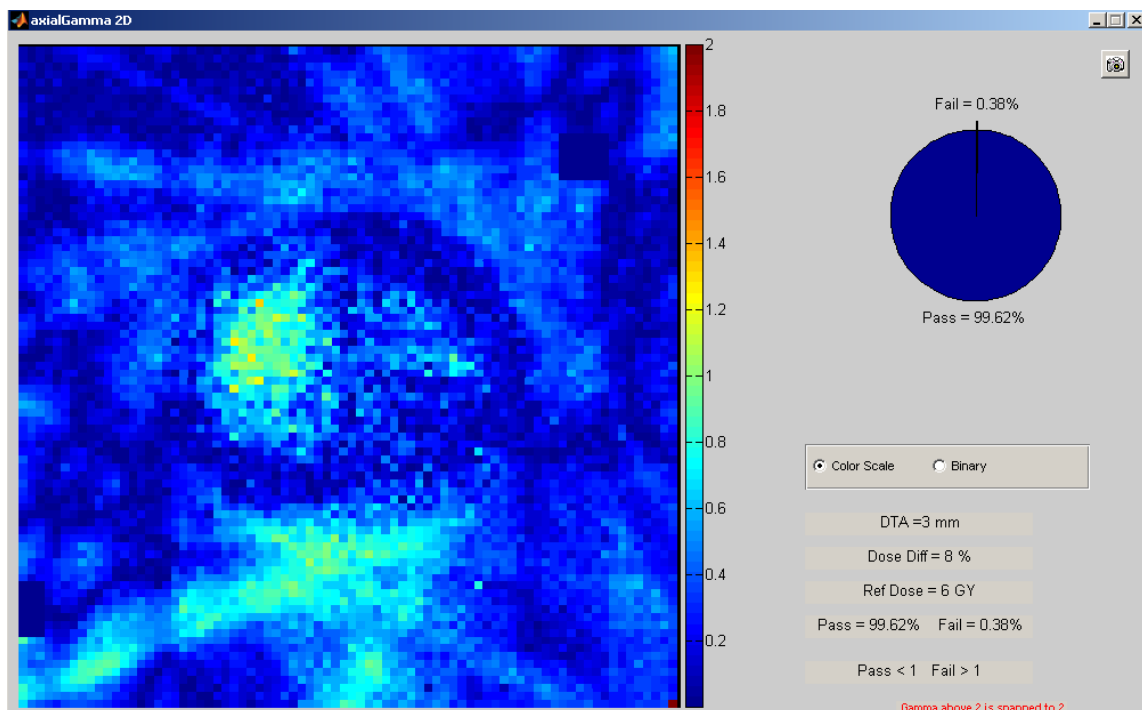


Figure 5.11 6 MV SBRT MDA 2D Gamma Index Results: $\pm 8\%/3\text{mm}$, Axial Plane, Irradiation #2

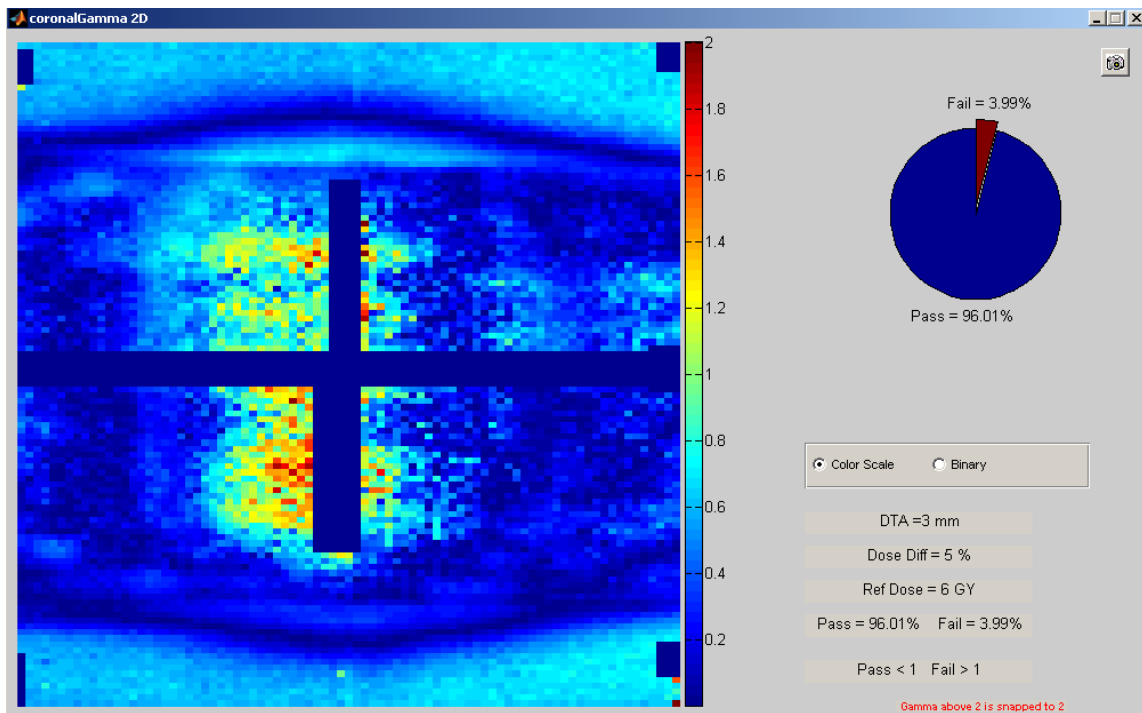


Figure 5.12 6 MV SBRT MDA 2D Gamma Index Results: $\pm 5\%/3\text{mm}$, Coronal Plane, Irradiation #2

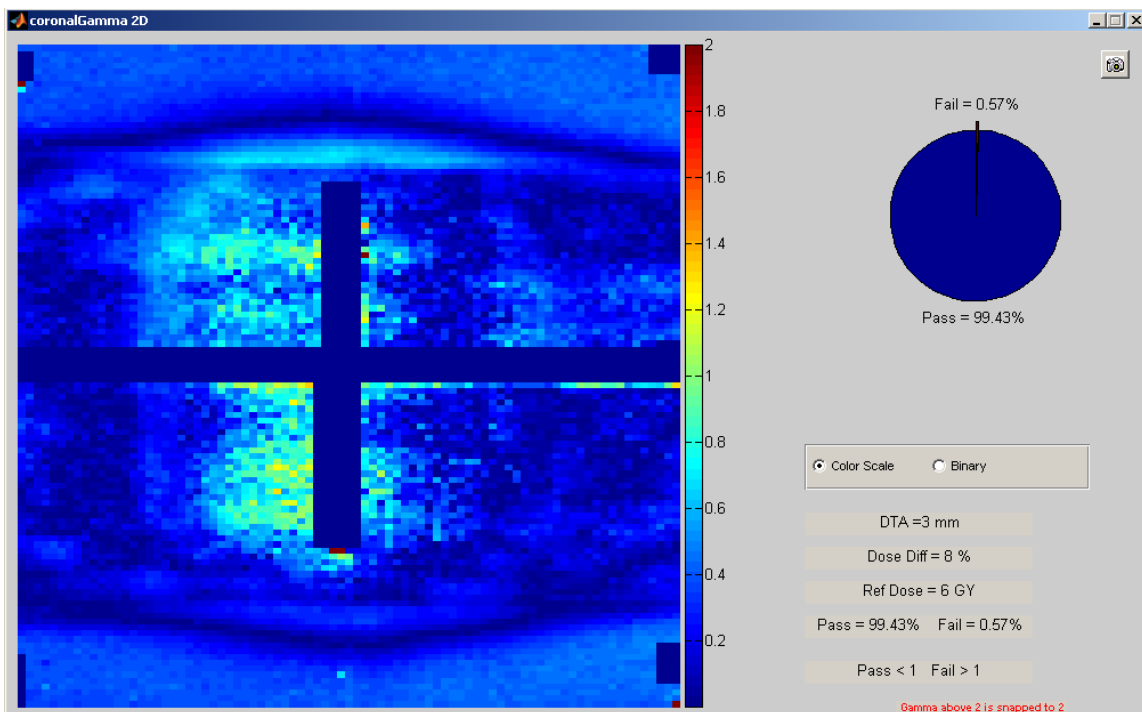


Figure 5.13 6 MV SBRT MDA 2D Gamma Index Results: $\pm 8\%/3\text{mm}$, Coronal Plane, Irradiation #2

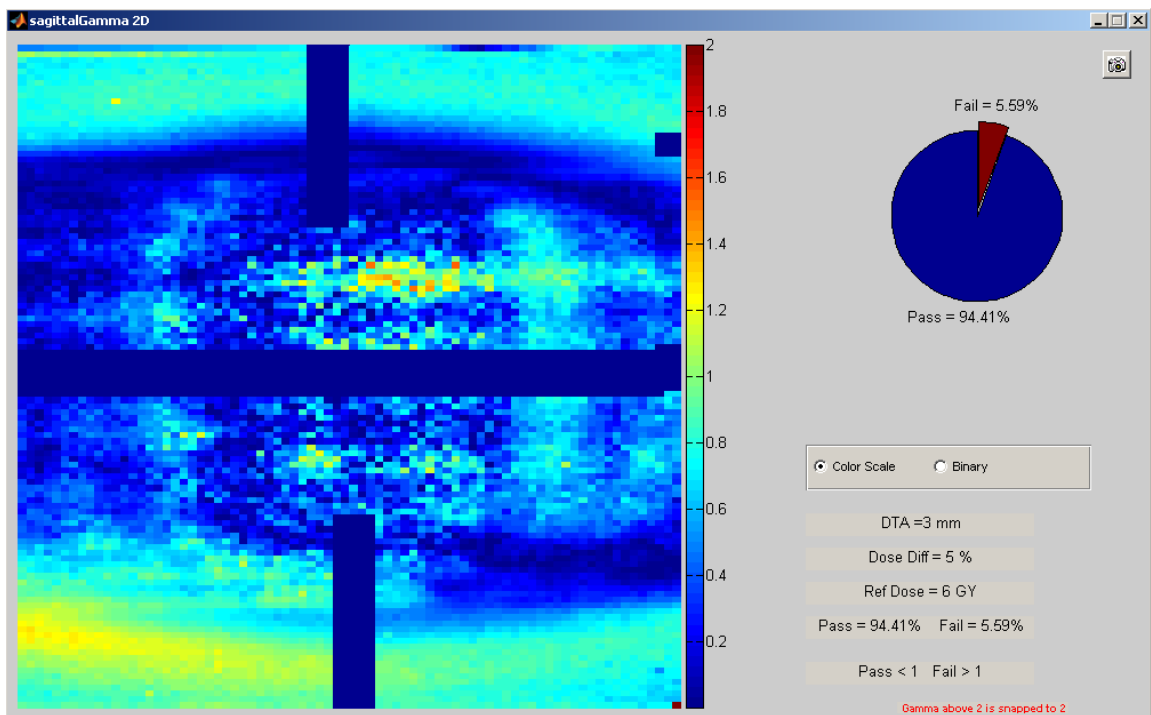


Figure 5.14 6 MV SBRT MDA 2D Gamma Index Results: $\pm 5\%/3\text{mm}$, Sagittal Plane, Irradiation #2

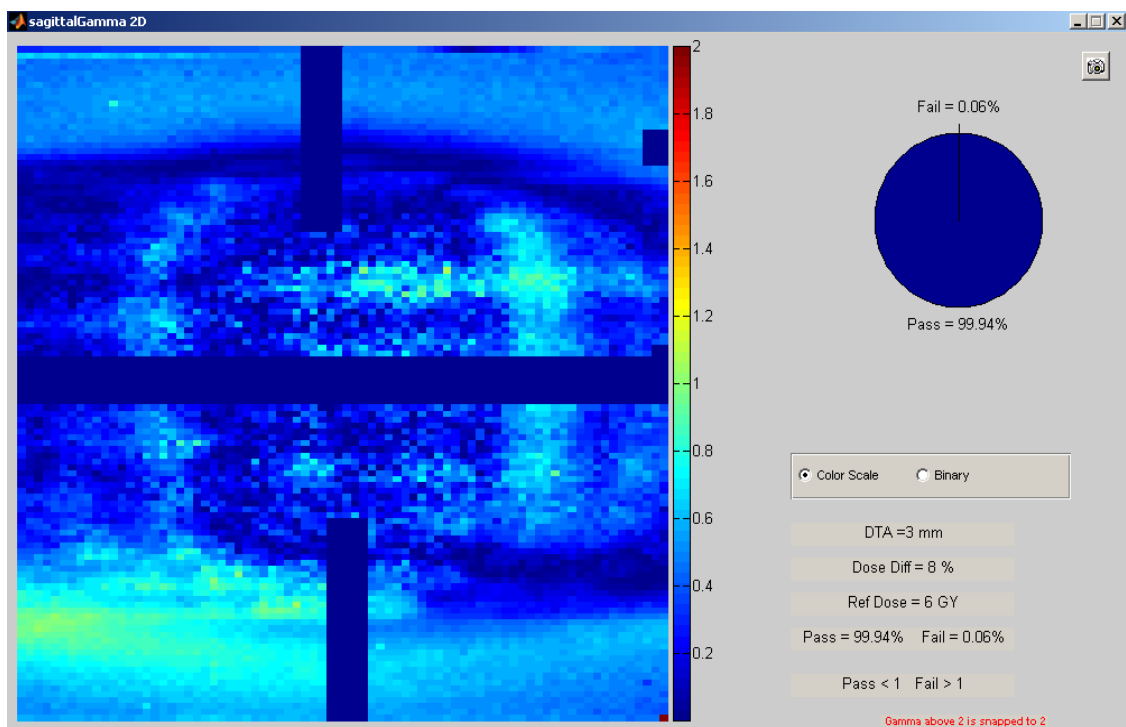


Figure 5.15 6 MV SBRT MDA 2D Gamma Index Results: $\pm 8\%/3\text{mm}$, Sagittal Plane, Irradiation #2

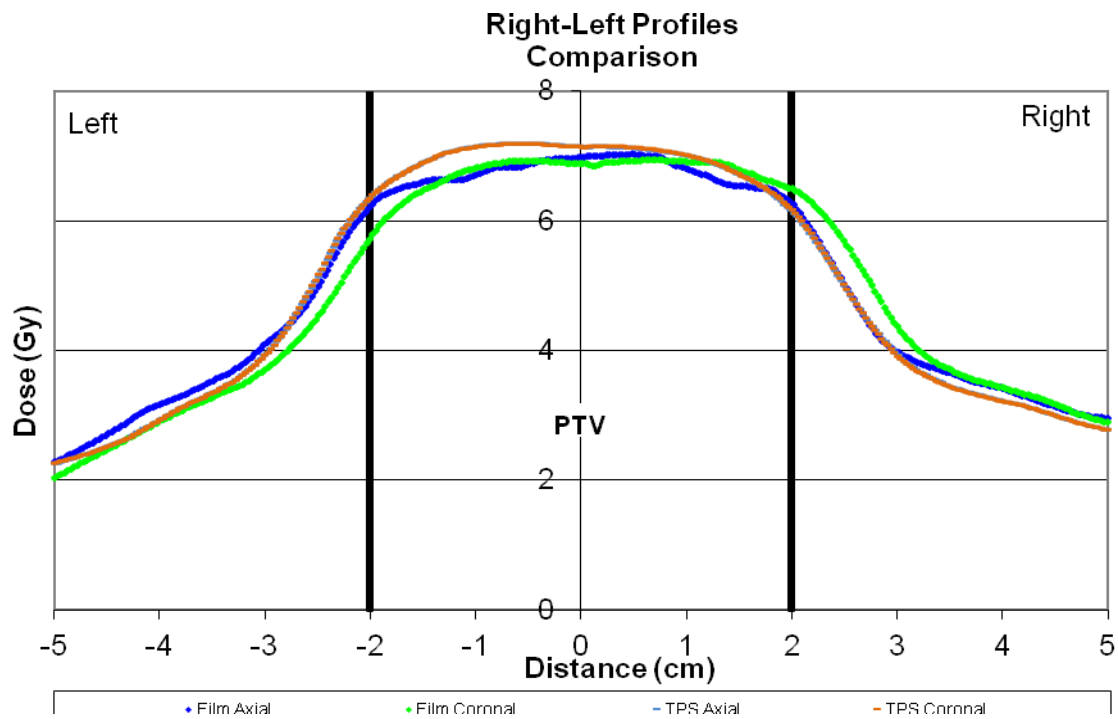


Figure 5.16 6 MV SBRT MDA 1D Right-Left Dose Profiles: Irradiation #2

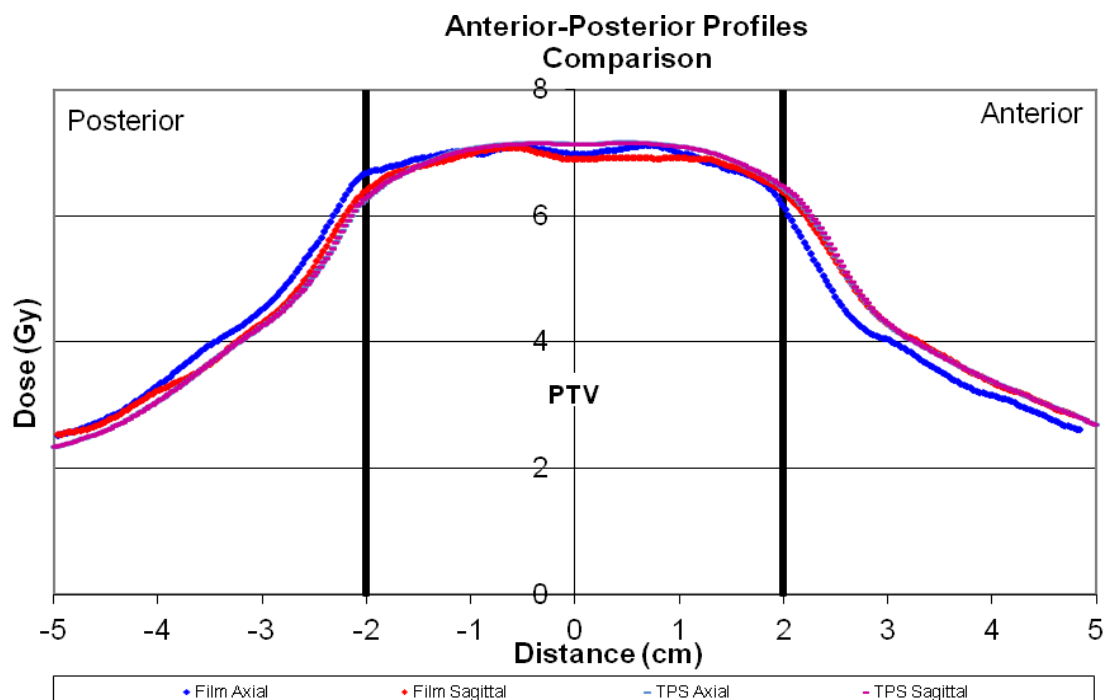


Figure 5.17 6 MV SBRT MDA 1D Anterior-Posterior Dose Profiles: Irradiation #2

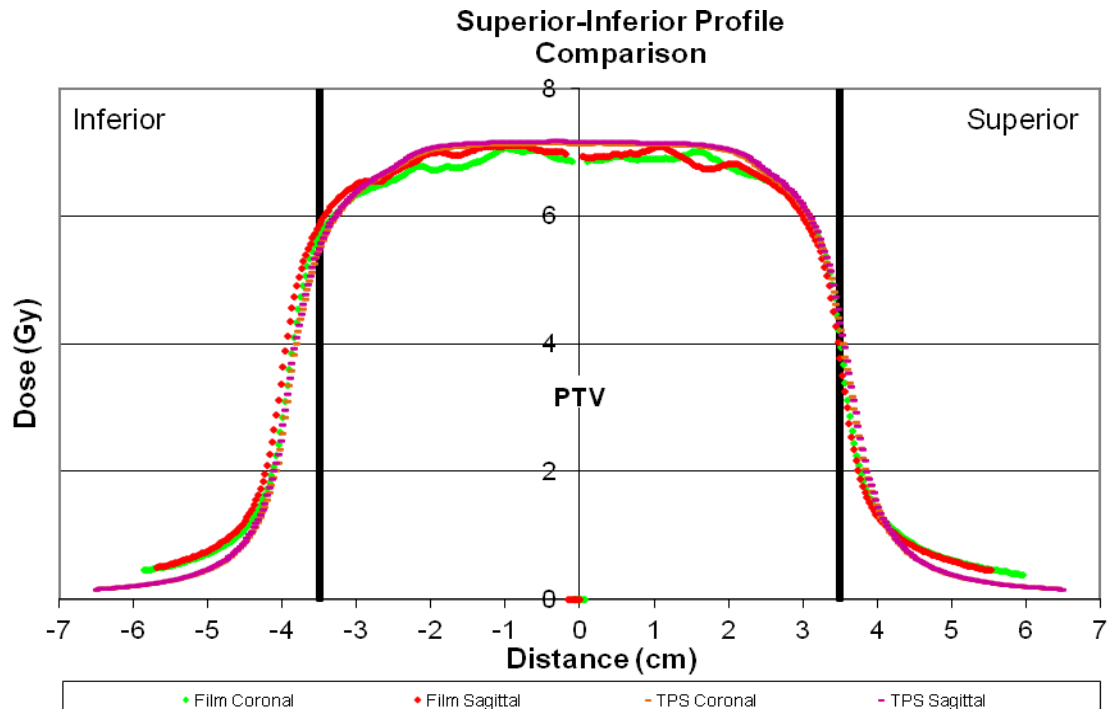


Figure 5.18 6 MV SBRT MDA 1D Superior-Inferior Dose Profiles: Irradiation #2

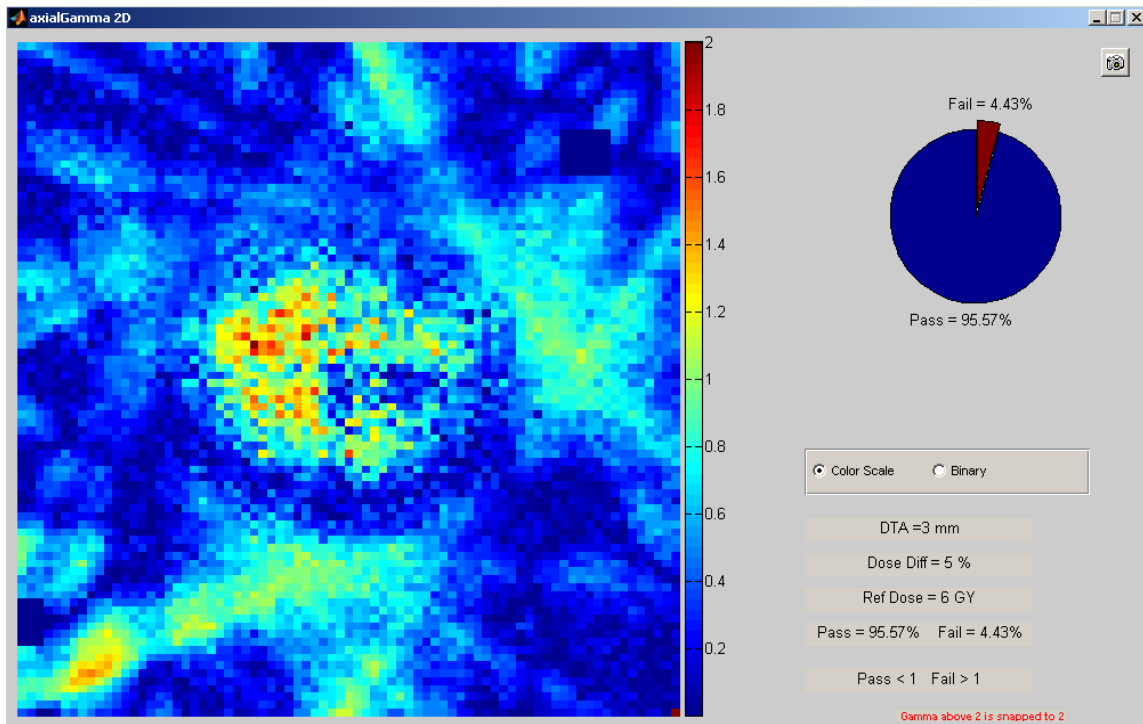


Figure 5.19 6 MV SBRT MDA 2D Gamma Index Results: $\pm 5\%/3\text{mm}$, Axial Plane, Irradiation #3

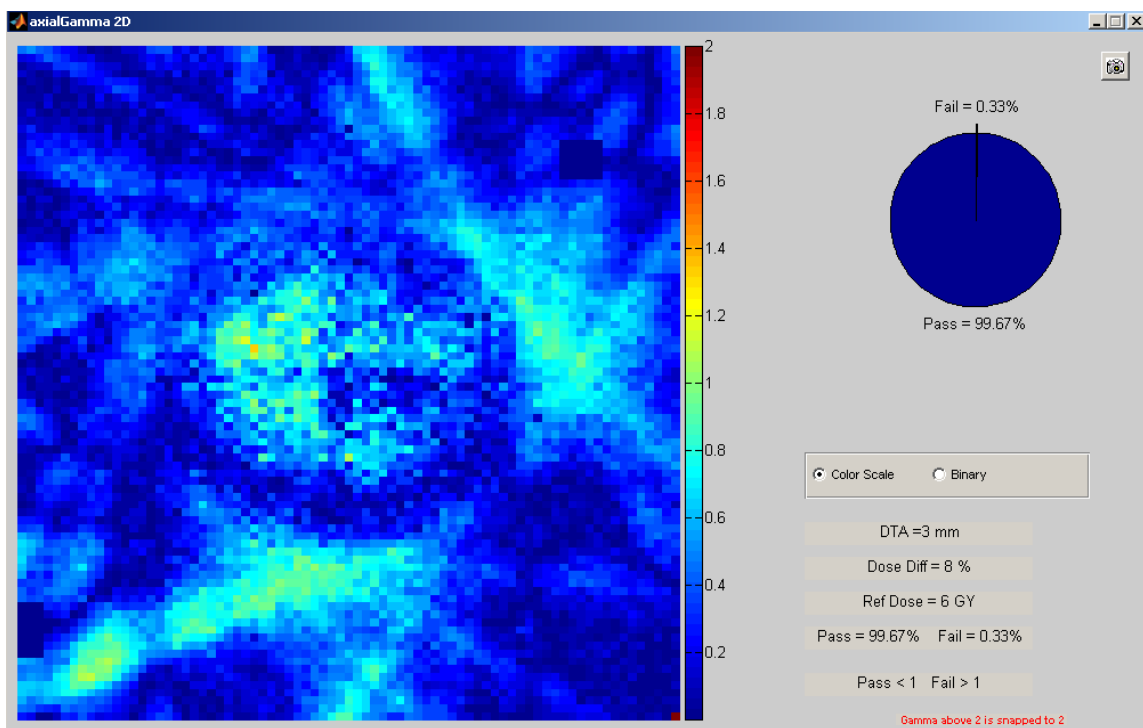


Figure 5.20 6 MV SBRT MDA 2D Gamma Index Results: $\pm 8\%/3\text{mm}$, Axial Plane, Irradiation #3

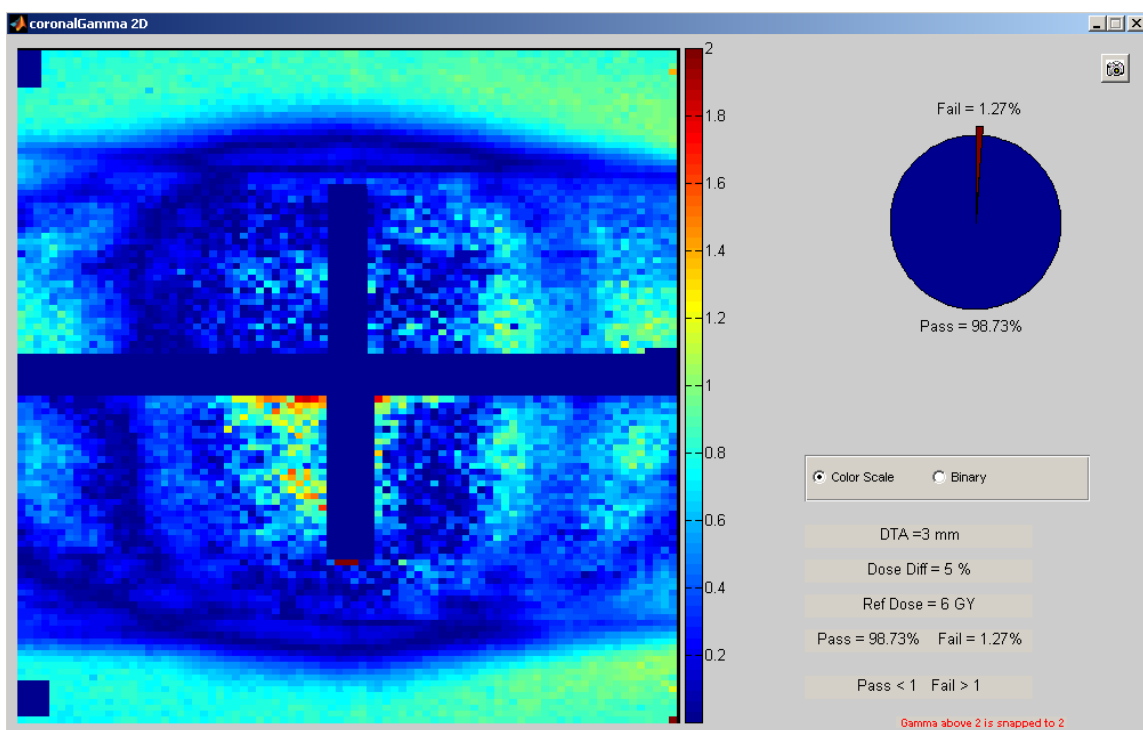


Figure 5.21 6 MV SBRT MDA 2D Gamma Index Results: $\pm 5\%/3\text{mm}$, Coronal Plane, Irradiation #3

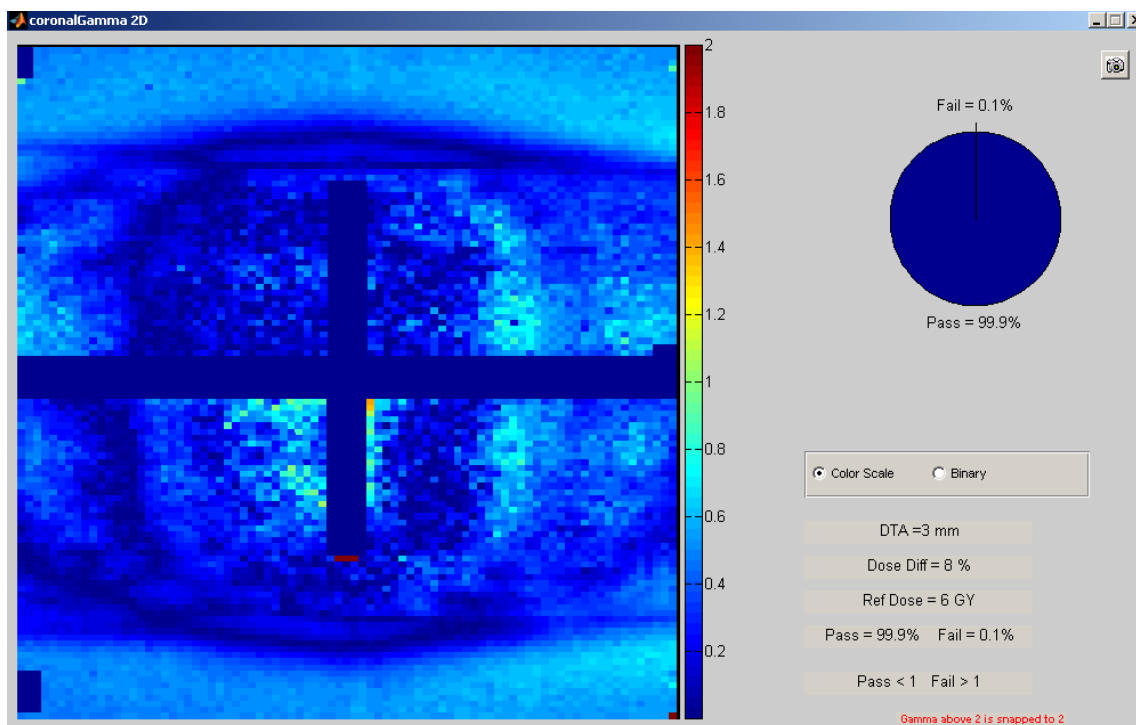


Figure 5.22 6 MV SBRT MDA 2D Gamma Index Results: $\pm 8\%/3\text{mm}$, Coronal Plane, Irradiation #3

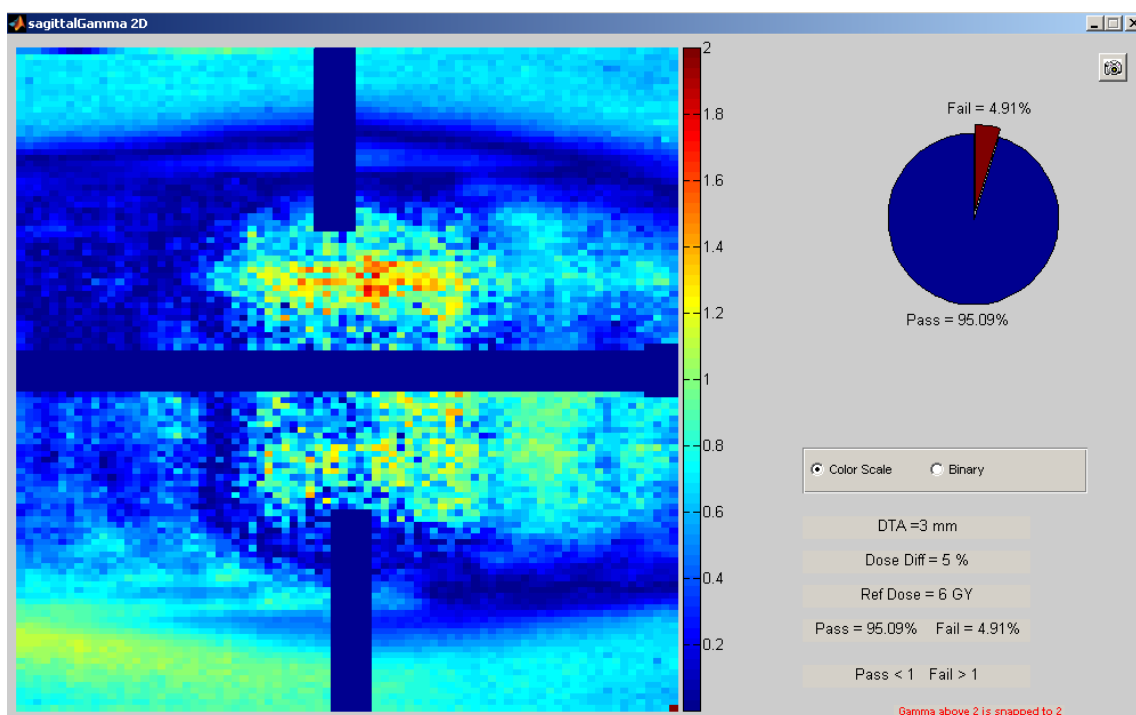


Figure 5.23 6 MV SBRT MDA 2D Gamma Index Results: $\pm 5\%/3\text{mm}$, Sagittal Plane, Irradiation #3

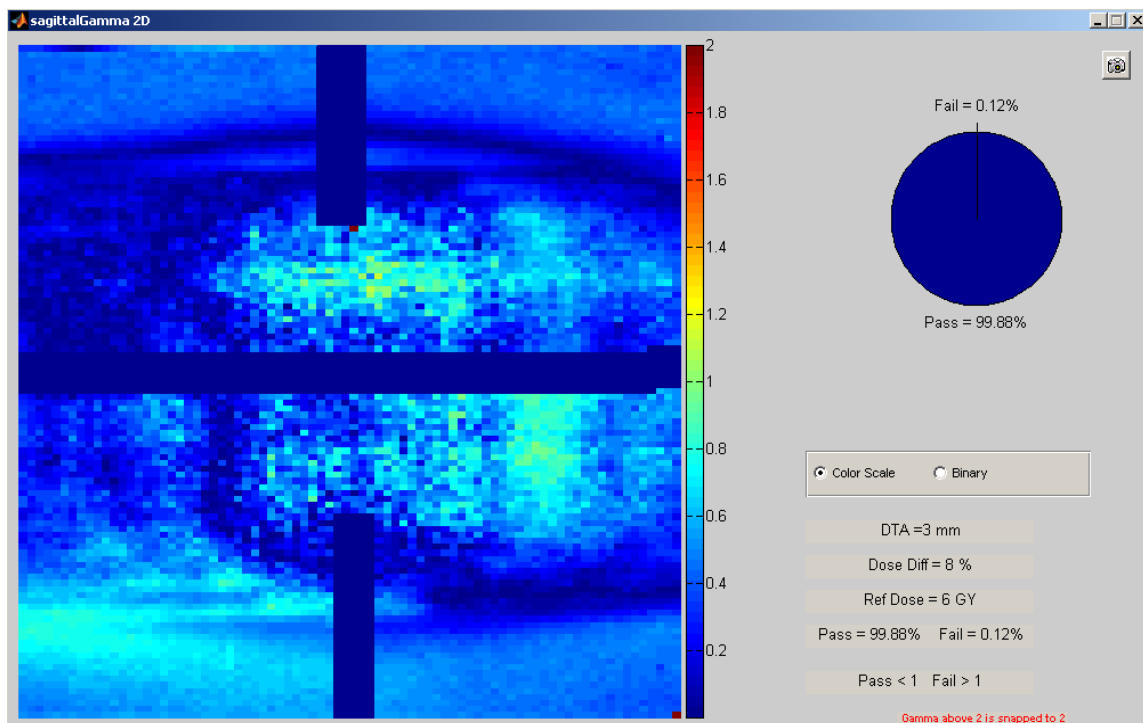


Figure 5.24 6 MV SBRT MDA 2D Gamma Index Results: $\pm 8\%/3\text{mm}$, Sagittal Plane, Irradiation #3

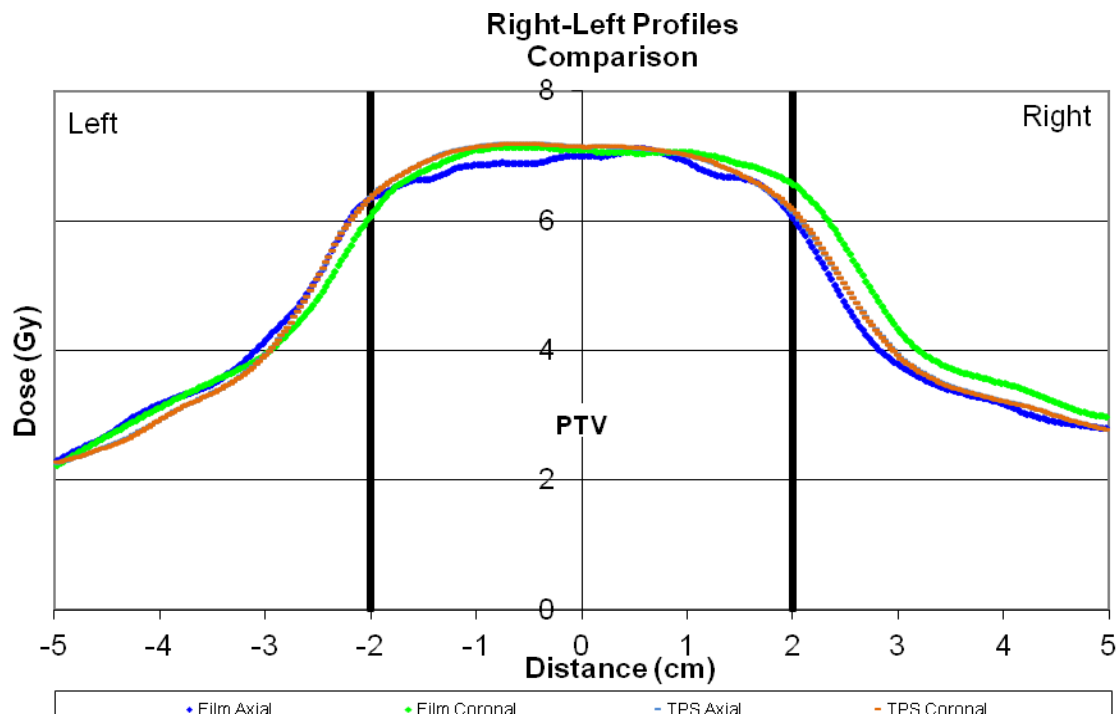


Figure 5.25 6 MV SBRT MDA 1D Right-Left Dose Profiles: Irradiation #3

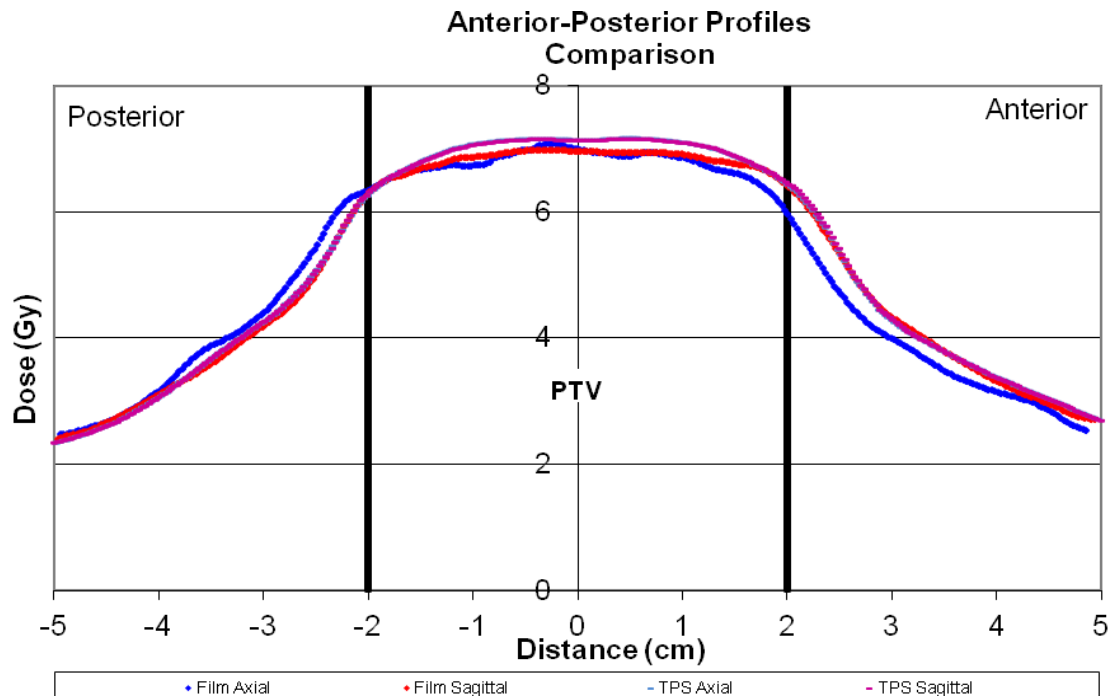


Figure 5.26 6 MV SBRT MDA 1D Anterior-Posterior Dose Profiles: Irradiation #3

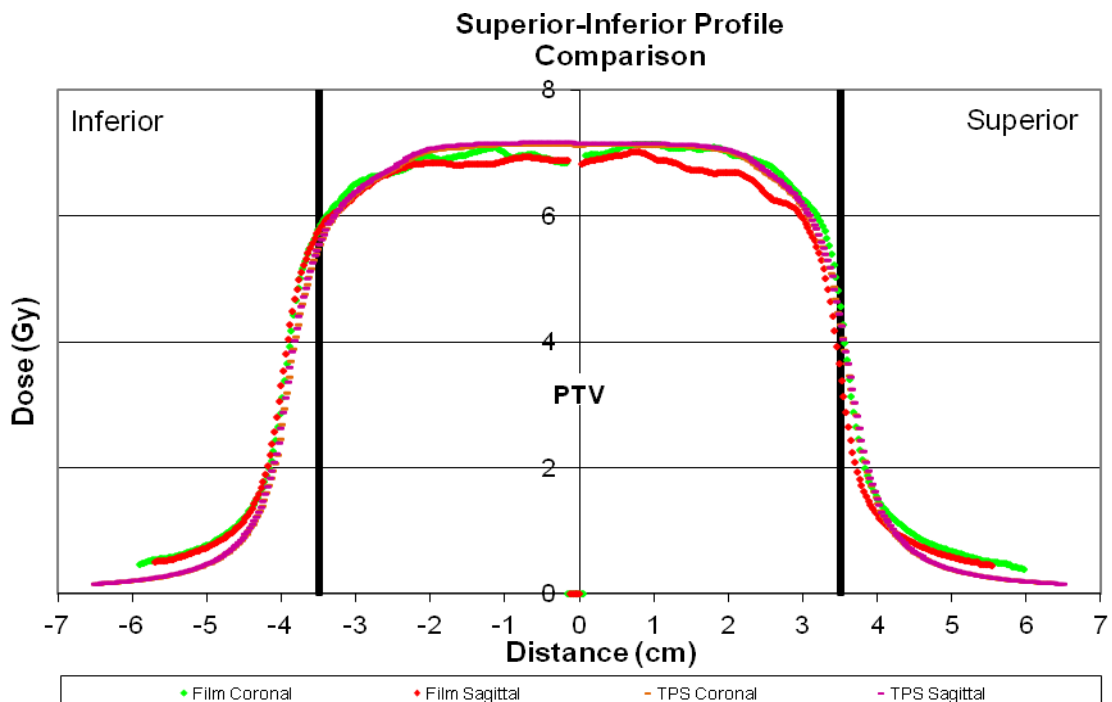


Figure 5.27 6 MV SBRT MDA 1D Superior-Inferior Dose Profiles: Irradiation #3

5.2 18 MV SBRT MD Anderson CANCER CENTER 2D Gamma Index Maps and Dose Profiles

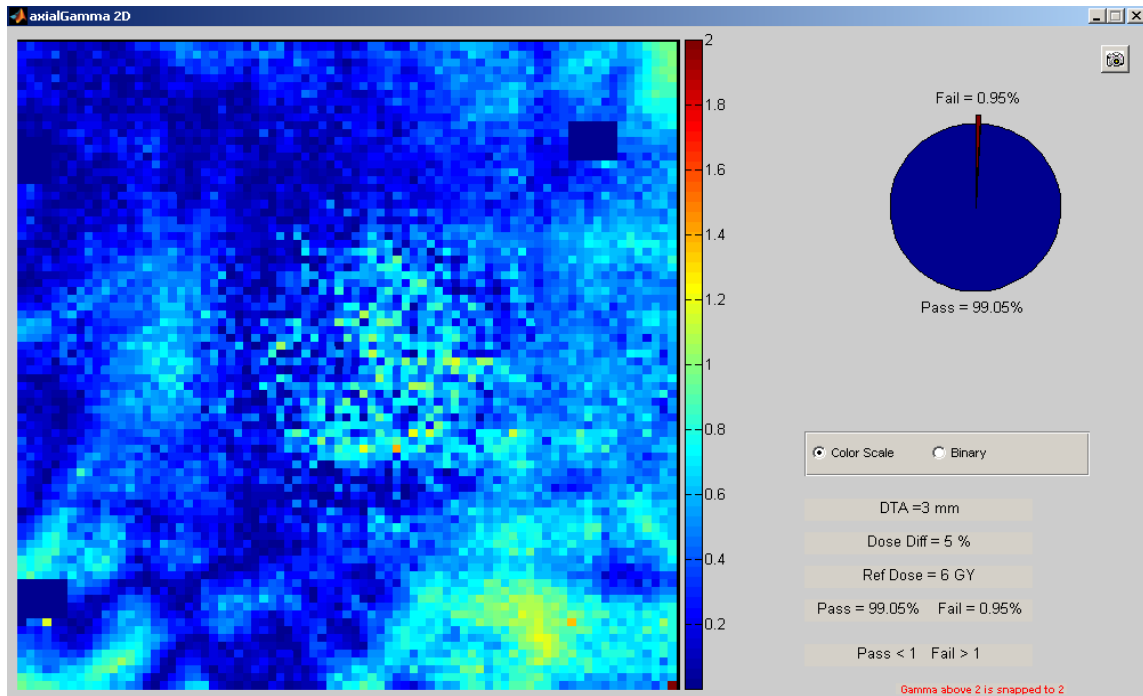


Figure 5.28 18 MV SBRT MDA 2D Gamma Index Results: $\pm 5\%/3\text{mm}$, Axial Plane, Irradiation #1

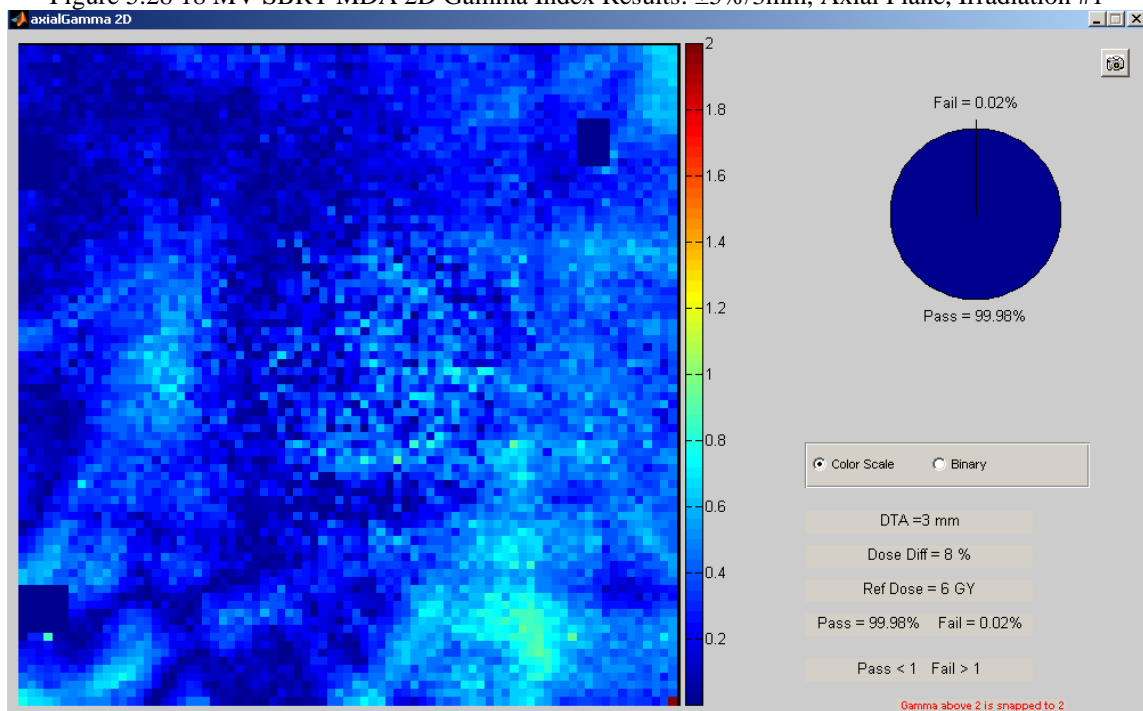


Figure 5.29 18 MV SBRT MDA 2D Gamma Index Results: $\pm 8\%/3\text{mm}$, Axial Plane, Irradiation #1

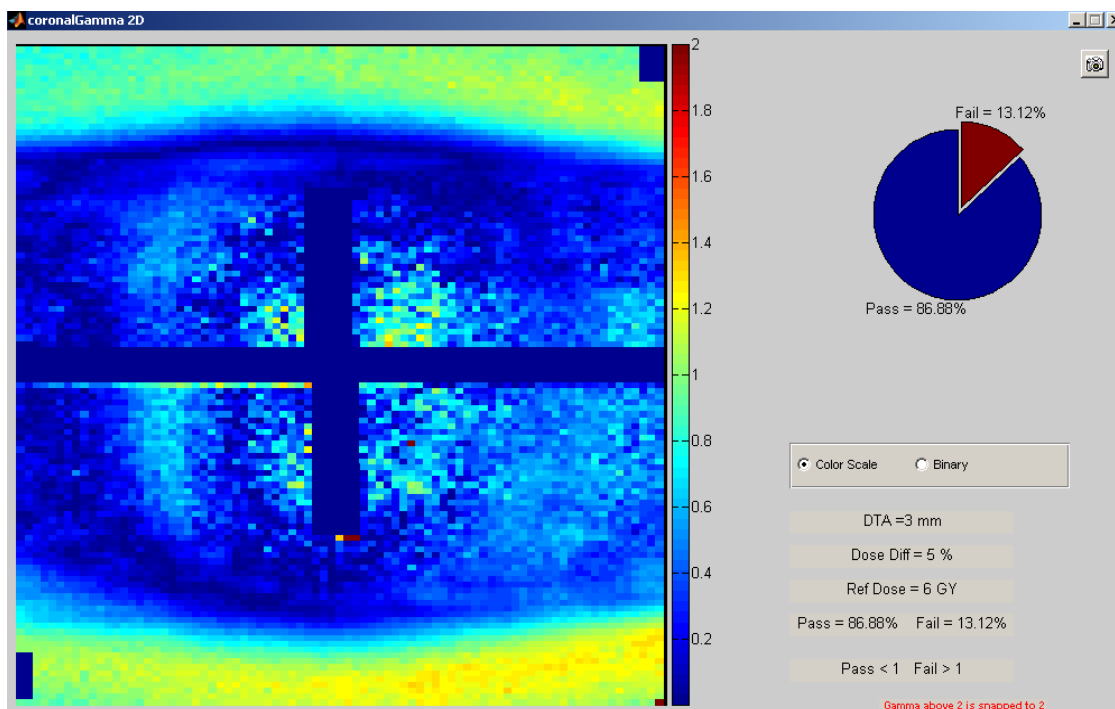


Figure 5.30 18 MV SBRT MDA 2D Gamma Index Results: $\pm 5\%/3\text{mm}$, Coronal Plane, Irradiation #1

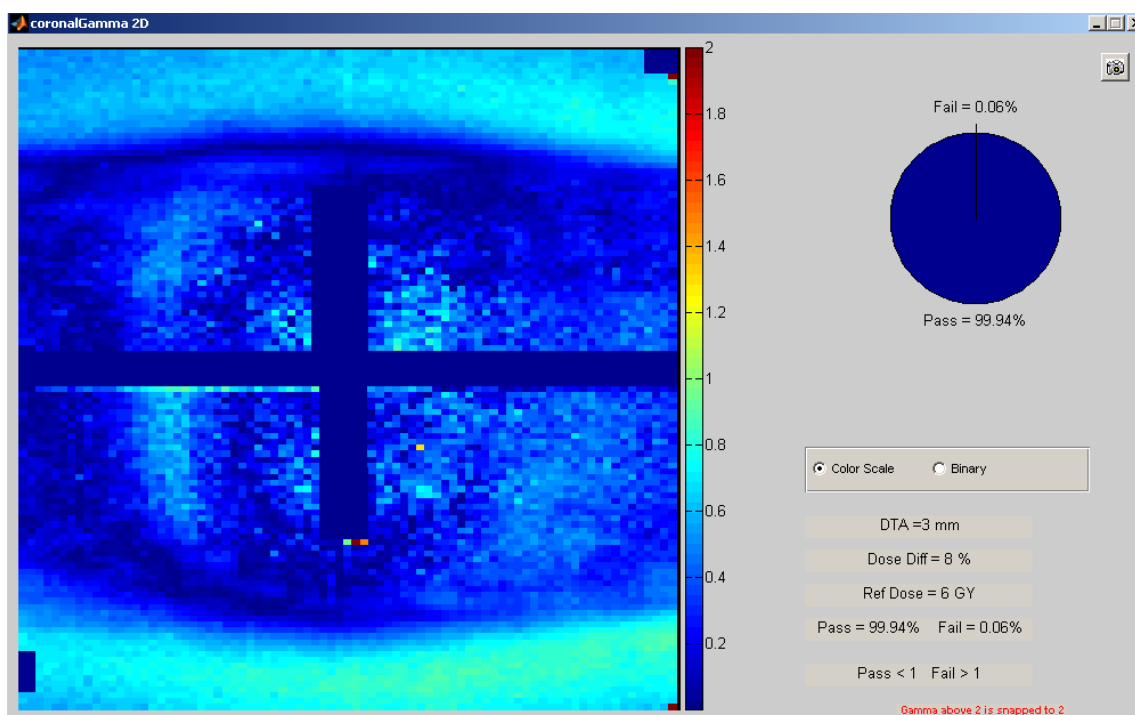


Figure 5.31 18 MV SBRT MDA 2D Gamma Index Results: $\pm 8\%/3\text{mm}$, Coronal Plane, Irradiation #1

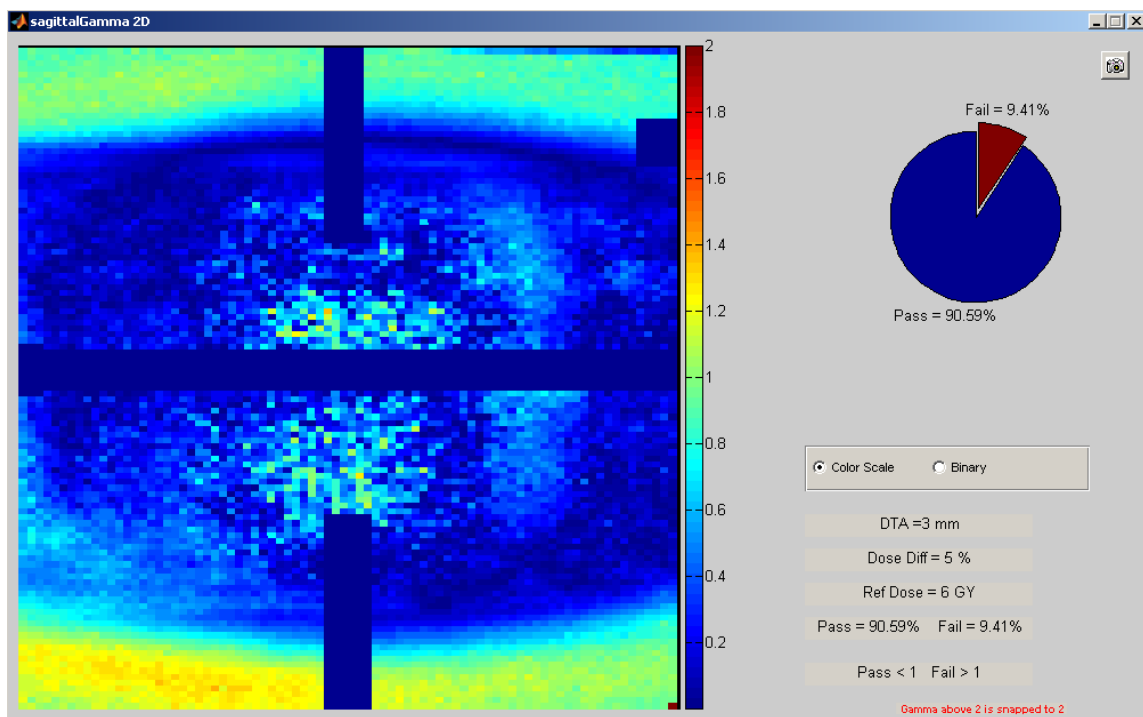


Figure 5.32 18 MV SBRT MDA 2D Gamma Index Results: $\pm 5\%/3\text{mm}$, Sagittal Plane, Irradiation #1

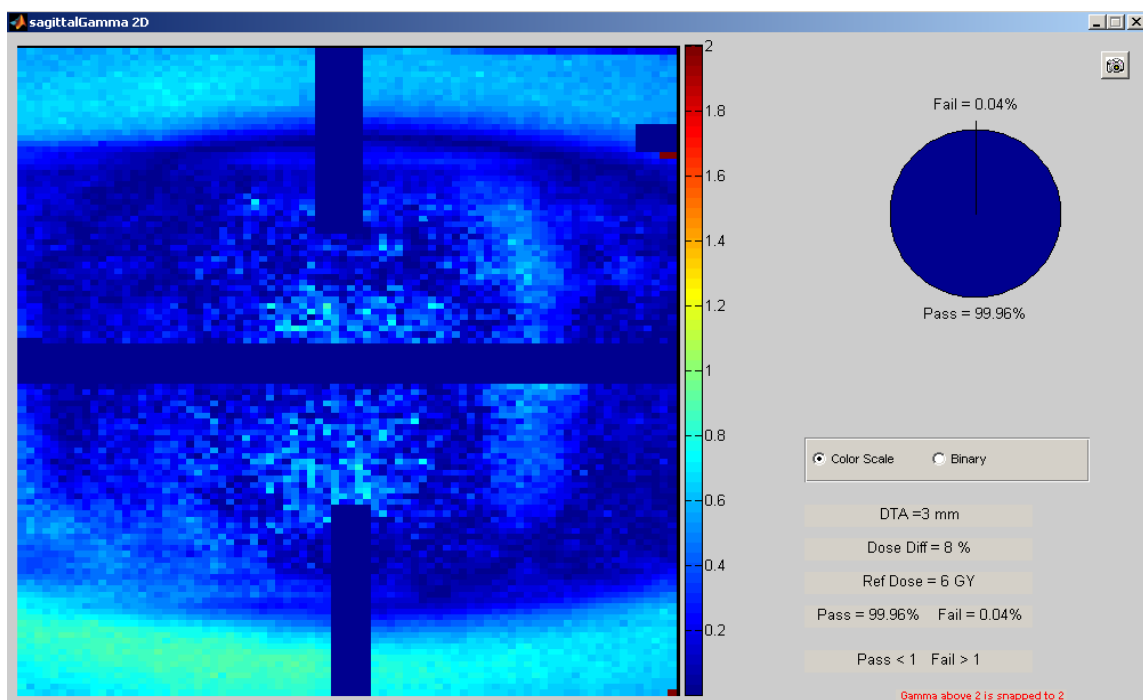


Figure 5.33 18 MV SBRT MDA 2D Gamma Index Results: $\pm 8\%/3\text{mm}$, Sagittal Plane, Irradiation #1

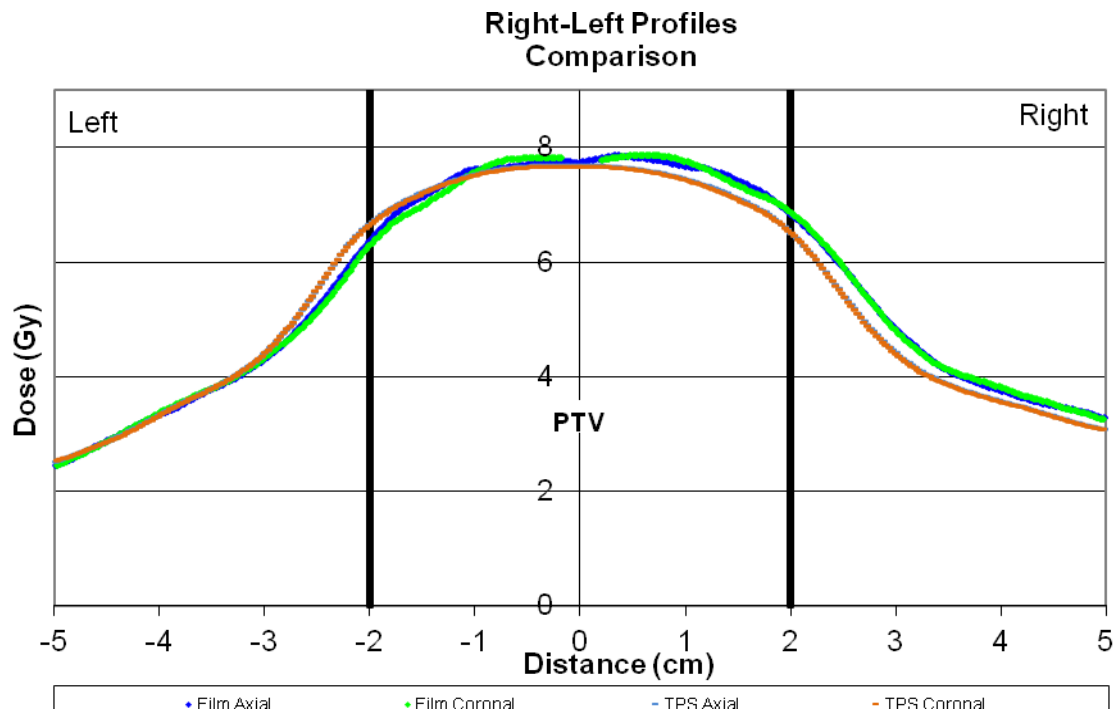


Figure 5.34 18 MV SBRT MDA 1D Right-Left Dose Profiles: Irradiation #1

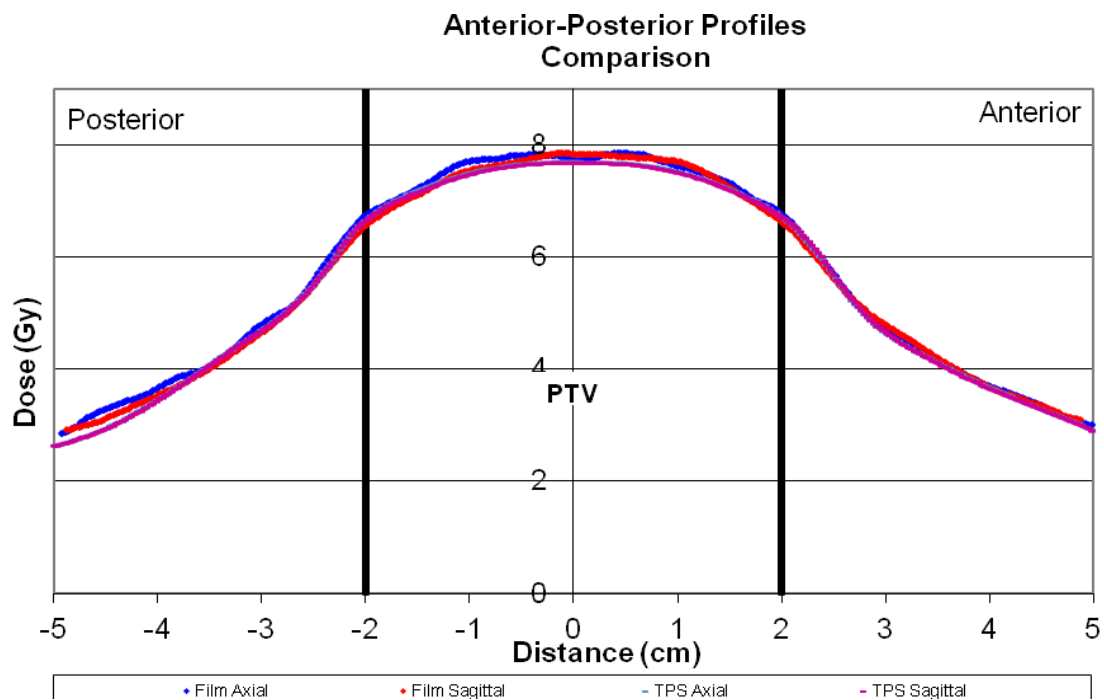


Figure 5.35 18 MV SBRT MDA 1D Anterior-Posterior Dose Profiles: Irradiation #1

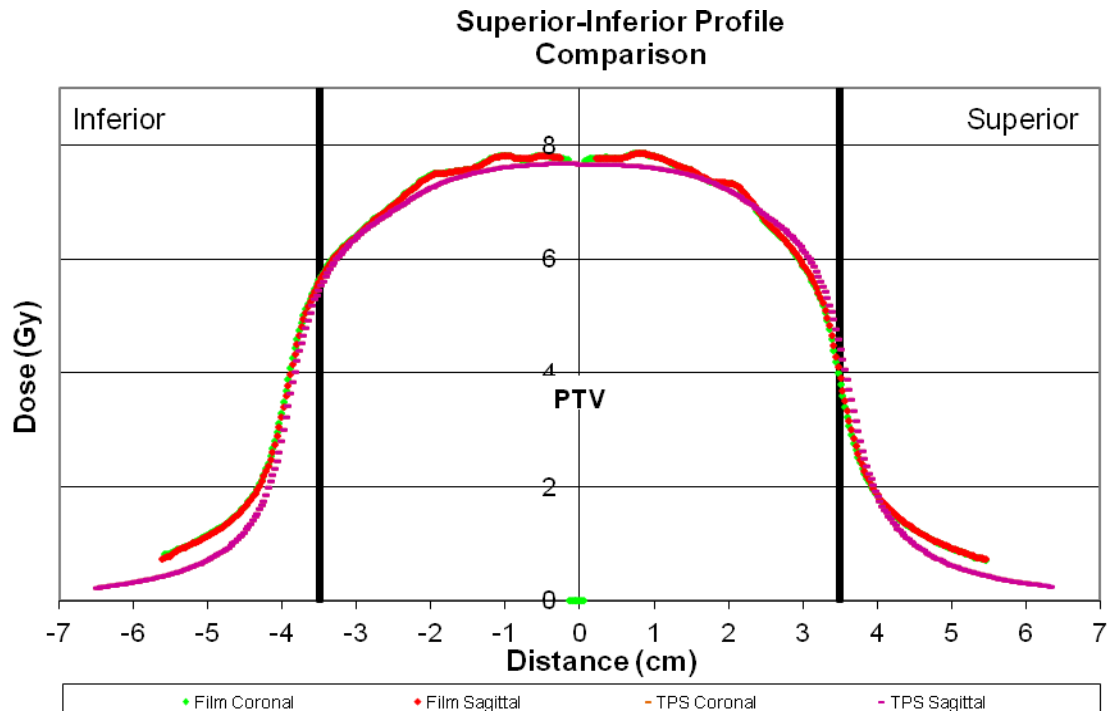


Figure 5.36 18 MV SBRT MDA 1D Superior-Inferior Dose Profiles: Irradiation #1

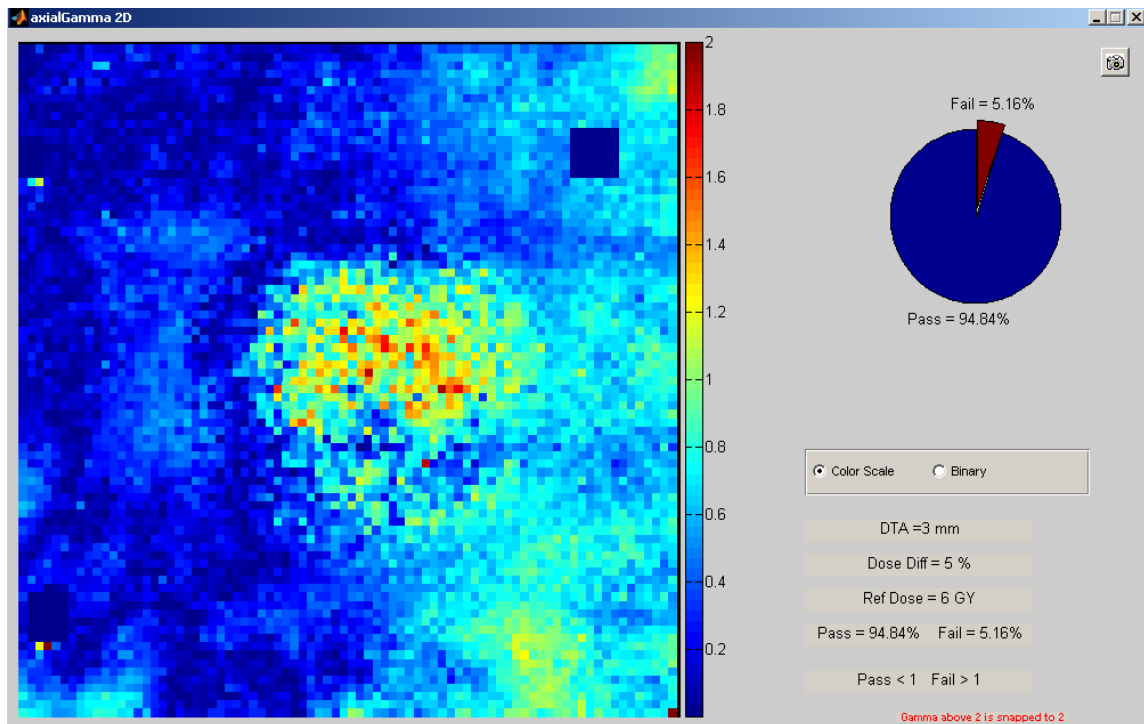


Figure 5.37 18 MV SBRT MDA 2D Gamma Index Results: $\pm 5\%/3\text{mm}$, Axial Plane, Irradiation #2

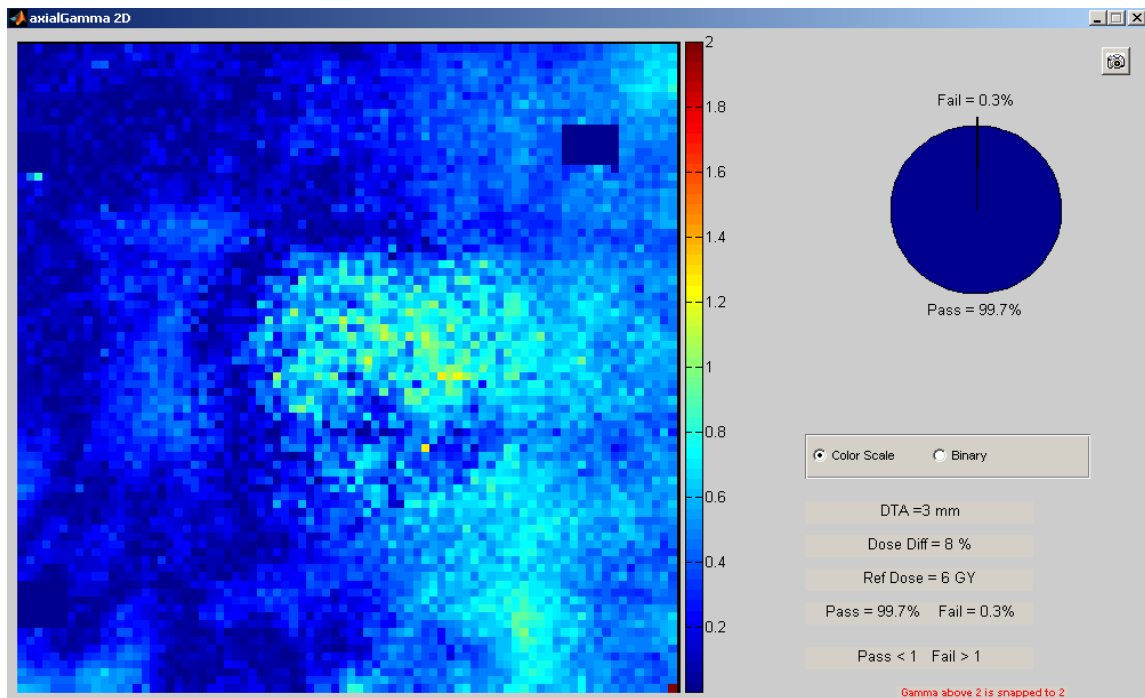


Figure 5.38 18 MV SBRT MDA 2D Gamma Index Results: $\pm 8\%/3\text{mm}$, Axial Plane, Irradiation #2

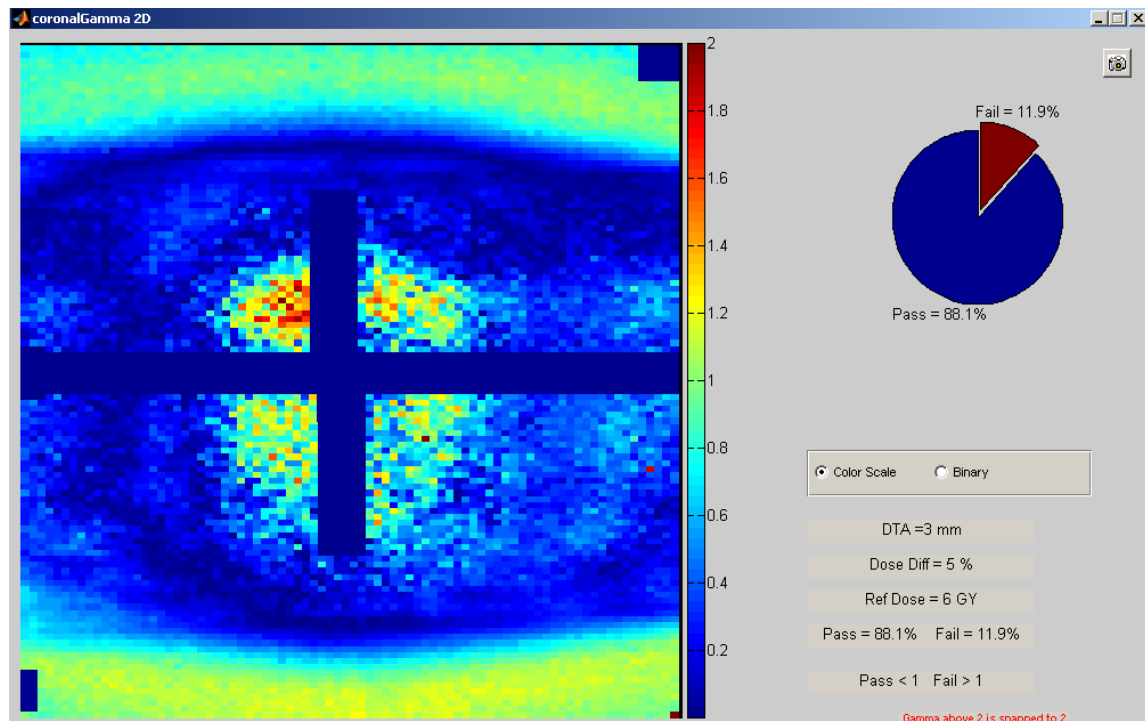


Figure 5.39 18 MV SBRT MDA 2D Gamma Index Results: $\pm 5\%/3\text{mm}$, Coronal Plane, Irradiation #2

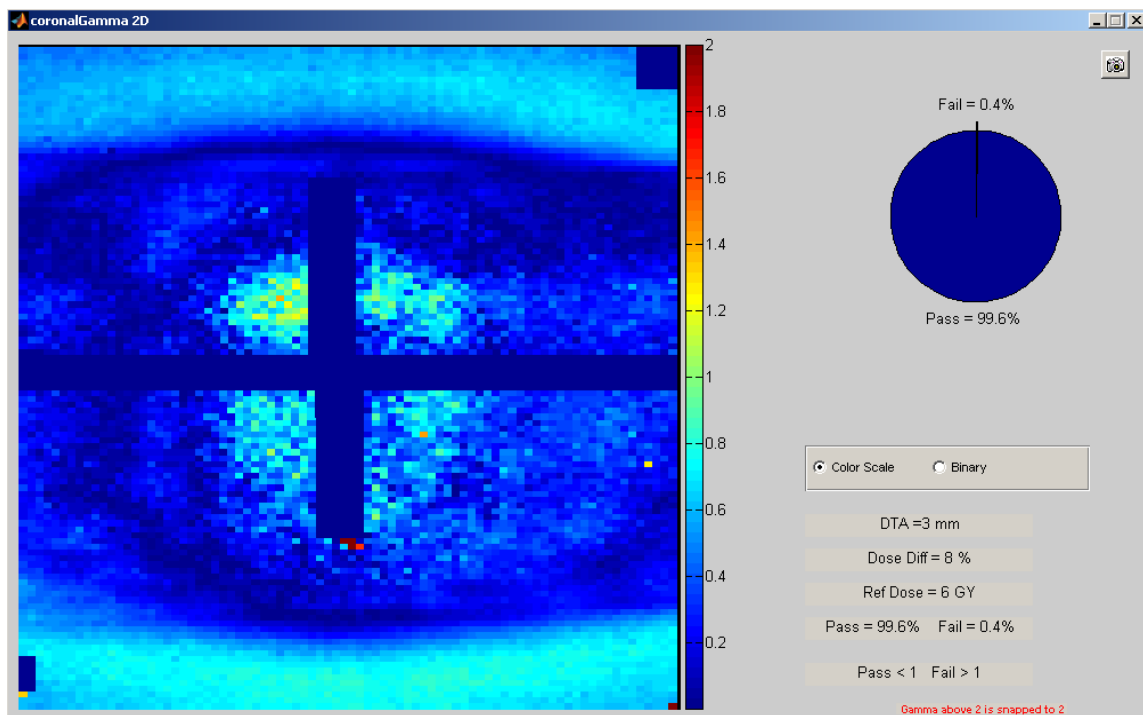


Figure 5.40 18 MV SBRT MDA 2D Gamma Index Results: $\pm 8\%/3\text{mm}$, Coronal Plane, Irradiation #2

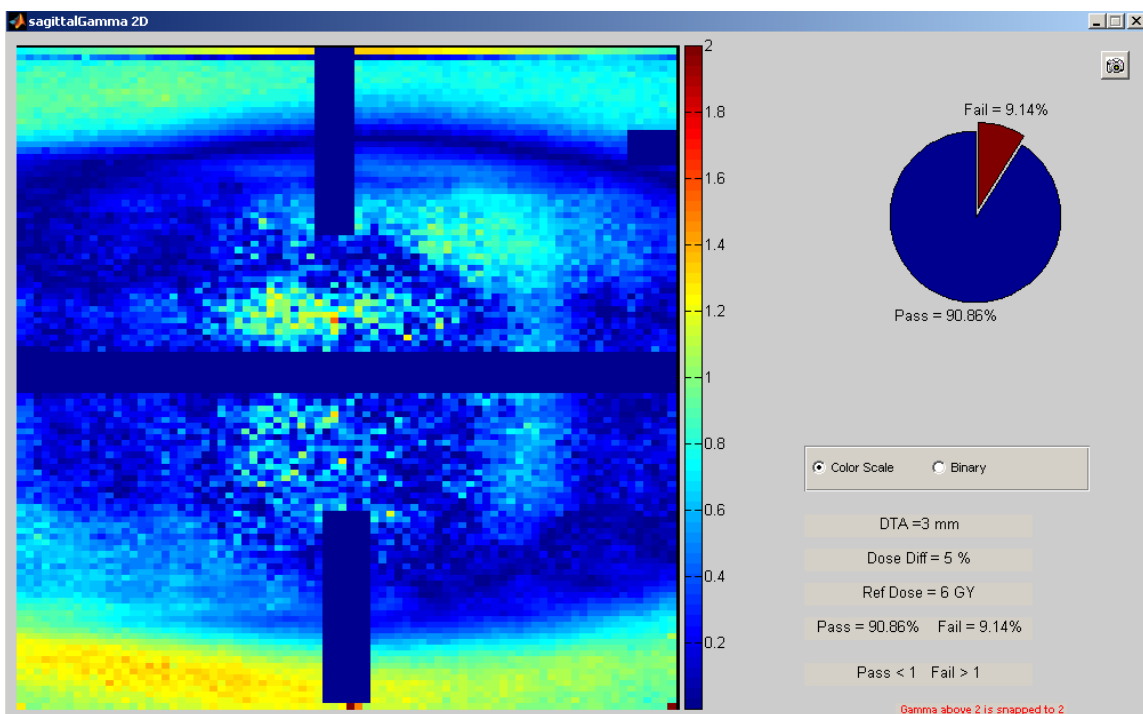


Figure 5.41 18 MV SBRT MDA 2D Gamma Index Results: $\pm 5\%/3\text{mm}$, Sagittal Plane, Irradiation #2

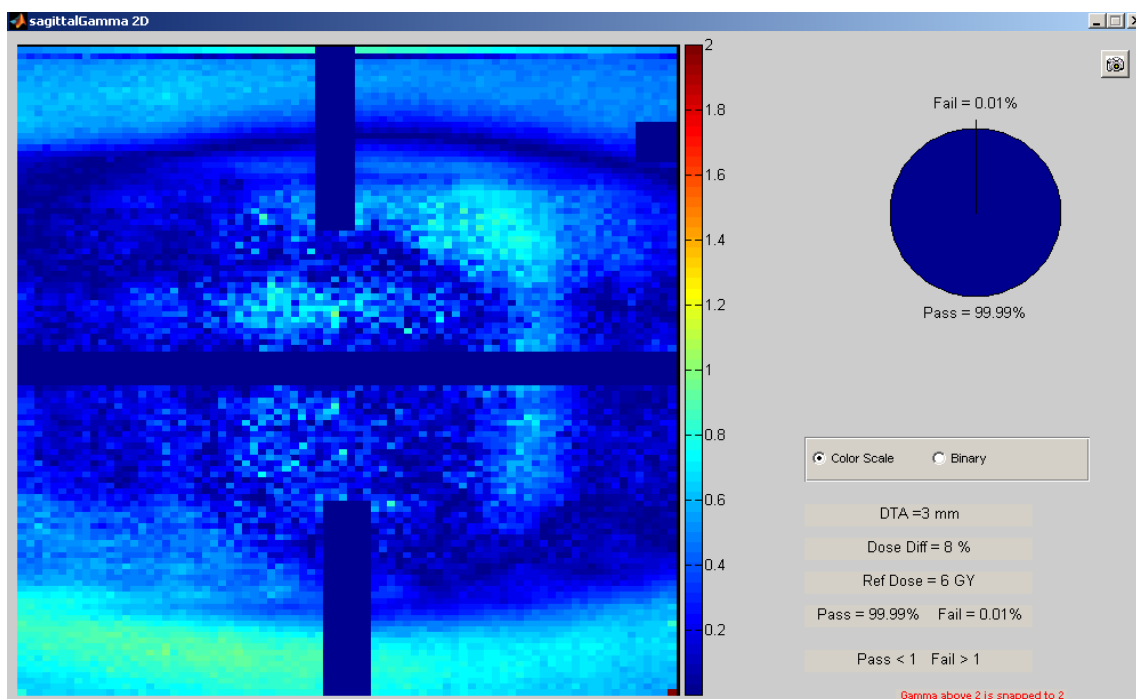


Figure 5.42 18 MV SBRT MDA 2D Gamma Index Results: $\pm 8\%/3\text{mm}$, Sagittal Plane, Irradiation #2

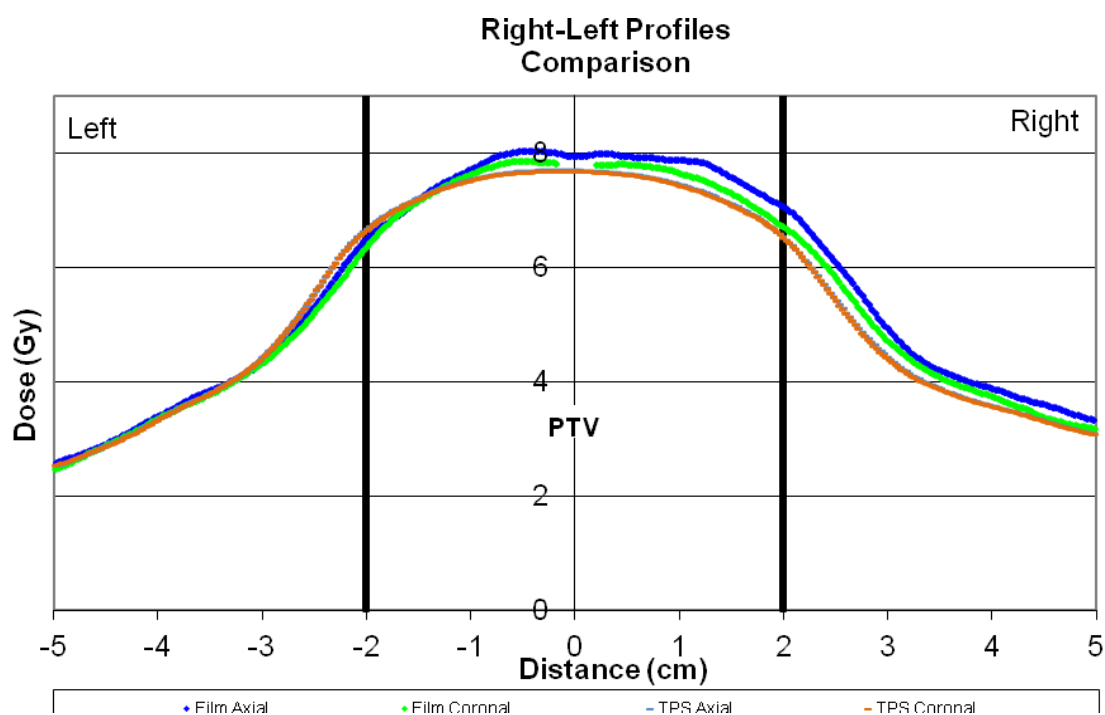


Figure 5.43 18 MV SBRT MDA 1D Right-Left Dose Profiles: Irradiation #2

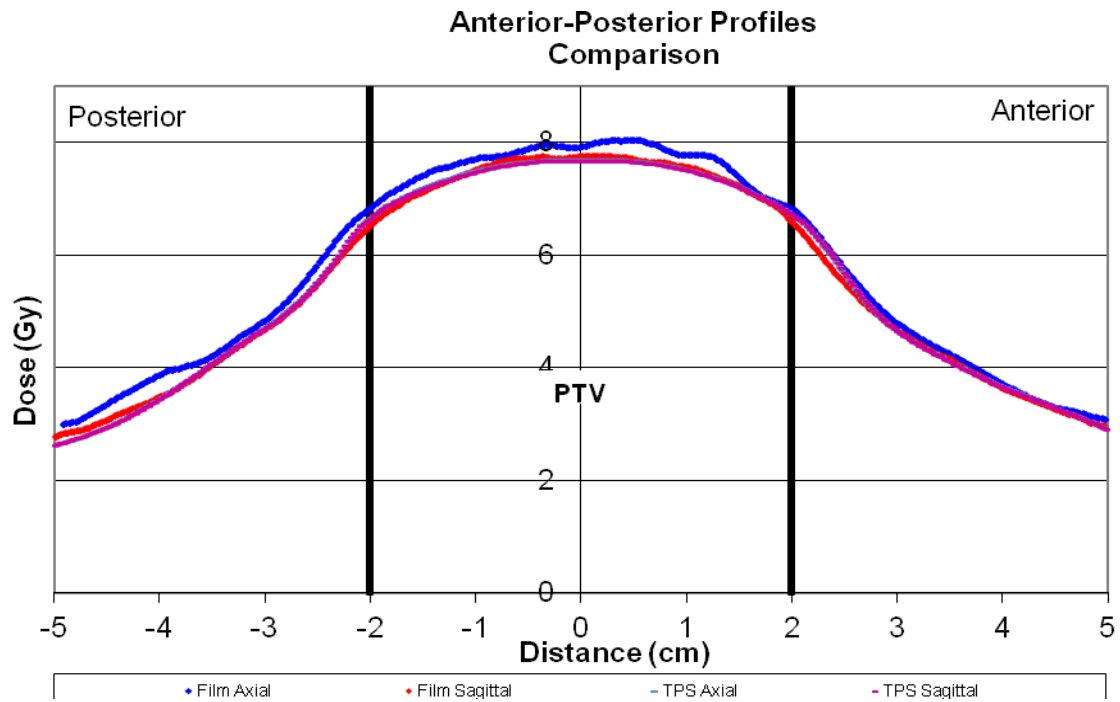


Figure 5.44 18 MV SBRT MDA 1D Anterior-Posterior Dose Profiles: Irradiation #2

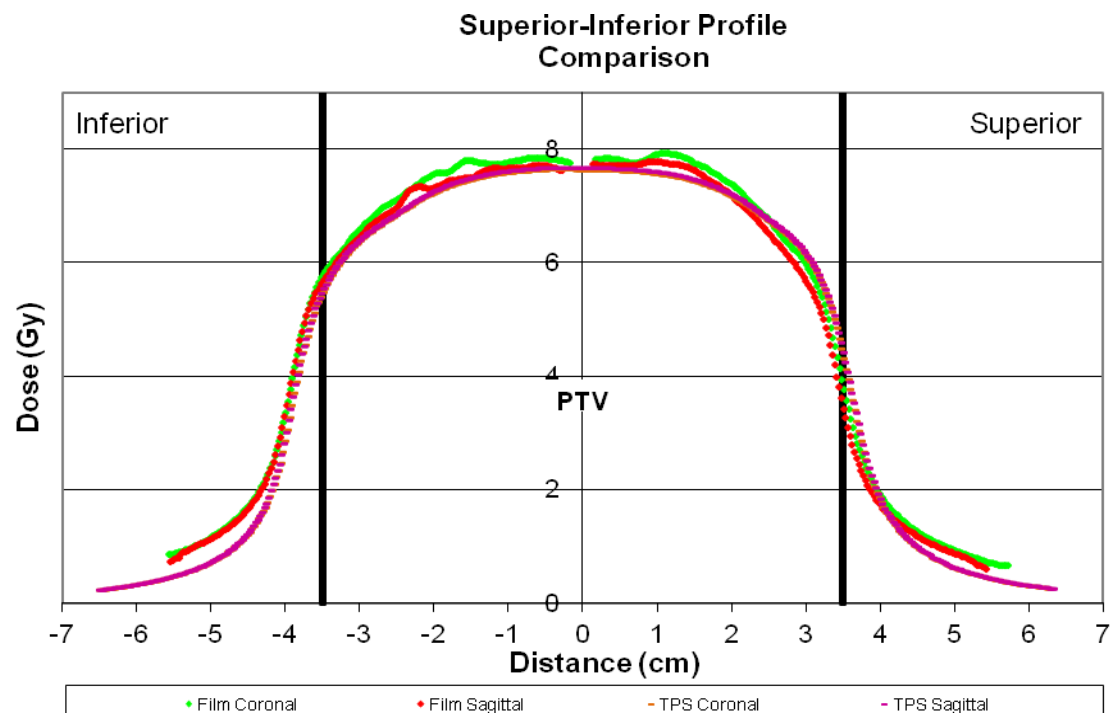


Figure 5.45 18 MV SBRT MDA 1D Superior-Inferior Dose Profiles: Irradiation #2

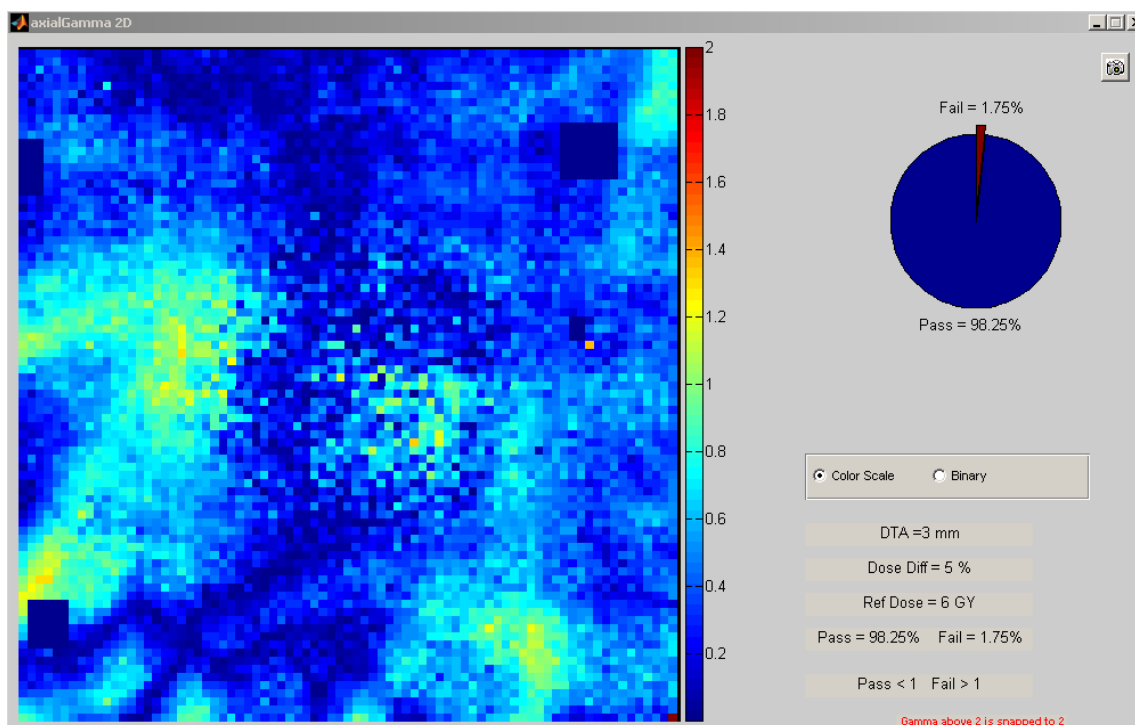


Figure 5.46 18 MV SBRT MDA 2D Gamma Index Results: $\pm 5\%/3\text{mm}$, Axial Plane, Irradiation #3

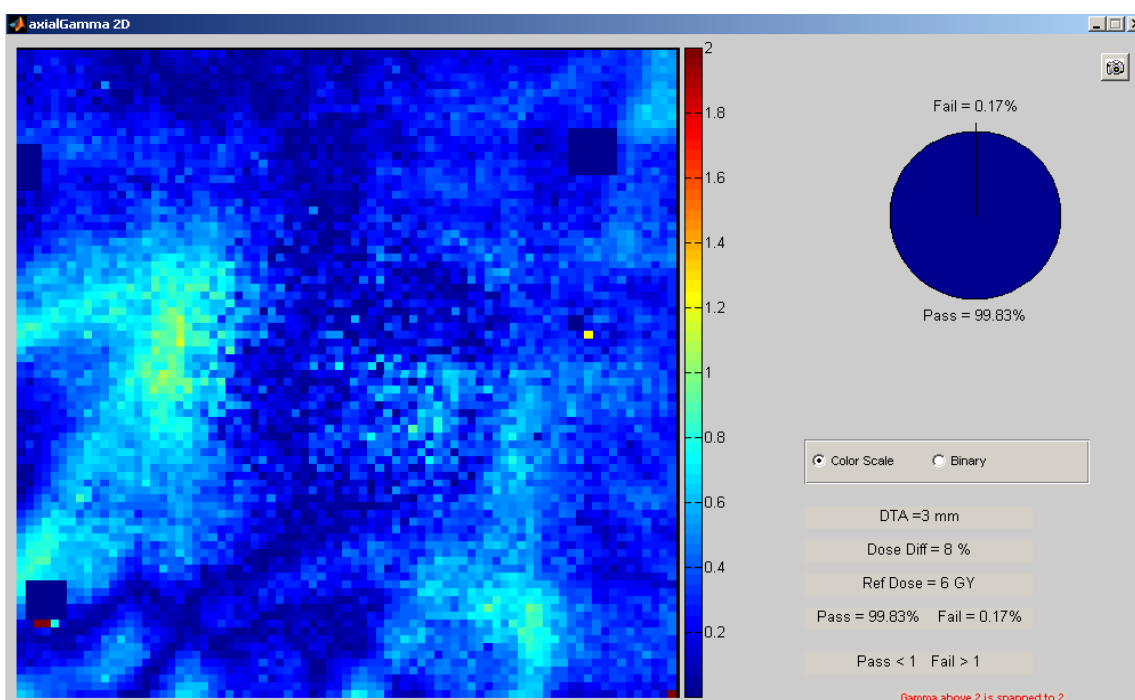


Figure 5.47 18 MV SBRT MDA 2D Gamma Index Results: $\pm 8\%/3\text{mm}$, Axial Plane, Irradiation #3

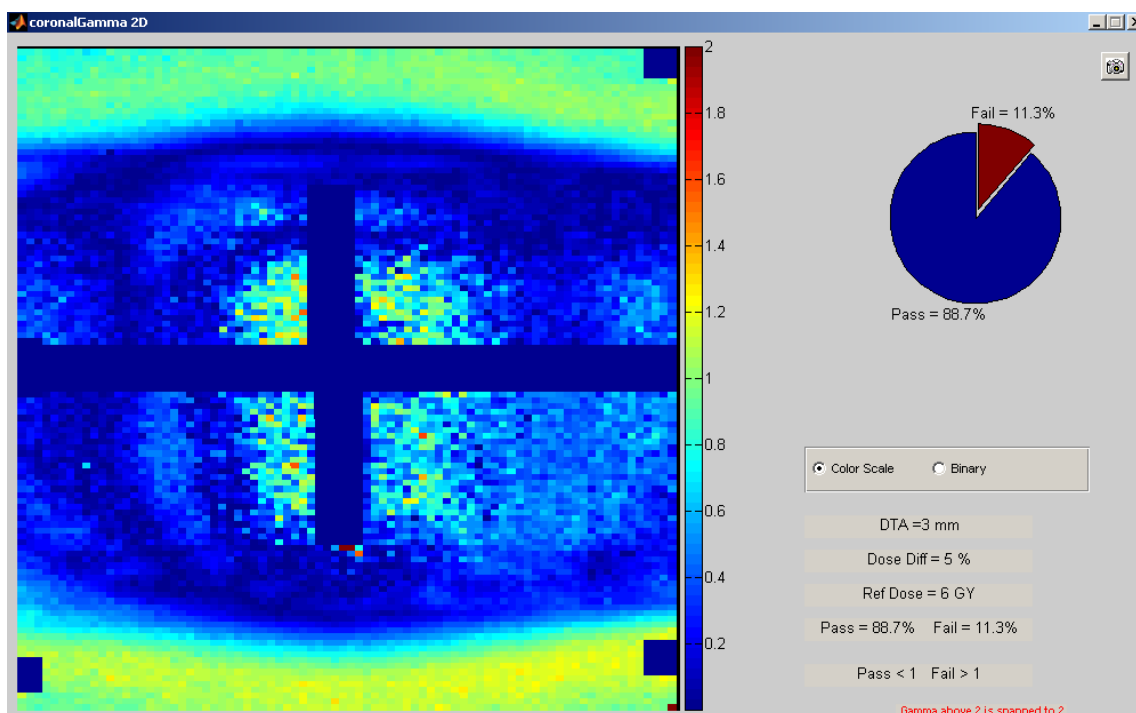


Figure 5.48 18 MV SBRT MDA 2D Gamma Index Results: $\pm 5\%/3\text{mm}$, Coronal Plane, Irradiation #3

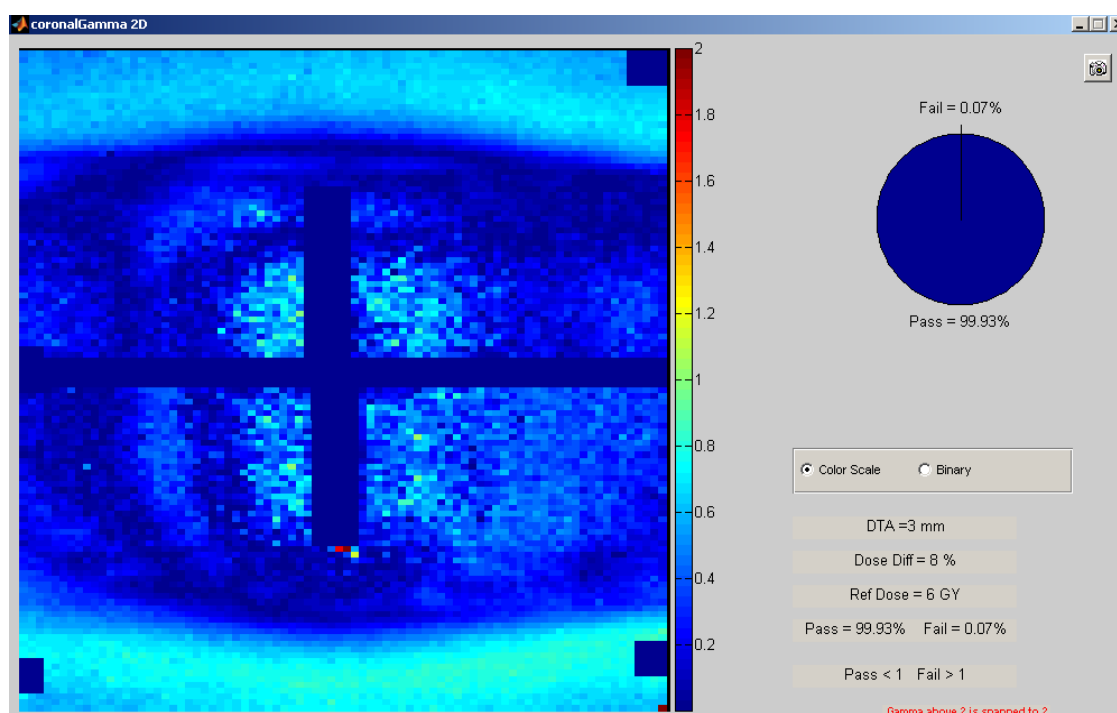


Figure 5.49 18 MV SBRT MDA 2D Gamma Index Results: $\pm 8\%/3\text{mm}$, Coronal Plane, Irradiation #3

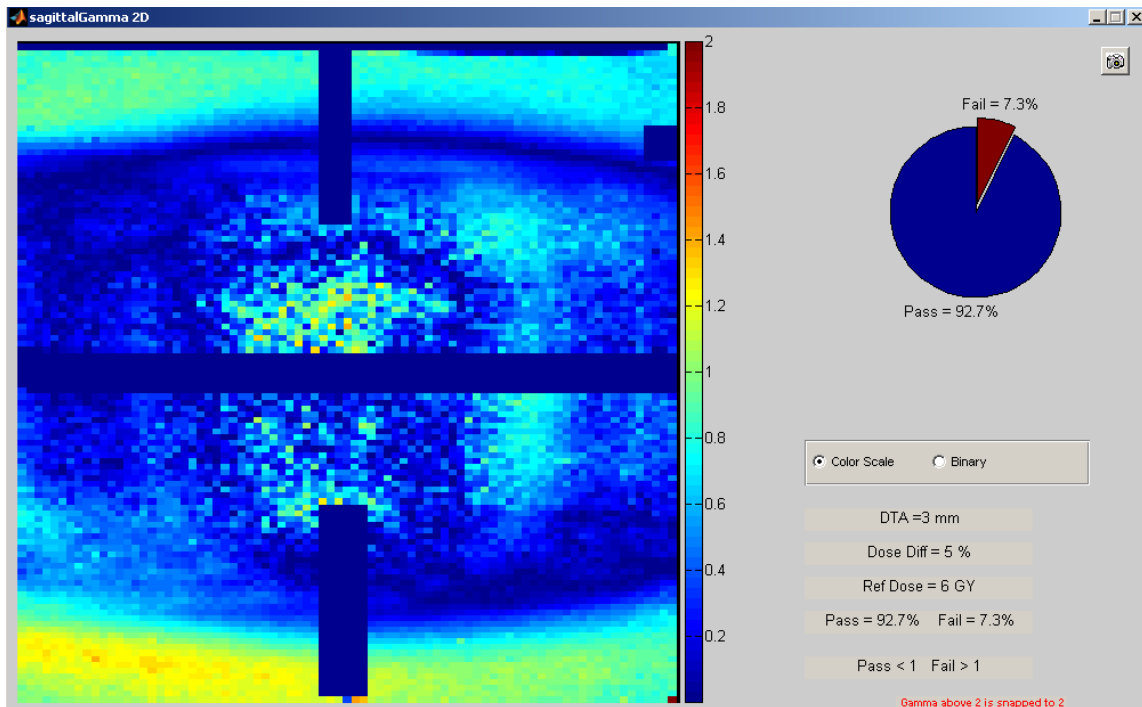


Figure 5.50 18 MV SBRT MDA 2D Gamma Index Results: $\pm 5\%/3\text{mm}$, Sagittal Plane, Irradiation #3

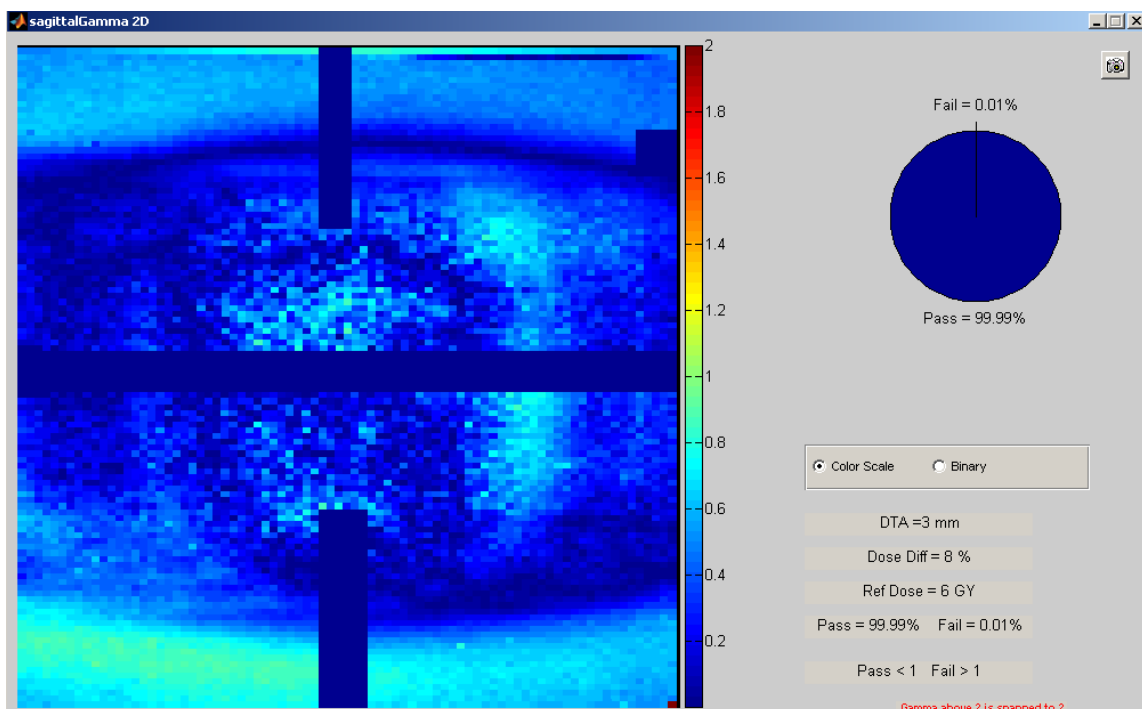


Figure 5.51 18 MV SBRT MDA 2D Gamma Index Results: $\pm 8\%/3\text{mm}$, Sagittal Plane, Irradiation #3

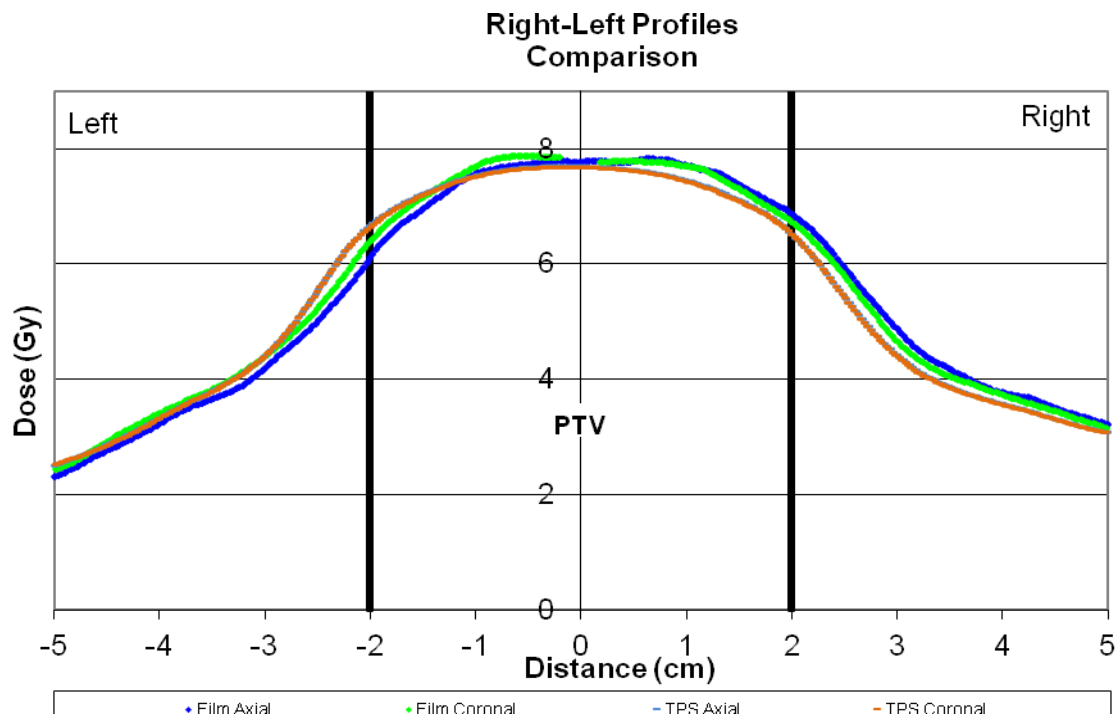


Figure 5.52 18 MV SBRT MDA 1D Right-Left Dose Profiles: Irradiation #3

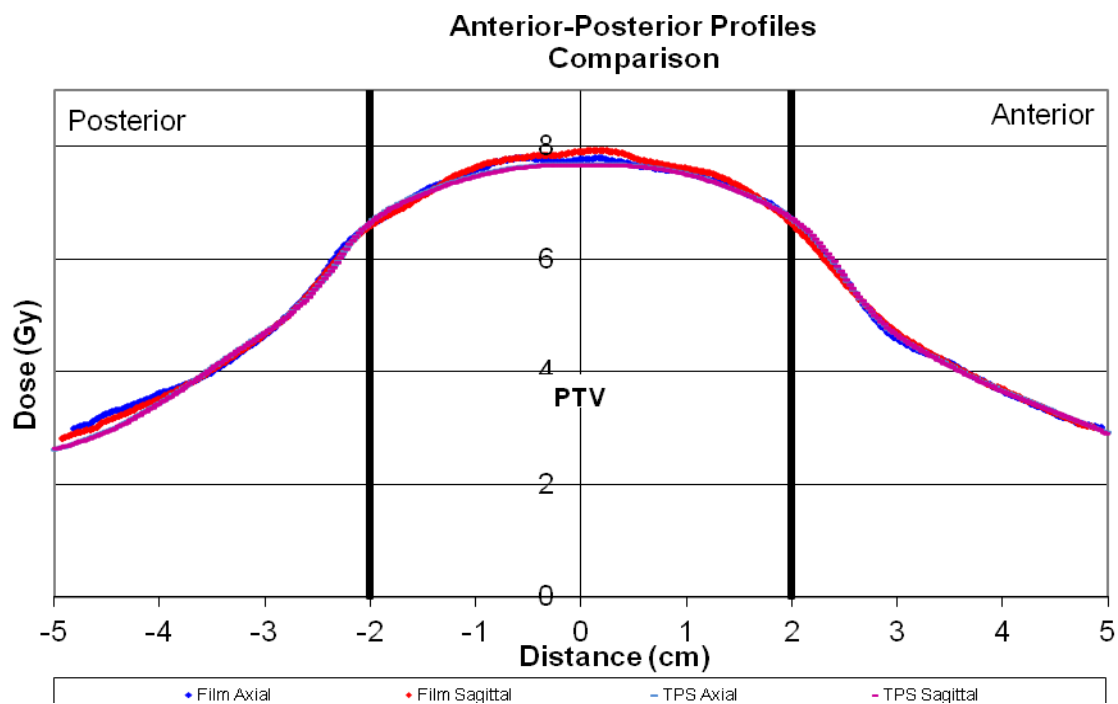


Figure 5.53 18 MV SBRT MDA 1D Anterior-Posterior Dose Profiles: Irradiation #3

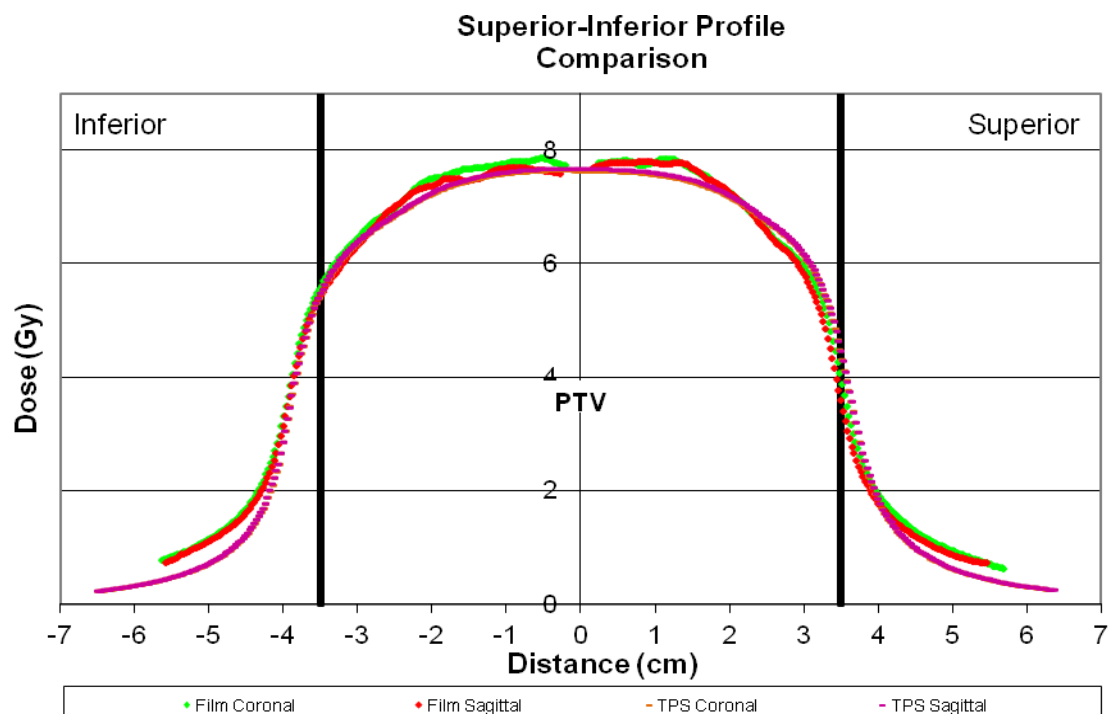


Figure 5.54 18 MV SBRT MDA 1D Superior-Inferior Dose Profiles: Irradiation #3

5.3 6 MV SBRT University of Alabama MEDICAL CENTER 2D Gamma Index

Maps and Dose Profiles

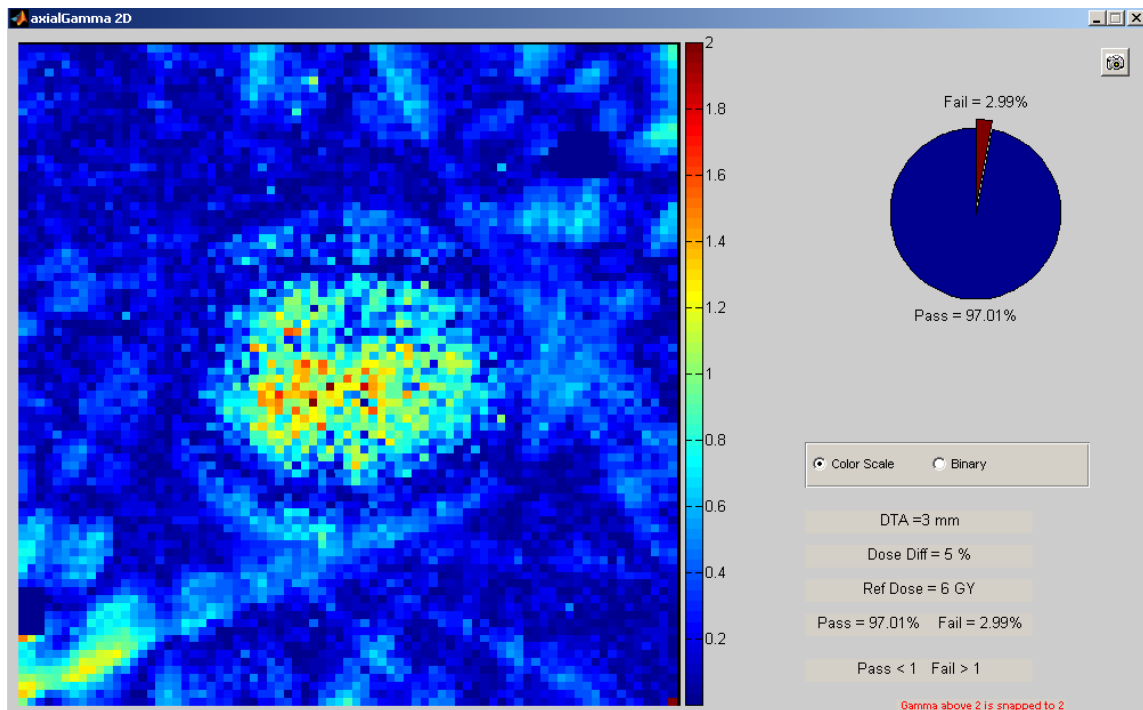


Figure 5.55 6 MV SBRT UAB 2D Gamma Index Results: $\pm 5\%/3\text{mm}$, Axial Plane, Irradiation #1

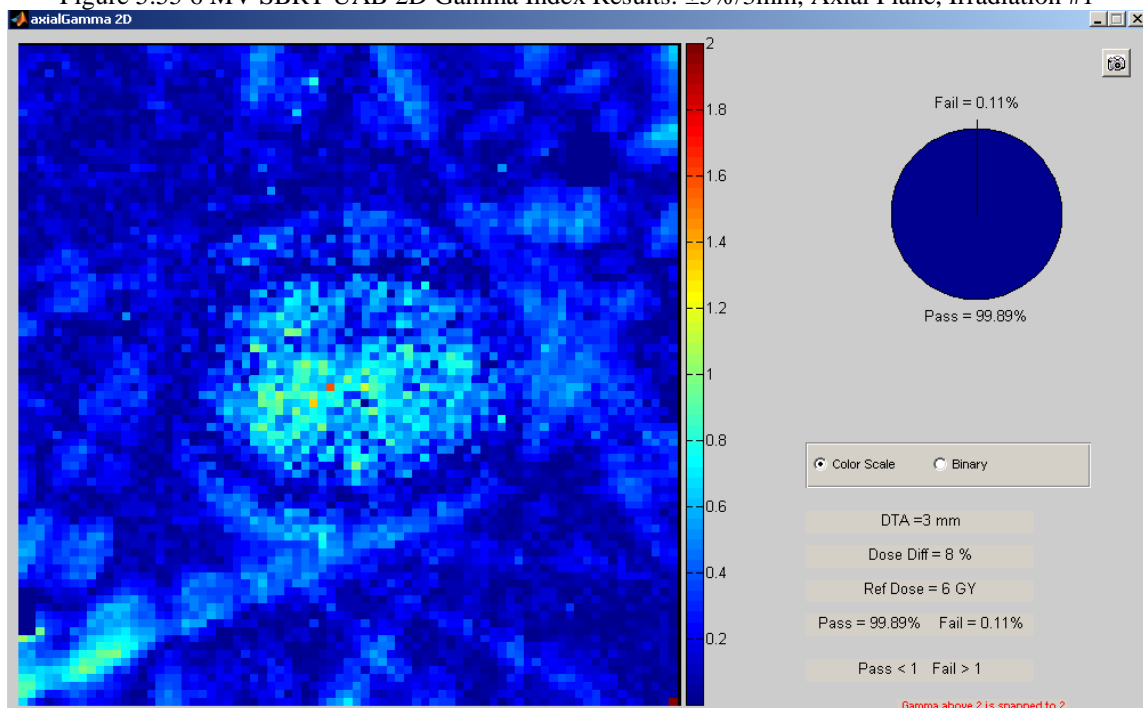


Figure 5.56 6 MV SBRT UAB 2D Gamma Index Results: $\pm 8\%/3\text{mm}$, Axial Plane, Irradiation #1

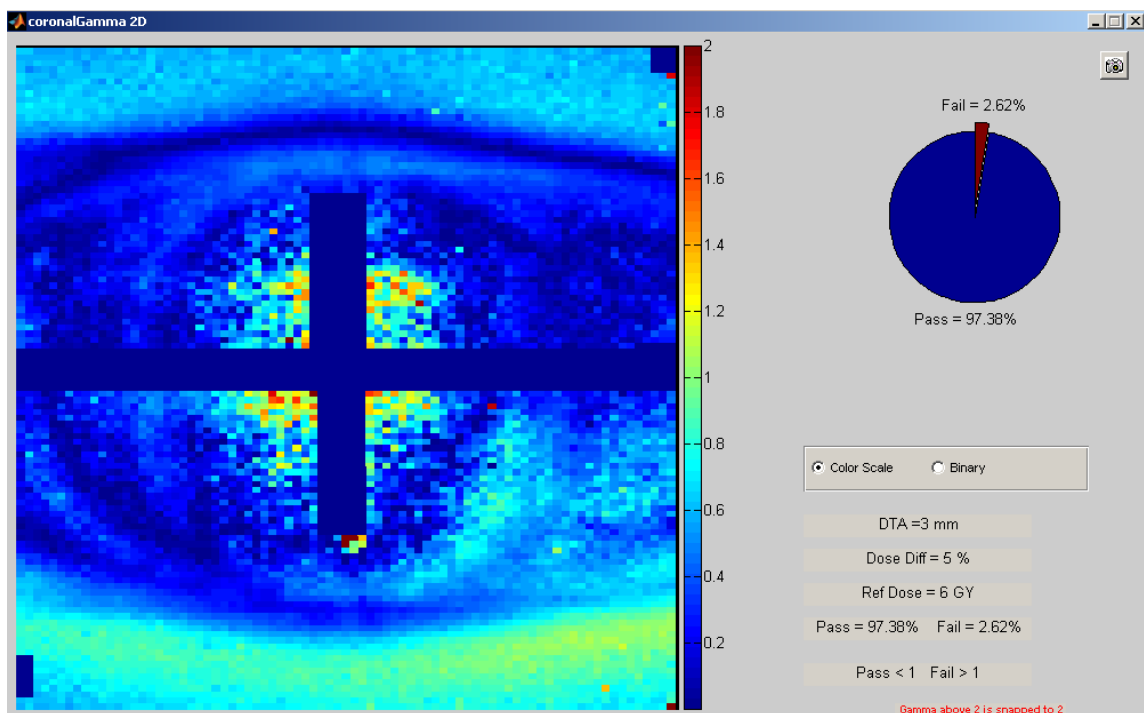


Figure 5.57 6 MV SBRT UAB 2D Gamma Index Results: $\pm 5\%/3\text{mm}$, Coronal Plane, Irradiation #1

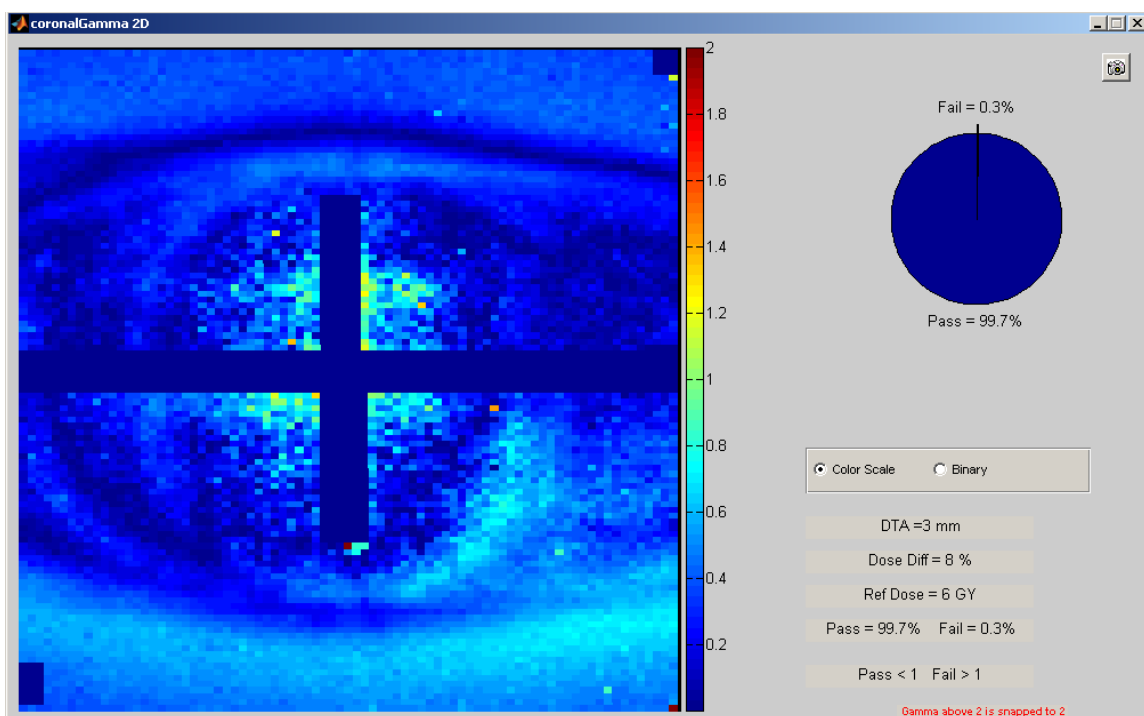


Figure 5.58 6 MV SBRT UAB 2D Gamma Index Results: $\pm 8\%/3\text{mm}$, Coronal Plane, Irradiation #1

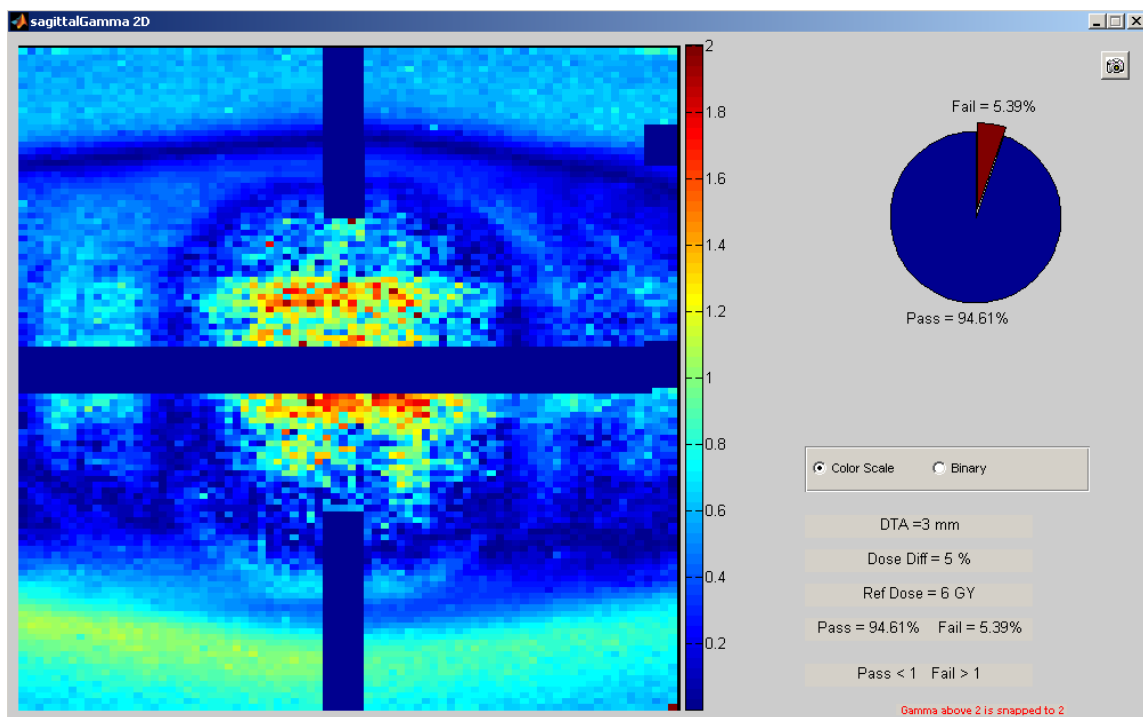


Figure 5.59 6 MV SBRT UAB 2D Gamma Index Results: $\pm 5\%/3\text{mm}$, Sagittal Plane, Irradiation #1

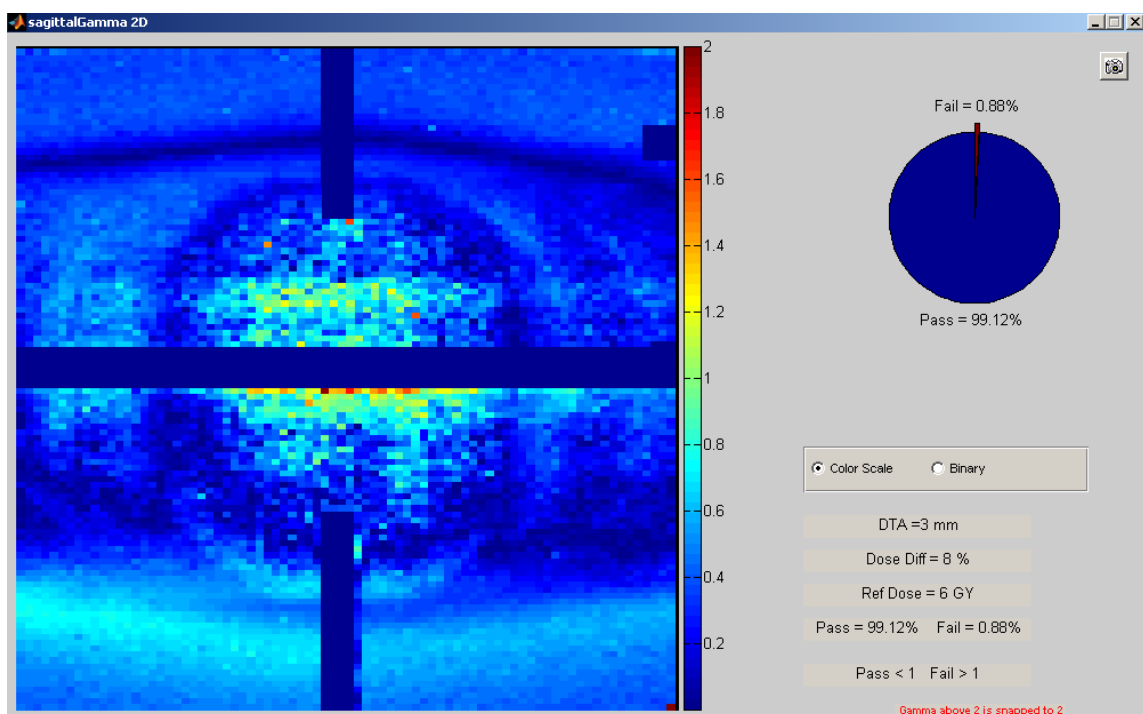


Figure 5.60 6 MV SBRT UAB 2D Gamma Index Results: $\pm 8\%/3\text{mm}$, Sagittal Plane, Irradiation #1

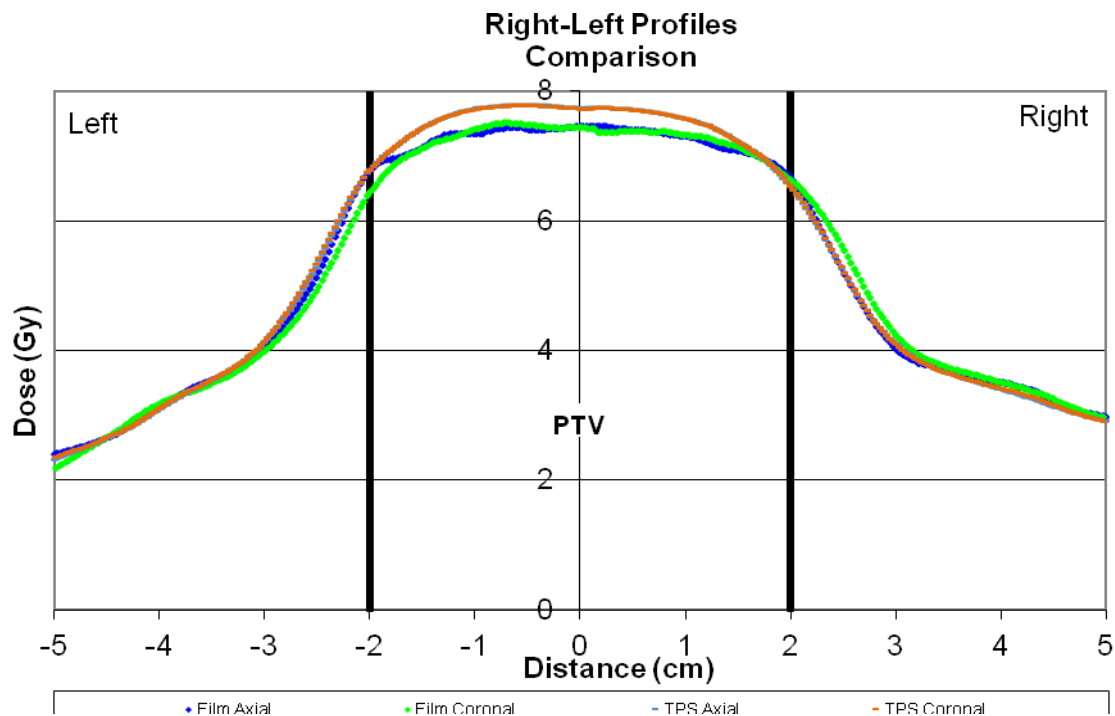


Figure 5.61 6 MV SBRT UAB 1D Right-Left Dose Profiles: Irradiation #1

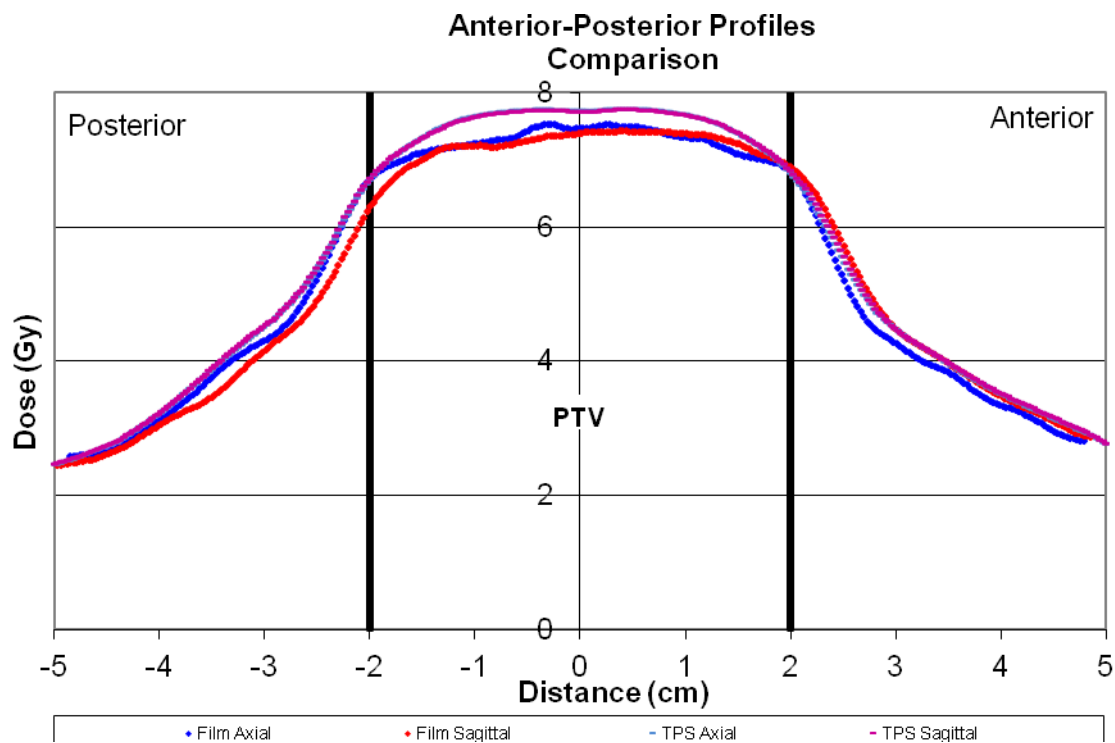


Figure 5.62 6 MV SBRT UAB 1D Anterior-Posterior Dose Profiles: Irradiation #1

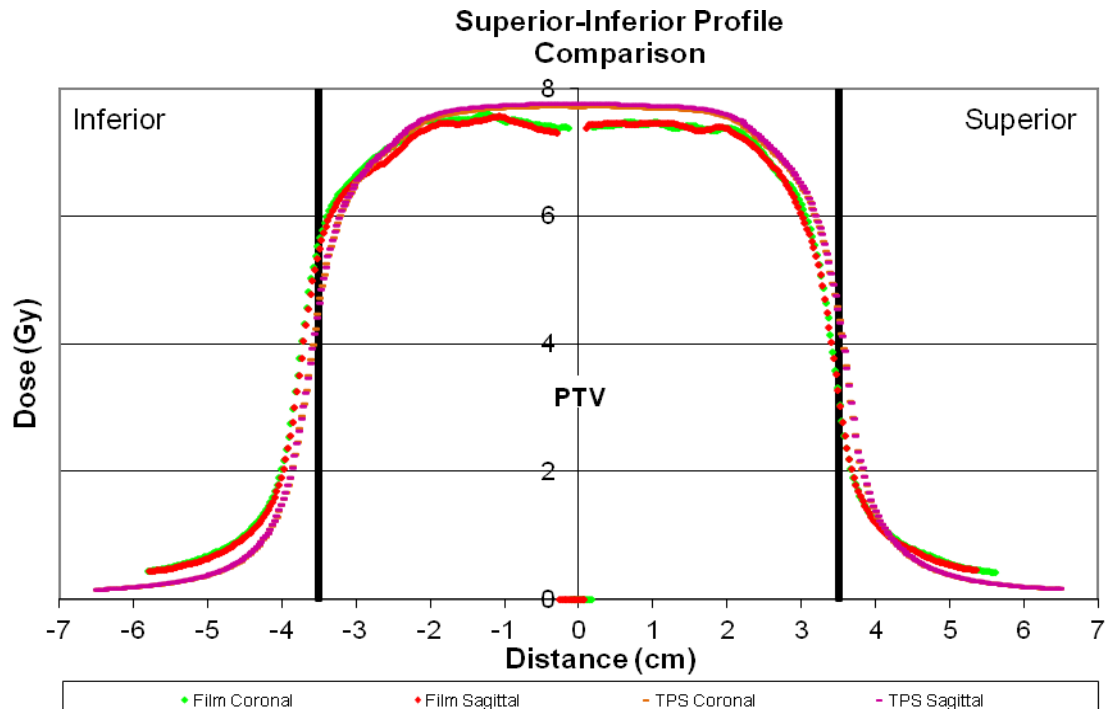


Figure 5.63 6 MV SBRT UAB 1D Superior-Inferior Dose Profiles: Irradiation #1

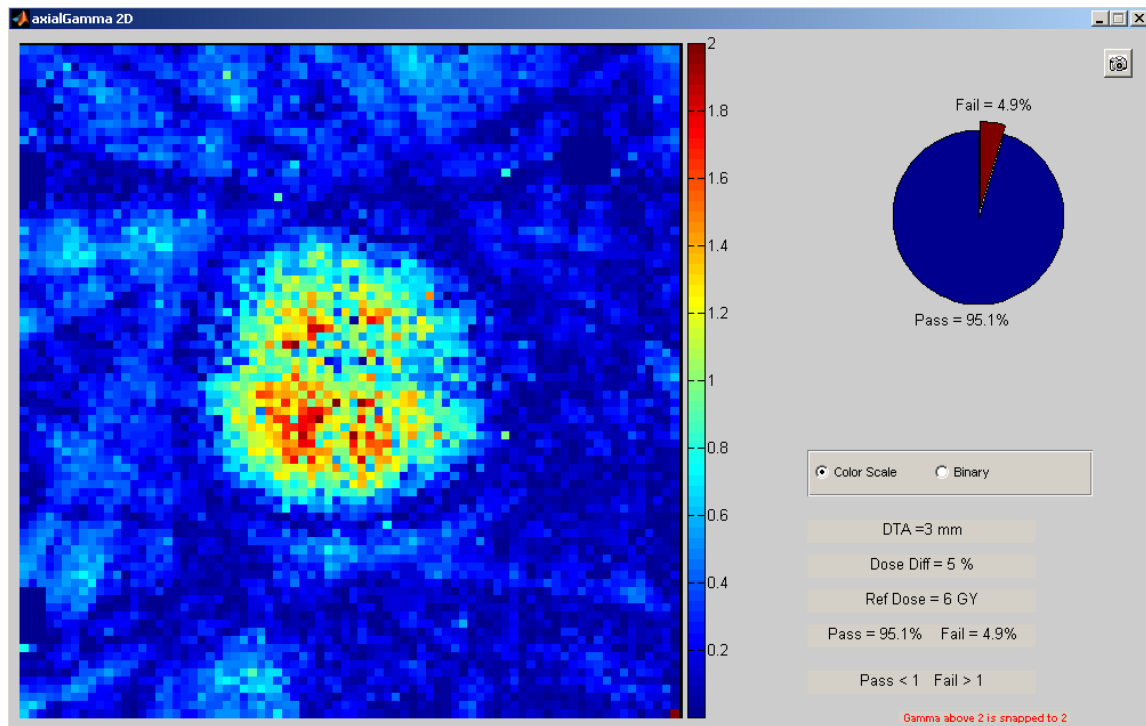


Figure 5.64 6 MV SBRT UAB 2D Gamma Index Results: $\pm 5\%/3\text{mm}$, Axial Plane, Irradiation #2

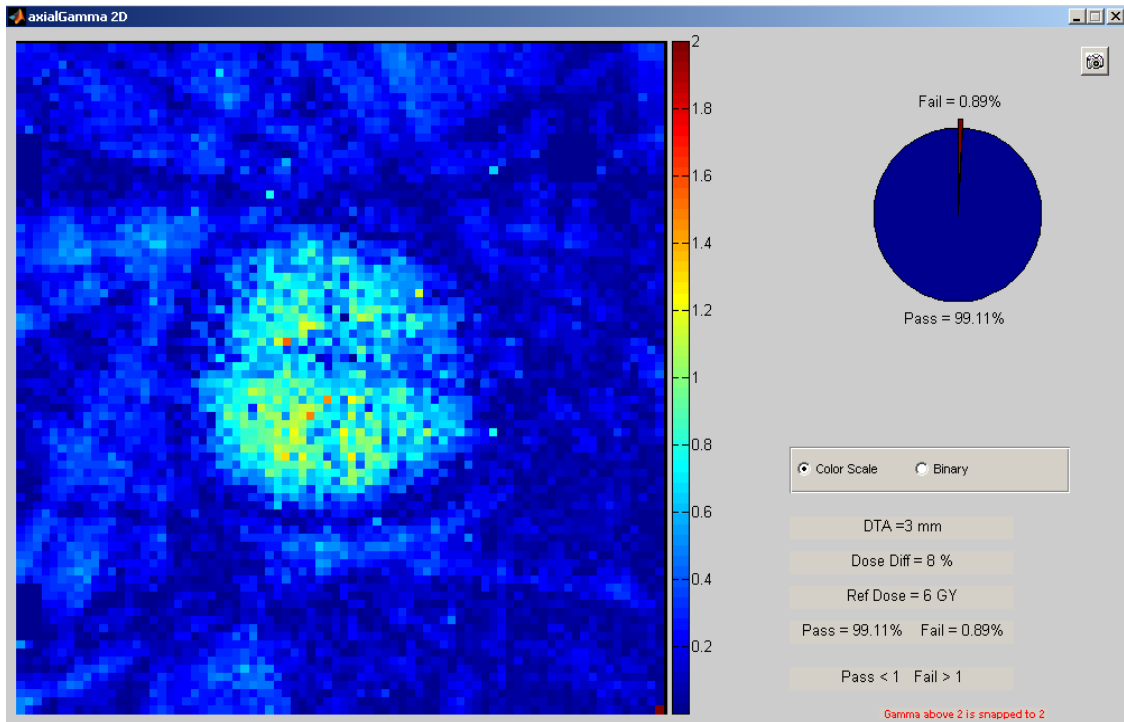


Figure 5.65 6 MV SBRT UAB 2D Gamma Index Results: $\pm 8\%/3\text{mm}$, Axial Plane, Irradiation #2

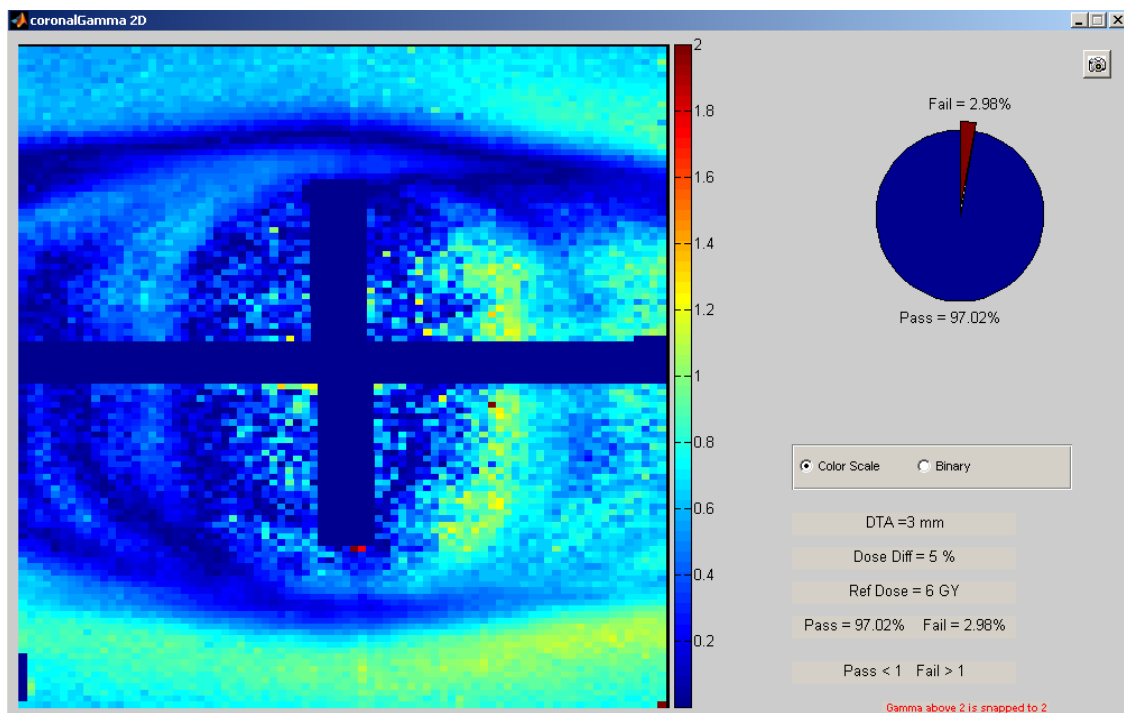


Figure 5.66 6 MV SBRT UAB 2D Gamma Index Results: $\pm 5\%/3\text{mm}$, Coronal Plane, Irradiation #2

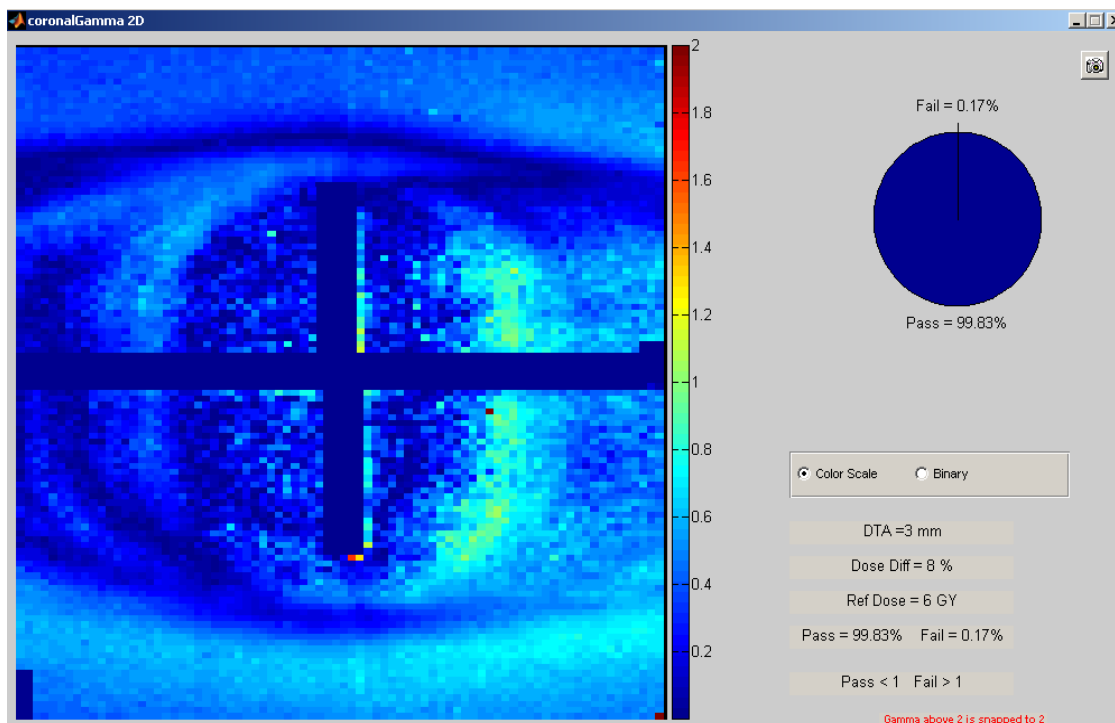


Figure 5.67 6 MV SBRT UAB 2D Gamma Index Results: $\pm 8\%/3\text{mm}$, Coronal Plane, Irradiation #2

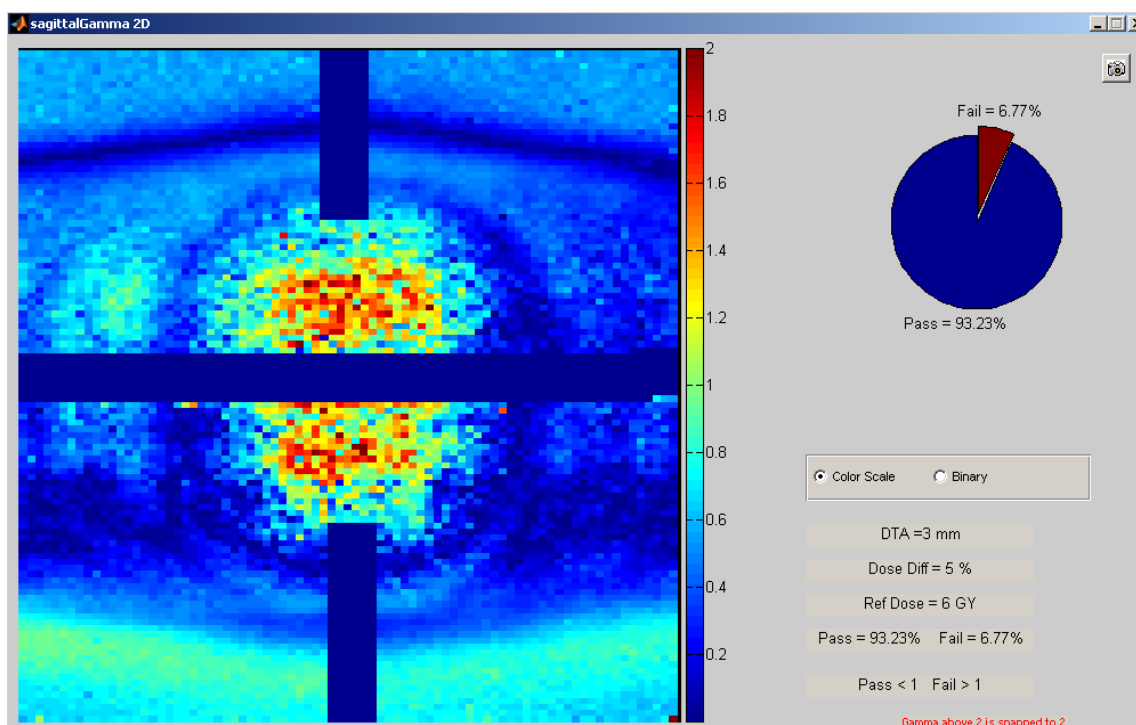


Figure 5.68 6 MV SBRT UAB 2D Gamma Index Results: $\pm 5\%/3\text{mm}$, Sagittal Plane, Irradiation #2

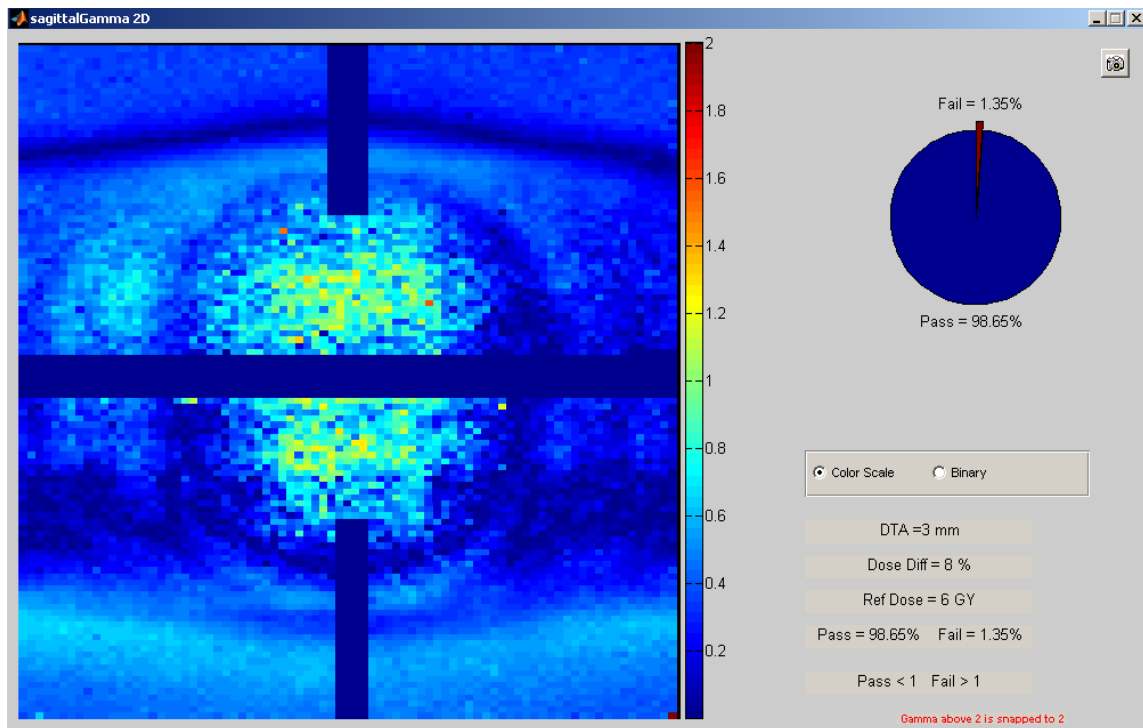


Figure 5.69 6 MV SBRT UAB 2D Gamma Index Results: $\pm 8\%/3\text{mm}$, Sagittal Plane, Irradiation #2

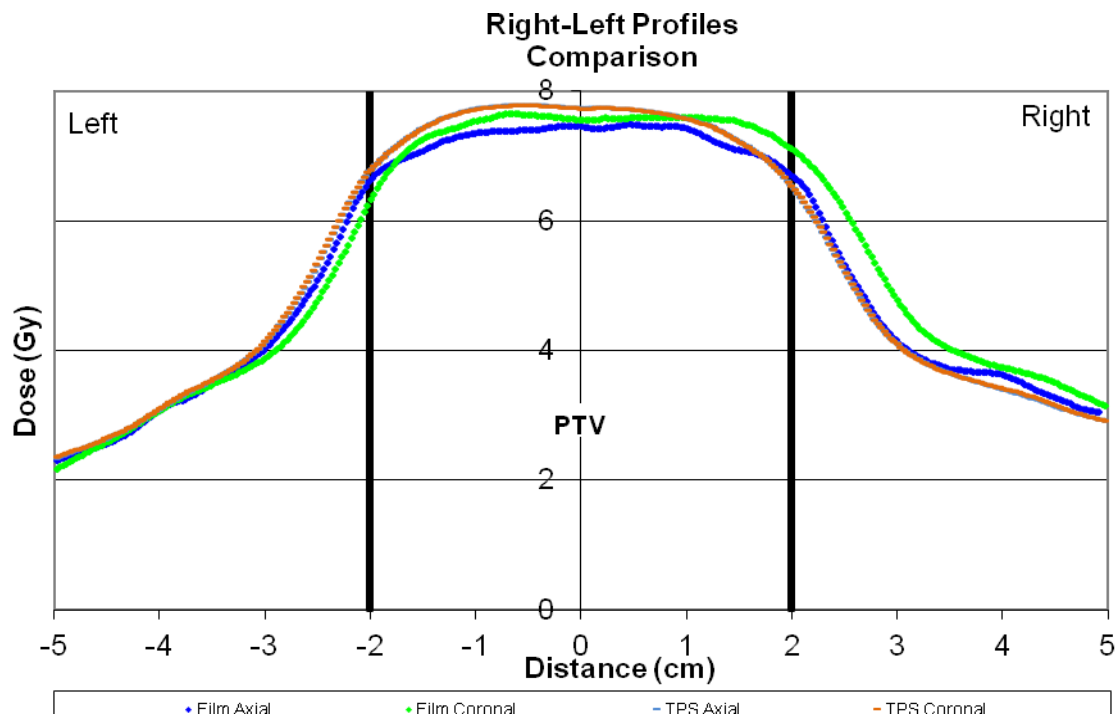


Figure 5.70 6 MV SBRT UAB 1D Right-Left Dose Profiles: Irradiation #2

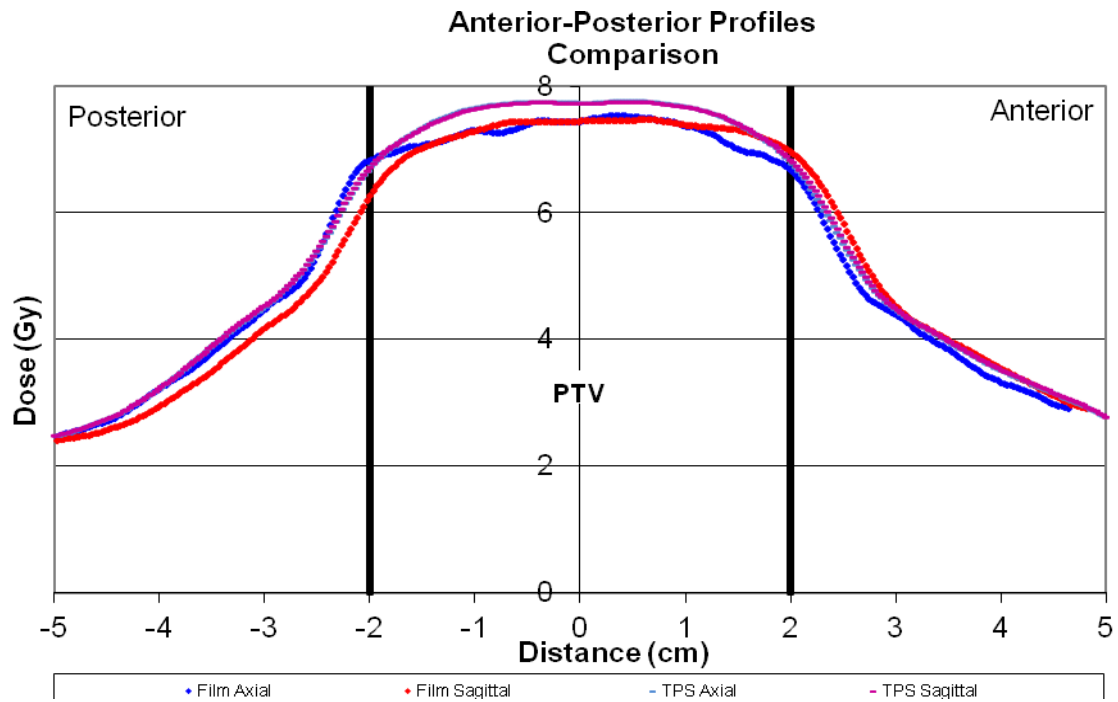


Figure 5.71 6 MV SBRT UAB 1D Anterior-Posterior Dose Profiles: Irradiation #2

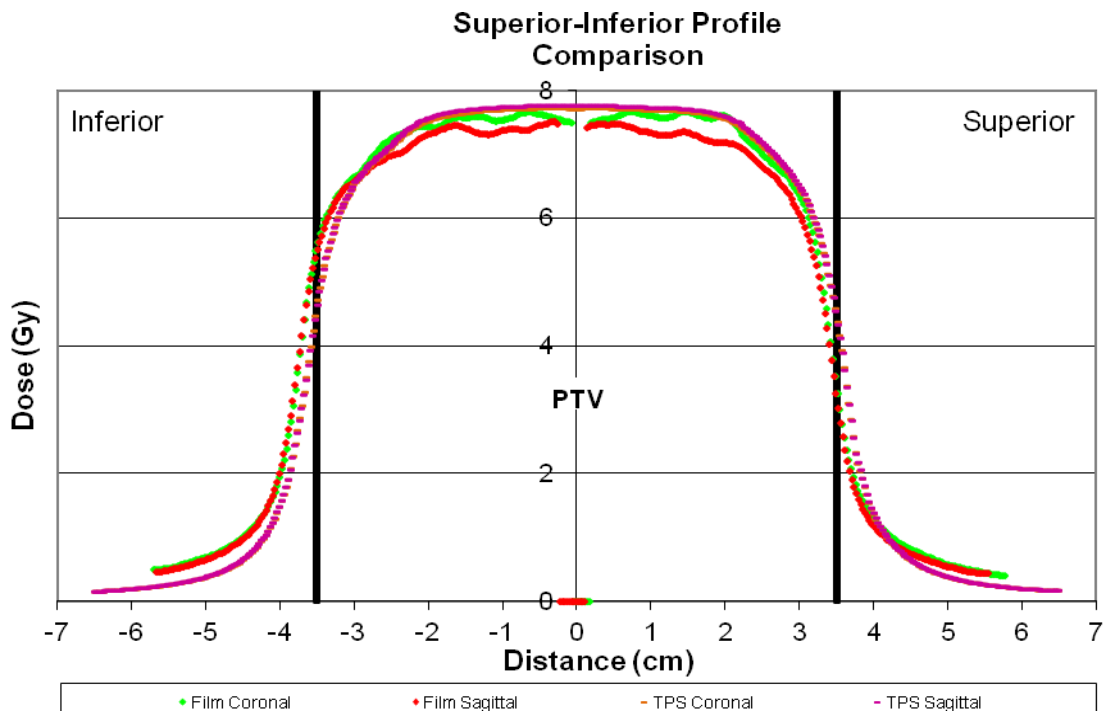


Figure 5.72 6 MV SBRT UAB 1D Superior-Inferior Dose Profiles: Irradiation #2

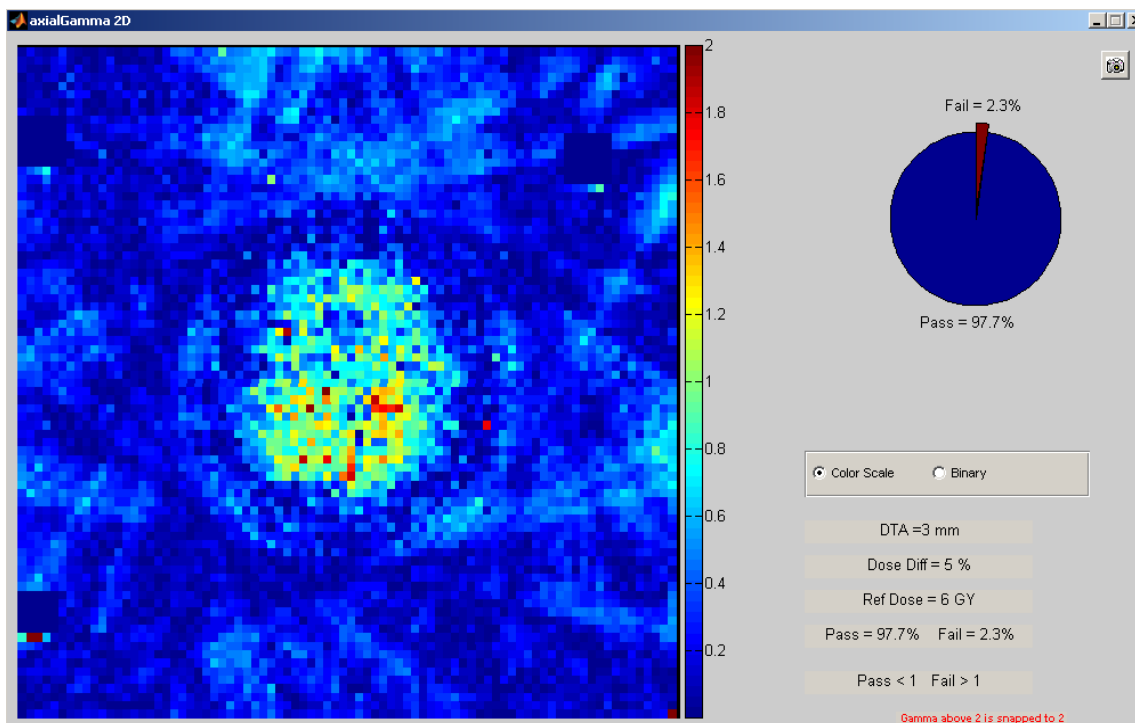


Figure 5.73 6 MV SBRT UAB 2D Gamma Index Results: $\pm 5\%/3\text{mm}$, Axial Plane, Irradiation #3

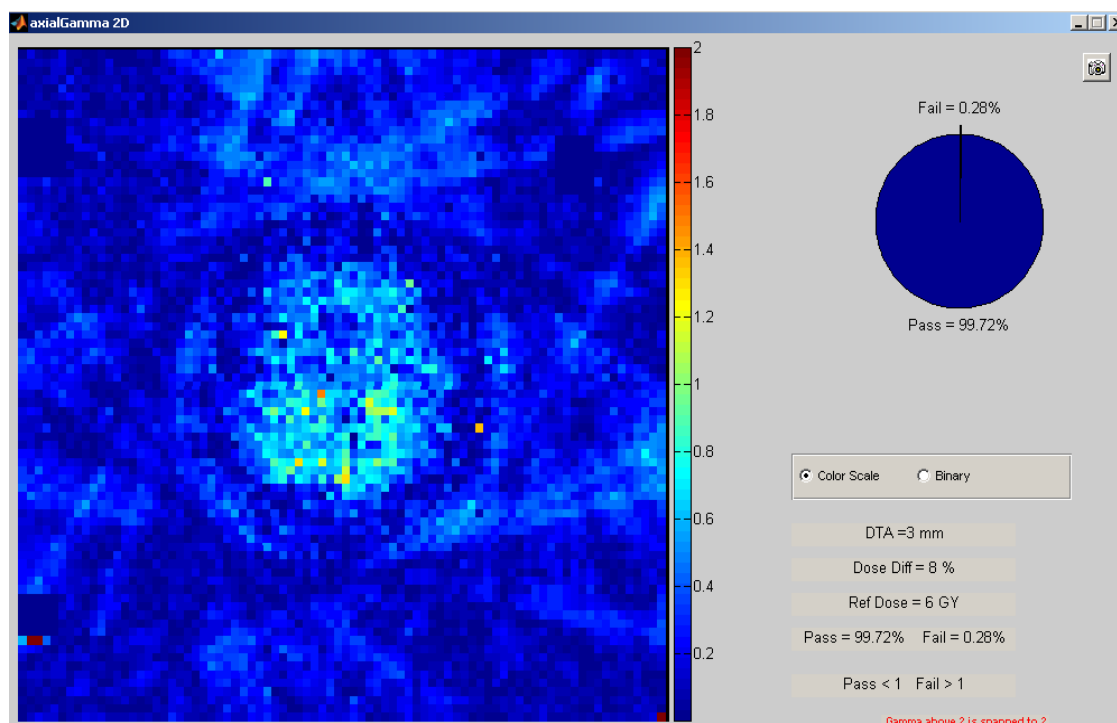


Figure 5.74 6 MV SBRT UAB 2D Gamma Index Results: $\pm 8\%/3\text{mm}$, Axial Plane, Irradiation #3

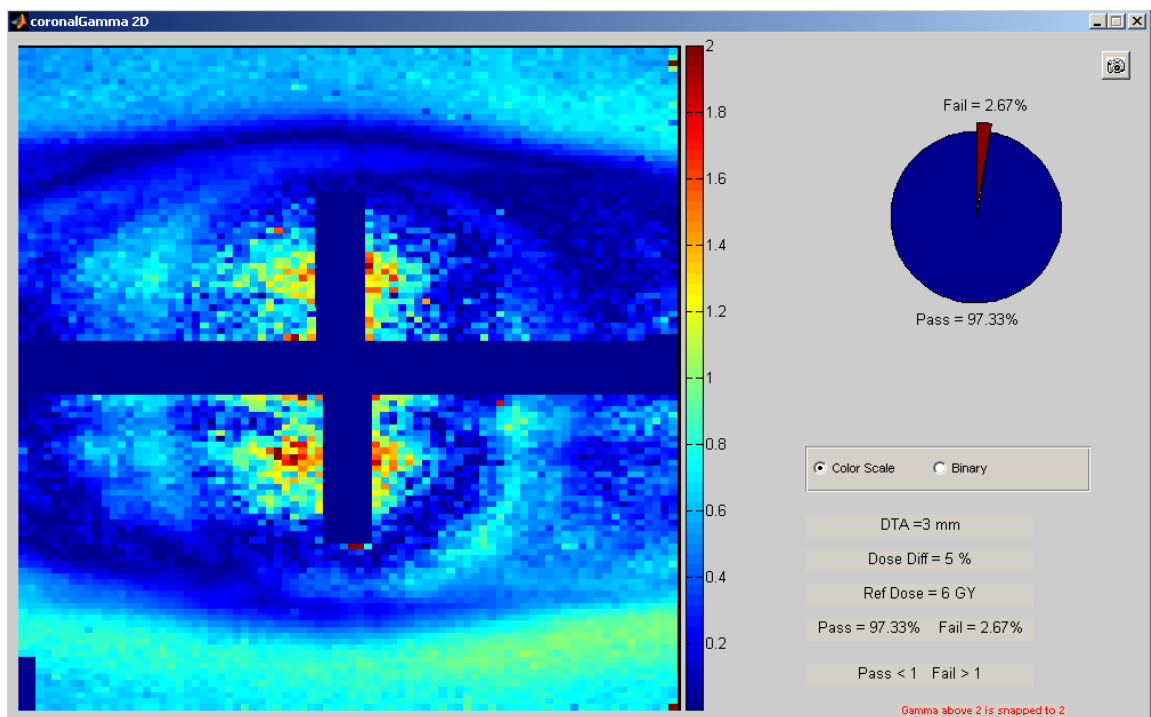


Figure 5.75 6 MV SBRT UAB 2D Gamma Index Results: $\pm 5\%/3\text{mm}$, Coronal Plane, Irradiation #3

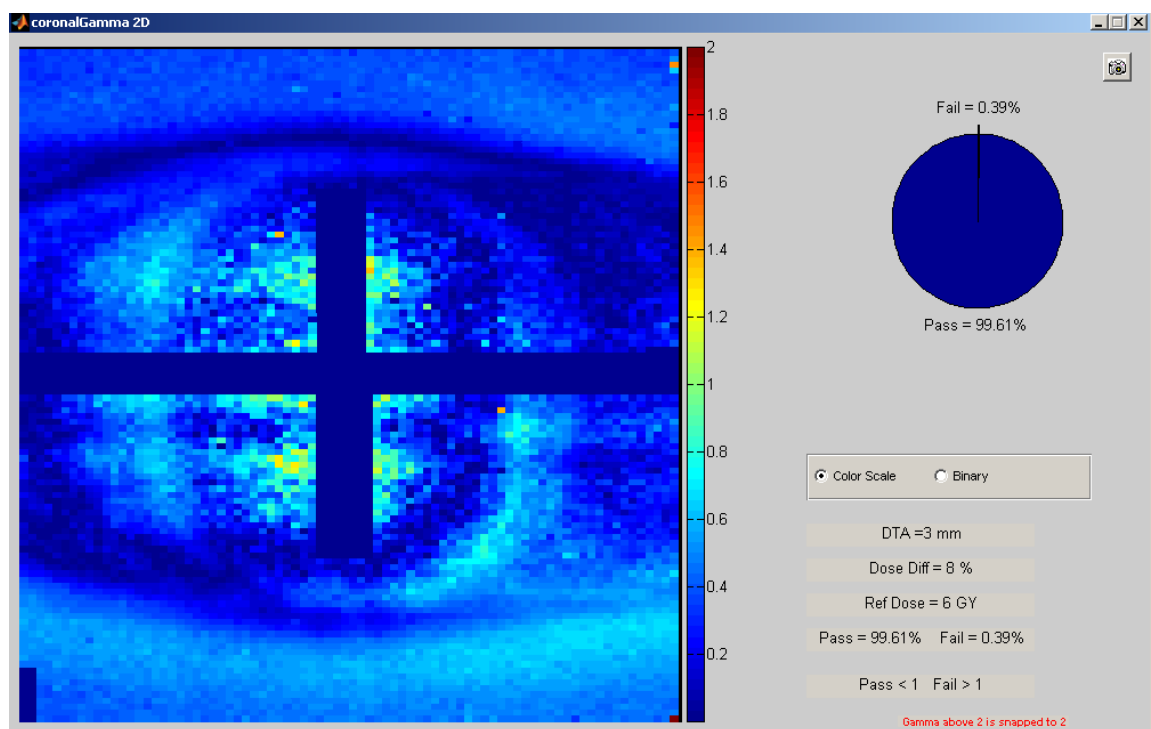


Figure 5.76 6 MV SBRT UAB 2D Gamma Index Results: $\pm 8\%/3\text{mm}$, Coronal Plane, Irradiation #3

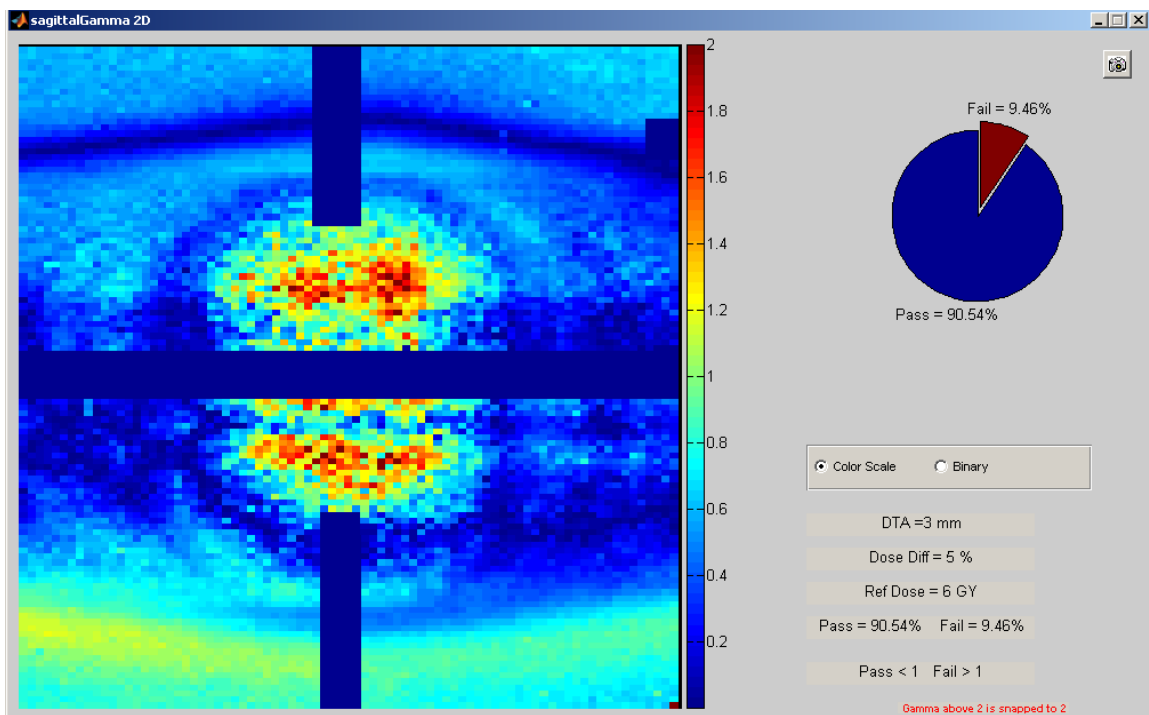


Figure 5.77 6 MV SBRT UAB 2D Gamma Index Results: $\pm 5\%/3\text{mm}$, Sagittal Plane, Irradiation #3

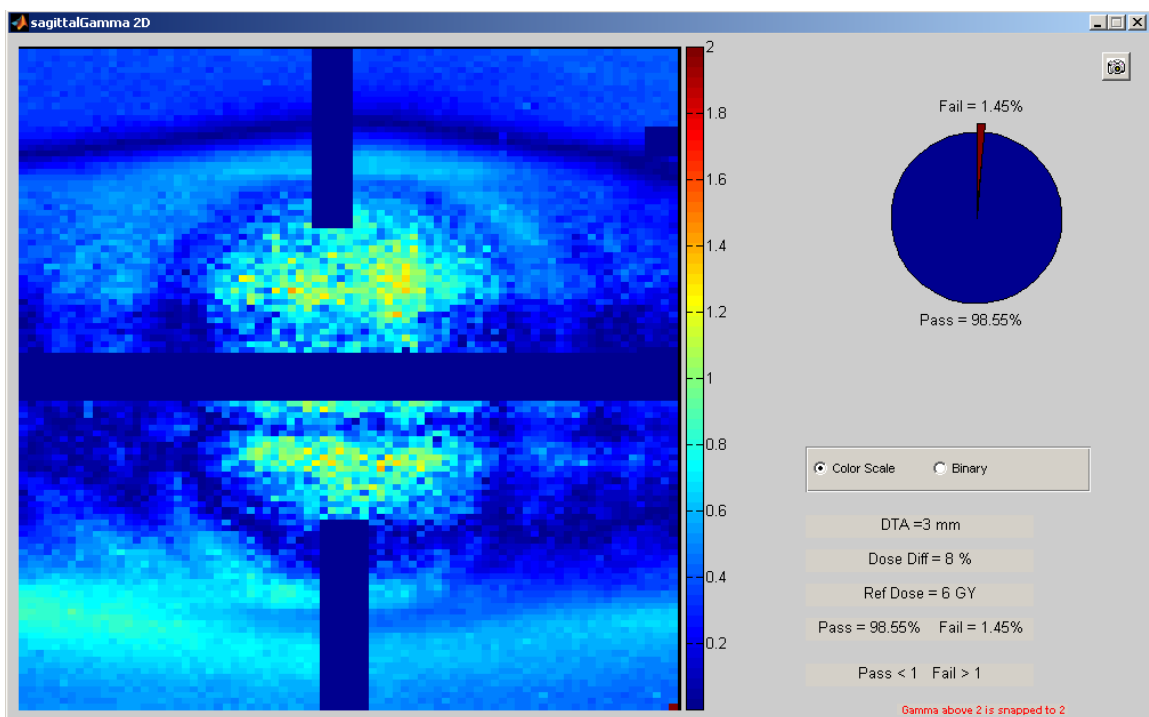


Figure 5.78 6 MV SBRT UAB 2D Gamma Index Results: $\pm 8\%/3\text{mm}$, Sagittal Plane, Irradiation #3

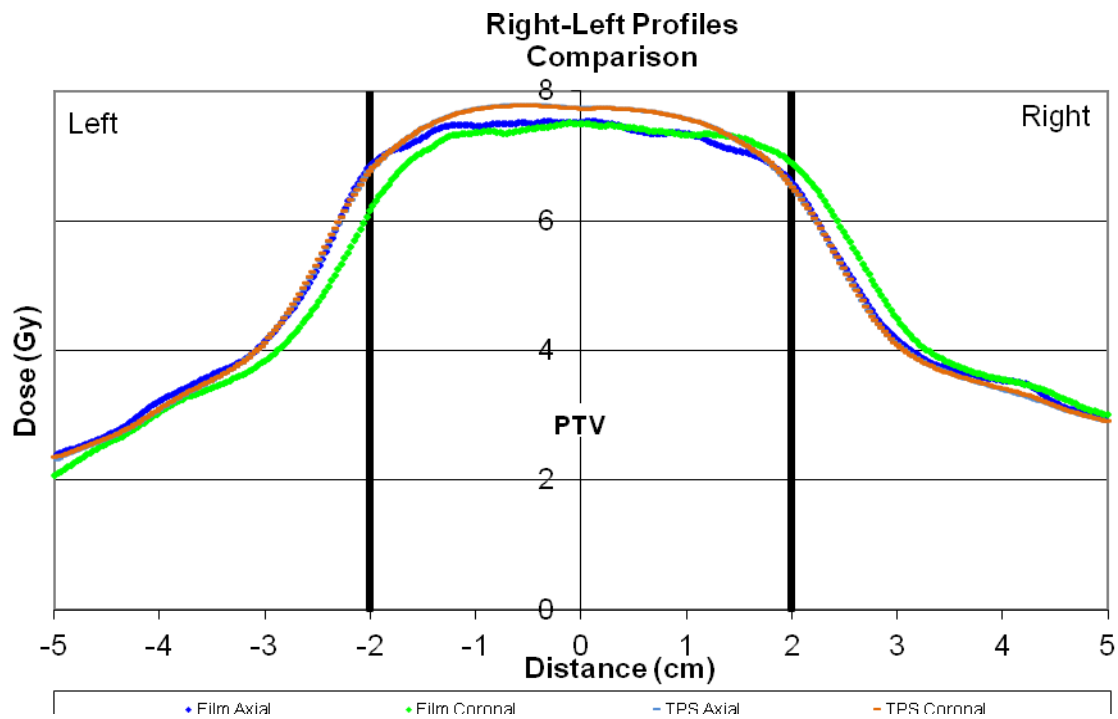


Figure 5.79 6 MV SBRT UAB 1D Right-Left Dose Profiles: Irradiation #3

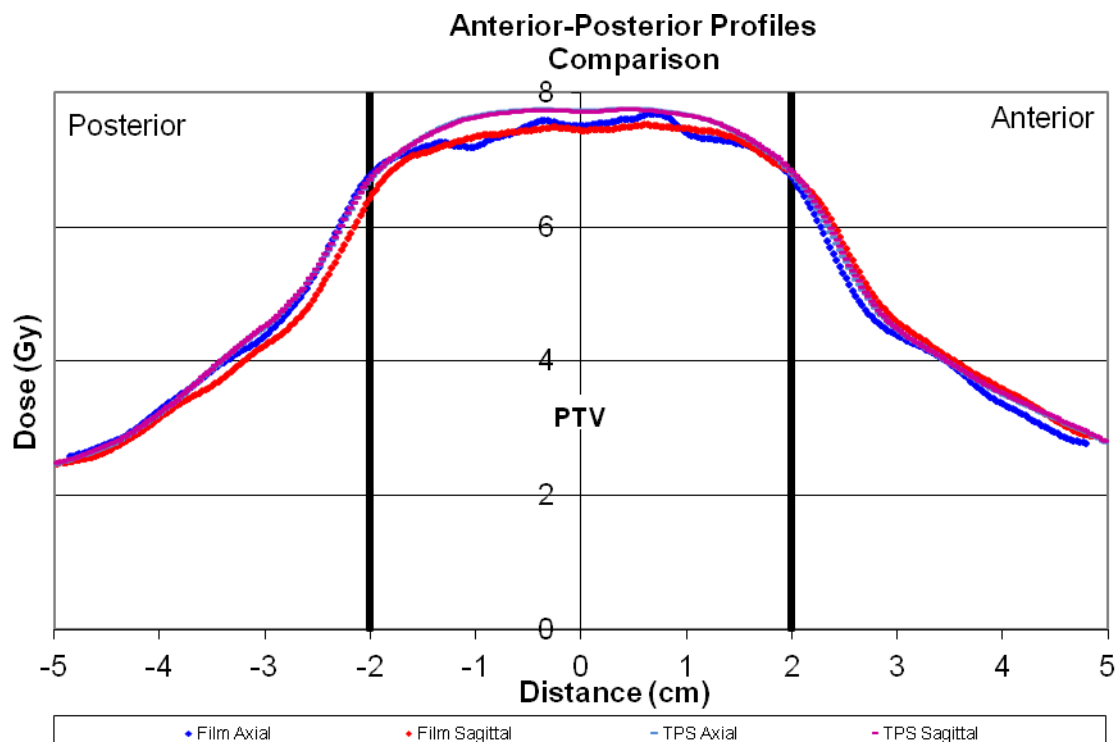


Figure 5.80 6 MV SBRT UAB 1D Anterior-Posterior Dose Profiles: Irradiation #1

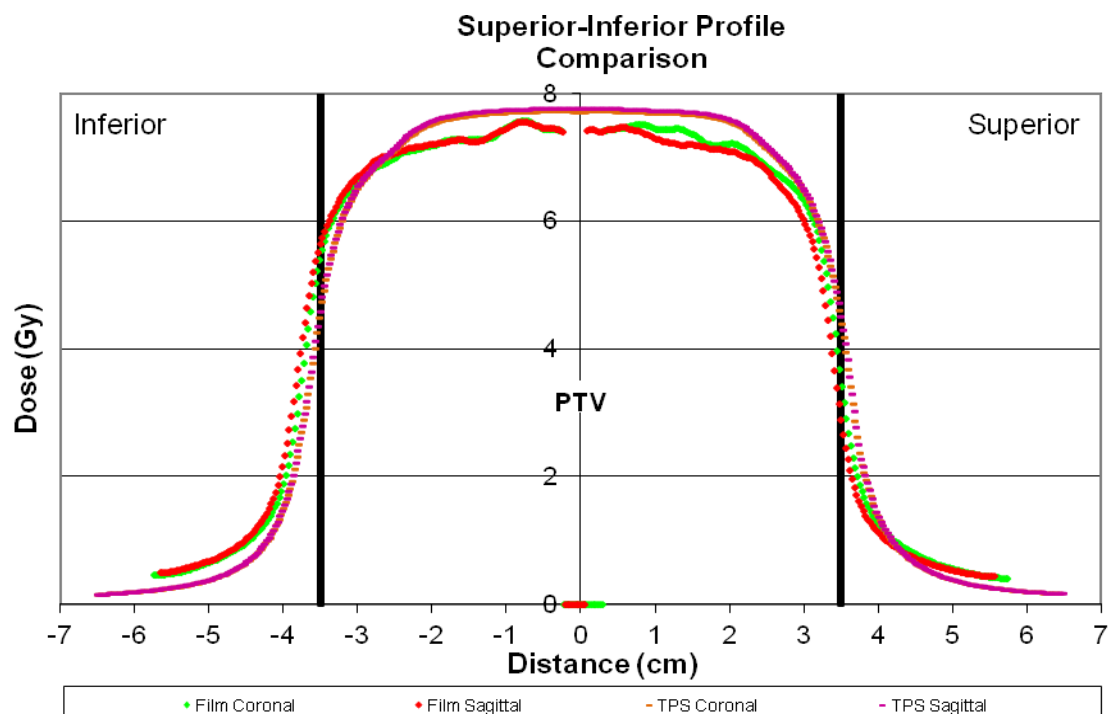


Figure 5.81 6 MV SBRT UAB 1D Superior-Inferior Dose Profiles: Irradiation #1

5.4 15 MV SBRT University of Alabama MEDICAL CENTER 2D Gamma Index

Maps and Dose Profiles

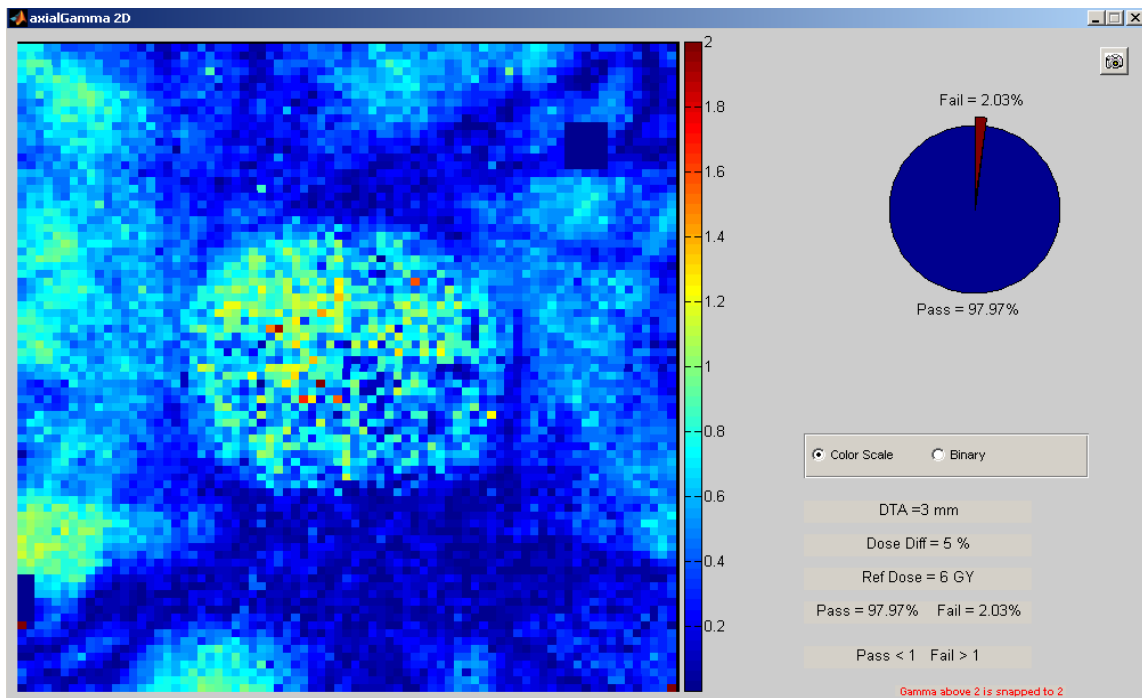


Figure 5.82 15 MV SBRT UAB 2D Gamma Index Results: $\pm 5\%/3\text{mm}$, Axial Plane, Irradiation #1

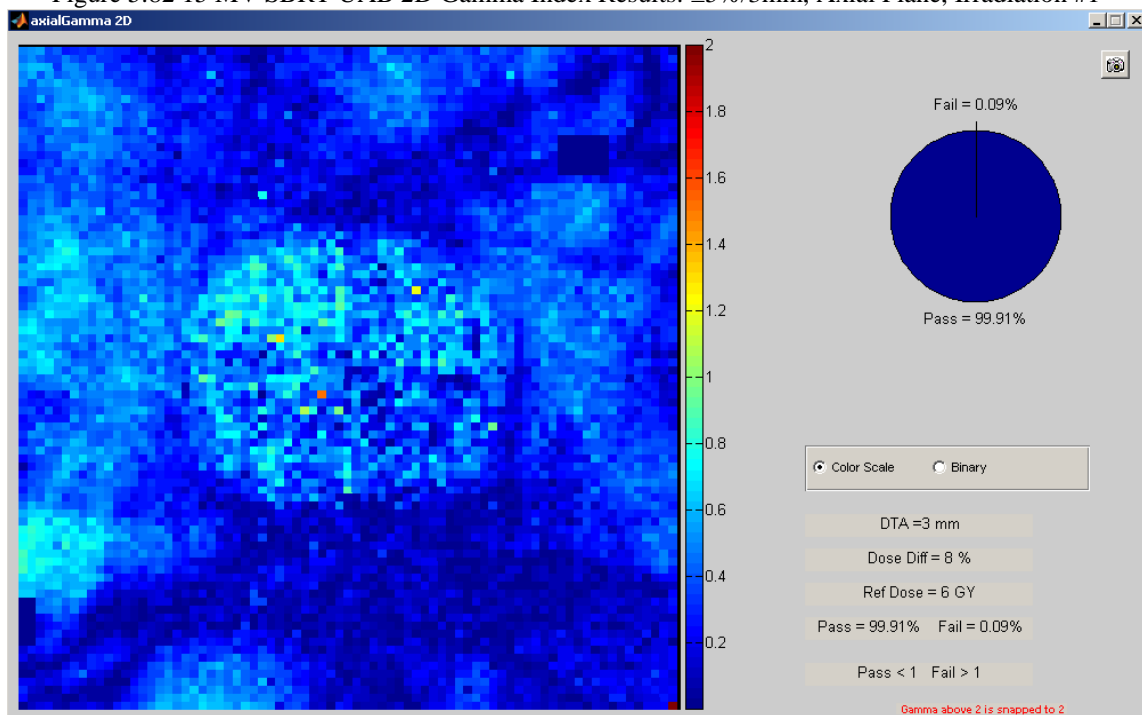


Figure 5.83 15 MV SBRT UAB 2D Gamma Index Results: $\pm 8\%/3\text{mm}$, Axial Plane, Irradiation #1

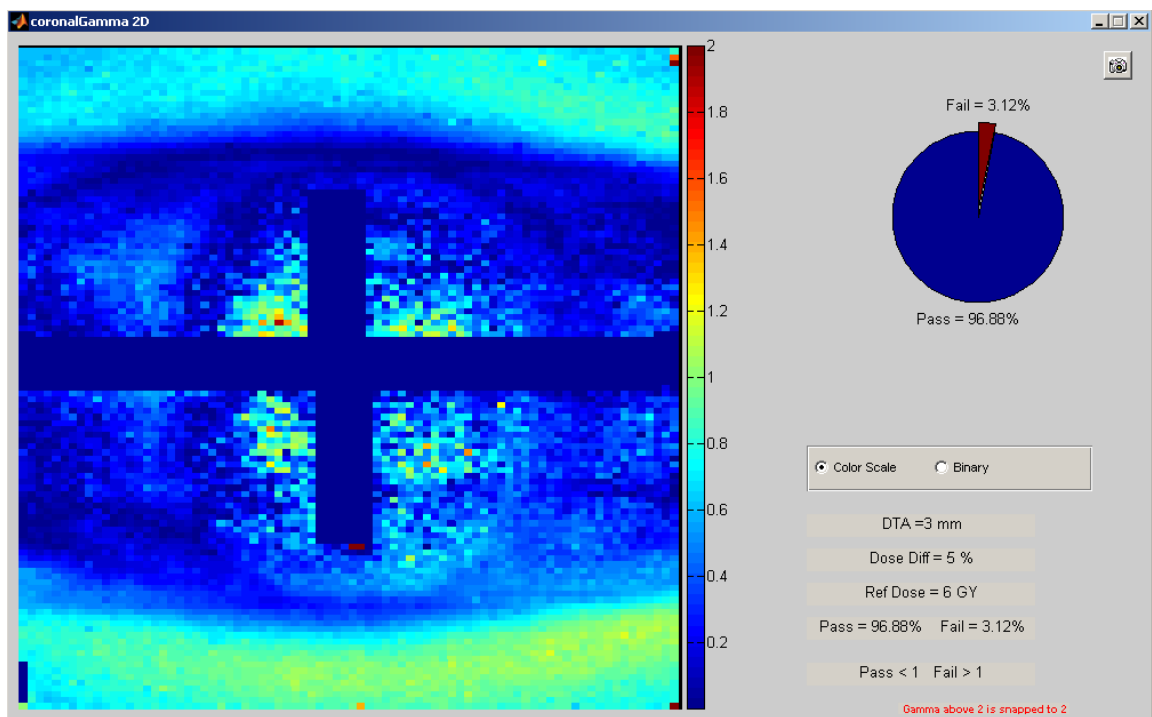


Figure 5.84 15 MV SBRT UAB 2D Gamma Index Results: $\pm 5\%/3\text{mm}$, Coronal Plane, Irradiation #1

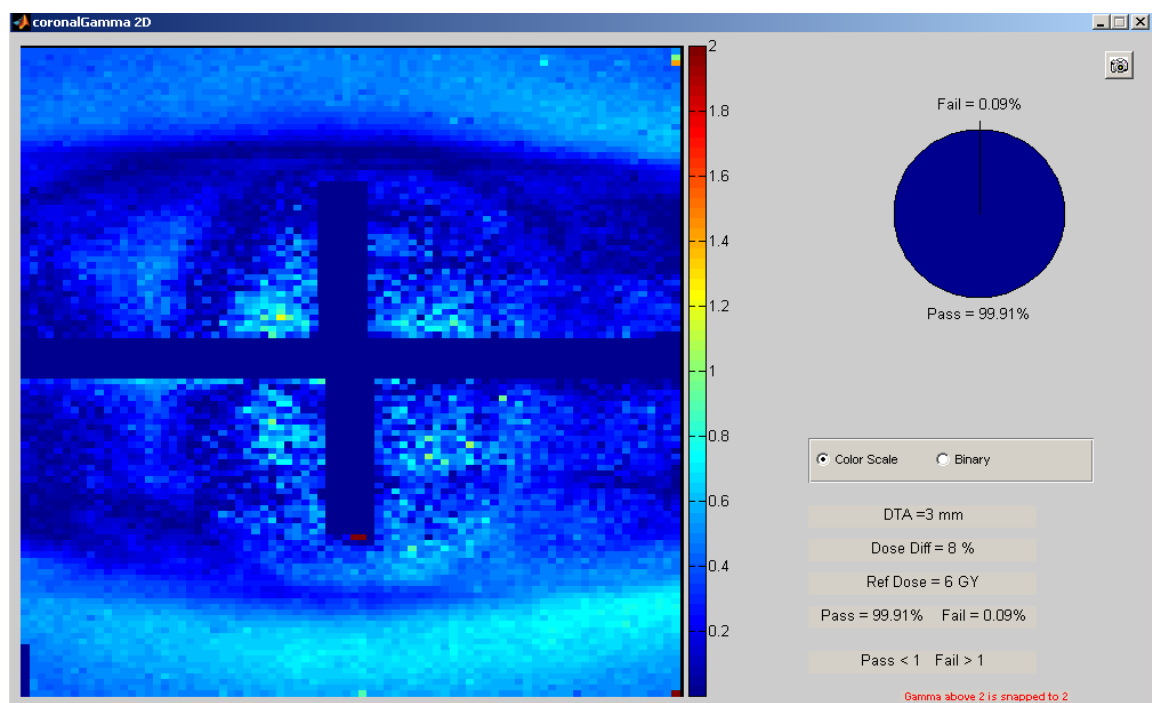


Figure 5.85 15 MV SBRT UAB 2D Gamma Index Results: $\pm 8\%/3\text{mm}$, Coronal Plane, Irradiation #1

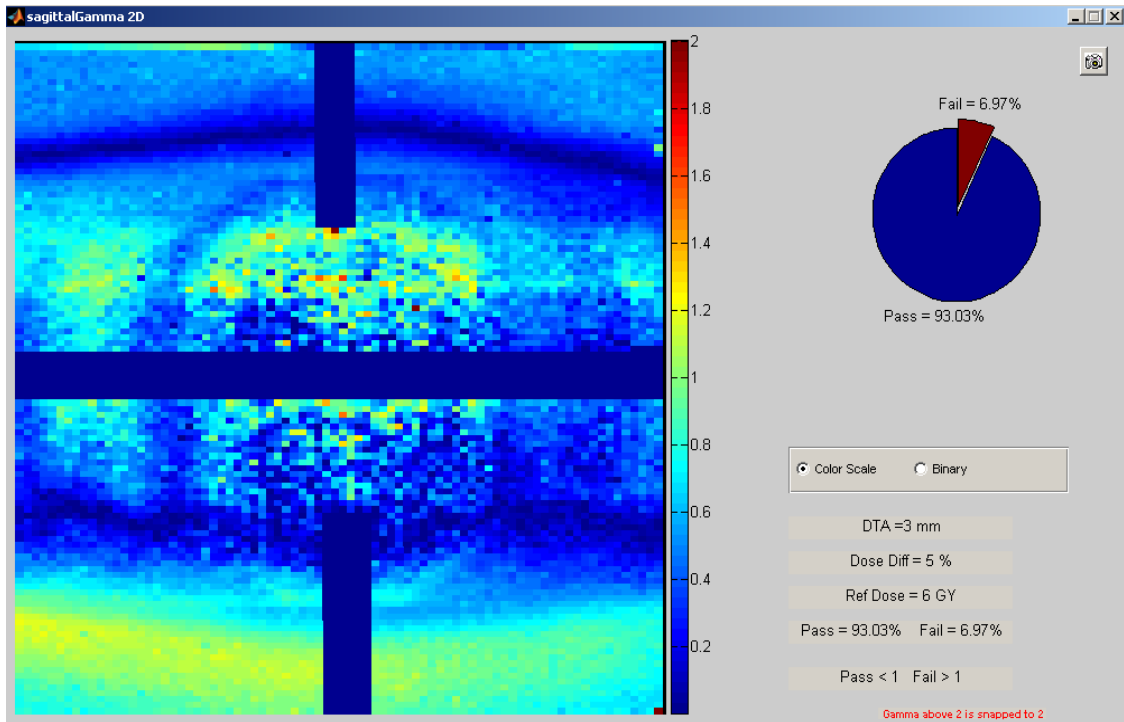


Figure 5.86 15 MV SBRT UAB 2D Gamma Index Results: $\pm 5\%/3\text{mm}$, Sagittal Plane, Irradiation #1

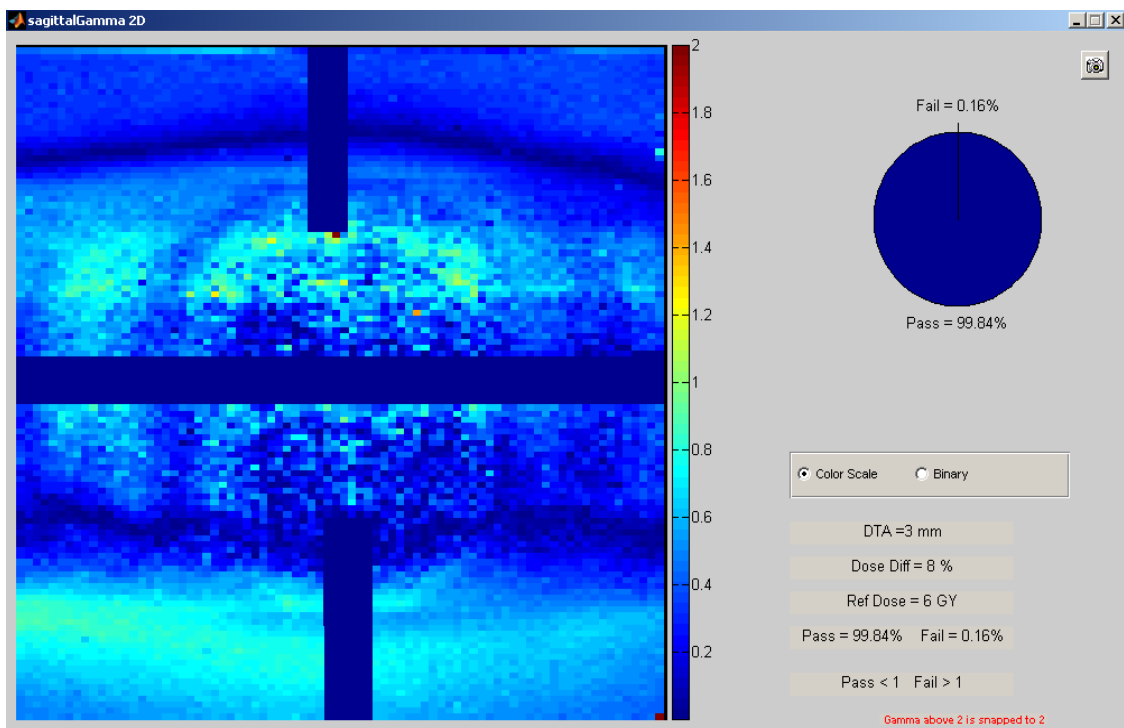


Figure 5.87 15 MV SBRT UAB 2D Gamma Index Results: $\pm 8\%/3\text{mm}$, Sagittal Plane, Irradiation #1

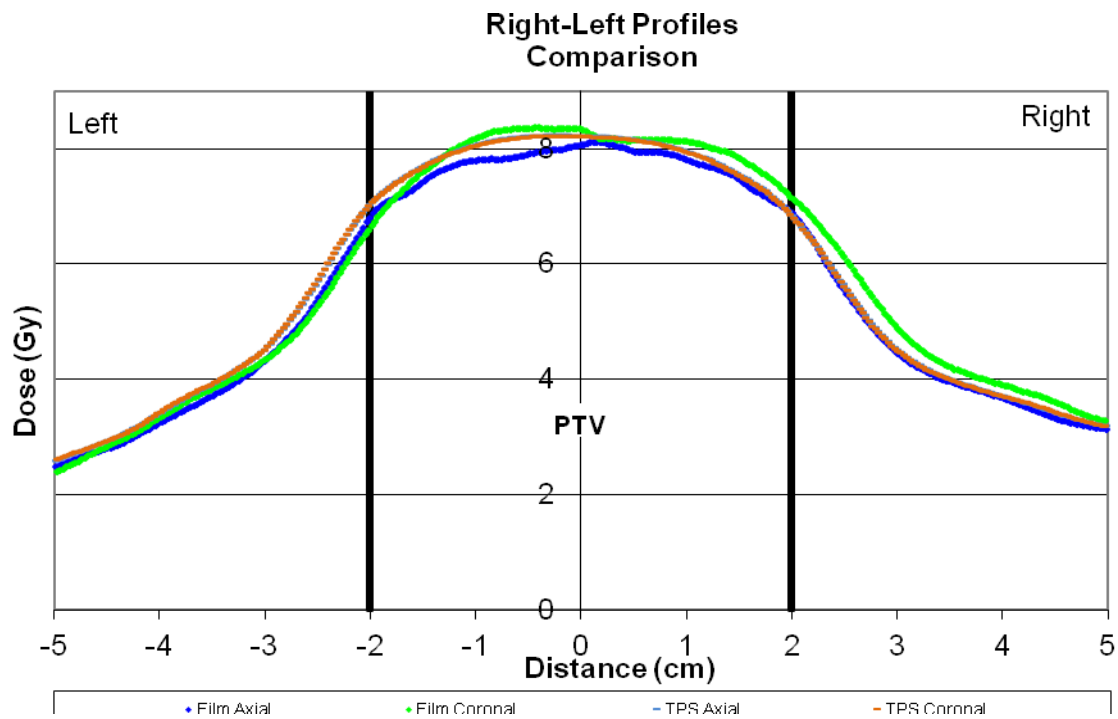


Figure 5.88 15 MV SBRT UAB 1D Right-Left Dose Profiles: Irradiation #1

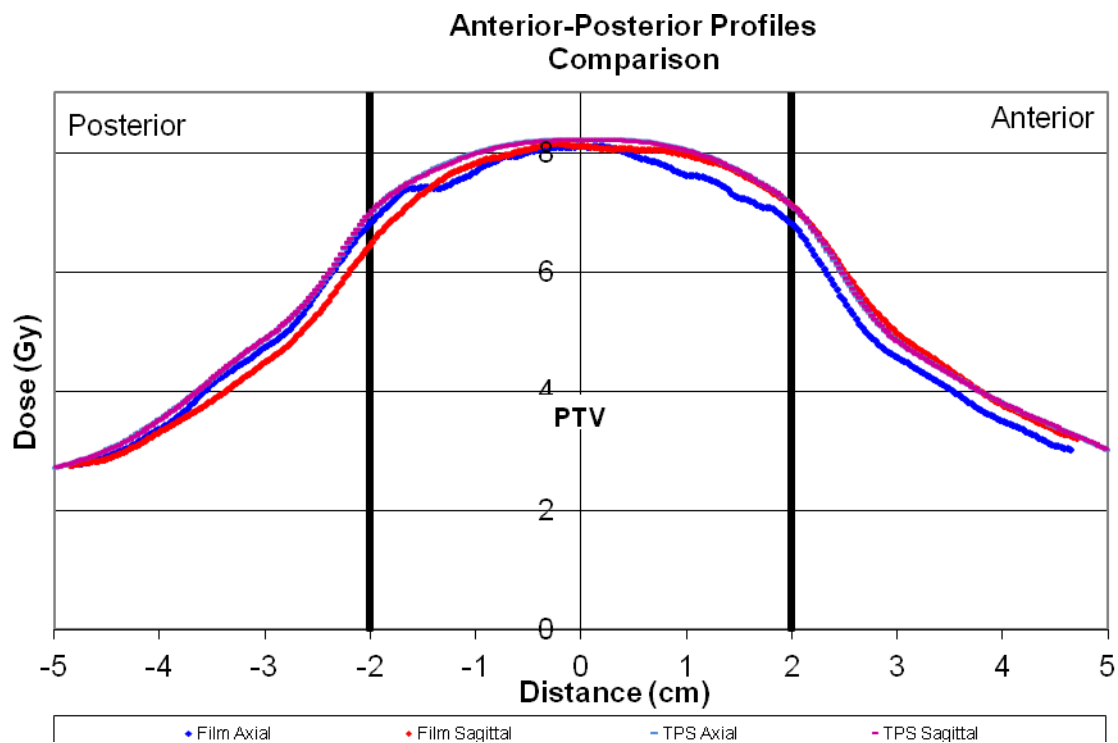


Figure 5.89 15 MV SBRT UAB 1D Anterior-Posterior Dose Profiles: Irradiation #1

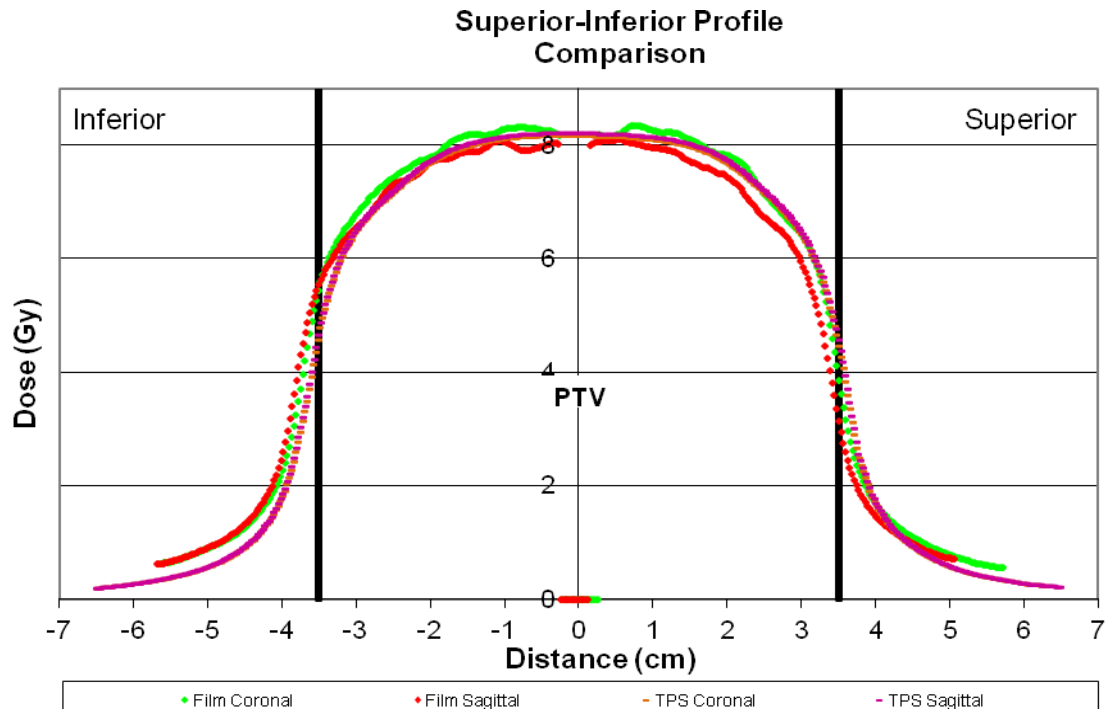


Figure 5.90 15 MV SBRT UAB 1D Superior-Inferior Dose Profiles: Irradiation #1

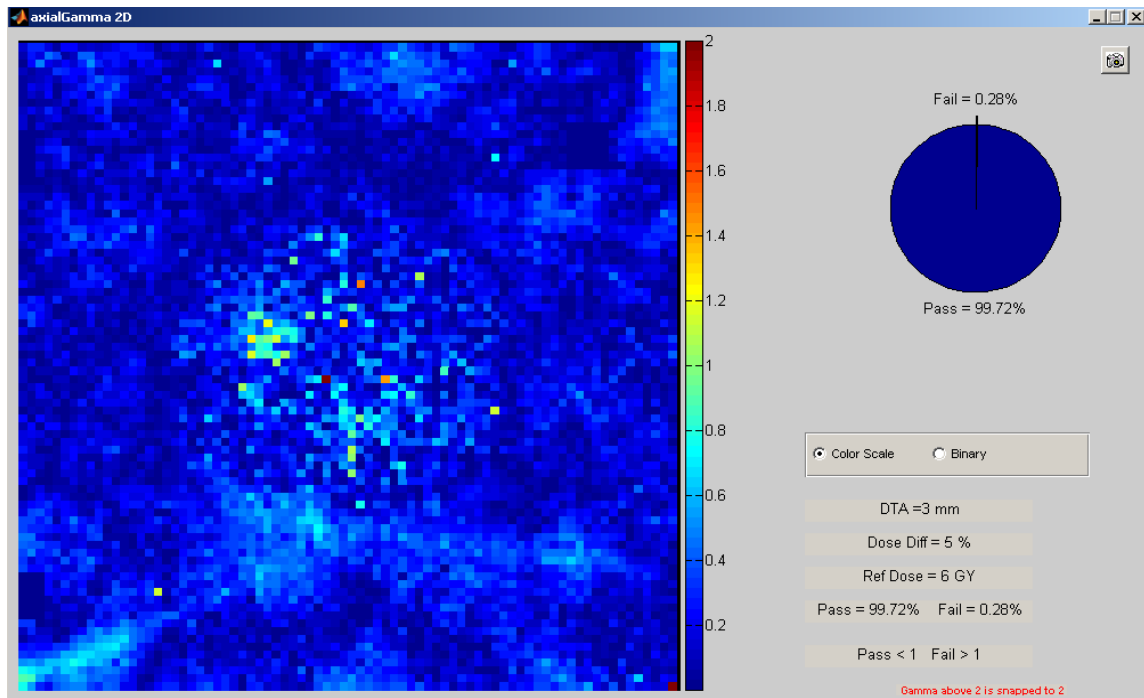


Figure 5.91 15 MV SBRT UAB 2D Gamma Index Results: $\pm 5\%/3\text{mm}$, Axial Plane, Irradiation #2

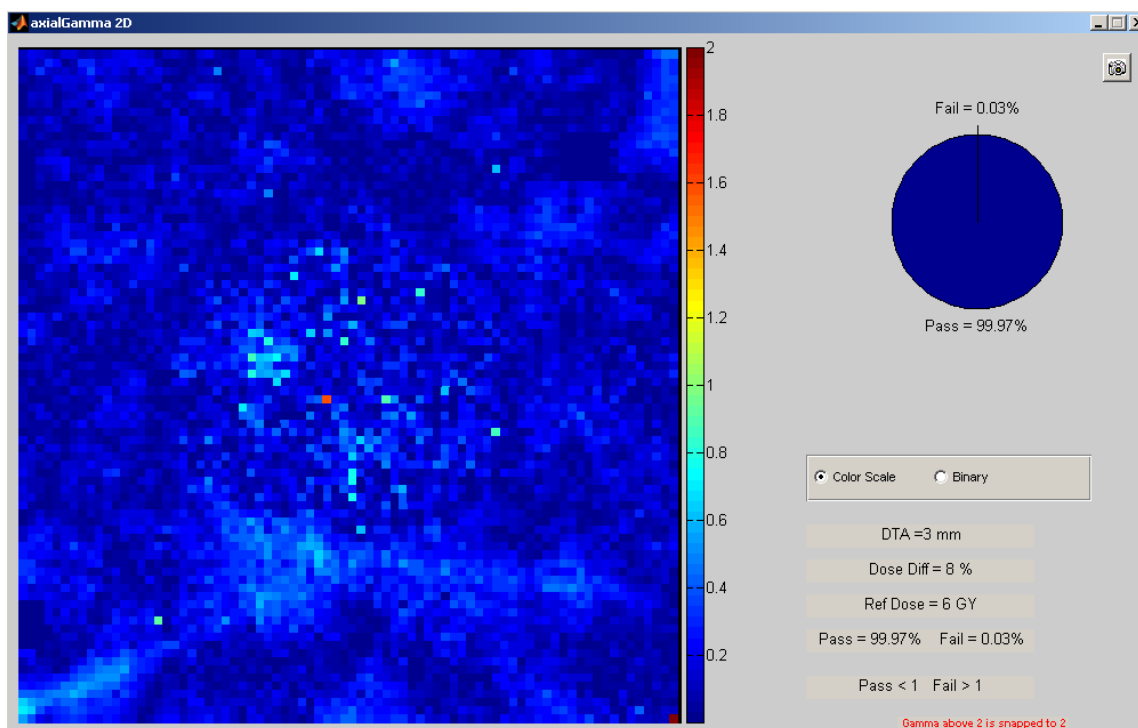


Figure 5.92 15 MV SBRT UAB 2D Gamma Index Results: $\pm 8\%/3\text{mm}$, Axial Plane, Irradiation #2

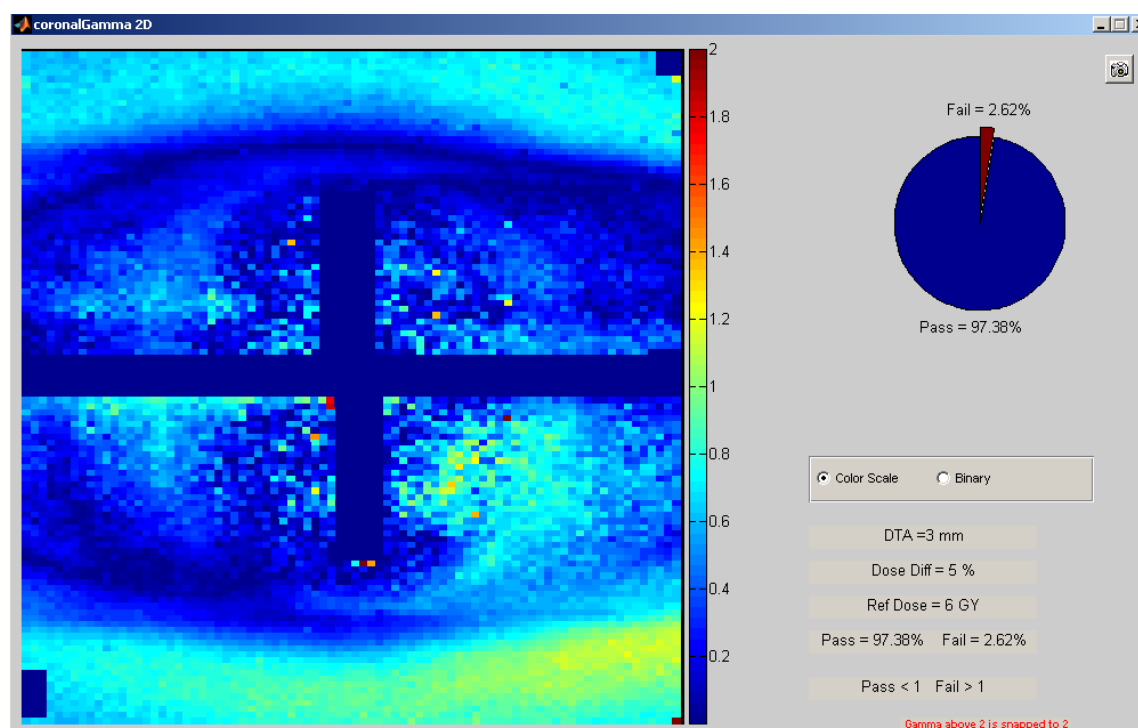


Figure 5.93 15 MV SBRT UAB 2D Gamma Index Results: $\pm 5\%/3\text{mm}$, Coronal Plane, Irradiation #2

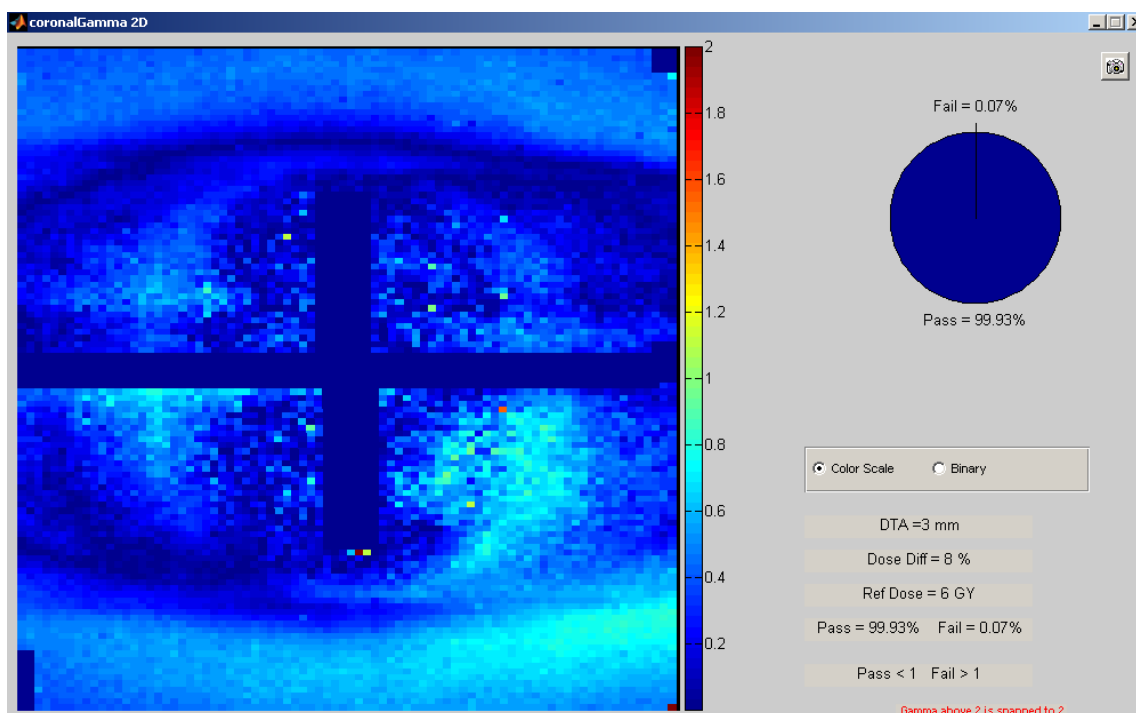


Figure 5.94 15 MV SBRT UAB 2D Gamma Index Results: $\pm 8\%/3\text{mm}$, Coronal Plane, Irradiation #2

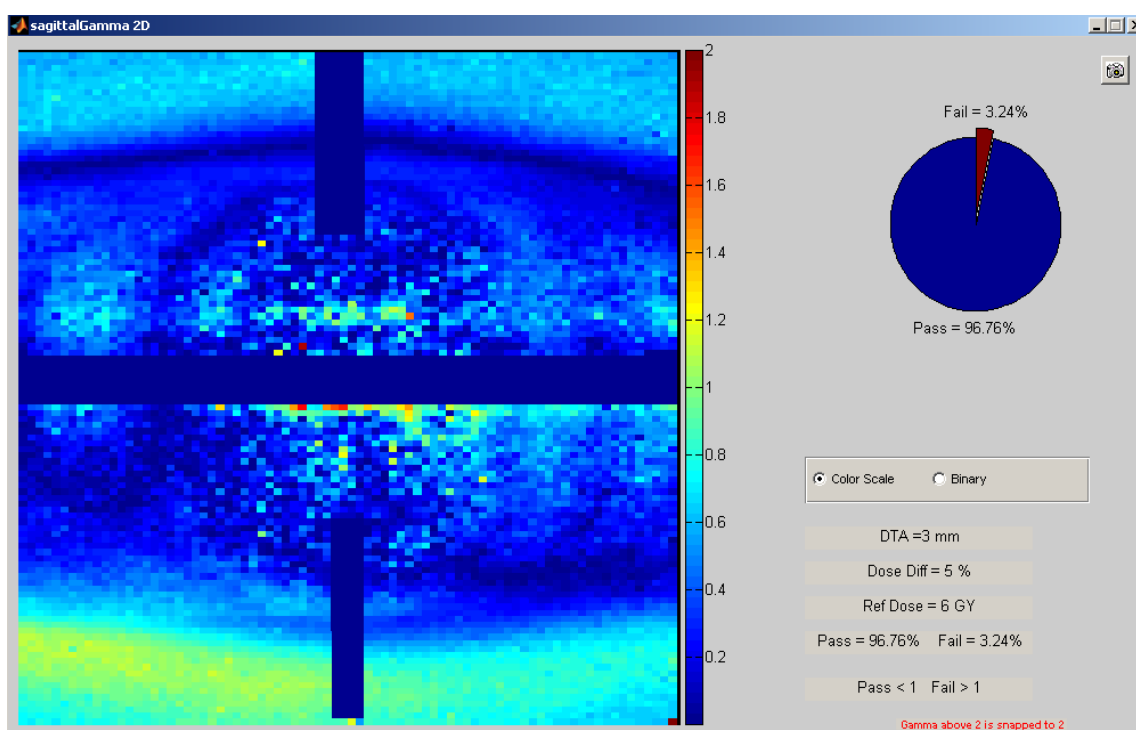


Figure 5.95 15 MV SBRT UAB 2D Gamma Index Results: $\pm 5\%/3\text{mm}$, Sagittal Plane, Irradiation #2

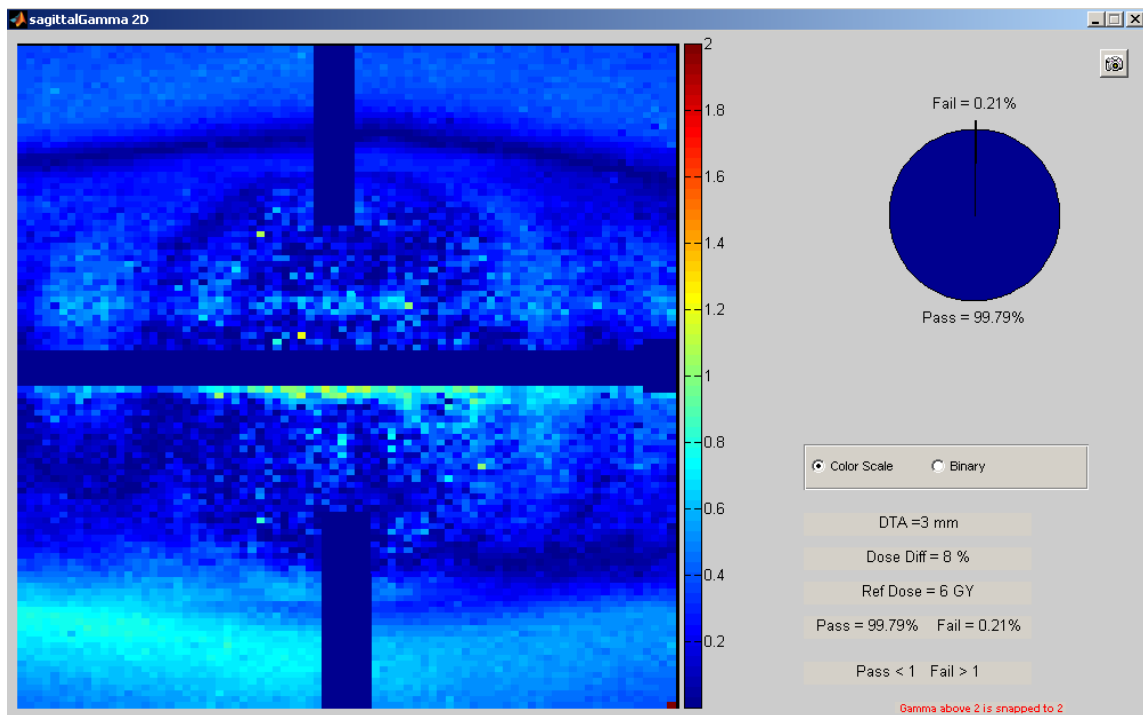


Figure 5.96 15 MV SBRT UAB 2D Gamma Index Results: $\pm 8\%/3\text{mm}$, Sagittal Plane, Irradiation #2

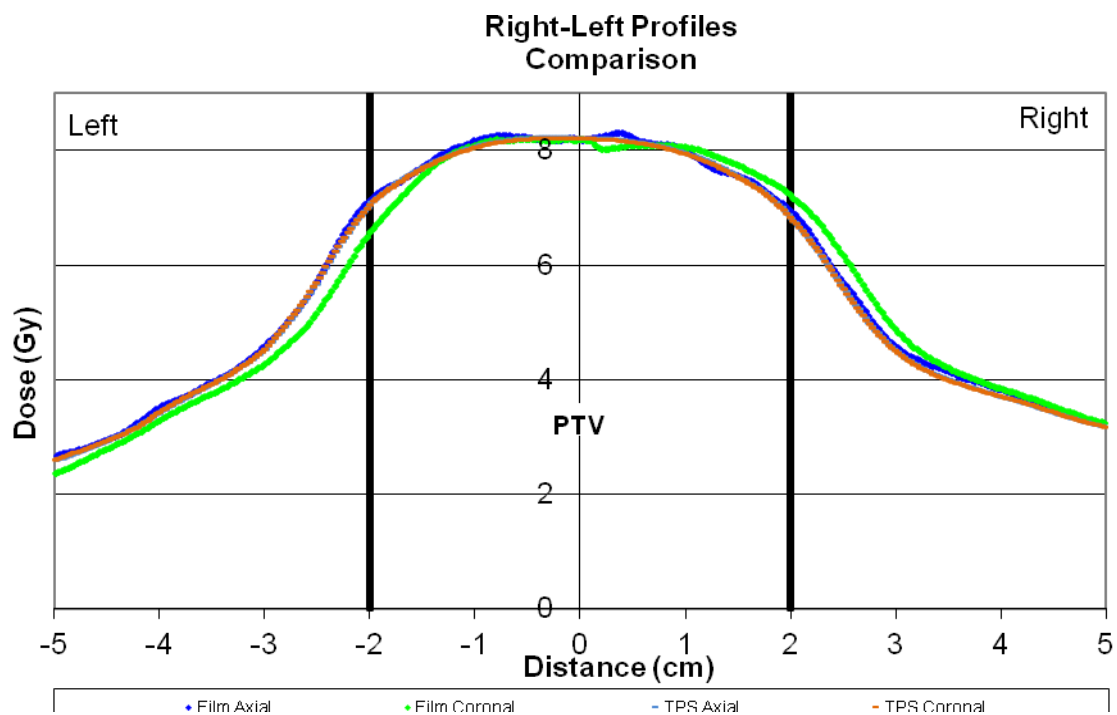


Figure 5.97 15 MV SBRT UAB 1D Right-Left Dose Profiles: Irradiation #2

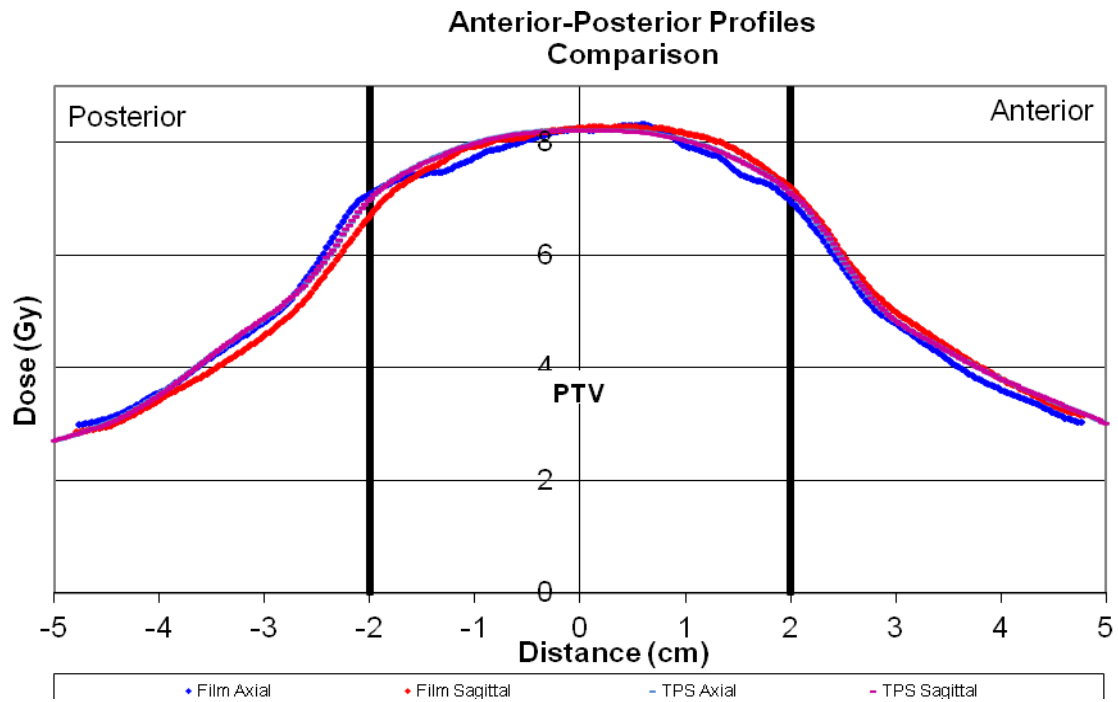


Figure 5.98 15 MV SBRT UAB 1D Anterior-Posterior Dose Profiles: Irradiation #2

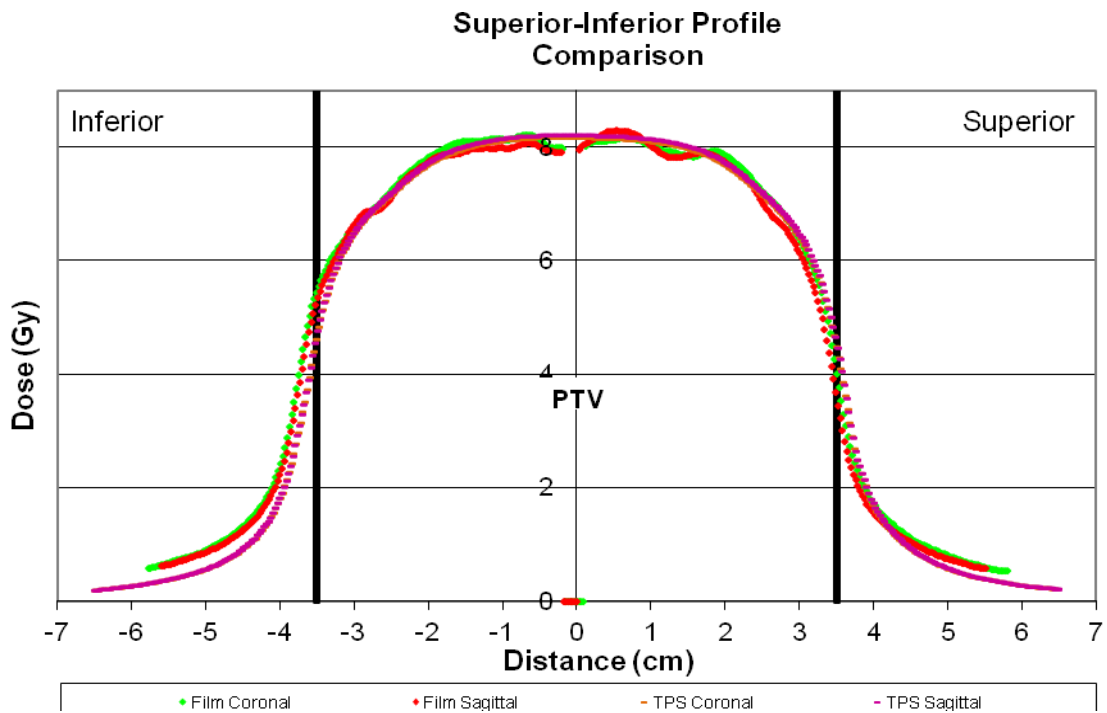


Figure 5.99 15 MV SBRT UAB 1D Superior-Inferior Dose Profiles: Irradiation #2

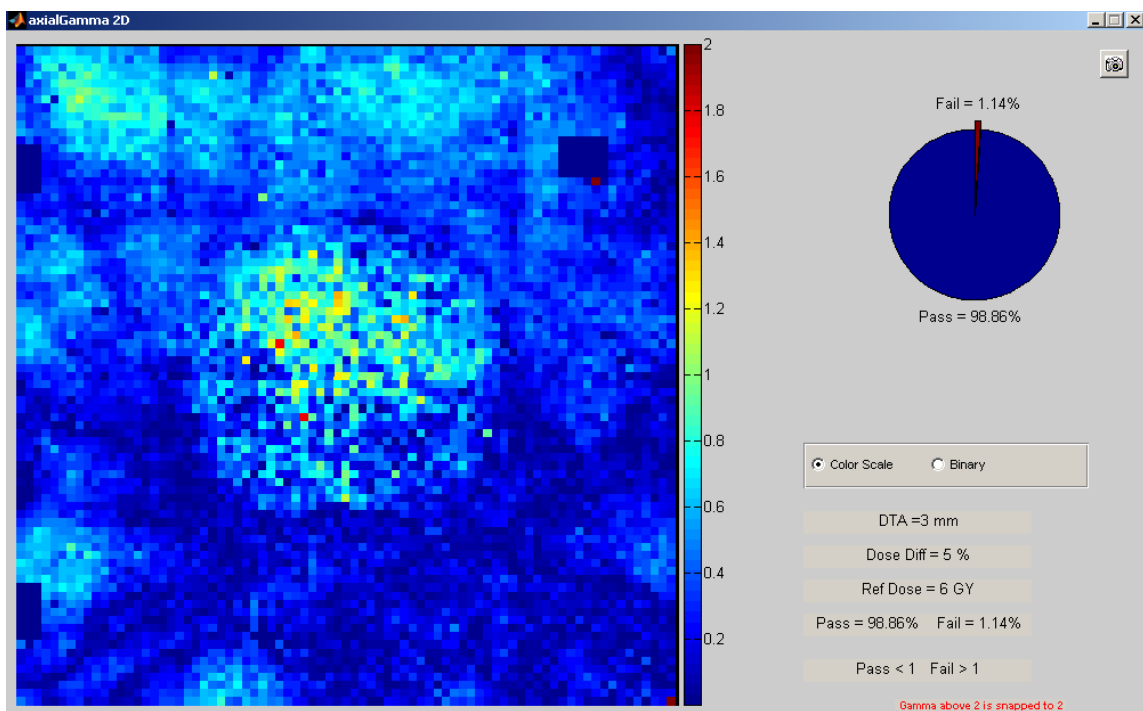


Figure 5.100 15 MV SBRT UAB 2D Gamma Index Results: $\pm 5\%/3\text{mm}$, Axial Plane, Irradiation #3

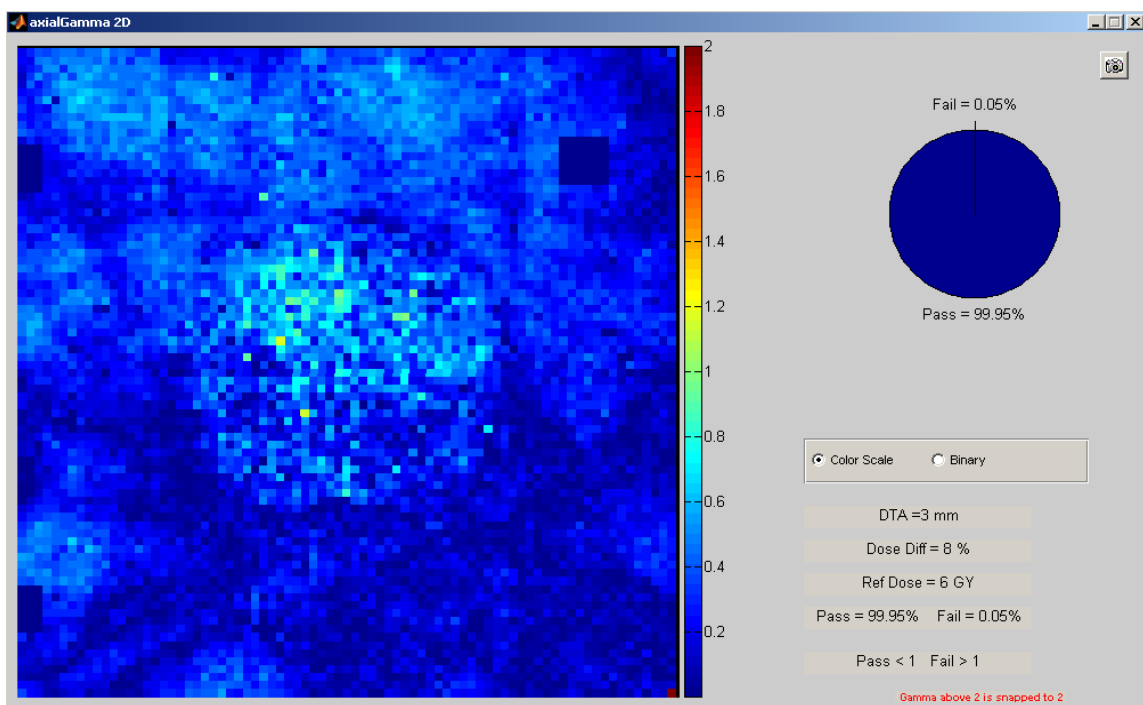


Figure 5.101 15 MV SBRT UAB 2D Gamma Index Results: $\pm 8\%/3\text{mm}$, Axial Plane, Irradiation #3

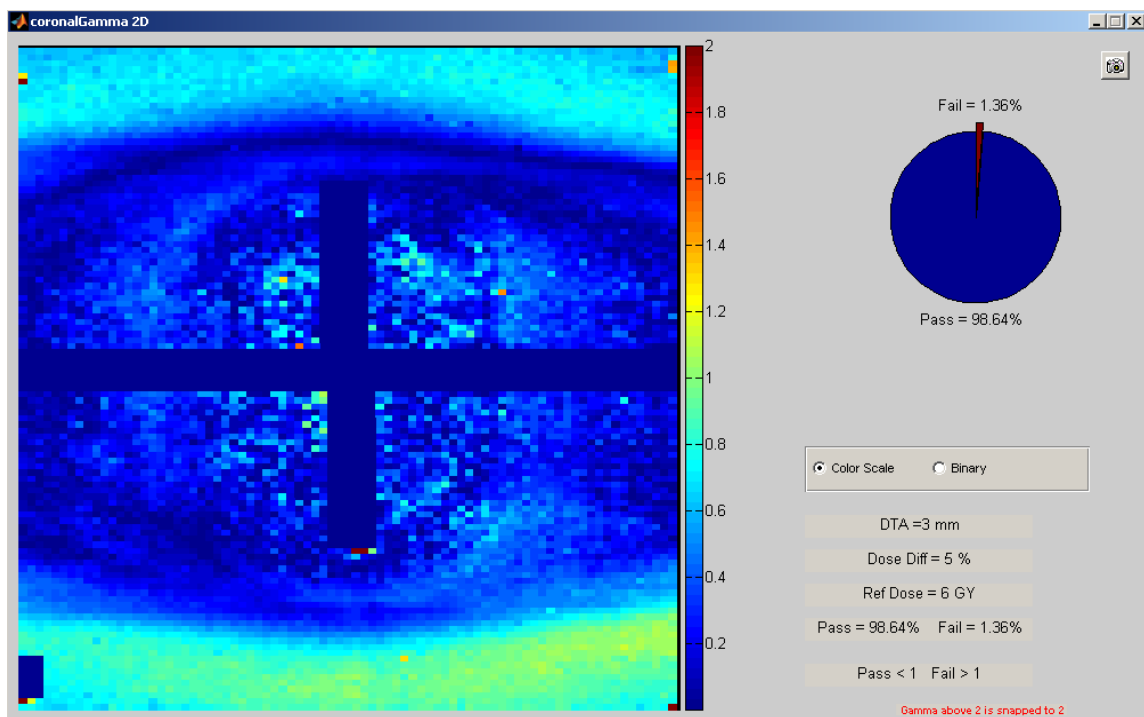


Figure 5.102 15 MV SBRT UAB 2D Gamma Index Results: $\pm 5\%/3\text{mm}$, Coronal Plane, Irradiation #3

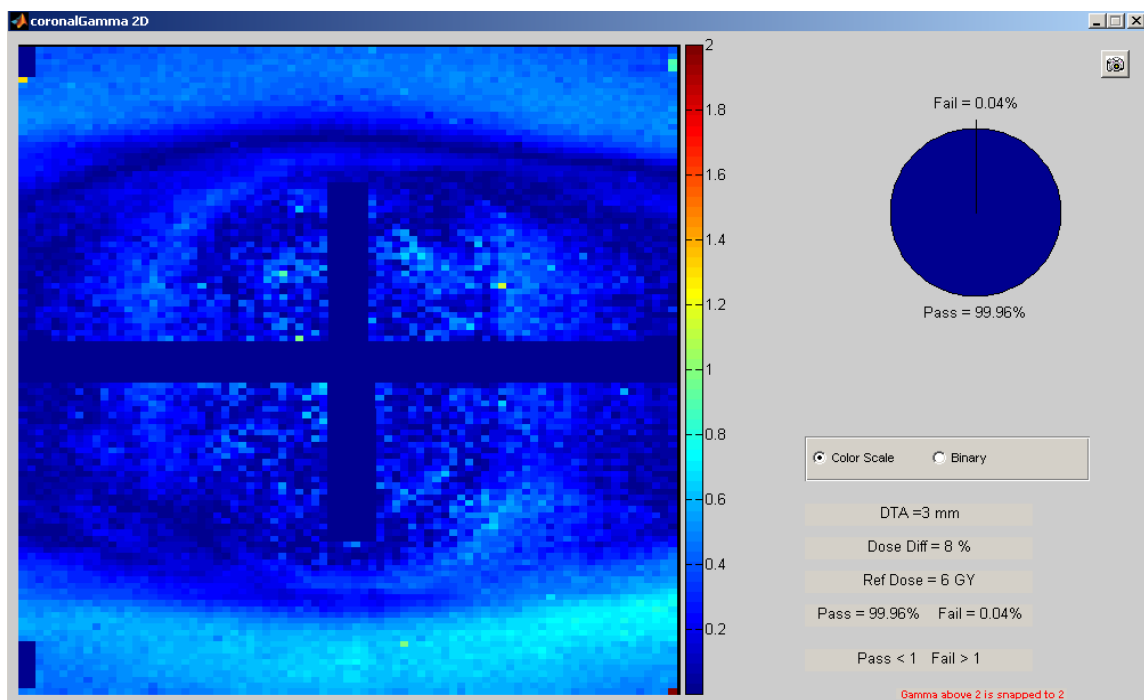


Figure 5.103 15 MV SBRT UAB 2D Gamma Index Results: $\pm 8\%/3\text{mm}$, Coronal Plane, Irradiation #3

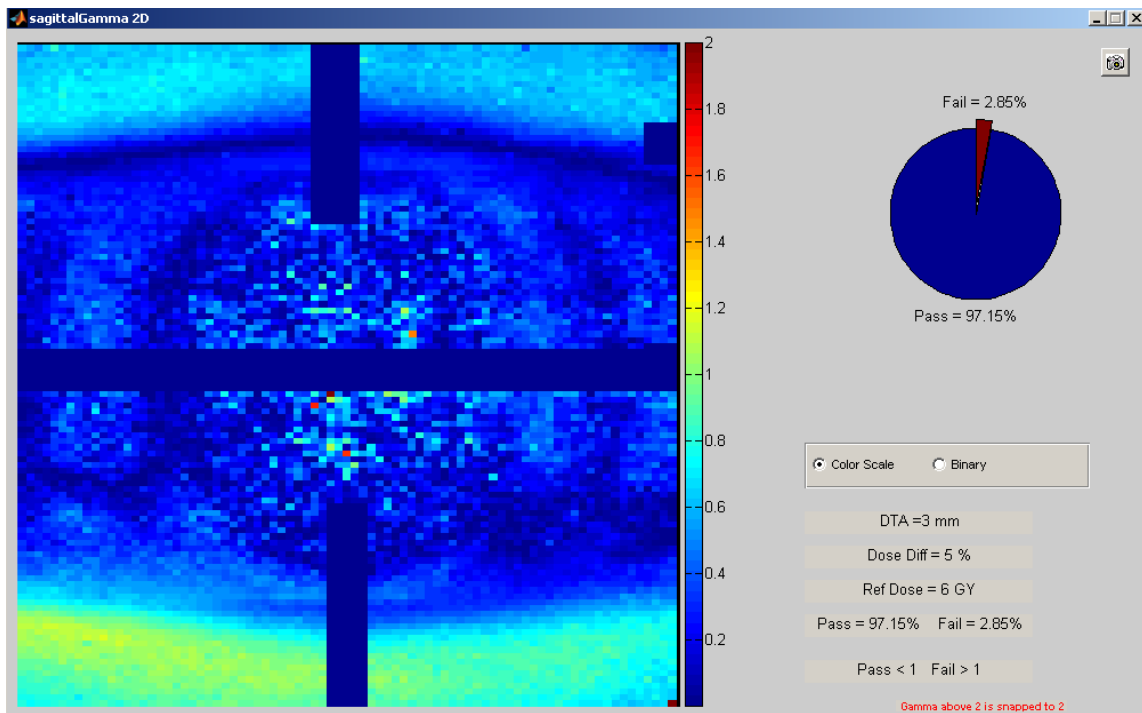


Figure 5.104 15 MV SBRT UAB 2D Gamma Index Results: $\pm 5\%/3\text{mm}$, Sagittal Plane, Irradiation #3

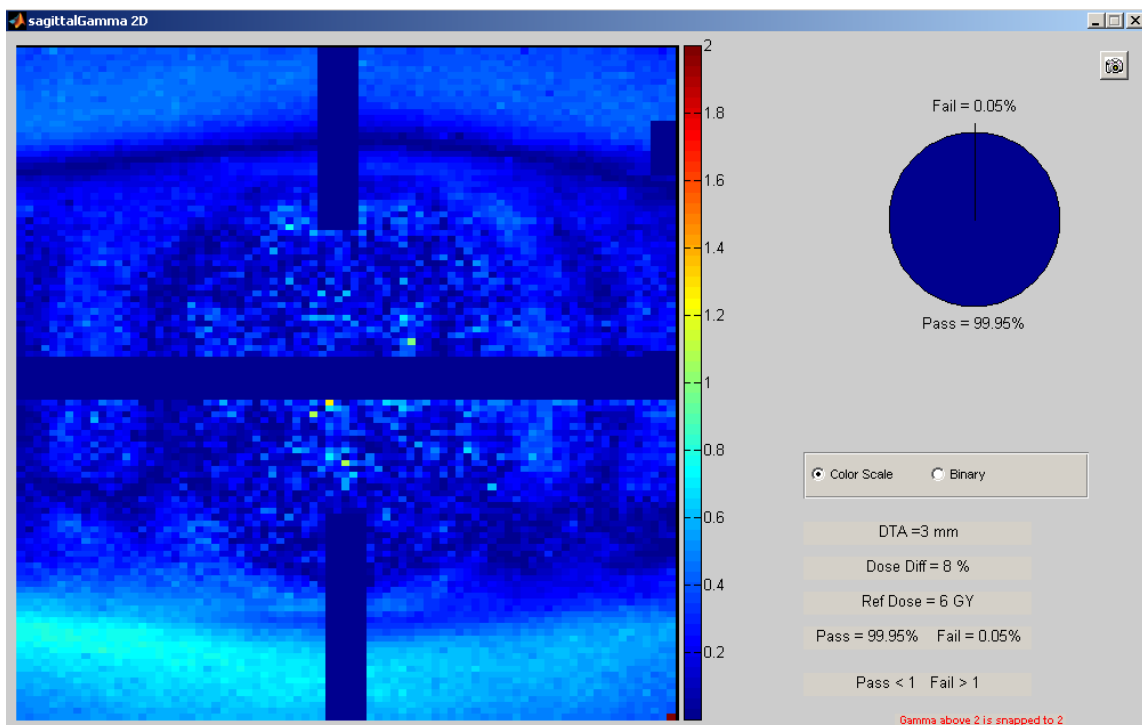


Figure 5.105 15 MV SBRT UAB 2D Gamma Index Results: $\pm 8\%/3\text{mm}$, Sagittal Plane, Irradiation #3

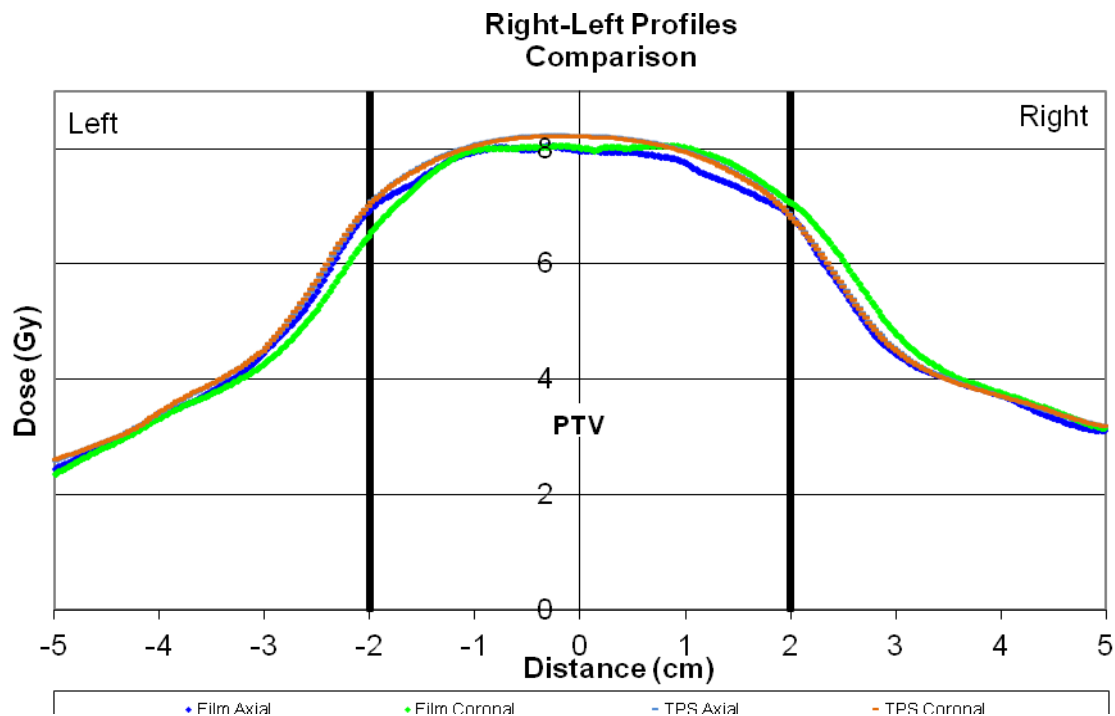


Figure 5.106 15 MV SBRT UAB 1D Right-Left Dose Profiles: Irradiation #3

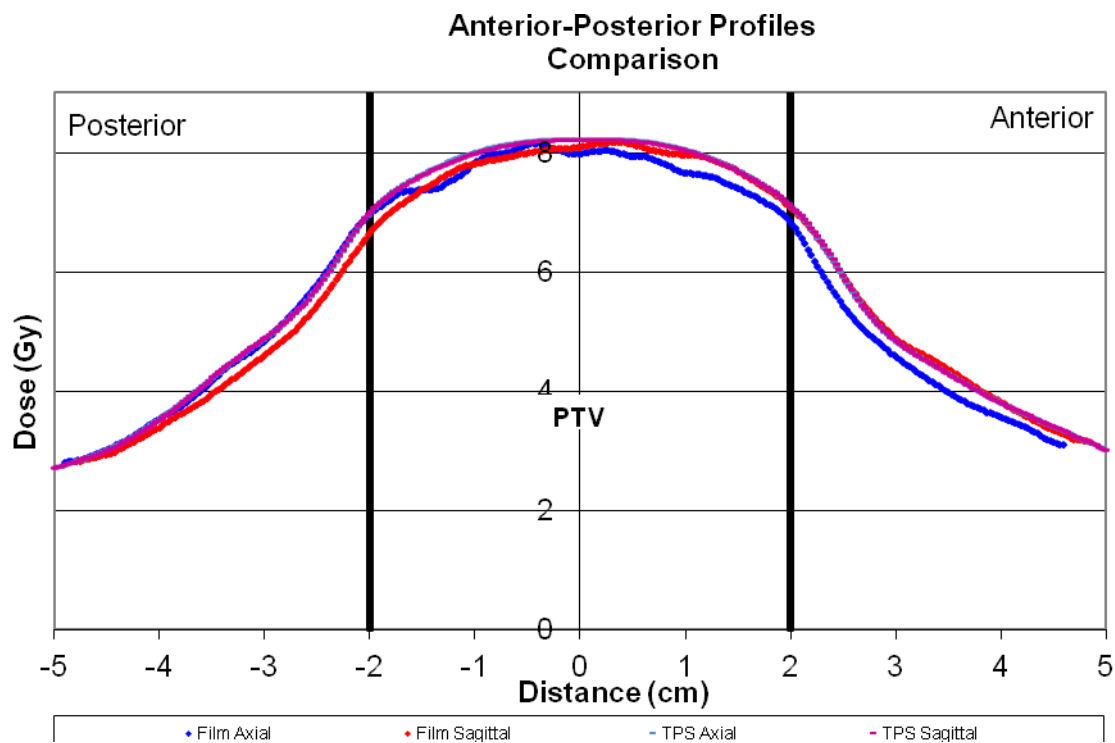


Figure 5.107 15 MV SBRT UAB 1D Anterior-Posterior Dose Profiles: Irradiation #3

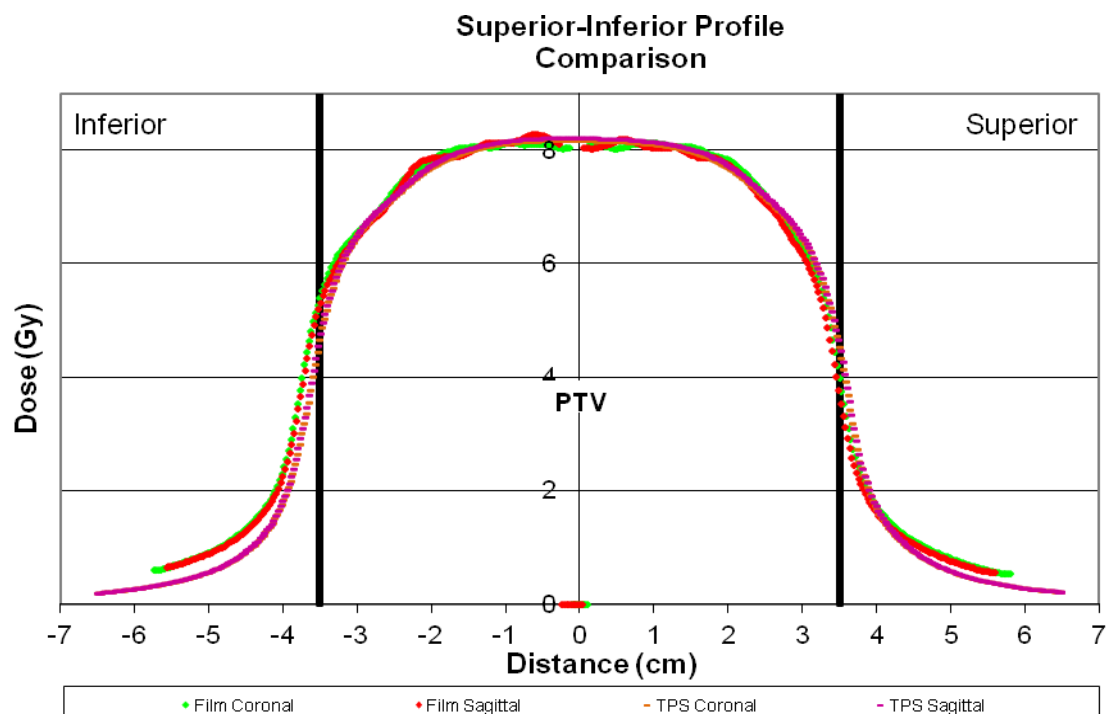


Figure 5.108 15 MV SBRT UAB 1D Superior-Inferior Dose Profiles: Irradiation #3

5.5 6 MV FFF SBRT University of Alabama MEDICAL CENTER 2D Gamma Index

Maps and Dose Profiles

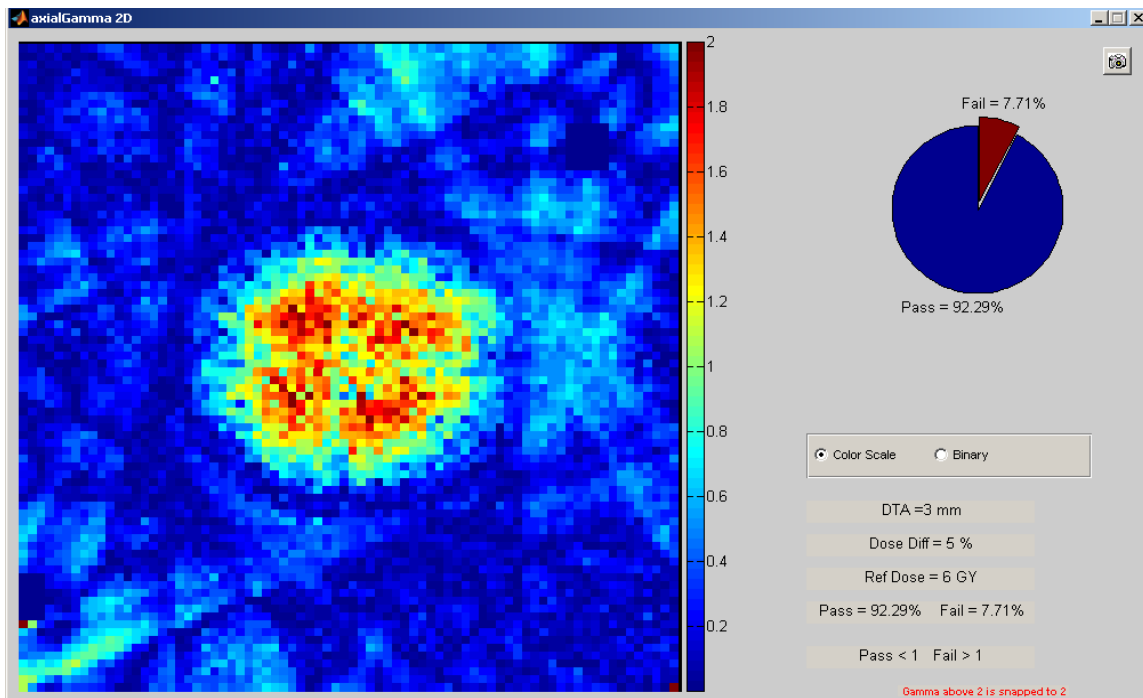


Figure 5.109 6 MV FFF SBRT UAB 2D Gamma Index Results: $\pm 5\%/3\text{mm}$, Axial Plane, Irradiation #1

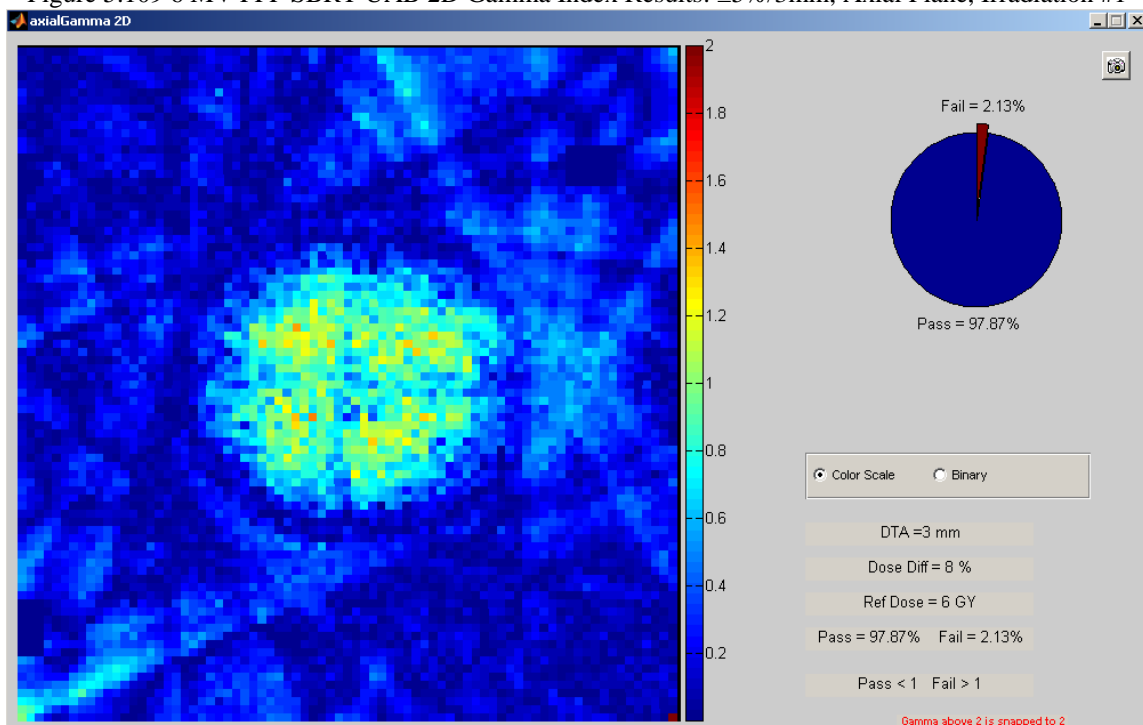


Figure 5.110 6 MV FFF SBRT UAB 2D Gamma Index Results: $\pm 8\%/3\text{mm}$, Axial Plane, Irradiation #1

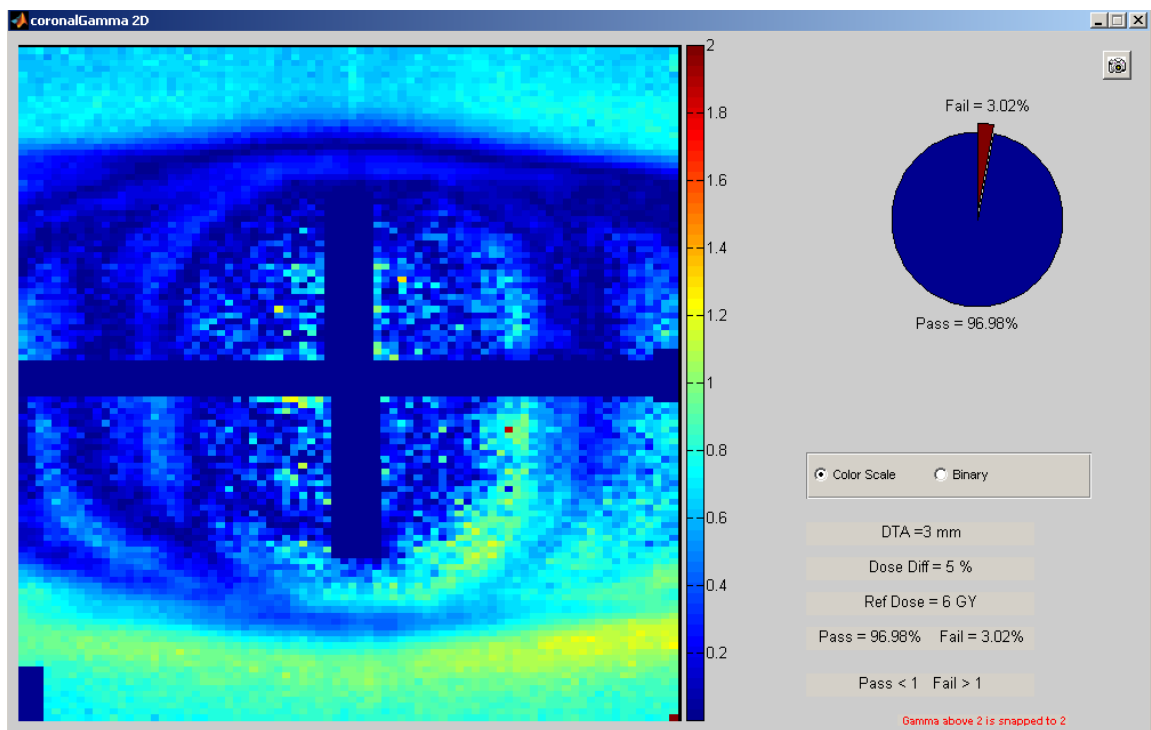


Figure 5.111 6 MV FFF SBRT UAB 2D Gamma Index Results: $\pm 5\%/3\text{mm}$, Coronal Plane, Irradiation #1

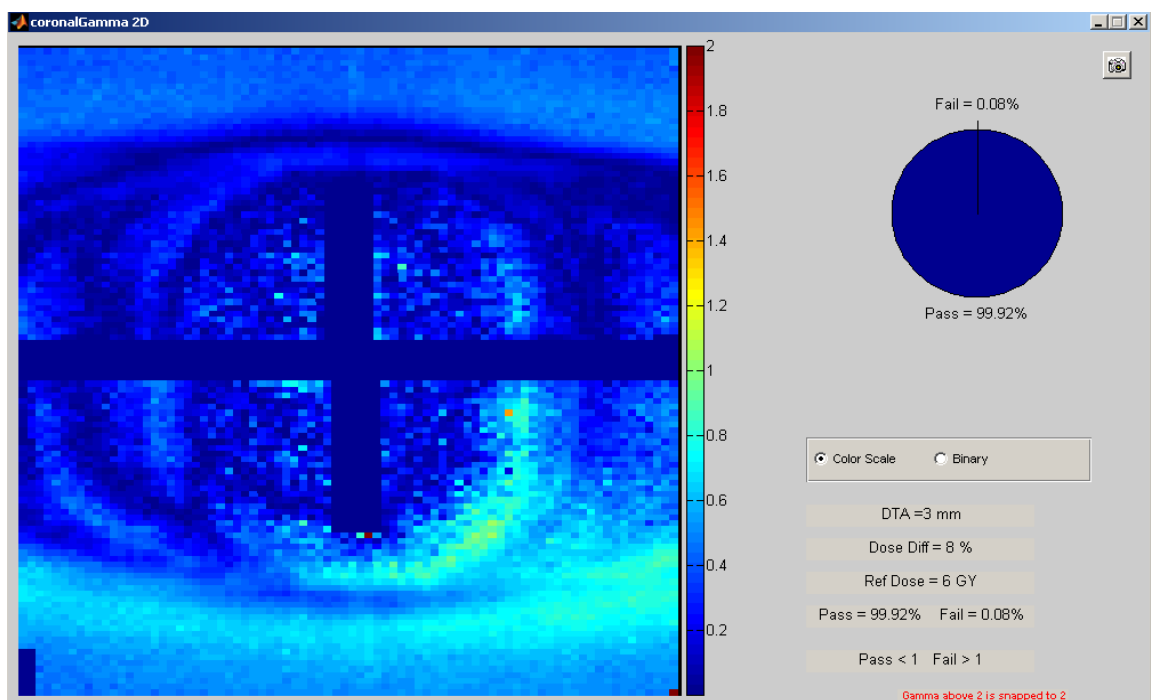


Figure 5.112 6 MV FFF SBRT UAB 2D Gamma Index Results: $\pm 8\%/3\text{mm}$, Coronal Plane, Irradiation #1

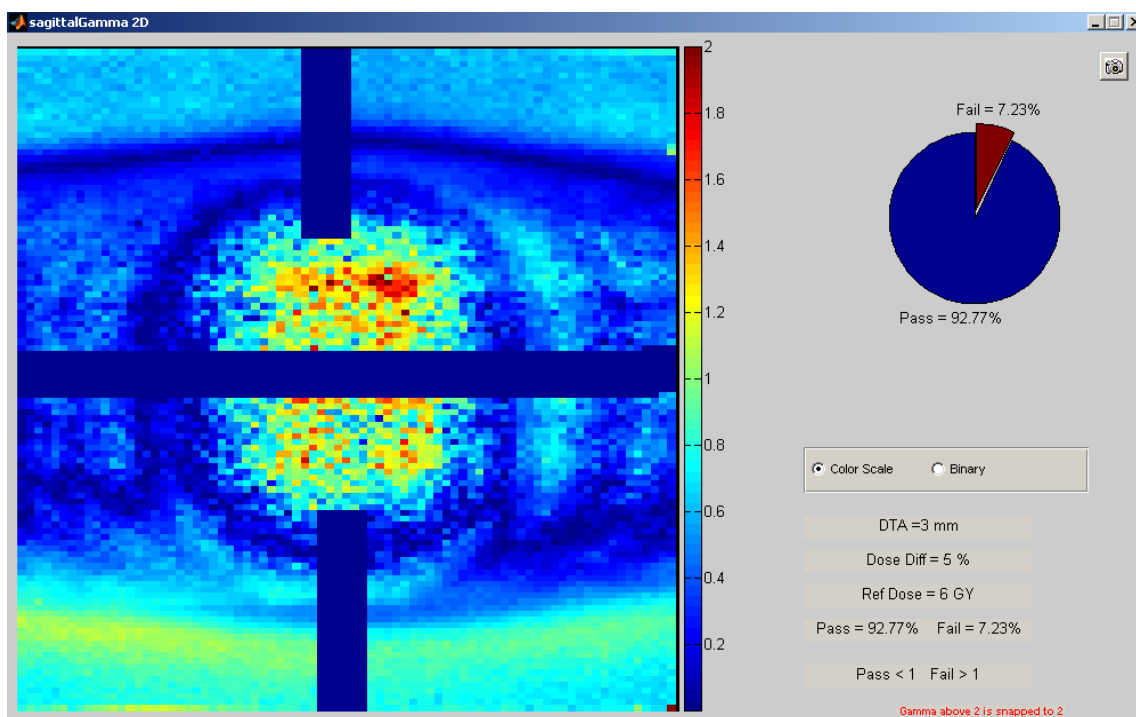


Figure 5.113 6 MV FFF SBRT UAB 2D Gamma Index Results: $\pm 5\%/3\text{mm}$, Sagittal Plane, Irradiation #1

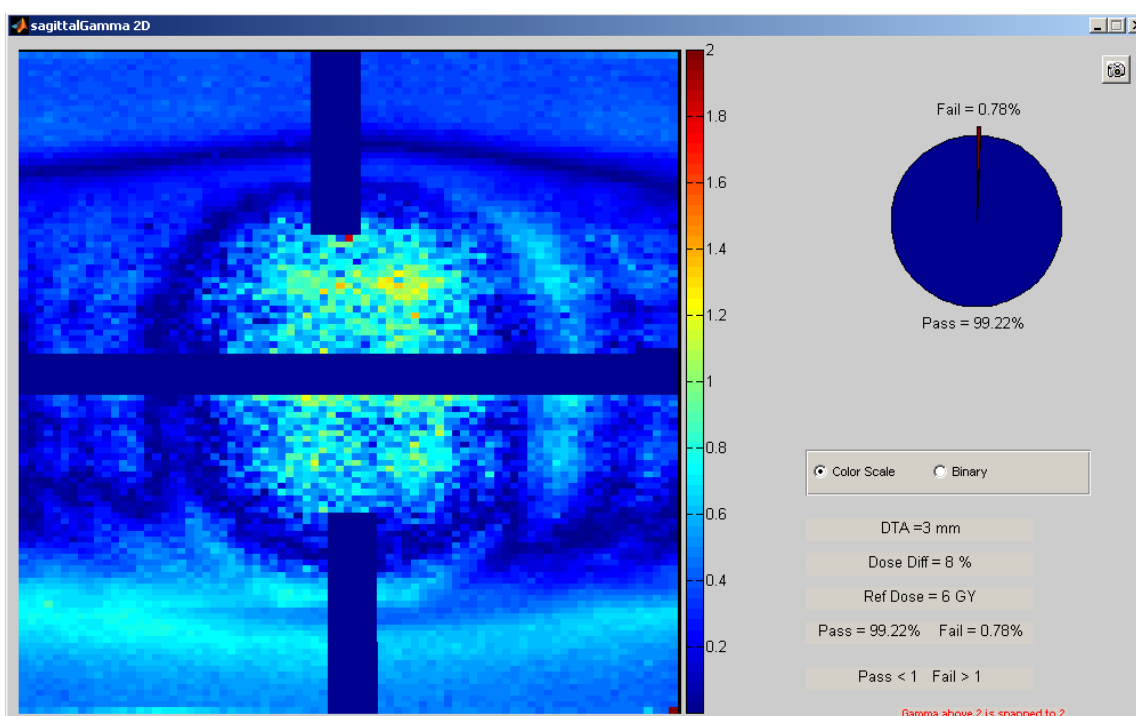


Figure 5.114 6 MV FFF SBRT UAB 2D Gamma Index Results: $\pm 8\%/3\text{mm}$, Sagittal Plane, Irradiation #1

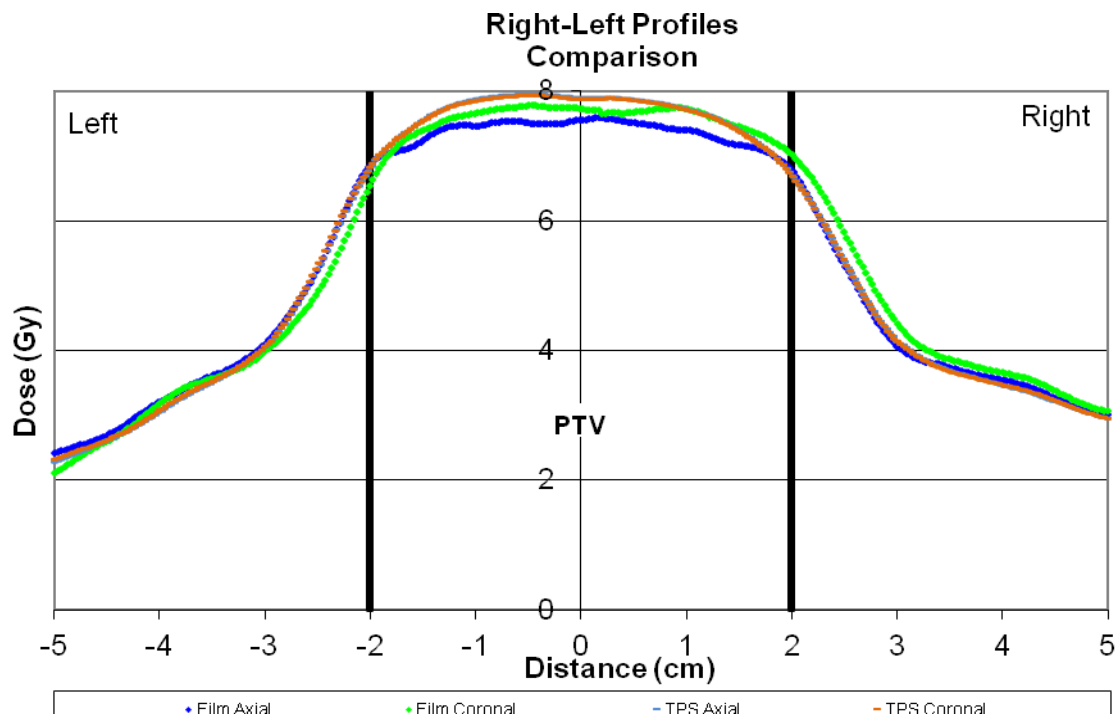


Figure 5.115 6 MV FFF SBRT UAB 1D Right-Left Dose Profiles: Irradiation #1

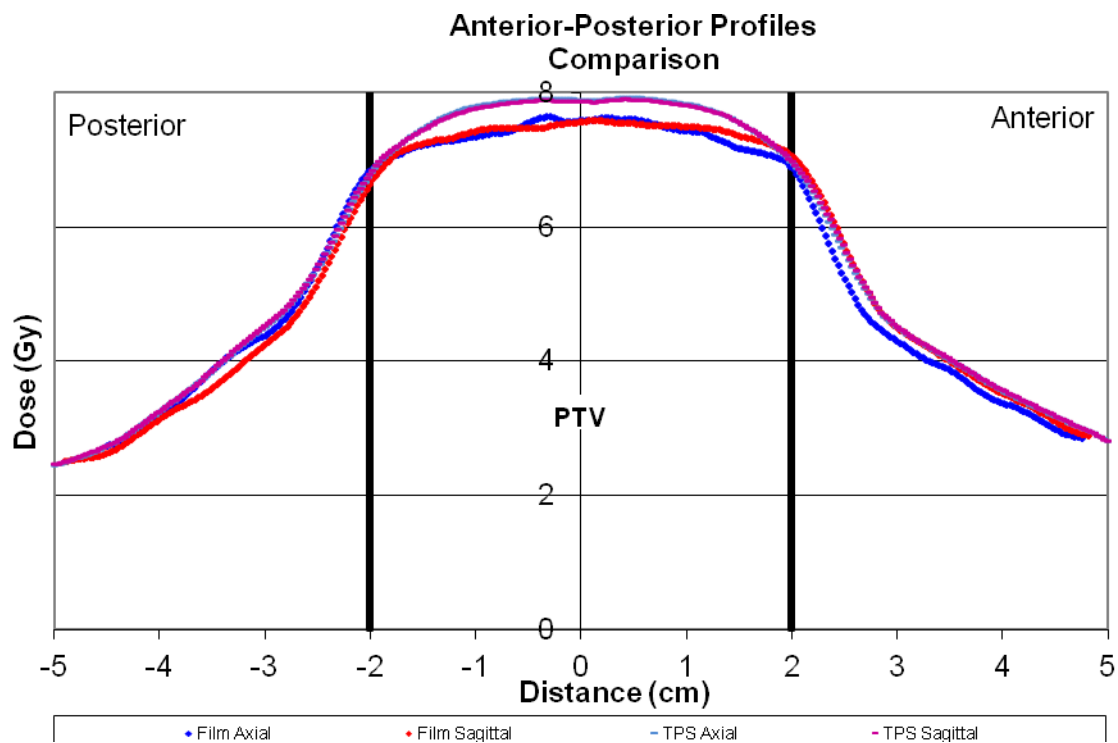


Figure 5.116 6 MV FFF SBRT UAB 1D Anterior-Posterior Dose Profiles: Irradiation #1

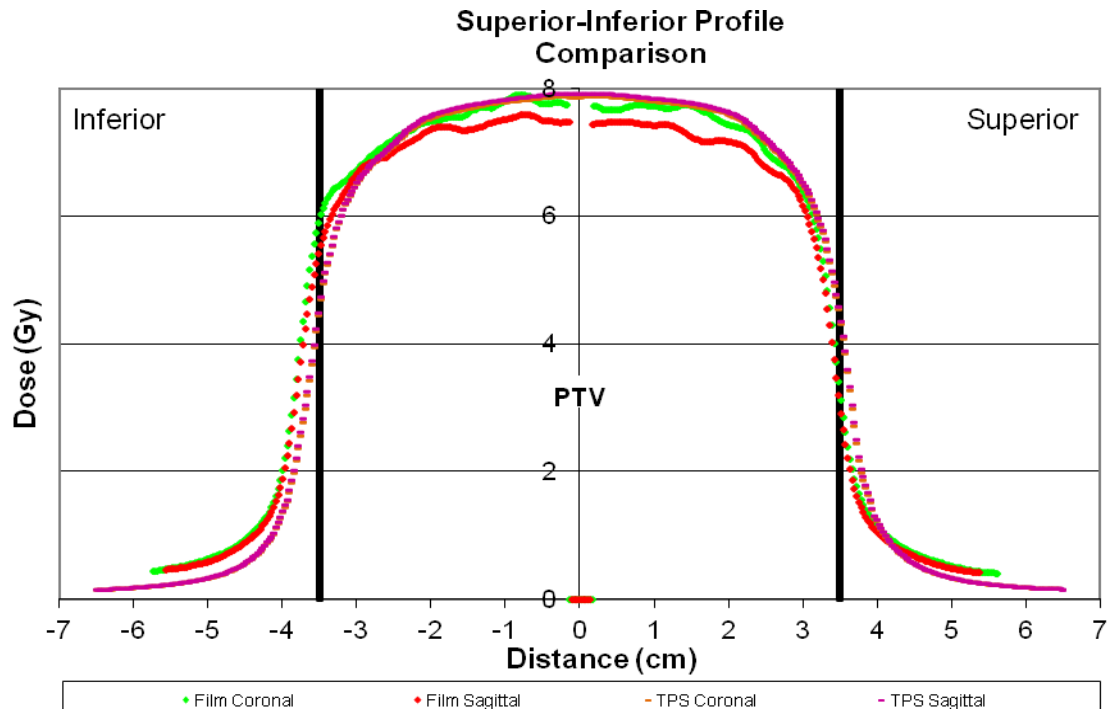


Figure 5.117 6 MV FFF SBRT UAB 1D Superior-Inferior Dose Profiles: Irradiation #1

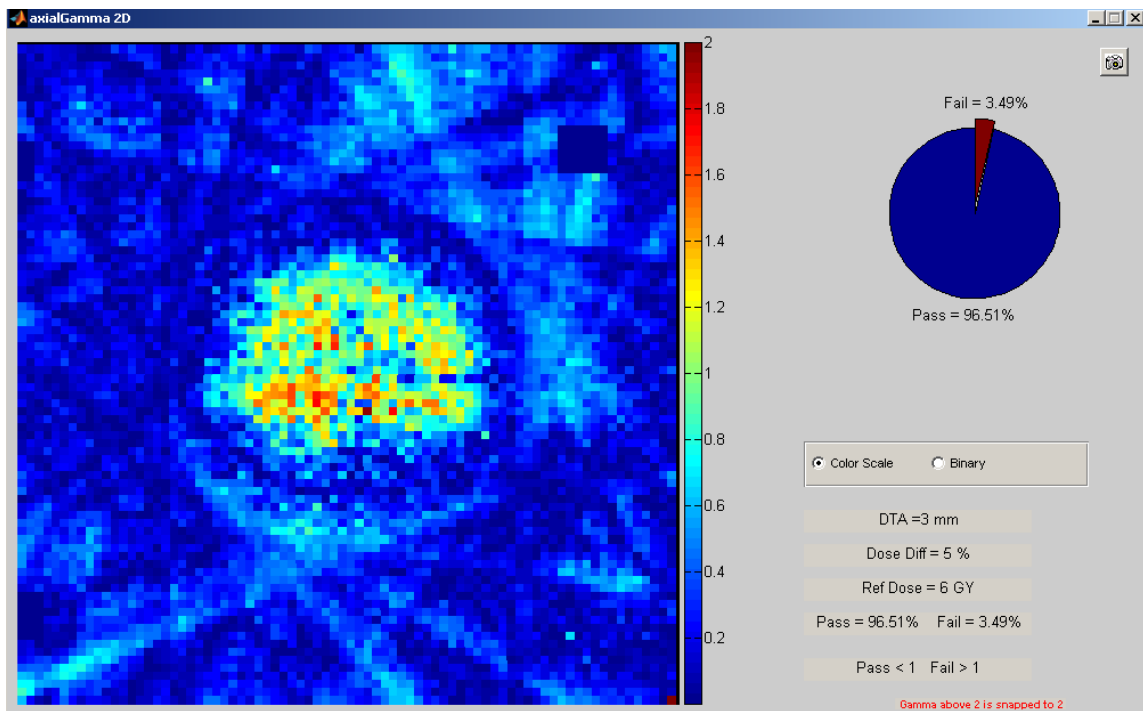


Figure 5.118 6 MV FFF SBRT UAB 2D Gamma Index Results: $\pm 5\%/3\text{mm}$, Axial Plane, Irradiation #2

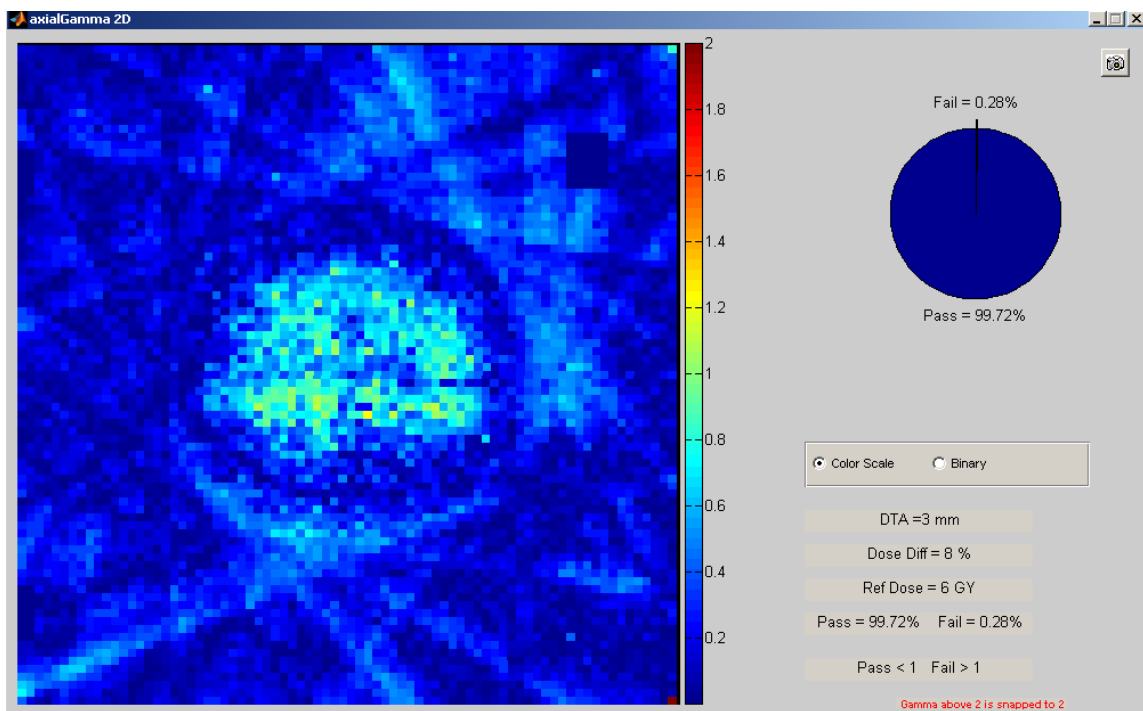


Figure 5.119 6 MV FFF SBRT UAB 2D Gamma Index Results: $\pm 8\%/3\text{mm}$, Axial Plane, Irradiation #2

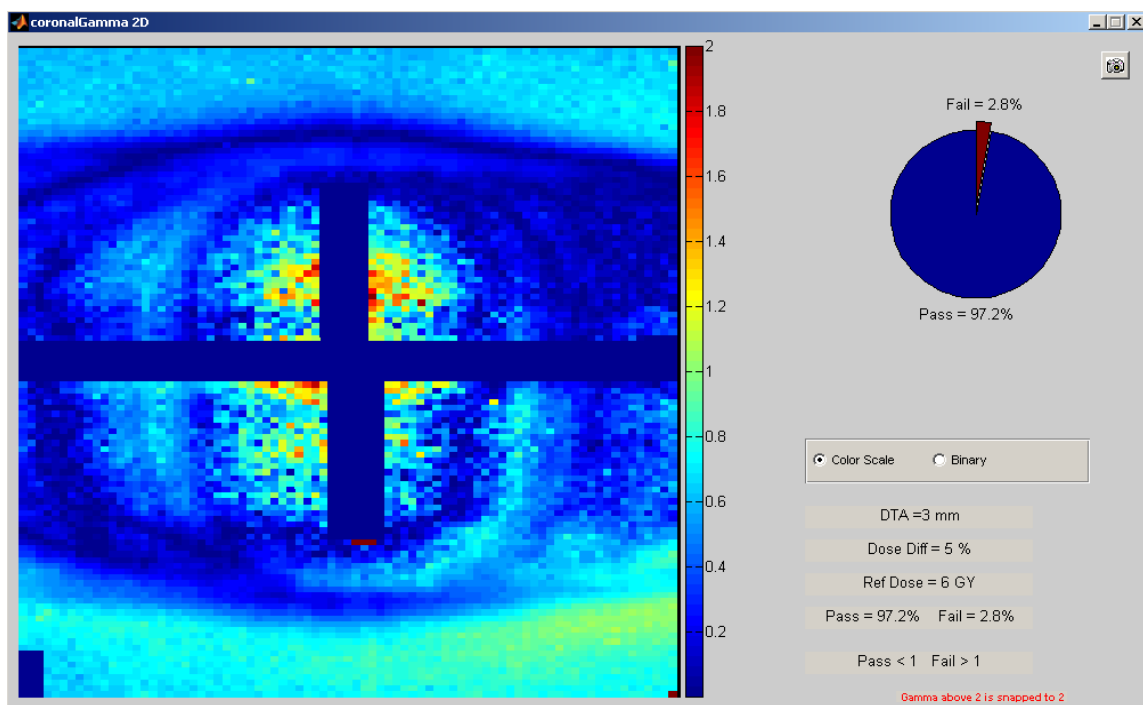


Figure 5.120 6 MV FFF SBRT UAB 2D Gamma Index Results: $\pm 5\%/3\text{mm}$, Coronal Plane, Irradiation #2

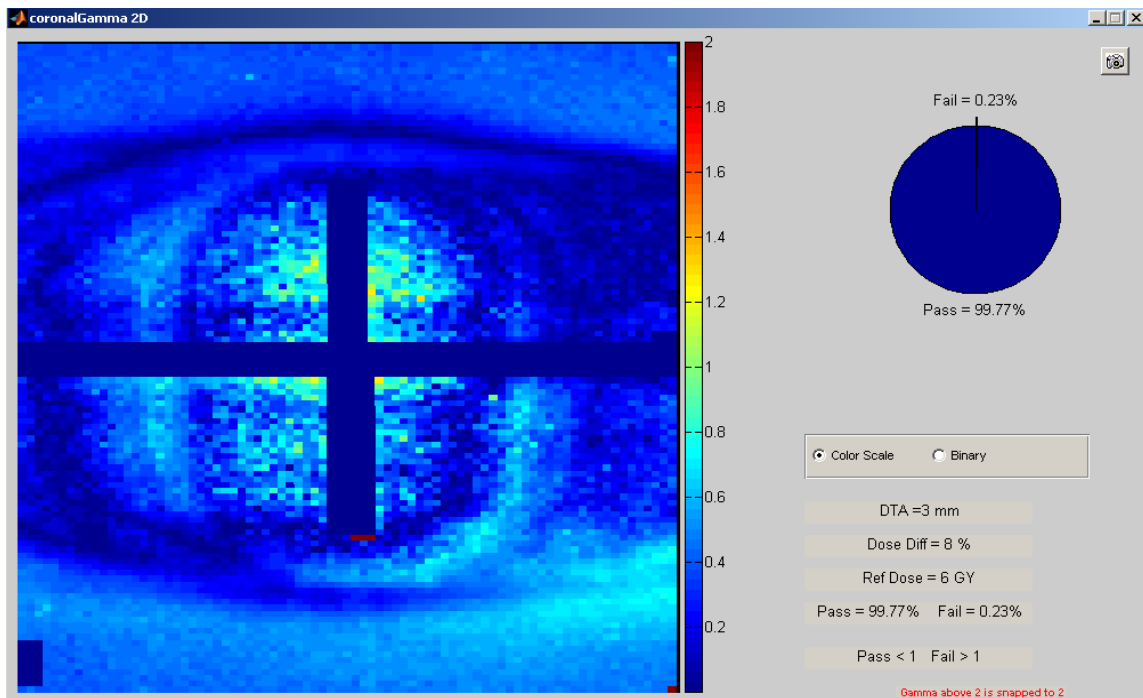


Figure 5.121 6 MV FFF SBRT UAB 2D Gamma Index Results: $\pm 8\%/3\text{mm}$, Coronal Plane, Irradiation #2

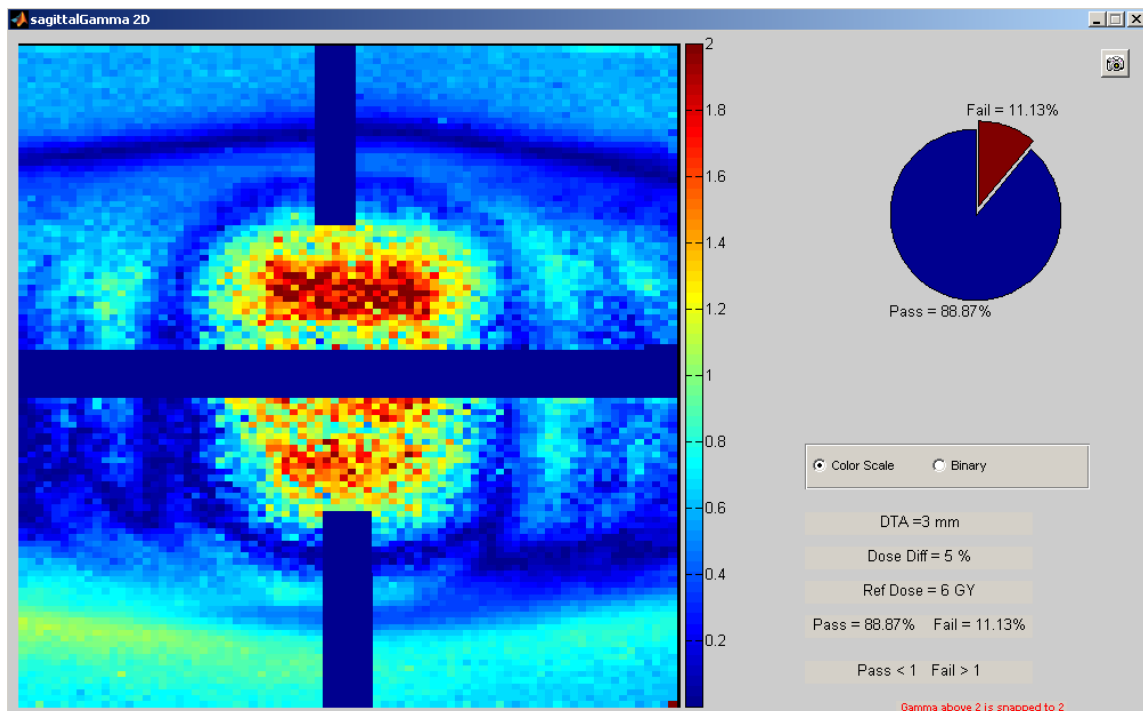


Figure 5.122 6 MV FFF SBRT UAB 2D Gamma Index Results: $\pm 5\%/3\text{mm}$, Sagittal Plane, Irradiation #2

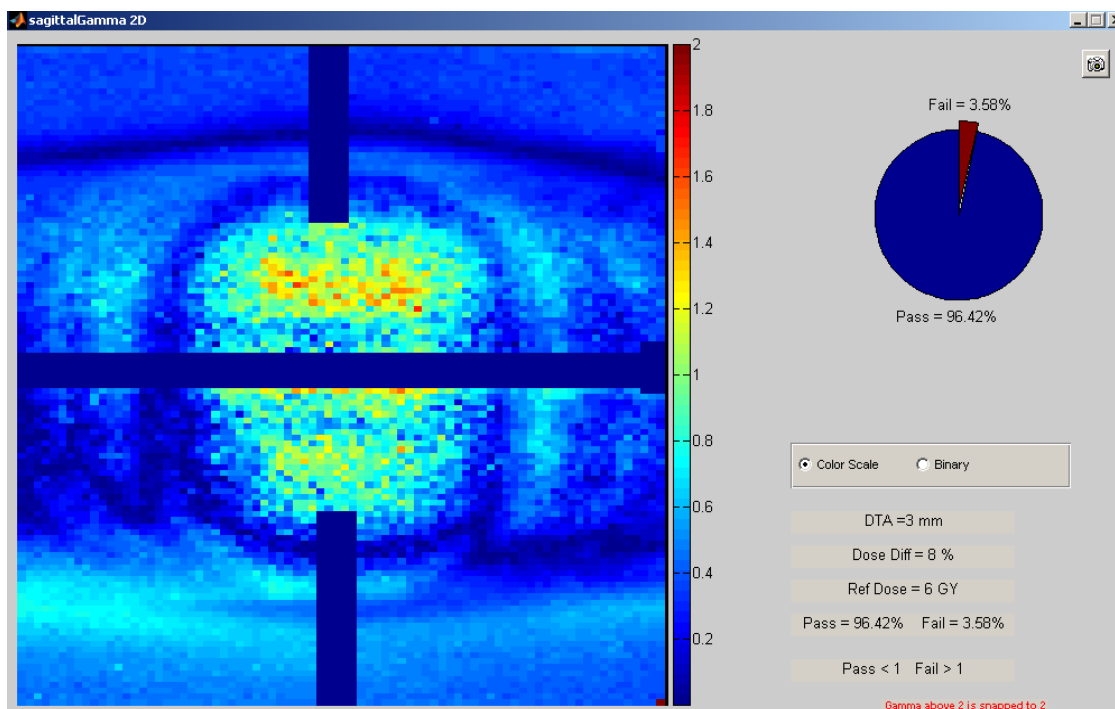


Figure 5.123 6 MV FFF SBRT UAB 2D Gamma Index Results: $\pm 8\%/3\text{mm}$, Sagittal Plane, Irradiation #2

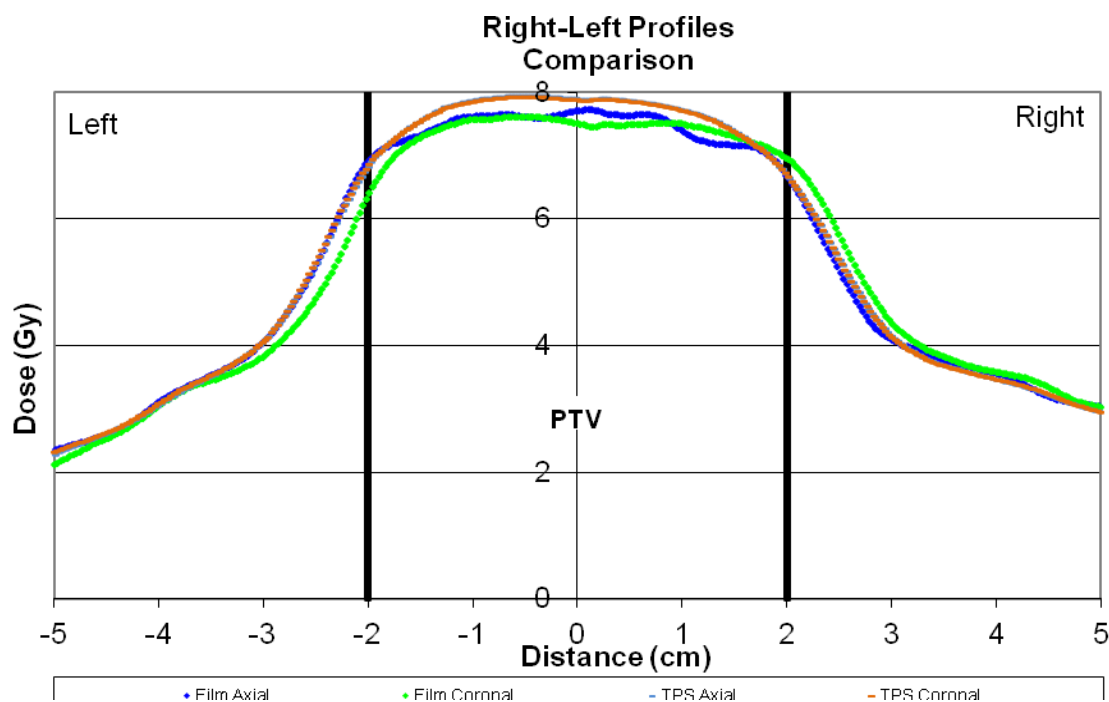


Figure 5.124 6 MV FFF SBRT UAB 1D Right-Left Dose Profiles: Irradiation #2

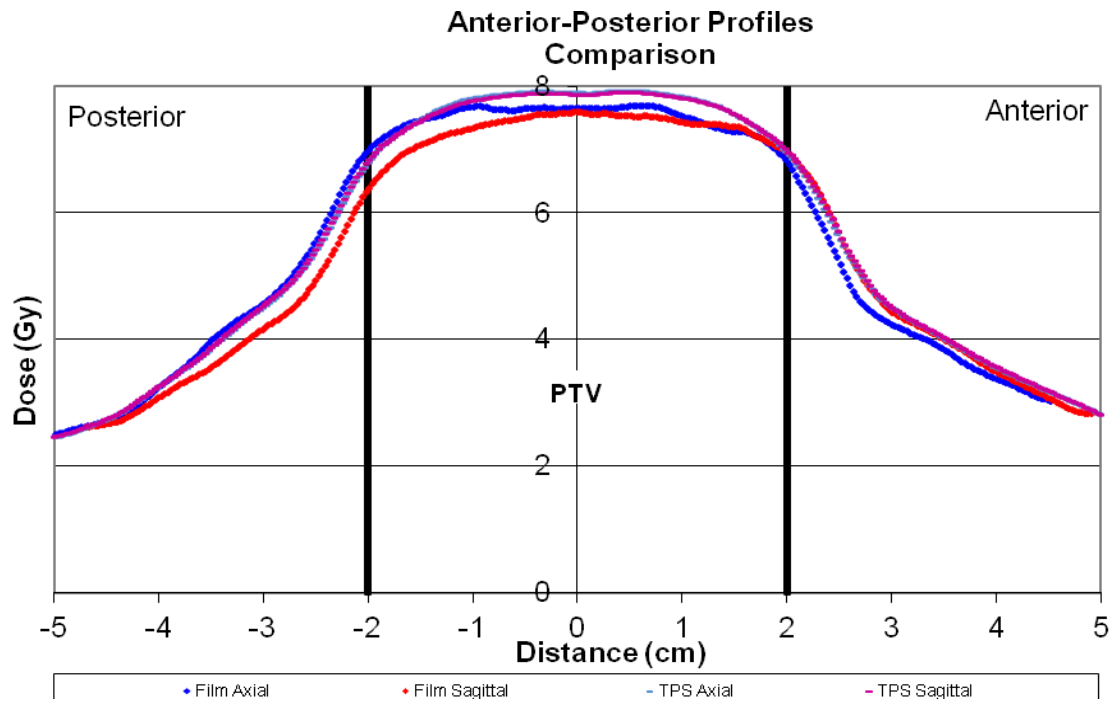


Figure 5.125 6 MV FFF SBRT UAB 1D Anterior-Posterior Dose Profiles: Irradiation #2

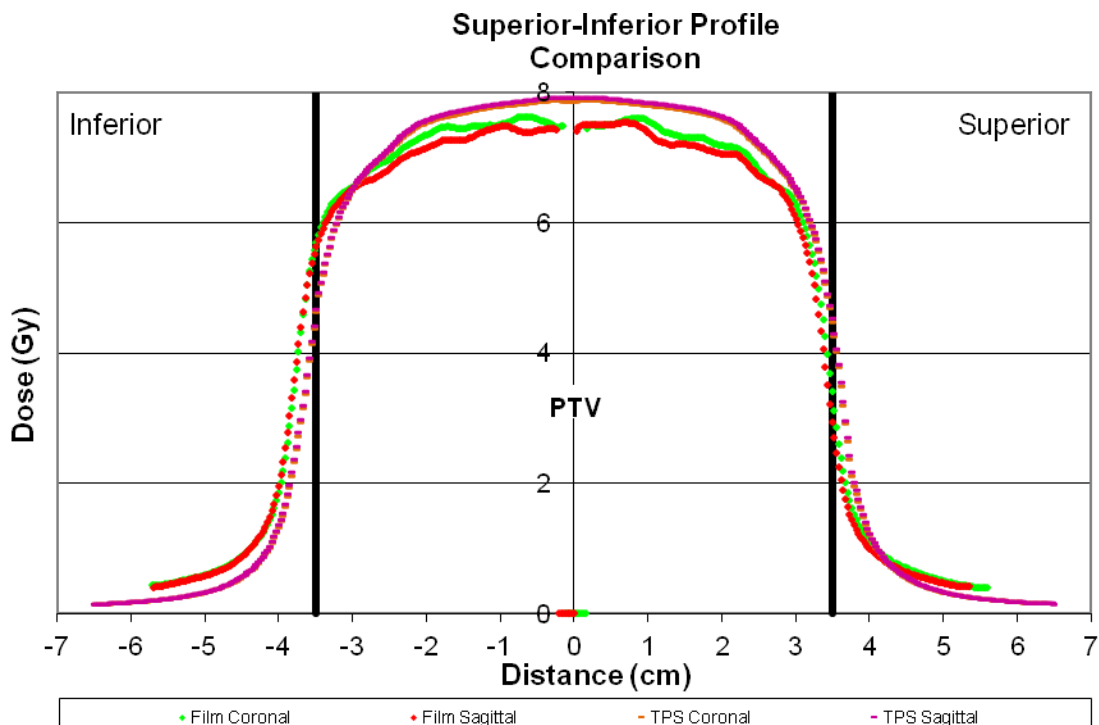


Figure 5.126 6 MV FFF SBRT UAB 1D Superior-Inferior Dose Profiles: Irradiation #2

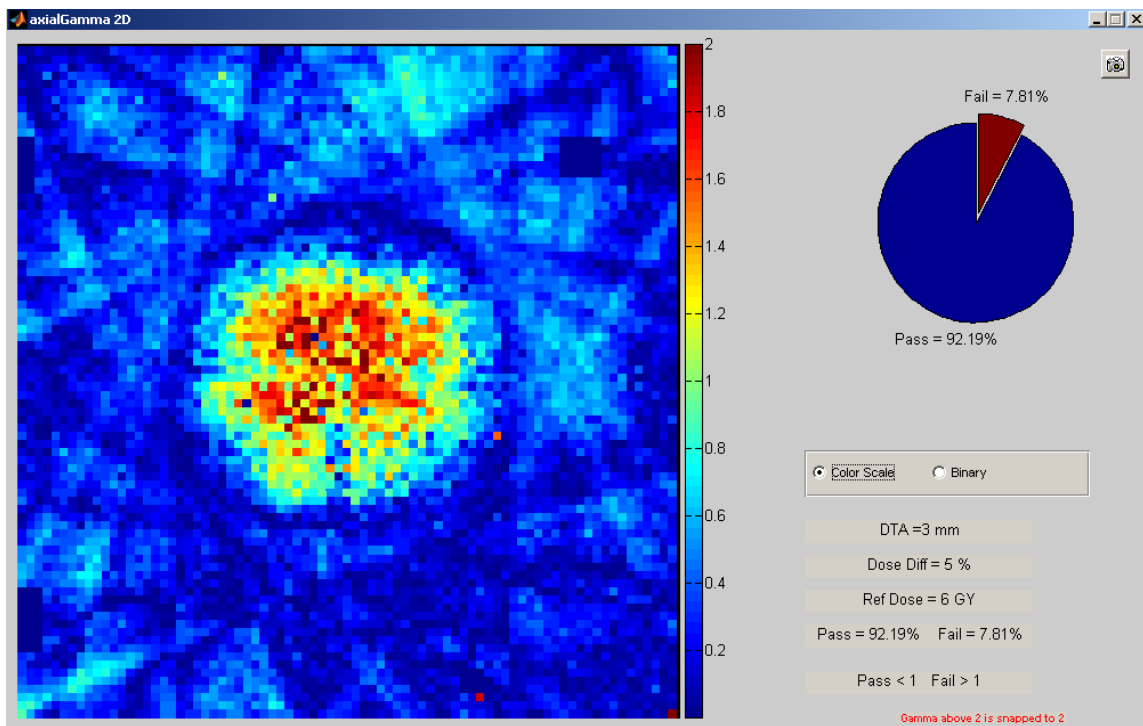


Figure 5.127 6 MV FFF SBRT UAB 2D Gamma Index Results: $\pm 5\%/3\text{mm}$, Axial Plane, Irradiation #3

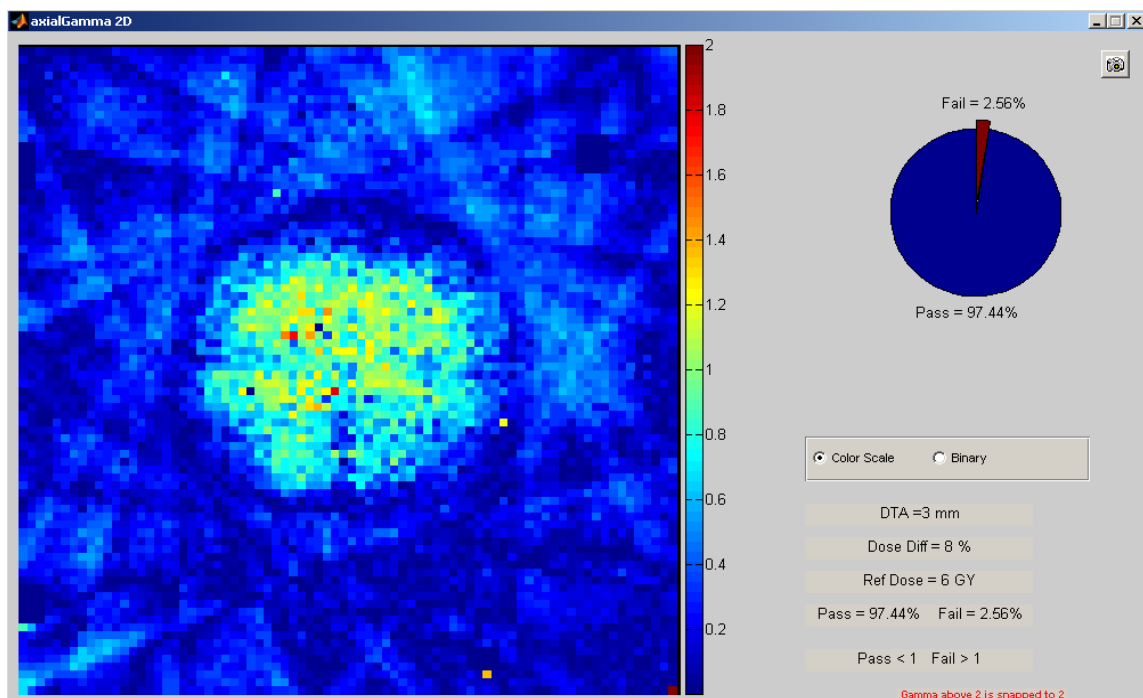


Figure 5.128 6 MV FFF SBRT UAB 2D Gamma Index Results: $\pm 8\%/3\text{mm}$, Axial Plane, Irradiation #3

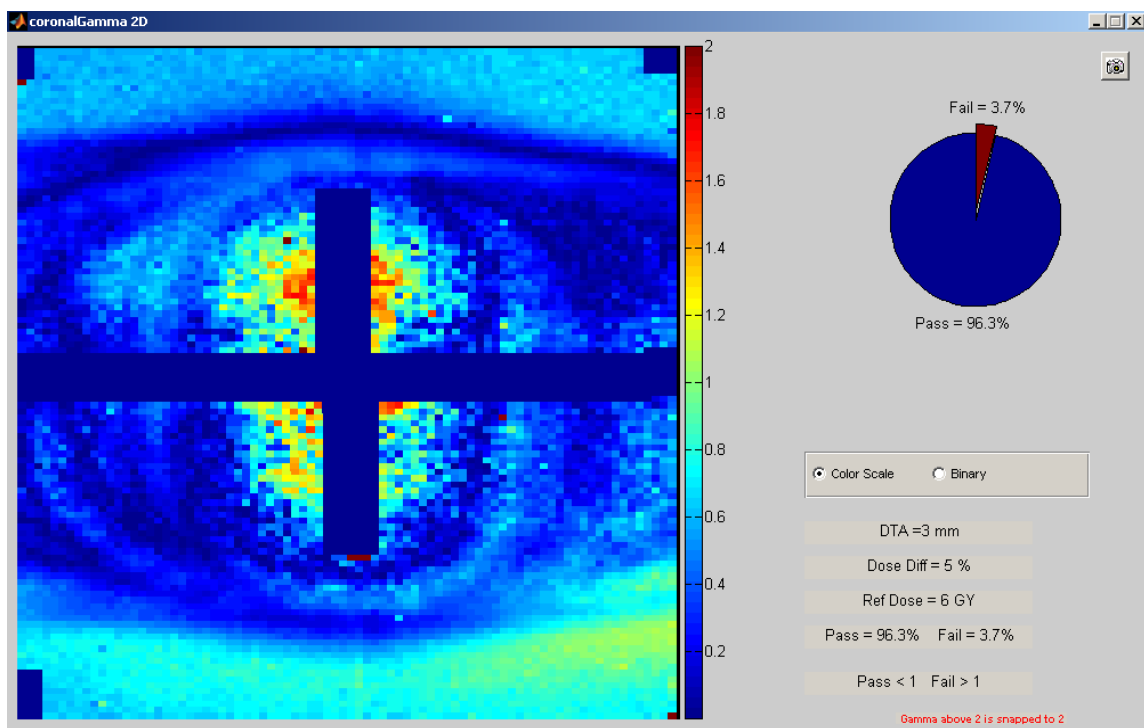


Figure 5.129 6 MV FFF SBRT UAB 2D Gamma Index Results: $\pm 5\%/3\text{mm}$, Coronal Plane, Irradiation #3

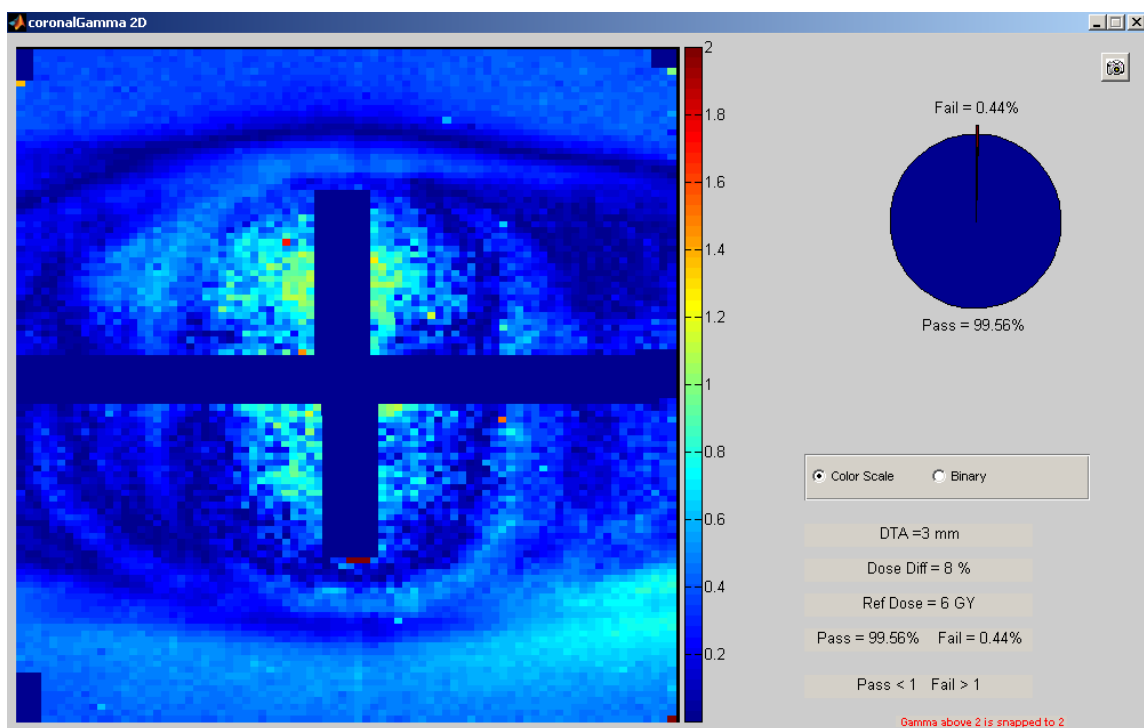


Figure 5.130 6 MV FFF SBRT UAB 2D Gamma Index Results: $\pm 8\%/3\text{mm}$, Coronal Plane, Irradiation #3

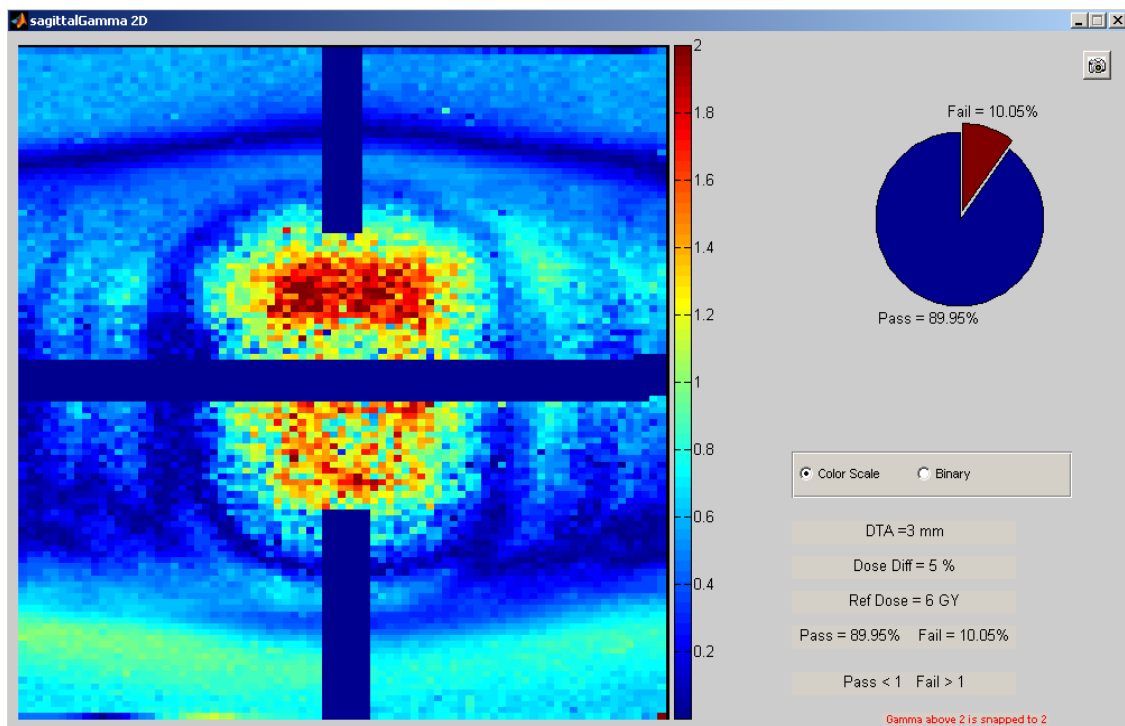


Figure 5.131 6 MV FFF SBRT UAB 2D Gamma Index Results: $\pm 5\%/3\text{mm}$, Sagittal Plane, Irradiation #3

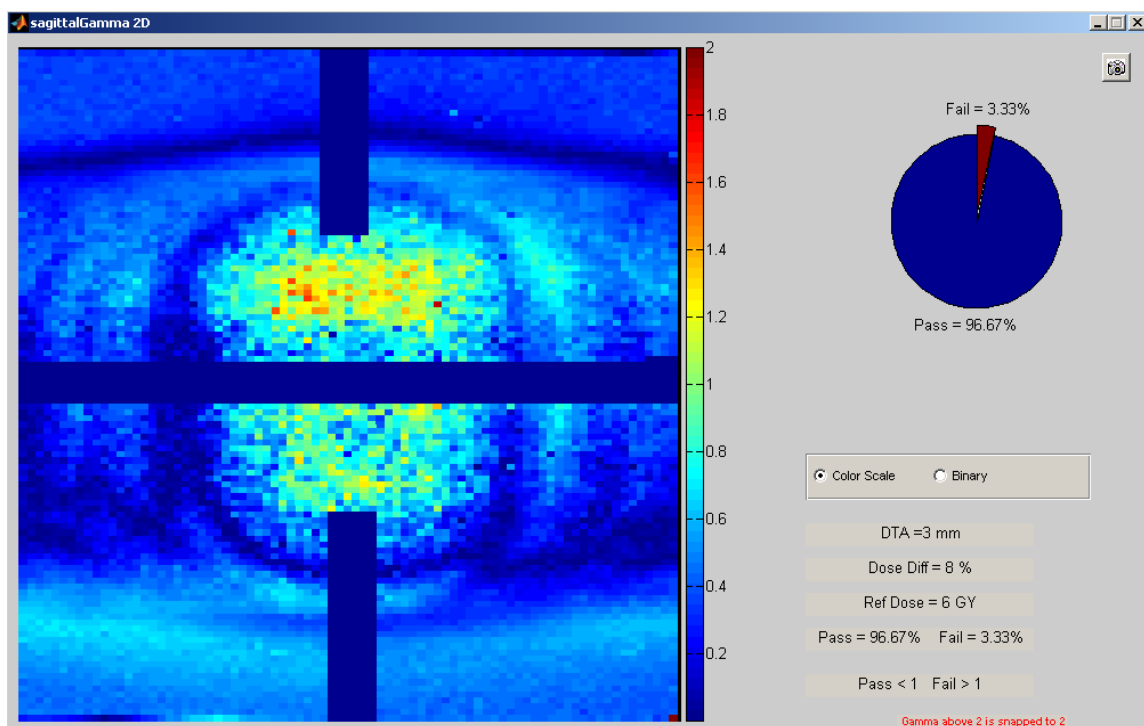


Figure 5.132 6 MV FFF SBRT UAB 2D Gamma Index Results: $\pm 8\%/3\text{mm}$, Sagittal Plane, Irradiation #3

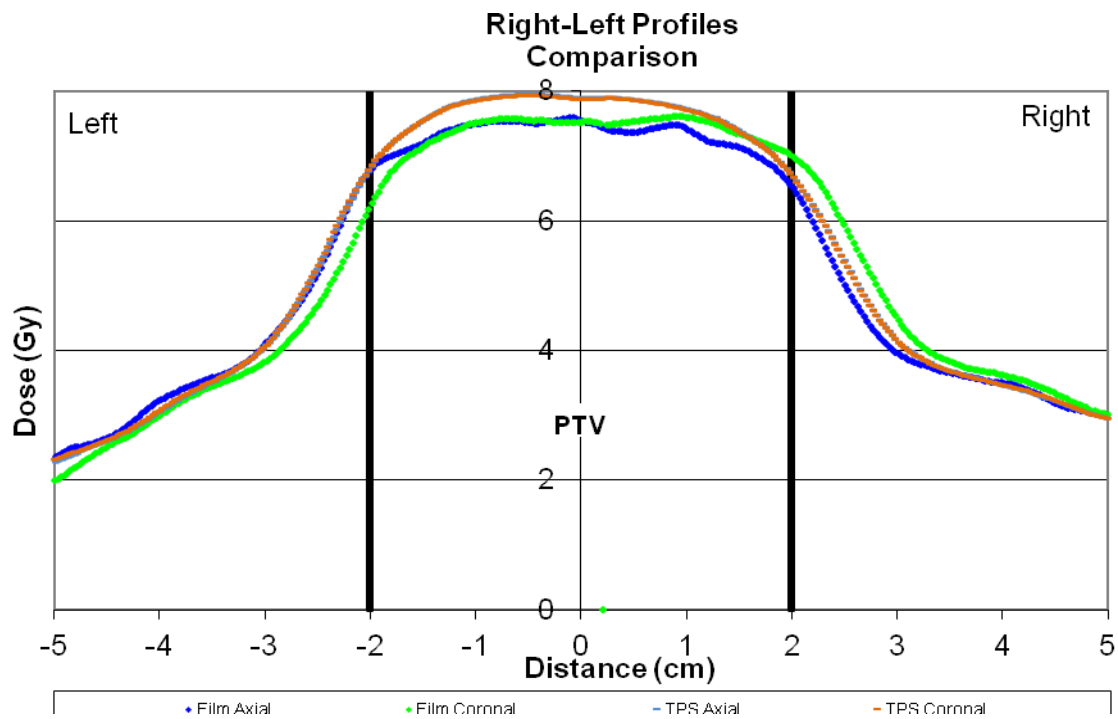


Figure 5.133 6 MV FFF SBRT UAB 1D Right-Left Dose Profiles: Irradiation #3

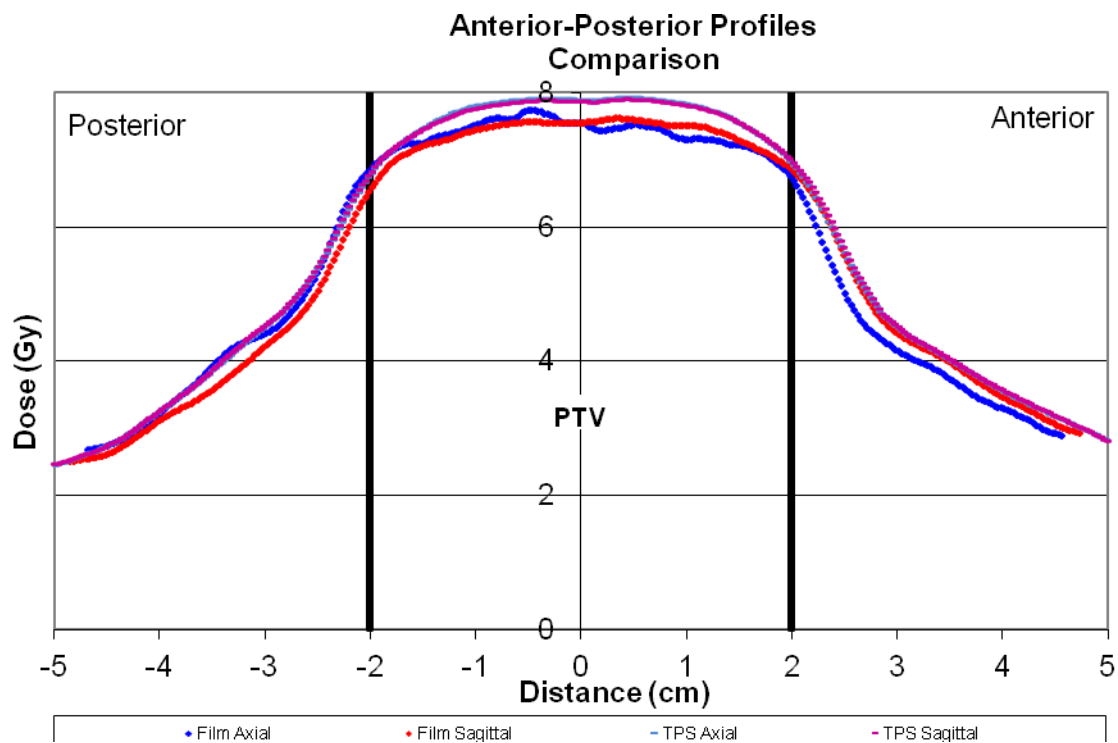


Figure 5.134 6 MV FFF SBRT UAB 1D Anterior-Posterior Dose Profiles: Irradiation #3

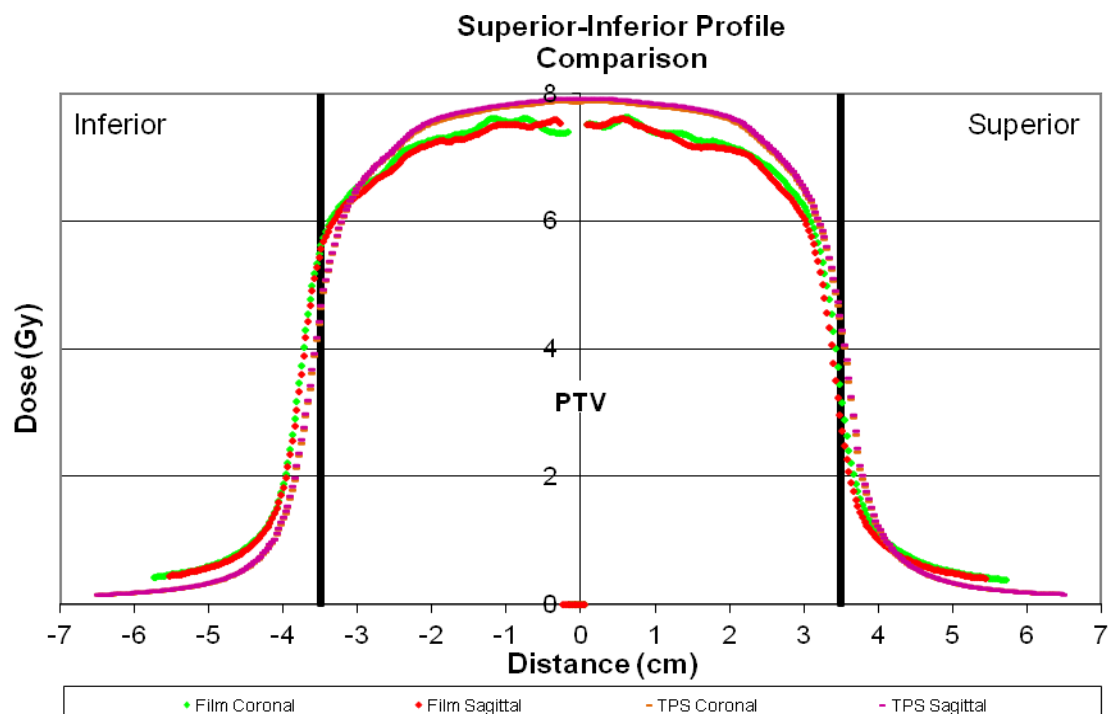


Figure 5.135 6 MV FFF SBRT UAB 1D Superior-Inferior Dose Profiles: Irradiation #3

5.6 10 MV FFF SBRT University of Alabama MEDICAL CENTER 2D Gamma

Index Maps and Dose Profiles

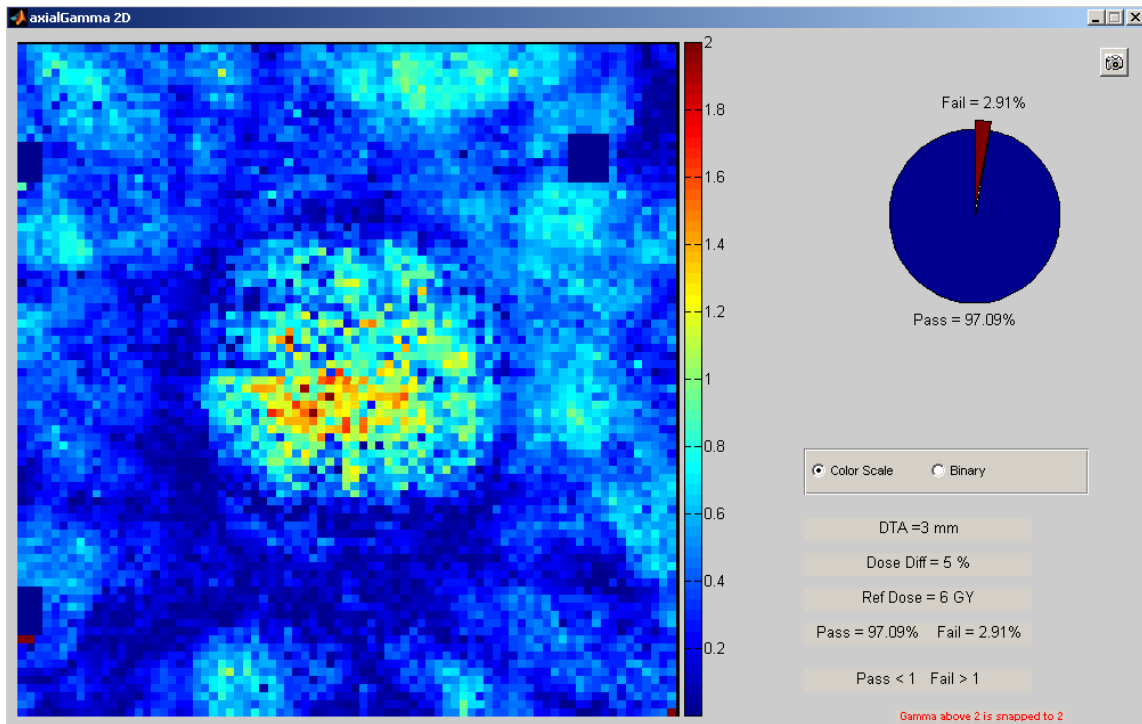


Figure 5.136 10 MV FFF SBRT UAB 2D Gamma Index Results: $\pm 5\%/3\text{mm}$, Axial Plane, Irradiation #1

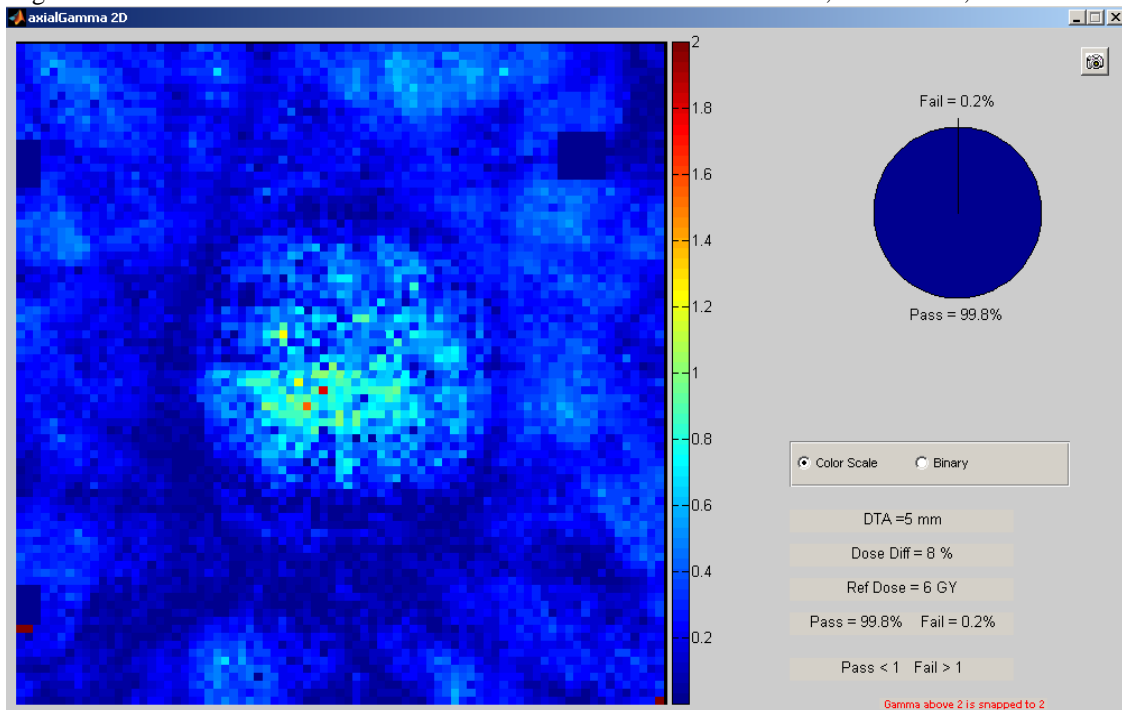


Figure 5.137 10 MV FFF SBRT UAB 2D Gamma Index Results: $\pm 8\%/3\text{mm}$, Axial Plane, Irradiation #1

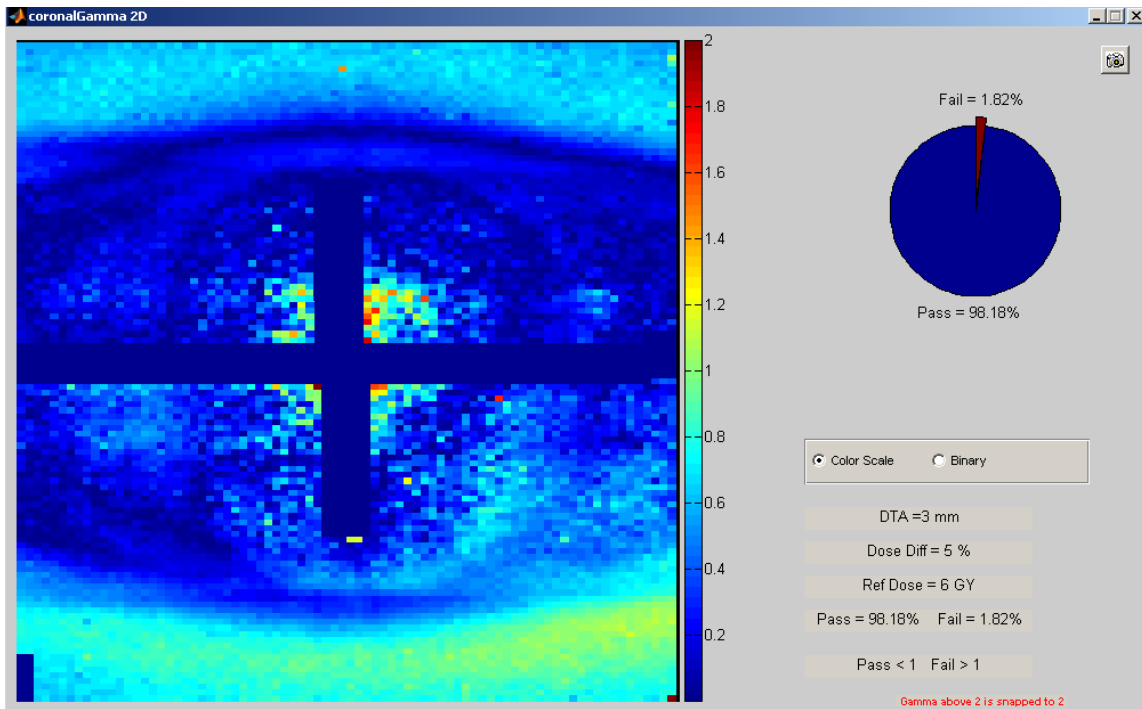


Figure 5.138 10 MV FFF SBRT UAB 2D Gamma Index Results: $\pm 5\%/3\text{mm}$, Coronal Plane, Irradiation #1

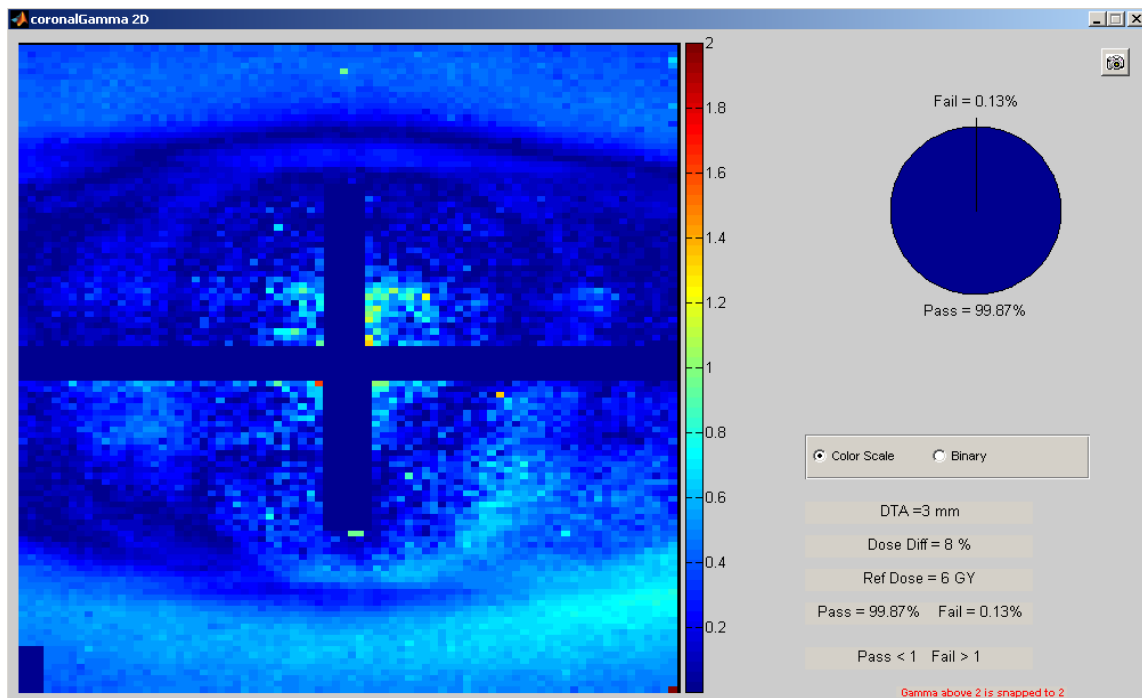


Figure 5.139 10 MV FFF SBRT UAB 2D Gamma Index Results: $\pm 8\%/3\text{mm}$, Coronal Plane, Irradiation #1

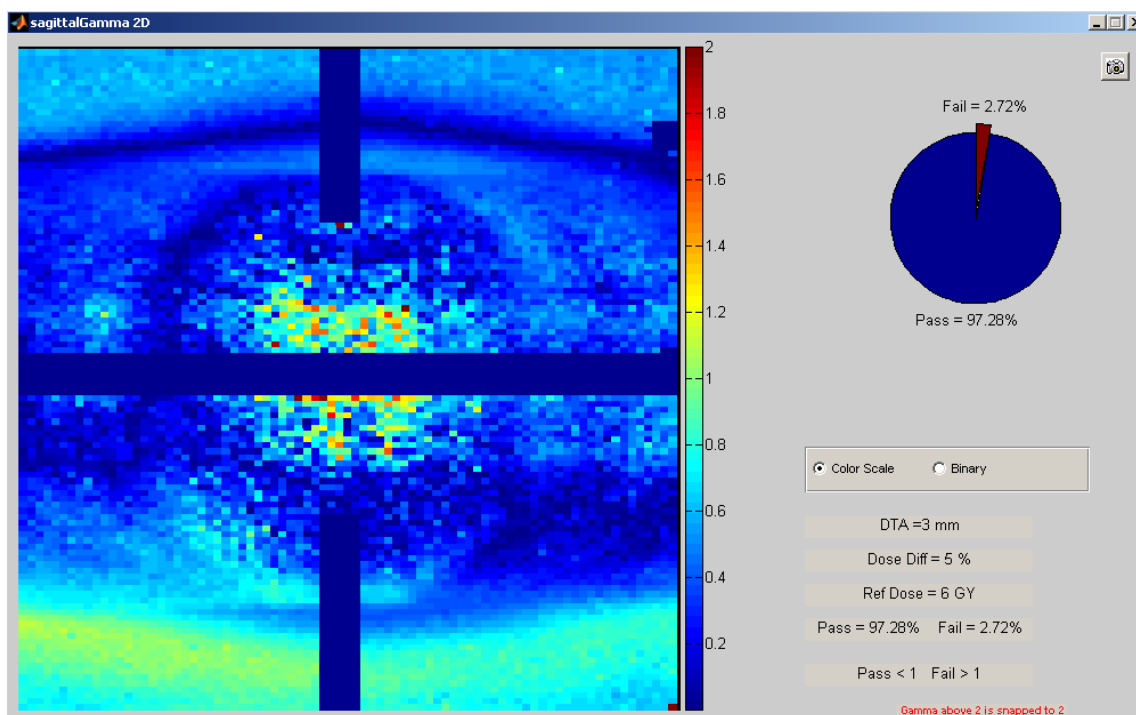


Figure 5.140 10 MV FFF SBRT UAB 2D Gamma Index Results: $\pm 5\%/3\text{mm}$, Sagittal Plane, Irradiation #1

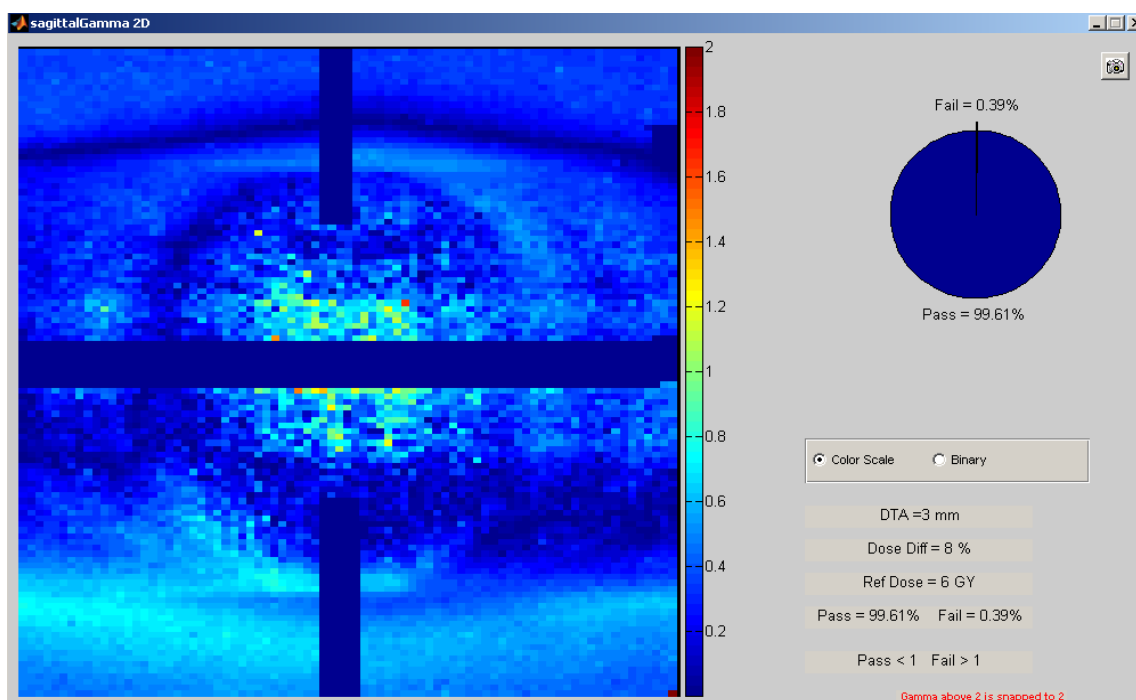


Figure 5.141 10 MV FFF SBRT UAB 2D Gamma Index Results: $\pm 8\%/3\text{mm}$, Sagittal Plane, Irradiation #1

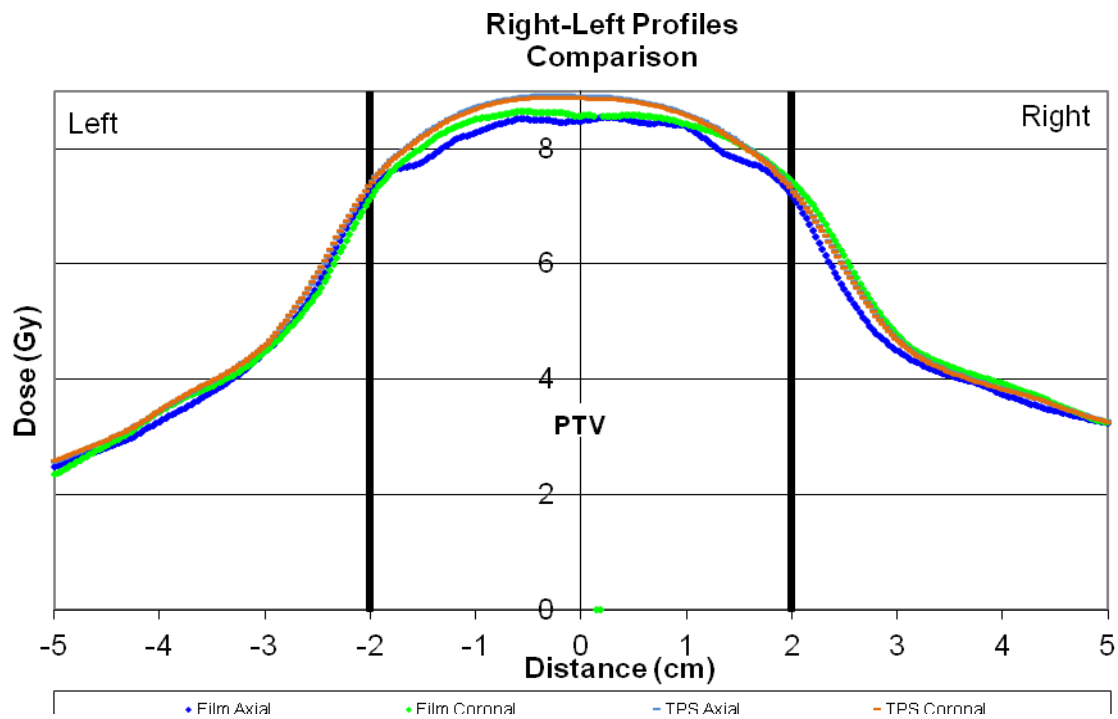


Figure 5.142 10 MV FFF SBRT UAB 1D Right-Left Dose Profiles: Irradiation #1

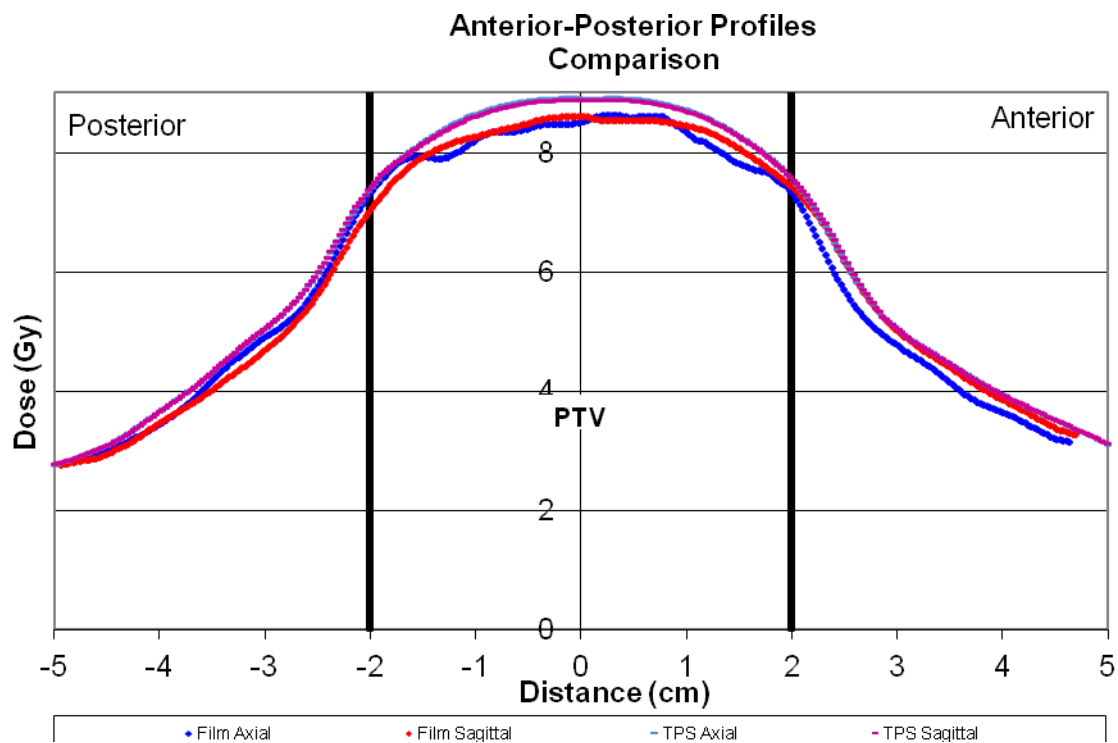


Figure 5.143 10 MV FFF SBRT UAB 1D Anterior-Posterior Dose Profiles: Irradiation #1

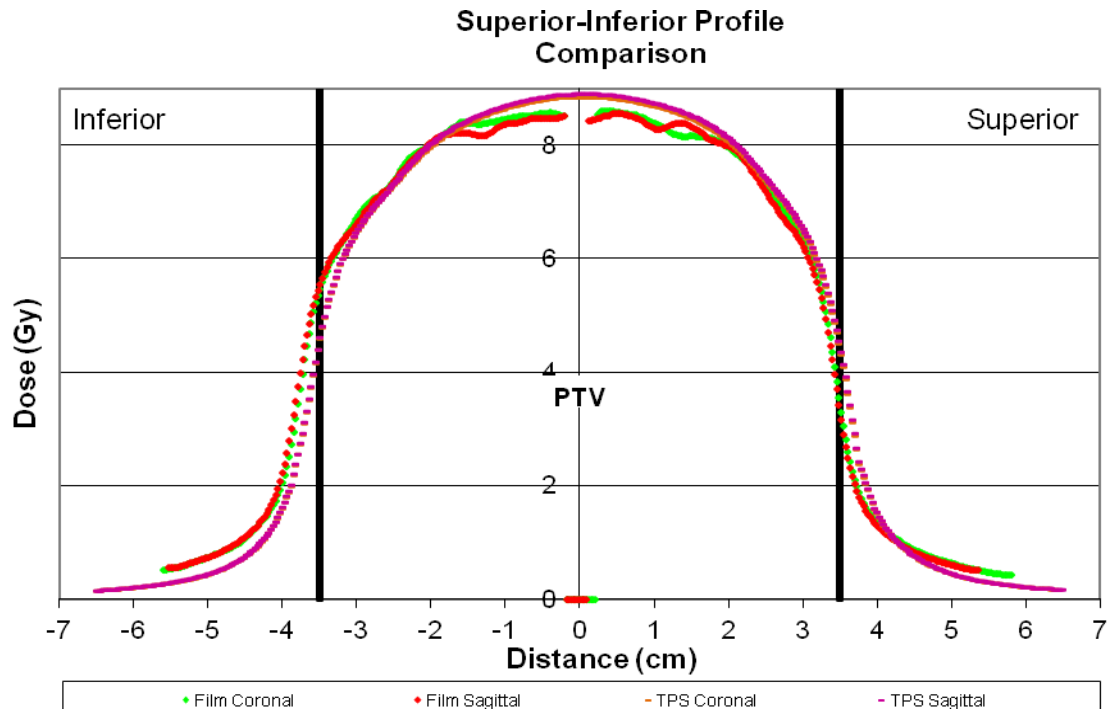


Figure 5.144 10 MV FFF SBRT UAB 1D Superior-Inferior Dose Profiles: Irradiation #1

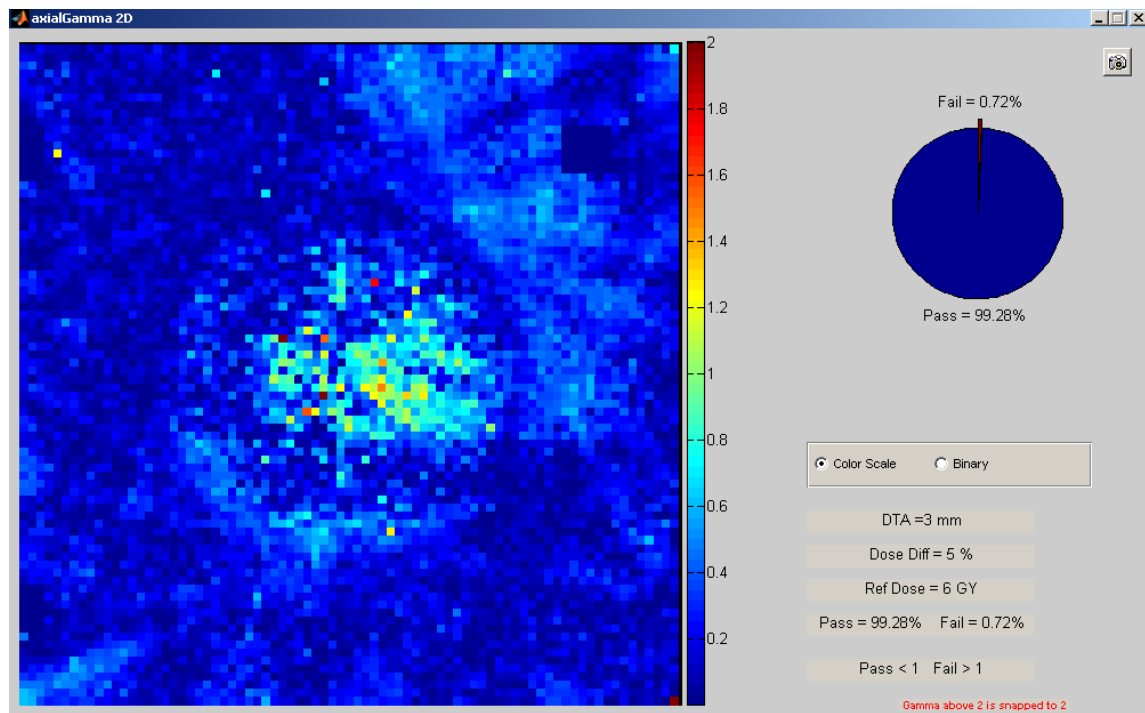


Figure 5.145 10 MV FFF SBRT UAB 2D Gamma Index Results: $\pm 5\%/3\text{mm}$, Axial Plane, Irradiation #2

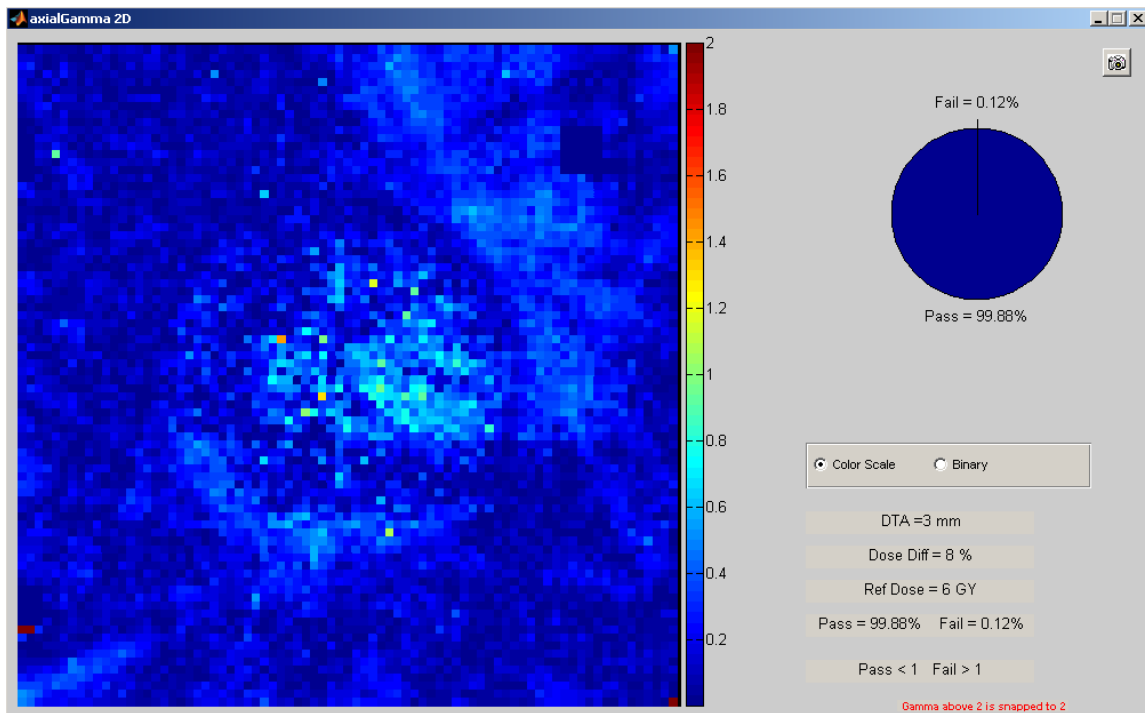


Figure 5.146 10 MV FFF SBRT UAB 2D Gamma Index Results: $\pm 8\%/3\text{mm}$, Axial Plane, Irradiation #2

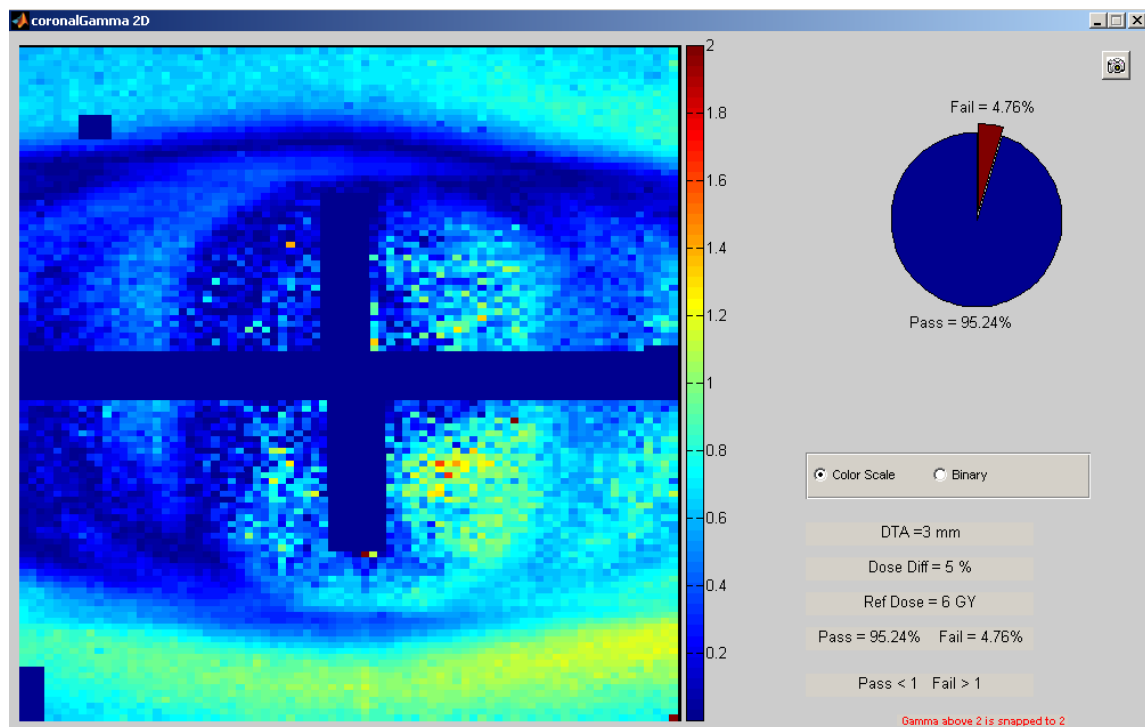


Figure 5.147 10 MV FFF SBRT UAB 2D Gamma Index Results: $\pm 5\%/3\text{mm}$, Coronal Plane, Irradiation #2

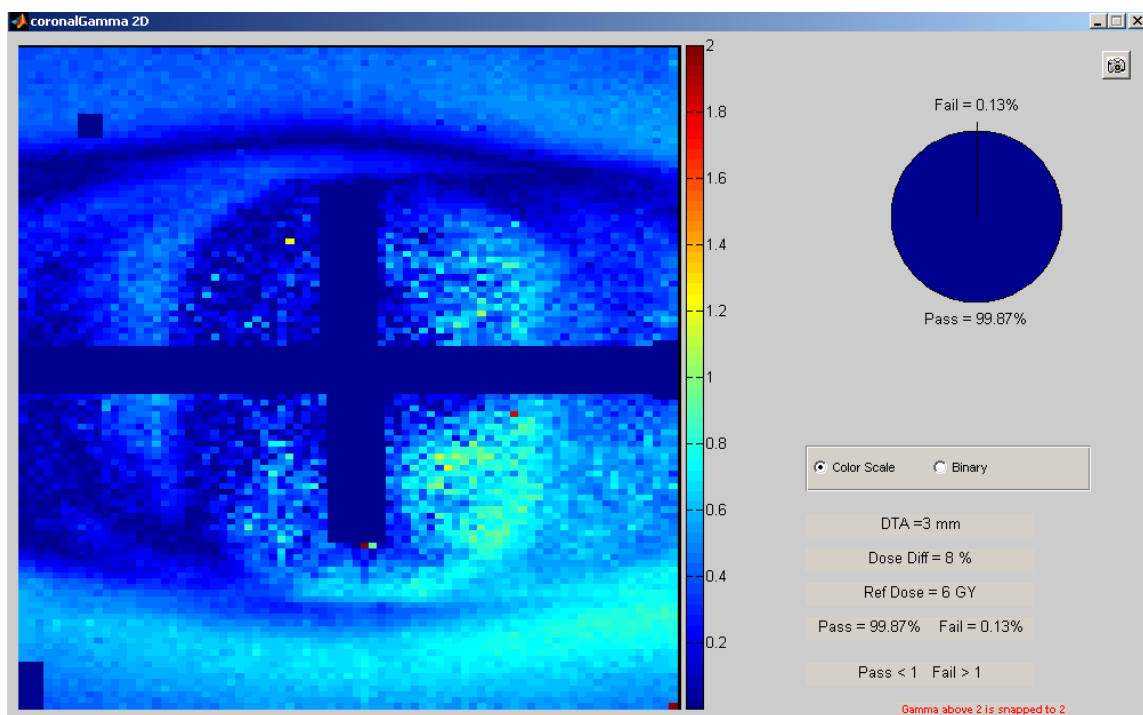


Figure 5.148 10 MV FFF SBRT UAB 2D Gamma Index Results: $\pm 8\%/3\text{mm}$, Coronal Plane, Irradiation #2

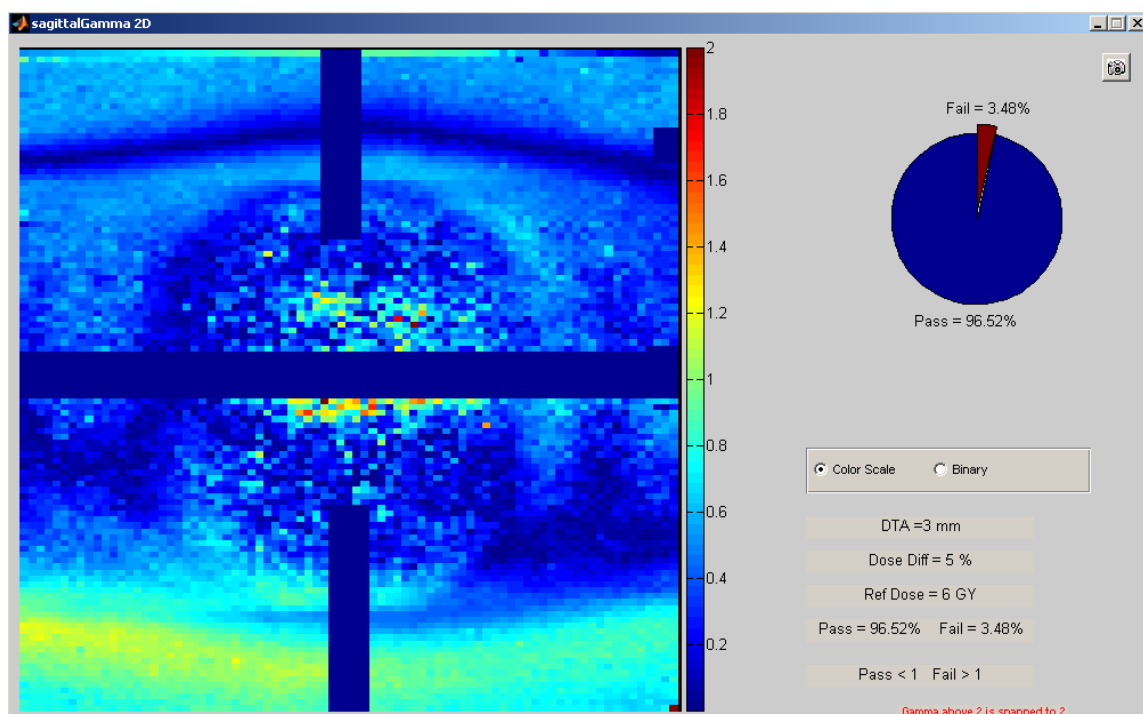


Figure 5.149 10 MV FFF SBRT UAB 2D Gamma Index Results: $\pm 5\%/3\text{mm}$, Sagittal Plane, Irradiation #2

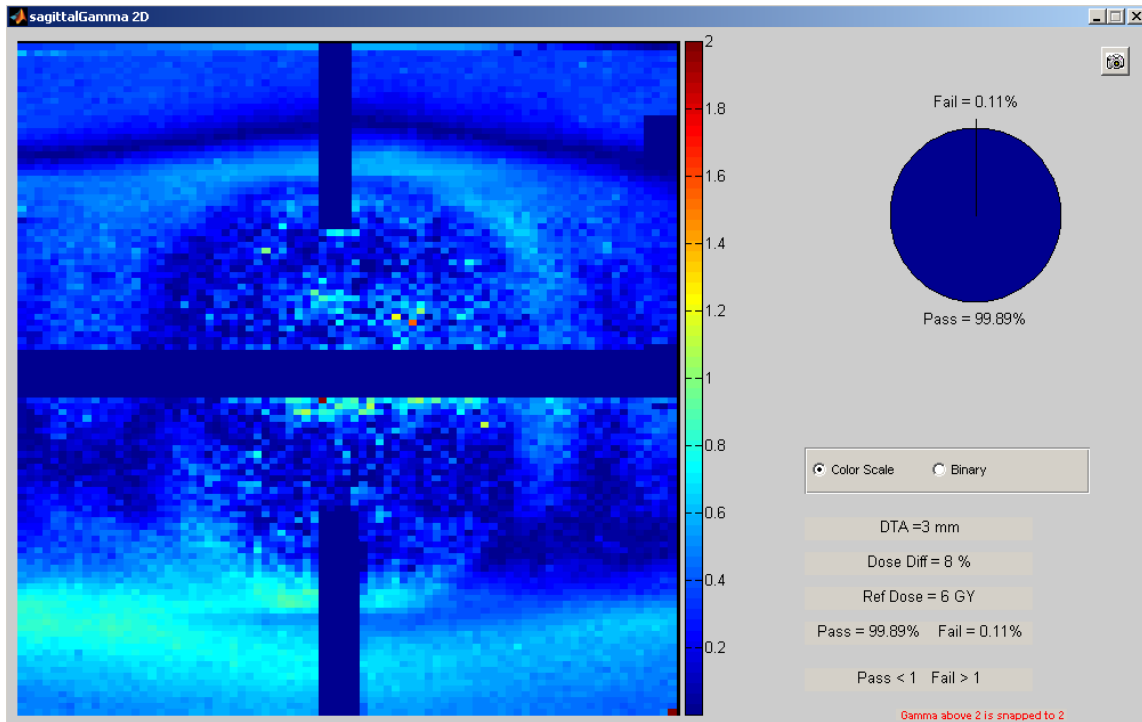


Figure 5.150 10 MV FFF SBRT UAB 2D Gamma Index Results: $\pm 8\%/3\text{mm}$, Sagittal Plane, Irradiation #2

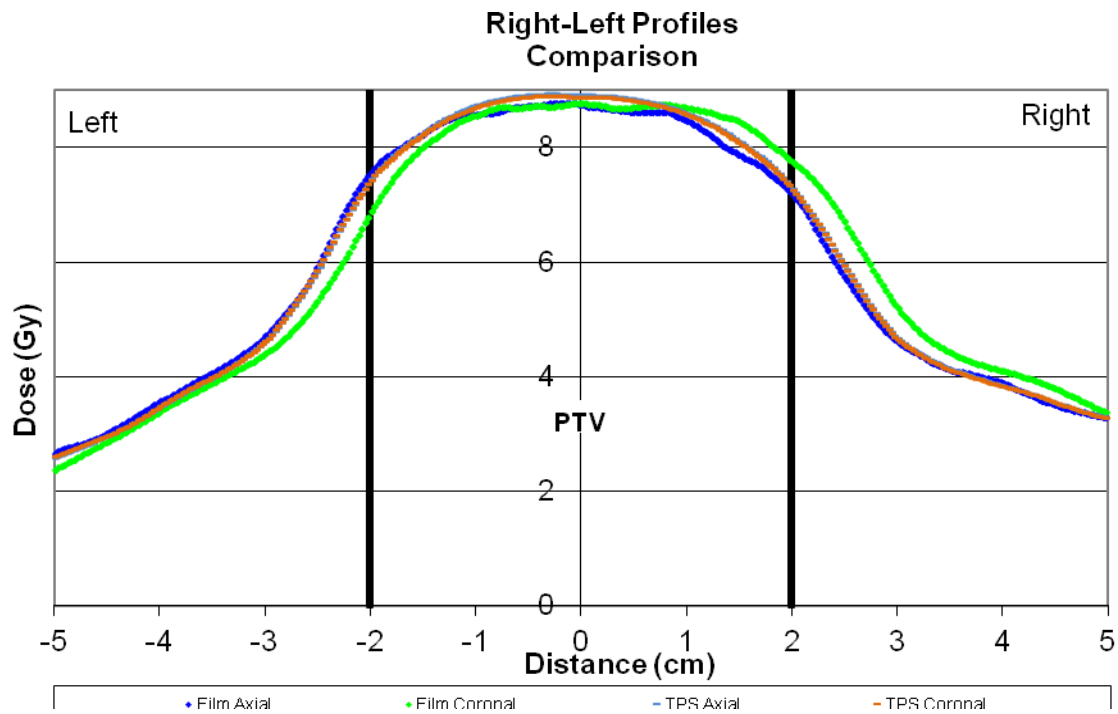


Figure 5.151 10 MV FFF SBRT UAB 1D Right-Left Dose Profiles: Irradiation #2

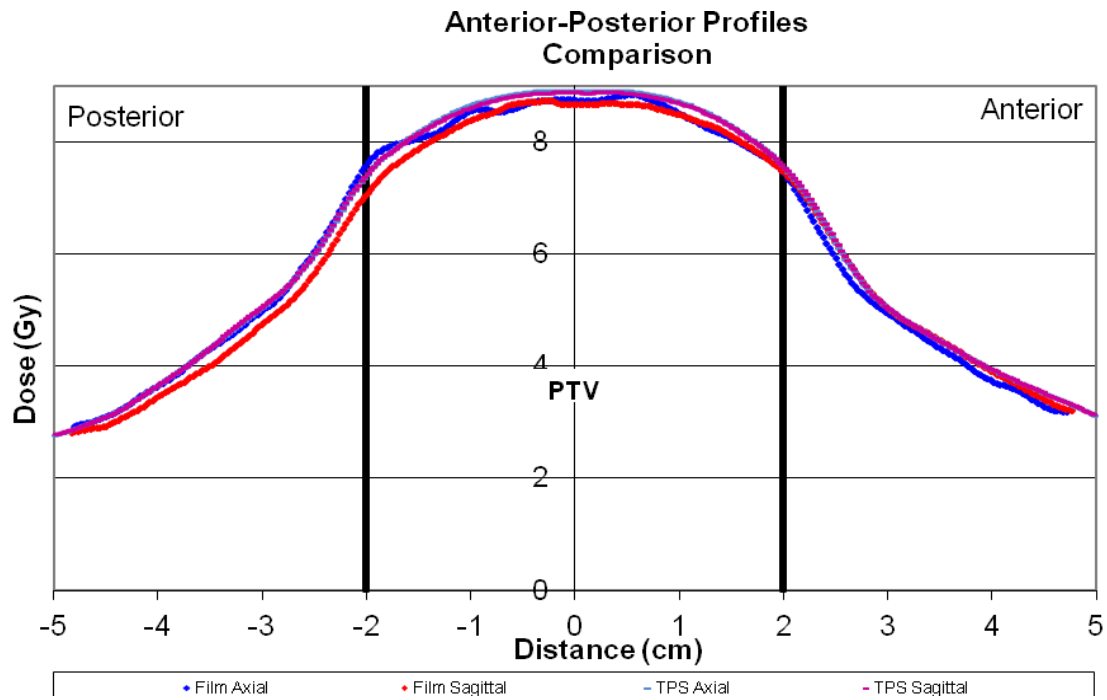


Figure 5.152 10 MV FFF SBRT UAB 1D Anterior-Posterior Dose Profiles: Irradiation #2

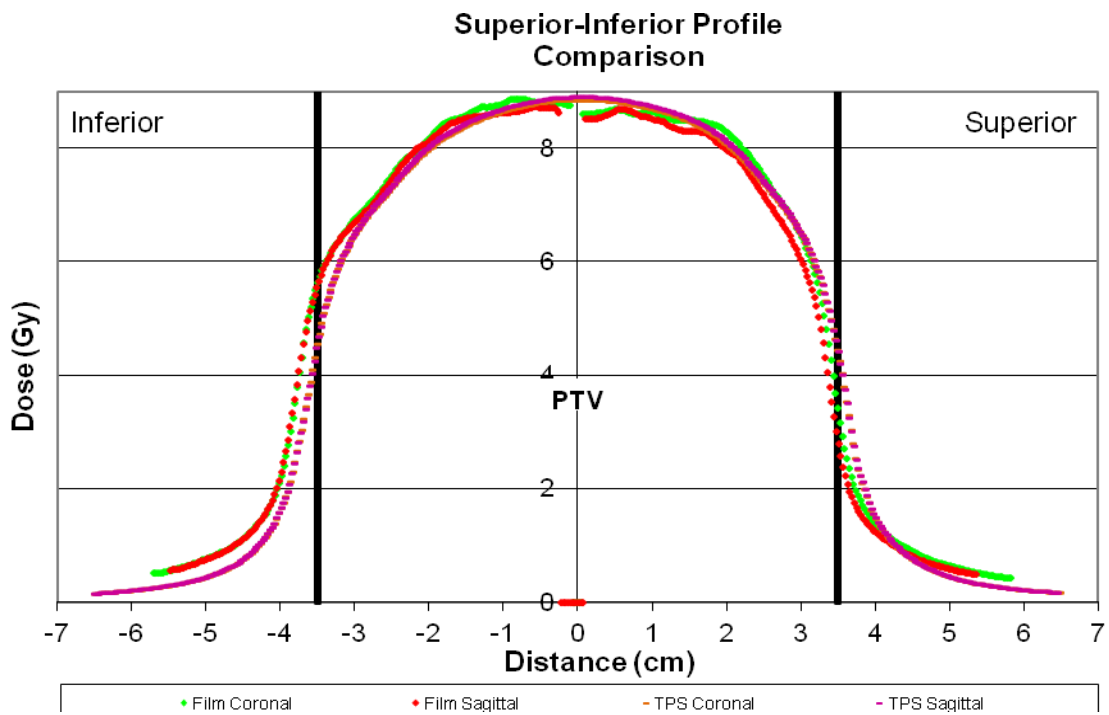


Figure 5.153 10 MV FFF SBRT UAB 1D Superior-Inferior Dose Profiles: Irradiation #2

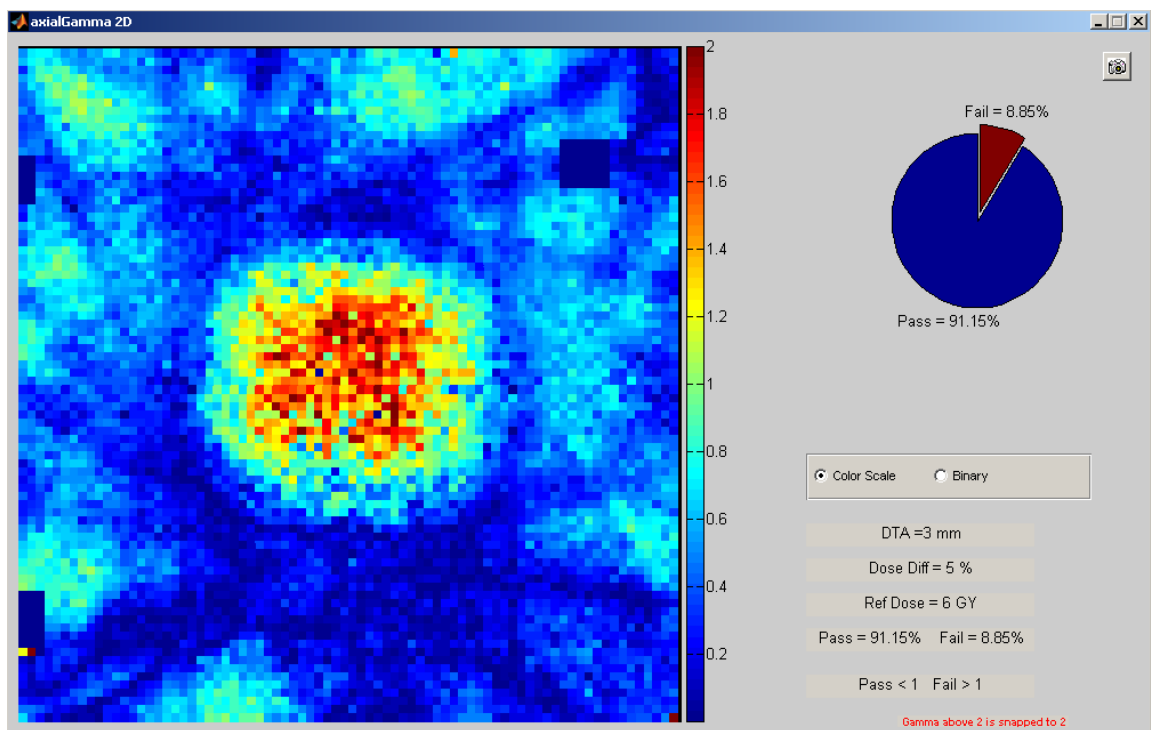


Figure 5.154 10 MV FFF SBRT UAB 2D Gamma Index Results: $\pm 5\%/3\text{mm}$, Axial Plane, Irradiation #3

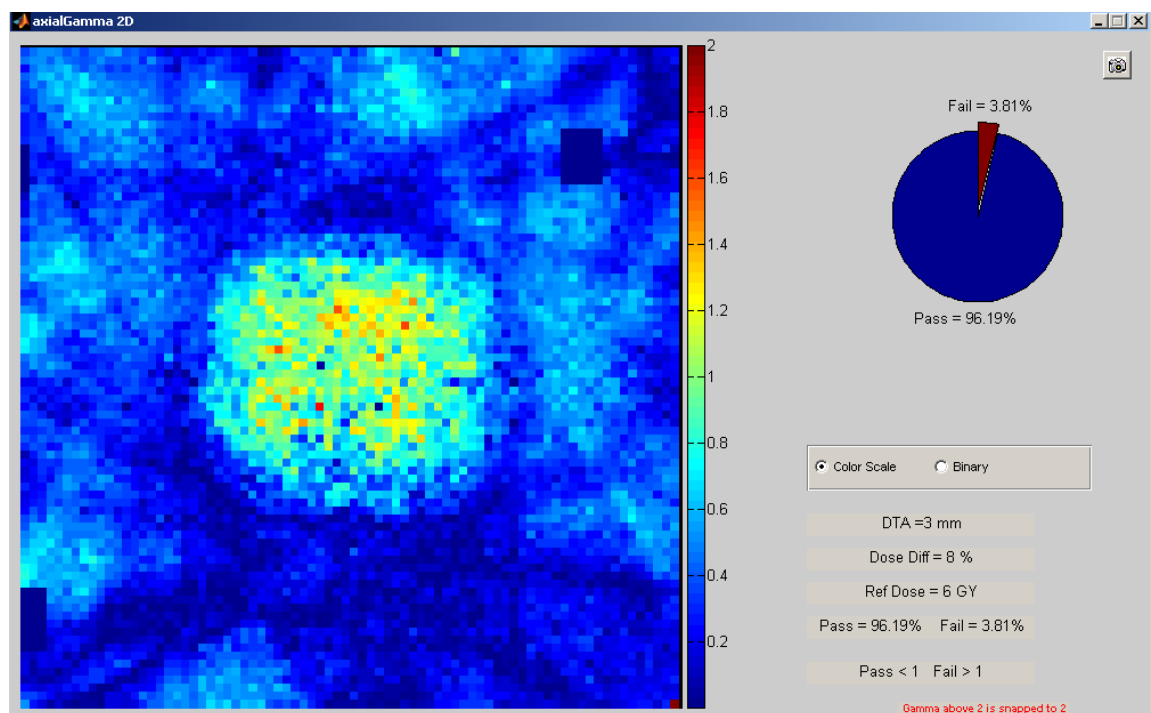


Figure 5.155 10 MV FFF SBRT UAB 2D Gamma Index Results: $\pm 8\%/3\text{mm}$, Axial Plane, Irradiation #3

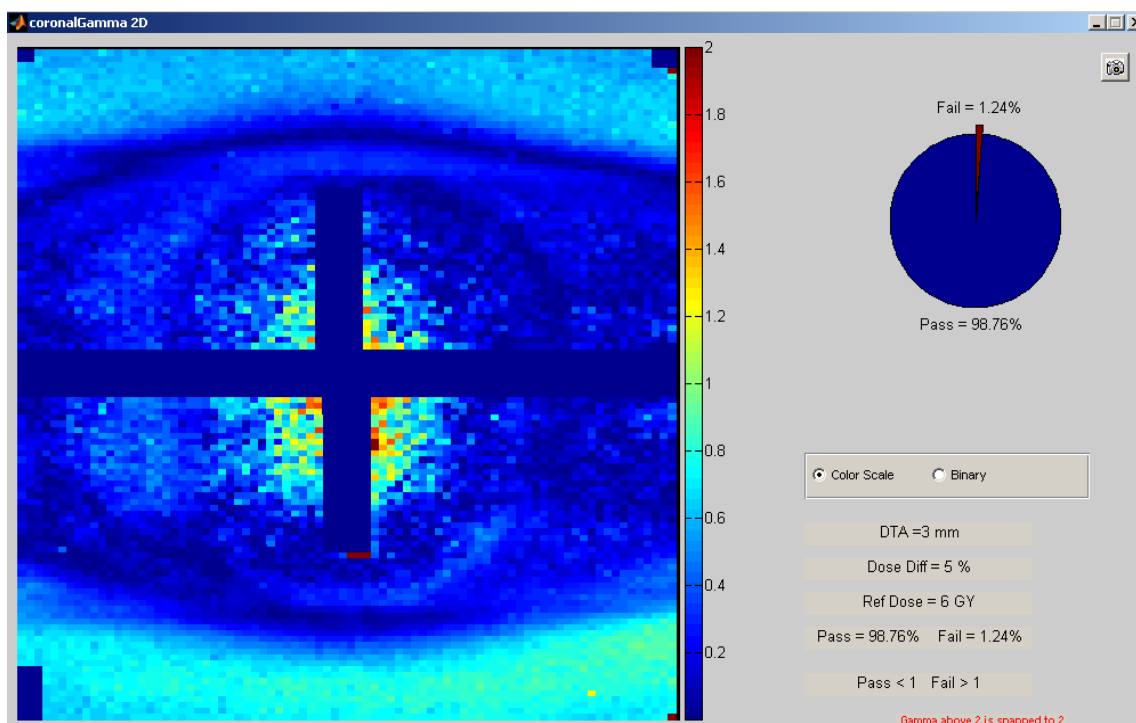


Figure 5.156 10 MV FFF SBRT UAB 2D Gamma Index Results: $\pm 5\%/3\text{mm}$, Coronal Plane, Irradiation #3

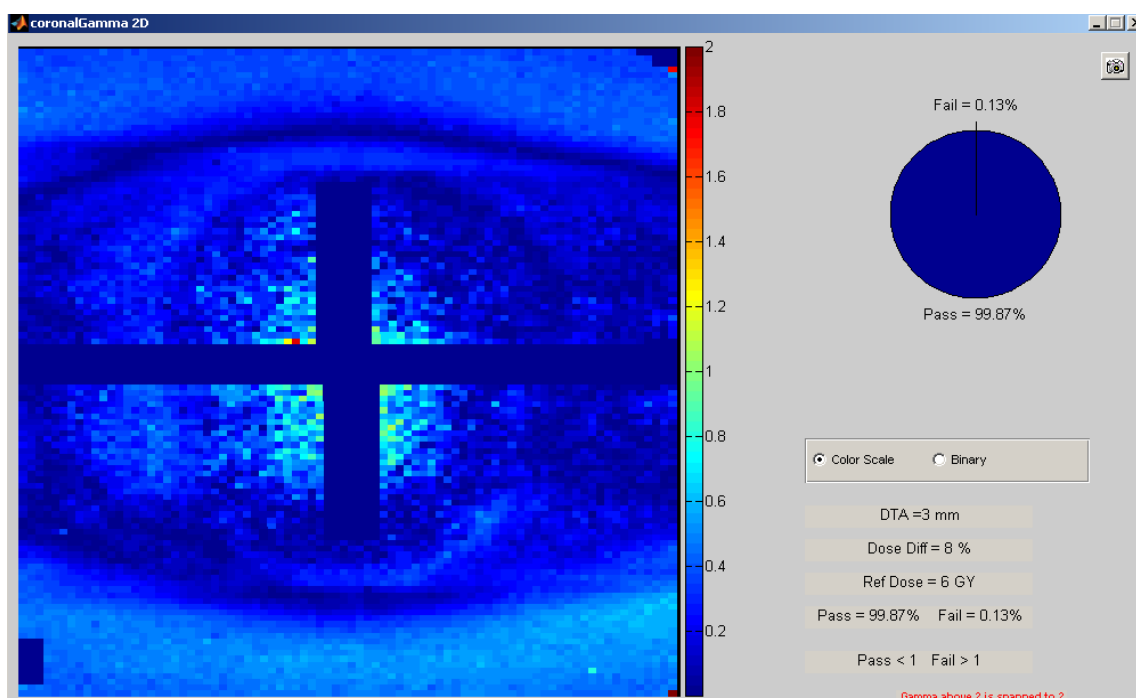


Figure 5.157 10 MV FFF SBRT UAB 2D Gamma Index Results: $\pm 8\%/3\text{mm}$, Coronal Plane, Irradiation #3

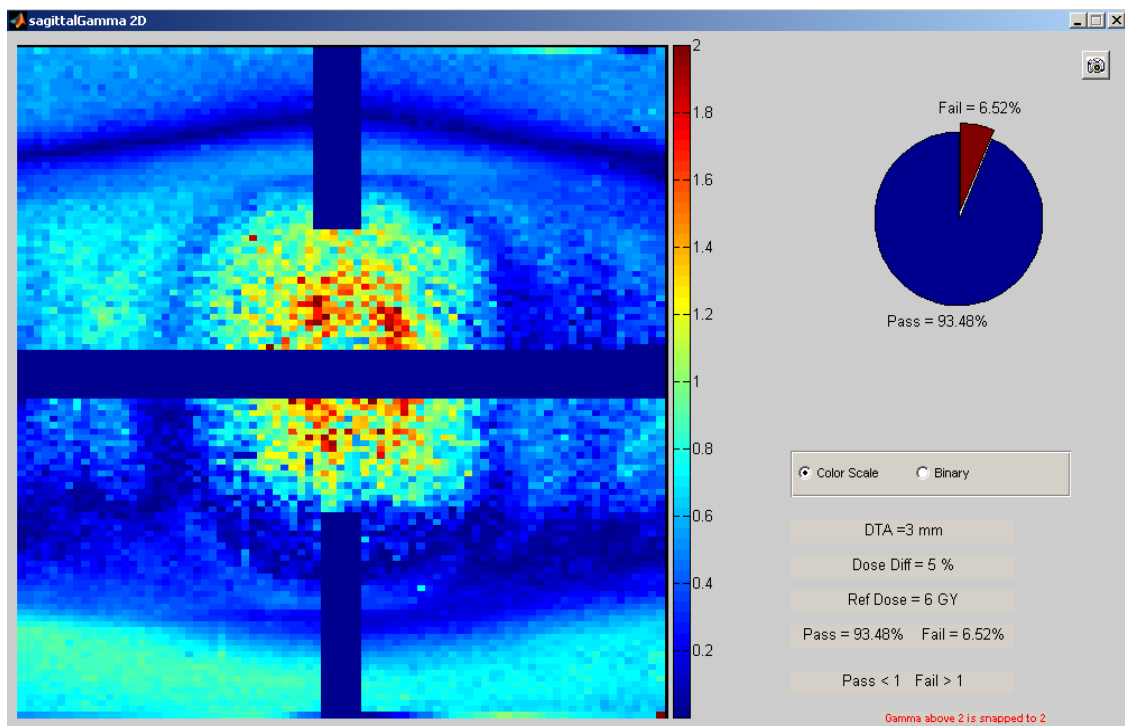


Figure 5.158 10 MV FFF SBRT UAB 2D Gamma Index Results: $\pm 5\%/3\text{mm}$, Sagittal Plane, Irradiation #3

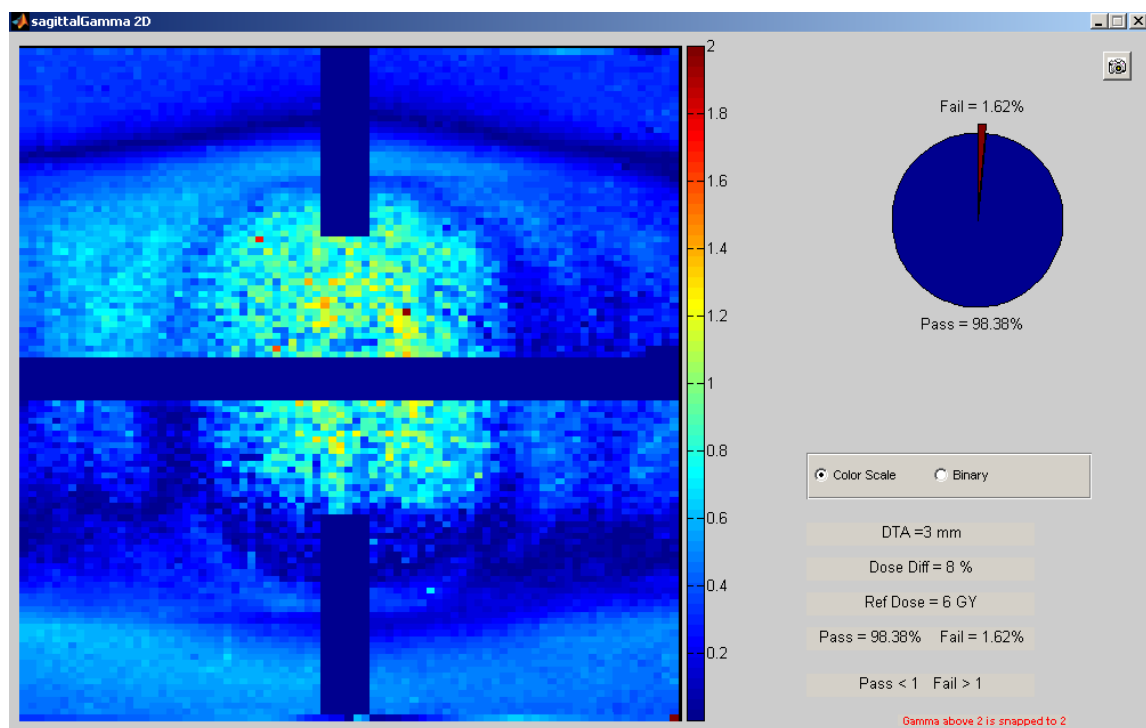


Figure 5.159 10 MV FFF SBRT UAB 2D Gamma Index Results: $\pm 8\%/3\text{mm}$, Sagittal Plane, Irradiation #3

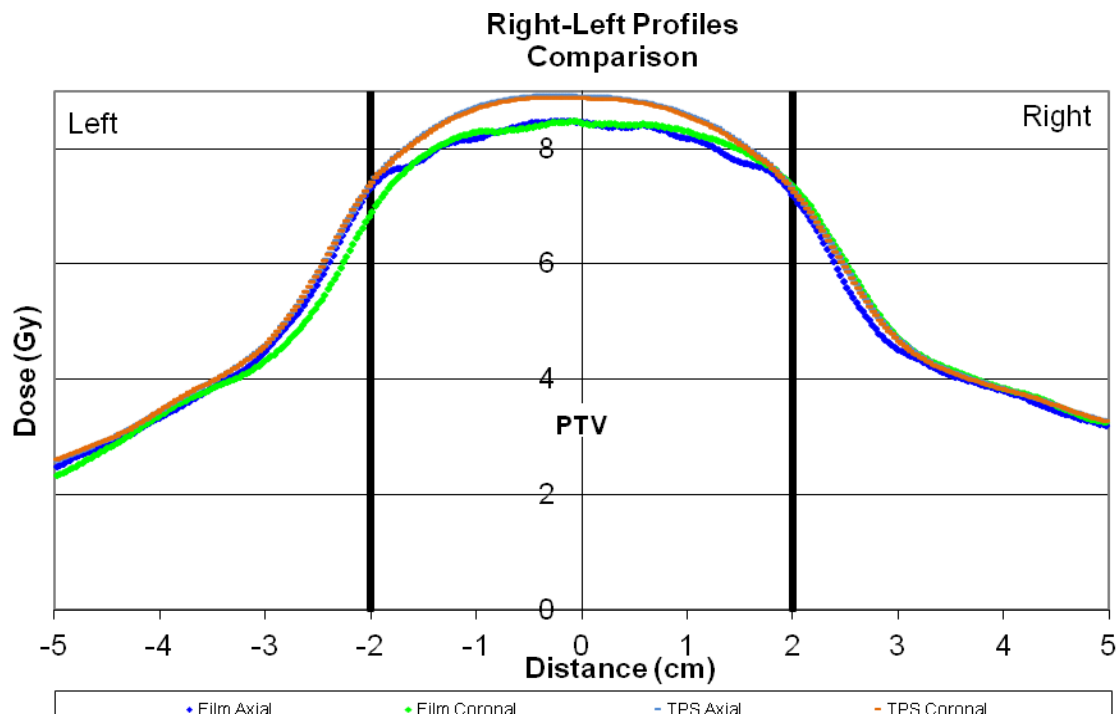


Figure 5.160 10 MV FFF SBRT UAB 1D Right-Left Dose Profiles: Irradiation #3

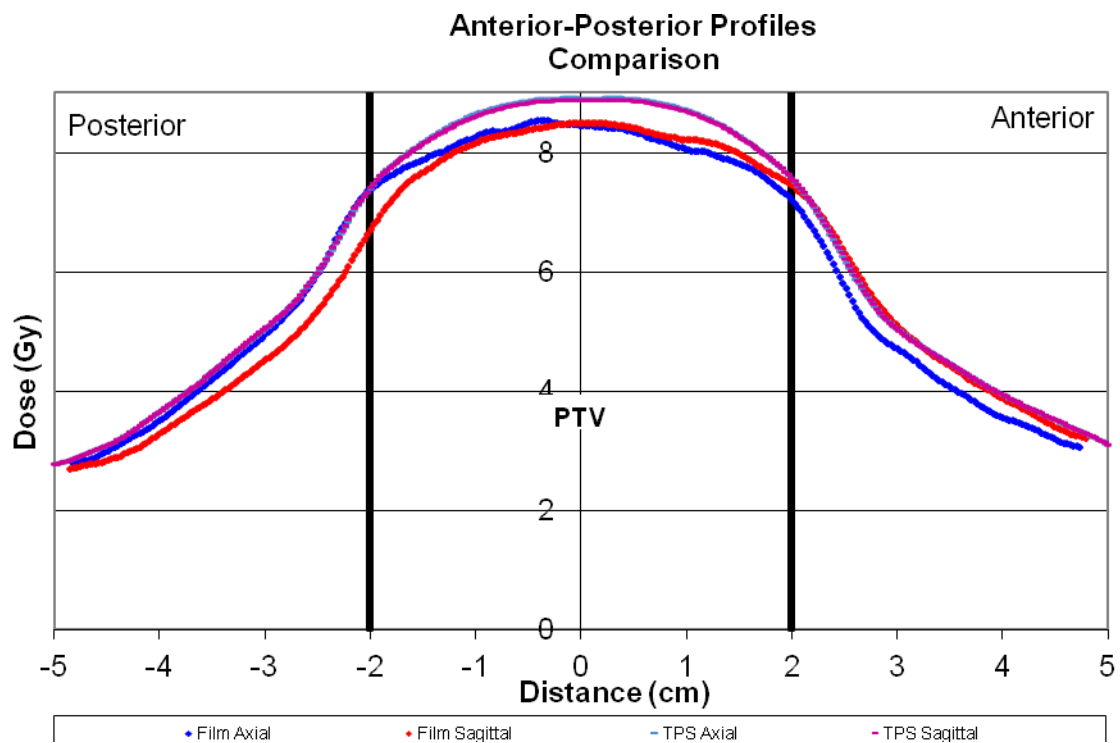


Figure 5.161 10 MV FFF SBRT UAB 1D Anterior-Posterior Dose Profiles: Irradiation #3

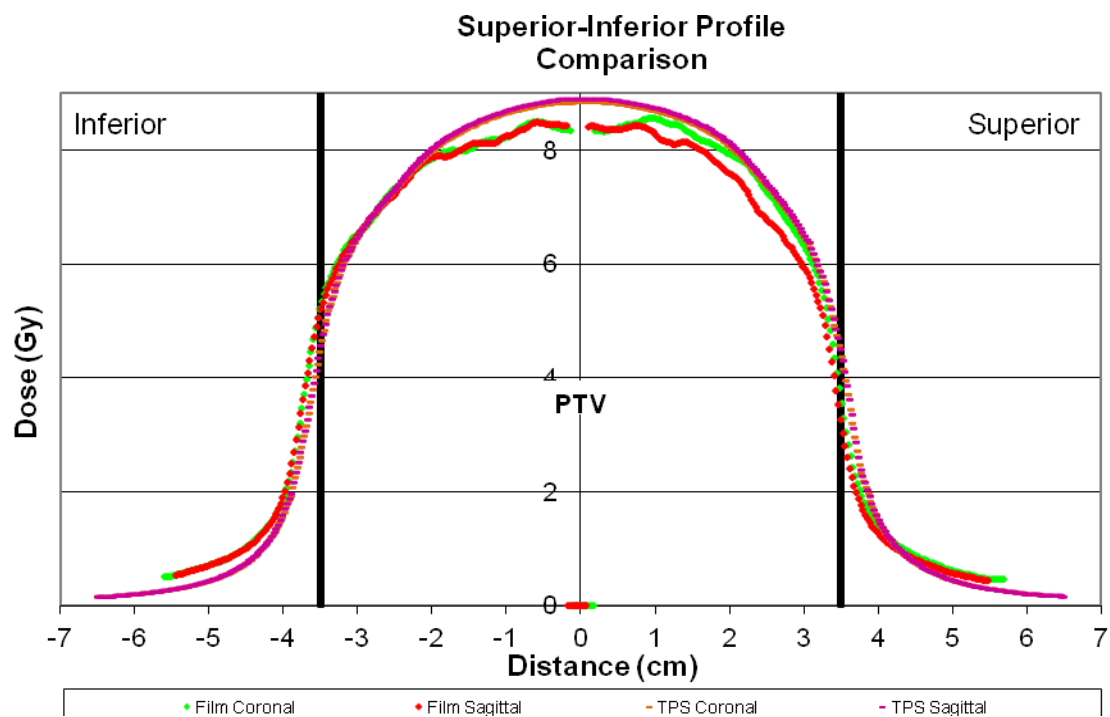


Figure 5.162 10 MV FFF SBRT UAB 1D Superior-Inferior Dose Profiles: Irradiation #3

Bibliography

1. D. Followill, D. Radford-Evans, C. Cherry, A. Molineu, G. Fisher, W. Hanson, and G. Ibbott, "Design, Development, and Implementation of the Radiological Physics Center's Pelvis and Thorax Anthropomorphic Quality Assurance Phantoms," *Med. Phys.* **34**(6), 2070-2076 (2007).
2. B. Fraass, K. Doppke, M. Hunt, G. Kutcher, G. Starkschall, R. Stern and J. Van Dyke, "American Association of Physicists in Medicine Radiation Therapy Committee Task Group 53: quality assurance for clinical radiotherapy treatment planning", *Med. Phys.* 25(10), 1773-1829 (1998).
3. K. Mah and J. Van Dyk, "On the impact of tissue inhomogeneity corrections in clinical thoracic radiation therapy", *International Journal of Radiation Oncology, Biology, Physics*, 21(5), 1257-1267 (1991).
4. K. Ekstrand and W. Barnes, "Pitfalls in the use of high energy X rays to treat tumors in the lung", *Int. J. Radiat. Oncol., Biol., Phys.* 18, 249–252 (1990).
5. E. Klein, A. Morrison, J. Purdy, M. Graham, and J. Matthews, "A volumetric study of measurements and calculations of lung density corrections for 6 and 18 MV photons", *Int. J. Radiat. Oncol., Biol., Phys.* 37, 1163–1170 (1997).

6. S. Davidson, G. Ibbott, K. Prado, L. Dong, Z. Liao, and D. Followill, "Accuracy of two heterogeneity dose calculation algorithms for IMRT in treatment plans designed using an anthropomorphic thorax phantom," *Med Phys* 34 (5), 1850-1857 (2007).
7. N. Papanikolaou, J. Battista, A. Boyer, C. Kappas, E. Klein, T. Mackie, M. Sharpe and J. Van Dyk, "Tissue Inhomogeneity Corrections for Megavoltage Photon Beams. AAPM Task Group #65 Radiation Therapy Committee". M. P. Publishing. Madison, WI, AAPM (2004).
8. P. Alvarez, A. Molineu, N. Hernandez, D. Followill, and G. Ibbott, "TU-E-224A-01: Evaluation of Heterogeneity Corrections Algorithms Through the Irradiation of a Lung Phantom", *Med. Phys.* 33 (6), 2214 (2006).
9. D. Followill, P. Alvarez, A. Molineu, M. Gillin, and G. Ibbott, "SU-E-T-542: Evaluation of Lung Treatment Deliveries Using the Radiological Physics Center's (RPC) Thorax Phantom: Monte Carlo Heterogeneity Correction Algorithms vs. All Other Modern Heterogeneity Correction Algorithms", *Med. Phys.* 38, 3614 (2011).
10. L. Wang, E. Yorke, G. Desobry, and C. Chui, "Dosimetric advantage of using 6 MV over 15 MV photons in conformal therapy of lung cancer: Monte Carlo studies in patient geometries", *Journal of Applied Clinical Medical Physics* 3 (1), 51-59 (2002).
11. G. Ding, D. Duggan, B. Lu, D. Hallahan, A. Cmelak, A. Malcolm, J. Newton, M. Deeley, and C. Coffey, "Impact of inhomogeneity corrections on dose coverage in the treatment of lung cancer using stereotactic body radiation therapy", *Med. Phys.* 34, 2985 (2007).

12. Varian Medical Systems, “Eclipse Algorithms Reference Guide”, (2009).
13. L. Tillikainen, H. Helminen, T. Torsti, S. Siljamäki, J. Alakuijala, J. Pyyry, and W. Ulmer, “A 3D pencil beam based superposition algorithm for photon dose calculation in heterogeneous media”, *Phys. Med. Biol.* 53 3821–3839 (2008).
14. Radiological Physics Center, “Guidelines for Planning and Irradiating the RPC Lung Phantom”, (March 2010).
15. RTOG 0618, “A Phase II Trial of Stereotactic Body Radiation Therapy (SBRT) in the Treatment of the Patients with Operable Stage I/II Non-Small Cell Lung Cancer”, (December 2010).
16. RTOG 0813, “Seamless Phase I/II Study of Stereotactic Lung Radiotherapy (SBRT) for Early Stage, Centrally Located, Non-small Cell Lung Cancer (NSCLC) in Medically Inoperable Patients”, (February 2011).
17. RTOG 0915, “A Randomized Phase II Study Comparing 2 Stereotactic Body Radiation Therapy (SBRT) Schedules for Medically Inoperable Patients with Stage I Peripheral Non-small Cell Lung Cancer”, (August 2010).

18. RTOG 1021, “A Randomized Phase III Study of Subtotal Resection (+/- Brachytherapy) versus Stereotactic Body Radiation Therapy in High Risk Patients with Stage I Non-small Cell Lung Cancer (NSCLC)”, (March 2011).
19. J. Hrbacek, S. Lang, and S. Klock, “Commissioning Of Photon Beams of a Flattening Filter-Free linear Accelerator and The Accuracy of Beam Modeling Using an Anisotropic Analytical Algorithm”, *Int. J. Radiation Oncology Biol. Phys.*, Vol. 80, No. 4, pp. 1228–1237, (2011).
20. G. Kragl, F. Baier, S. Lutz, D. Albrich, M. Dalaryd, B. Kroupa, T. Wiezorek, T. Knöös, D. Georg, “Flattening filter free beams in SBRT and IMRT: dosimetric assessment of peripheral doses”, *Z Med Phys*; 21(2):91-101 (2011).
21. A. Niroomand-Rad, C. R. Blackwell, B. M. Coursey, K. P. Gall, J. M. Galvin, W. L. McLaughlin, A. S. Meigooni, R. Nath, J. E. Rodgers and C. G. Soares, "Radiochromic film dosimetry: recommendations of AAPM Radiation Therapy Committee Task Group 55", *Med. Phys.* 25(11): 2093 (1998).
22. B. Arjomandy, R. Tailor, A. Anand, N. Sahoo, M. Gillin, K. Prado, and M. Vivic, “Energy dependence and dose response of Gafchromic EBT2 film over a wide range of photon, electron, and proton beam energies”, *Med. Phys.* 37 (5), 1942-1947 (2010).
23. International Specialty Products, “Gafchromic® Ebt2 Self-Developing Film for Radiotherapy Dosimetry”, (2009).

24. T. Kirby, W. Hanson, and D. Johnston, "Uncertainty analysis of absorbed dose calculations from thermoluminescence dosimeters", *Med. Phys.* 19 (6), 1427-1433 (1992).
25. Radiological Physics Center, "Procedure for Calculating TLD Doses. Batch B11 (TG-51)", (2007).
26. G. Fisher, "The Accuracy of 3-D Inhomogeneity Photon Algorithms In Commercial Treatment Planning Systems Using A Heterogeneous Lung Phantom", The University of Texas Health Science Center at Houston Graduate School of Biomedical Sciences, Houston, TX, Master's Thesis (2005).
27. J. Deasy, A. Blanco, and V. Clark, "CERR: a computational environment for radiotherapy research," *Med Phys* 30 (5), 979-985 (2003).
28. D. Low and J. Dempsey, "Evaluation of the gamma dose distribution comparison method", *Med. Phys.* 30(9), 2455-2464 (2003).
29. P. Alvarez, A. Molineu, N. Hernandez, D. Followill, and G. Ibbott, "SU-FF-T-403: Evaluation of Doses Delivered by SBRT to the Lung of An Anthropomorphic Thorax Phantom", *Med. Phys.* 32 (6), 2043-2044 (2005).

Vita

Roman Repchak was born in St. Sambir, Ukraine on April 17th, 1977, the son of Zinoviy and Maria Repchak. He attended the State University 'Lvivska Politechnika' in Lviv, Ukraine where he earned a Bachelor of Science in Electrical Engineering in 1998 and Master of Science in Electrical Engineering in 1999. For the next two years he worked as an engineer at 'Lviv Lisparkhosp'. In 2002 he immigrated to the United States where in 2003 he enlisted in the United States Air Force and in 2006 he was commissioned in the rank of 1st Lieutenant. In August of 2010, he entered The University of Texas Health Science Center at Houston Graduate School of Biomedical Sciences.

Permanent address:

7900 Cambridge St Apt 30-2G.

Houston, TX 77054